Aspects of N = 4 Super Yang-Mills: Amplitudes, Operators and Invariants

ALASTAIR JAMES DUNCAN STEWART

Aspects of $\mathcal{N} = 4$ Super Yang-Mills: Amplitudes, Operators and Invariants

Alastair James Duncan Stewart

A Thesis presented for the degree of
Doctor of Philosophy

Department of Mathematical Sciences
Durham University
United Kingdom

July 2021

Aspects of $\mathcal{N} = 4$ Super Yang-Mills: Amplitudes, Operators and Invariants

Alastair James Duncan Stewart

Submitted for the degree of Doctor of Philosophy

July 2021

Abstract: In this thesis, we study aspects of scattering amplitudes, half-BPS operators and Yangian Invariants in $\mathcal{N} = 4$ super Yang Mills.

We begin by exploring the geometry of Wilson loop diagrams. The Wilson loop in supertwistor space gives an explicit description of perturbative superamplitude integrands in $\mathcal{N} = 4$ super Yang-Mills as a sum of planar Feynman diagrams. Each Feynman diagram can be naturally associated with a geometrical object in the same space as the amplituhedron (although not uniquely). This suggests that the geometrical images of the diagrams would give a tessellation of the amplituhedron. This turns out to be true for NMHV amplitudes, however we prove that for N^2MHV and beyond this is not the case. Specifically, we show that there is no choice of geometric image of the Wilson loop Feynman diagrams that gives a geometric object with no spurious boundaries.

We then move to investigate a set of half-BPS operators in $\mathcal{N} = 4$ super Yang-Mills which are appropriate for describing single particle states of superstring theory on $AdS_5 \times S^5$; we refer to these as single particle operators. They are defined to have vanishing two-point function with all multi-trace operators, and so correspond to admixtures of single- and multi-traces. We find explicit formulae for these operators and their two-point function normalisation. We prove that single particle operators in the $U(N)$ gauge theory are

single particle operators in the $SU(N)$ theory, and show that at large N these operators interpolate between the single trace operator and the sphere giant graviton. A multipoint orthogonality theorem is presented and proved, which as a consequence enforces all near-extremal correlators to vanish. We compute all maximally and next-to-maximally extremal free correlators, and provide some explicit results for subsets of two- and three-point functions for multi-particle operators.

Finally, we calculate the N^2MHV Yangian invariants for $\mathcal{N} = 4$ SYM in amplituhedron coordinates, and see that some have suggestively simple forms.

Declaration

The work in this thesis is based on research carried out in the Department of Mathematical Sciences at Durham University. No part of this thesis has been submitted elsewhere for any degree or qualification.

Acknowledgements

First and foremost, I would like to thank my supervisor, Paul Heslop, for his help and encouragement through the whole time we have been working together. The projects that Paul has provided have been incredibly stimulating, and it has been a privilege to be able to learn from him over the last four years. I would particularly like to thank him for his patience during the tougher moments. This thesis certainly would not have been possible without his guidance.

Second, I would like to thank Michele Santagata, Hynek Paul, Francesco Aprile and James Drummond for the collaborative effort that went into the work presented in Chapter four of this thesis, and for their hospitality when we visited Southampton last year.

Third, I would like to thank my fellow CM301/CM135 office mates who have been part of my daily life over the last few years, with particular thanks to Matthew Renwick and Philip Glass who have been with me since day one. I will cherish the many tea and coffee breaks we have had over the years! I would also like to give special thanks to Gabriele Dian, whom I have had numerous stimulating and enjoyable conversations with over the last two years.

I would like to give a massive thank you to all the friends I have had the great fortune of meeting during my time at Ustinov College. Being part of such an intercultural and interdisciplinary community has made my time at Durham truly special, and taught me a great deal. I will not name you all as I am sure to forget someone, however special shout out needs to be given to the Spin Doctors ultimate-frisbee team and all the wonderful

people who have been a part of it over the years, and to all the people I have shared time with on the GCR committees gone by.

There are a few others who deserve special mention. To Anna, Armaan, Alex, Tom, Ed, Jake who I have had the pleasure of living with at some point or another over the last few years, thank you for providing an often well needed distraction. We have had many hilarious times together, and helped each other when we were feeling a bit blue. I couldn't have asked for better people to share a house with. For being my conference buddy, a bit of a mentor (though perhaps unintentionally!) when I first arrived in Durham, for introducing me to teching open mic nights and for being a great friend to me, I would like to thank Joe Farrow. I would like to give a special thanks to Diane Austry for her support, her kindness, and her friendship. We have shared many laughs together (the odd tear...) and had long discussions about many different aspects of life. I am grateful to have met you and to be able to call you my friend.

More close to home, I would like to thank my godfather Rick Finlay, as well as Janet and Lorraine for their kindness, support and encouragement throughout my life.

Most importantly, I would like to thank my Mum and Dad, Evan and May. Without your support, I would absolutely not be where I am today. I am truly thankful for everything you have done for me.

Final thanks to my examiners Arthur Lipstein and Sanjaye Ramgoolam for constructive comments on this thesis and very interesting discussions during the viva, and to STFC for funding this PhD.

Dedicated to

My parents, Evan and May,
for their never ending love and
support.

Thank you.

Contents

Abstract **iii**

List of Figures **xv**

List of Tables **xvii**

1 Introduction **1**

1.1 Introduction 1

1.1.1 Outline of the Thesis 5

2 Review of Concepts **9**

2.1 The $\mathcal{N} = 4$ Supersymmetric Yang-Mills Lagrangian and Field Content . 9

2.2 Scattering Amplitudes in Planar $\mathcal{N} = 4$ SYM 11

2.3 Super Momentum Twistors and Bosonisation to Amplituhedron Coordinates 13

2.3.1 Momentum Twistors and Supermomentum Twistors 14

2.3.2 Bosonisation of Supermomentum Twistors 17

2.4 Mathematical Preliminaries: Permutations and Partitions 19

2.4.1 The Symmetric Group 19

2.4.2 Conjugacy Classes of S_n 20

2.4.3 Dimension of S_n . . . 21
2.4.4 Characters . . . 22
2.4.5 Weights of $U(N)$ Representations . . . 24
2.4.6 Power Set . . . 25

3 The Twistor Wilson Loop and the Amplituhedron 27

3.1 Introduction . . . 27
3.1.1 Toy Model: polygons in P^2 . . . 30
3.2 WLDs and Volume Forms . . . 34
3.2.1 Planar Wilson Loop Diagrams in $\mathcal{N} = 4$ SYM . . . 35
3.2.2 Volume Forms in Amplituhedron Space from WLDs . . . 38
3.3 NMHV amplituhedron from WLDs . . . 40
3.3.1 Cancellation of spurious poles in NMHV WLDs . . . 41
3.3.2 Spurious boundary matching . . . 44
3.4 N^2MHV . . . 47
3.4.1 Cancellation of spurious poles in N^2MHV WLDs . . . 47
3.4.2 Spurious Boundary Matching for N^2MHV . . . 52
3.5 Concluding Remarks . . . 62

4 Single Particle Operators in $N = 4$ Super Yang-Mills 65

4.1 Introduction . . . 65
4.1.1 Half-BPS Operators in $N = 4$ SYM and the Trace Basis . . . 67
4.1.2 Other Bases of Half-BPS Operators . . . 71
4.1.3 Summary of Chapter . . . 74
4.2 Single-Particle Half-BPS Operators (SPOs) . . . 76

4.2.1 Definition of SPOs and Low Charge Examples 77
4.2.2 General Formulae for SPOs 80
4.2.3 SPOs interpolate between single-trace operators and giant gravitons 88
4.2.4 SPOs in $U(N)$ are SPOs in $SU(N)$ 90
4.2.5 Two-point Function Properties 93
4.2.6 On Multi-particle Operators 94
4.3 Multipoint Orthogonality 97
4.3.1 Proof of the Theorem 99
4.3.2 Vanishing Near-Extremal Correlators 102
4.4 Exact Results for Correlators of SPOs 106
4.4.1 Maximally-Extremal (ME) Correlators 107
4.4.2 Next-to-Maximally-Extremal Correlators 113
4.4.3 On correlators with lower extremality 118
4.4.4 3-Point Functions as Multi-Particle 2-Point Functions 121
4.4.5 Some Formulae for Two-Point Functions of Multi-Particle Operators 124
4.4.6 Three-point Functions of Multi-Particles Involving $\mathcal{O}_2$s 125
4.5 Conclusions 128

5 A Note on N^2MHV Yangian Invariants for $N = 4$ SYM **131**

5.1 Introduction 131
5.1.1 Yangian Invariants from the Grassmannian 132
5.1.2 Covariantising the Seven-Point Yangian Invariants 135
5.2 Results of N^2MHV Yangian Invariants 138
5.2.1 $n = 8$ Invariants 140

5.2.2 $n = 9$ Invariants 141

5.2.3 $n = 10$ Invariants 143

5.3 Concluding Remarks 143

6 Conclusion **145**

A Spurious Pole Cancellation for Special N^2MHV Three-Way Case **151**

B Character Polynomials **155**

C Trace Sector Formulae **159**

C.1 Double Trace Sector 159

C.2 Triple Trace Sector 160

D Prüfer Sequences and Trees **161**

List of Figures

2.1 The relation between momenta p_i and the dual momenta x_i, and an indication of the transformation to momentum twistors z_i. 15

3.1 Figures illustrating polygons in P^2 represented as a disc where opposite points of the disc are identified. In Figure a) we illustrate the fact that there are four triangles I, II, III, IV all of which have the same three vertices Z_1, Z_2, Z_3 and all having the same canonical form $\langle 123\rangle^2/(\langle Y12\rangle\langle Y23\rangle\langle Y31\rangle)$. In Figure b) we see a region (shaded area) which has the same canonical form as the quadrilateral $[Z_1Z_2Z_3Z_4]$, $\langle 123\rangle^2/(\langle Y12\rangle\langle Y23\rangle\langle Y31\rangle) + \langle 134\rangle^2/(\langle Y13\rangle\langle Y34\rangle\langle Y41\rangle)$ but which does not represent a good geometrical region as it has spurious boundaries. 32

3.2 Two possibilities for triangulating a polygon. BCFW gives a generalisation of the left hand side, whereas WLDs give a generalisation of the right hand side. (for NMHV). 34

3.3 Example of a Wilson loop diagram which contributes to the 8-point N^{4}MHV amplitude. 37

3.4 Examples of Feynman diagrams in twistor space that contribute to the 6-point NMHV / N^{2}MHV amplitude with their corresponding expressions following the rules given. 38

3.5 Spurious poles occur when the propagator end reaches the vertex. It is cancelled by the adjacent diagram. 42

3.6 A special case of the spurious pole cancellation that occurs when the propagator ends are on next-to-adjacent edges, and one propagator end moves to the vertex closest to the other end. 43

3.7 Three diagrams each having a new type of spurious pole occurring when the propagator ends touch. In the sum of the three diagrams, however, this pole cancels. Note that although this is drawn at six points for illustrative purposes, the cancellation only depends on the three sides taking part and can be directly repeated at n points. 48

3.8 Three diagrams which when summed cancel the spurious poles illustrated by the arrows on each diagram. This is a special case of the three way cancellation. 51

3.9 The two possibilities for three way boundary matching. We plot the range of α on a circle from $[-\infty, \infty]$ passing through 0 and 1. Black is the range of α in diagram D1, in red that of $\alpha(\beta)$ in D_2 and in blue the range of $\alpha(\gamma)$ in D_3. We see there is always a local pairwise matching of the three diagrams in both cases. In Case 1 D2 and D3 each only overlap with D1 and not with each other. For Case 2 all diagrams overlap the other two. . 54

6.1 Regions I and II clearly have a spurious boundary along the edge $[Z_1 Z_3]$ despite their canonical forms summing to cancel the associated spurious pole. 146

A.1 The WLDs corresponding to the special three way cancellation, with the limits of the residues illustrated by the arrows on each WLD. 151

D.1 Tree diagrams corresponding to the diagrams given in (4.4.8). The label i corresponds to the propagator T_{q_i} and the branches of the trees correspond to the propagators. 161

List of Tables

2.1 The character tables of S_2, S_3 and S_4. The labels along the top indicate the conjugacy classes, $\sigma_{q_1 \ldots q_m}$, of the symmetry groups, and the left column gives the Young diagram associated to the representation, R, in question. The main body of the tables give the characters $\chi_R(\sigma_{q_1 \ldots q_m})$. 23

4.1 Table showing the 1/2-BPS operators of weight 5 in the trace basis for a $U(N)$ gauge group on the left, with a representative of the conjugacy class each corresponds to on the right. For $SU(N)$ the field is traceless, therefore only T_3T_2 and T_5 survive. 69

B.1 The character table involving hook representations, using characters calculated using the generating function (B.0.1) 157

Chapter 1

Introduction

1.1 Introduction

Quantum Field Theory (QFT) is a very important part of the tool kit for any theoretical physicist due to its broad ranging applications that extend from condensed matter physics to particle physics and beyond. One of the biggest revolutions in theoretical physics in the last few decades is the AdS/CFT correspondence, a conjectural relation between string theory on a $d+1$ dimensional Anti-de-Sitter space and a conformal quantum field theory living on the d dimensional boundary [1–3]. The discovery of this correspondence intimately connected two of the most important unsolved problems in theoretical physics; how to understand non-perturbative gauge theory, and how to quantise gravity. The most remarkable aspect of the conjecture, and also the property that makes it extremely difficult to prove, is the strong-weak nature of the duality. The strongly coupled gauge theory is dual to the weakly interacting stringy physics and vice versa. Therefore, the strongly coupled regimes of both theories, which otherwise would have been very difficult to probe, can be studied by investigating the weakly coupled regime of the dual theory and then using the dictionary provided by the correspondence to move back to the theory of interest. For a thorough review of AdS/CFT and its many applications see for example [4]. Perhaps the most successful and most studied example of the correspondence is in $d = 4$

dimensions, where the maximally supersymmetric CFT known as $\mathcal{N} = 4$ super Yang-Mills is conjectured to be dual to type IIB string theory on $AdS_5 \times S^5$.

In order to define the Yang-Mills theory we require two parameters: the coupling $g_{\rm YM}$ and the rank N of the gauge group (where this thesis will include both $U(N)$ and $SU(N)$). It was shown by 't Hooft [5] that in the limit where the number of colours, N, of the gauge group becomes large and the 't Hooft coupling $\lambda = g^2_{\rm YM}N$ is kept finite, a huge amount of simplifications occur. This limit where $N \to \infty$ is known as the "planar" limit.

The simplified nature of $\mathcal{N} = 4$ SYM allows for interesting and unexpected physical and mathematical structures to be uncovered, and it is often regarded as a toy model to more realistic theories. Therefore, the study of links between $\mathcal{N} = 4$ SYM and its gravity dual remains at the forefront of current research today. It is hoped that this will lead to enough of an understanding of four-dimensional quantum field theories in general that properties of more realistic theories, that otherwise would have been far more difficult or impossible to explore, will be uncovered. This thesis will restrict to explorations of different aspects of $\mathcal{N} = 4$ SYM, particularly in the planar limit, though we will indicate how one or two of our results are consistent with the relevant results on the gravity side in Chapter 4.

A particularly important set of mathematical objects in any field theory is the set of scattering amplitudes. They are interpreted as the "probabilities" for a particular interaction to occur and are a key ingredient in the cross sections used by particle colliders. The ability to compute scattering amplitudes using Feynman rules derived from a Lagrangian was one of the earliest successes of quantum field theory. However, the calculations very quickly became intractable as the number of diagrams to compute increased very rapidly with the number of particles involved in the interaction. Moreover, many cancellations of the individual terms led to huge simplifications of the final result. The example often quoted that never ceases to be extremely impressive is the reduction of the 2-to-4 gluon amplitude result from six pages [6] to a single line [7]! Furthermore, this result only required slight modifications to give the 2-to-n gluon amplitude; unthinkable from the Feynman diagram point of view. The remarkable simplicity of the final expression heavily

indicated that whilst correct, the Feynman diagram approach was not an efficient method for calculating scattering amplitudes, and led to an explosion of progress in understanding scattering amplitudes on a more fundamental level.

Many techniques, broadly referred to as "on-shell methods", were then discovered that could be used to calculate scattering amplitudes without having to deal with the presence of the massive gauge redundancies present in the Feynman diagrams. The concept of "generalised unitarity" [8–10] was developed, which allowed for the evaluation of loop integrals that were previously inaccessible (see for example [11] and the references therein). New recursion relations were developed, including BCFW [12,13] and CSW [14] recursions, which enabled the computation of amplitudes of four points and more starting from three-point amplitudes, which were fixed purely by Poincaré invariance.

As amplitudes were becoming more well understood, unanticipated symmetries were found including dual superconformal symmetry [15–18]. The massive amount of symmetry led to the discovery of a remarkable duality between scattering amplitudes and Wilson loops [19–24]. In fact, this duality turned out to be a triality between Wilson loops, scattering amplitudes and correlation functions [25, 25–28]. It was then understood that the dual superconformal symmetry paired with the standard superconformal symmetry of $\mathcal{N} = 4$ SYM to form a full "Yangian" symmetry [29]. The duality between amplitudes and correlators has led to some astounding results. For example, the duality was used along with techniques in graph theory to calculate the 4-point amplitude to an impressive ten loops [30]. Furthermore, it is projected that any scattering amplitude for any n with any helicity structure at any loop order may be extractable from the four-point correlator. This was successfully tested up to seven points and two loops [31].

For the purposes of this thesis, however, we will take advantage of a different aspect of the triality: the duality between amplitudes and Wilson loops. The duality was first conjectured by Alday and Maldacena at strong coupling [19], and was later understood in a very geometrical way via a "fermionic T-duality" [32,33]. This maps a gluon scattering process to the expectation value of a polygonal Wilson loop with cusps and light-like

edges determined by the gluon momenta (see [34] for a review). The duality was also observed at weak coupling by Drummond, Korchemsky and Sokatchev [20], for a specific set of helicity configurations known as MHV amplitudes. On space-time, the conjecture has been checked for a number of examples. It was shown using anomalous conformal Ward identities conjectured in [35] and proven in [36] that the finite part of the $4-$ and $5-$point Wilson loop can be fixed (up to an additive constant), and the functional form is in agreement with the BDS conjecture [37] for the finite part of the n-point MHV amplitude when $n = 4, 5$. The Wilson loop/MHV amplitude duality has also been tested for arbitrary n at one loop in [21], and up to two loops at $n = 6$ [38–40].

Reformulating the Wilson loop in twistor space led to the conjecture that the *full* super-amplitude (with arbitrary external helicities) is related to a supersymmetric, holomorphic version of the Wilson loop in twistor space [23]. The conjecture has been proven at the level of the loop integrand [22, 41]; this thesis shall exploit this duality and remain restricted to the level of the integrand.

One of the most remarkable discoveries in recent years was the underlying Grassmannian structure of planar $\mathcal{N} = 4$ [42–46], which resulted in a fundamental reformulation of our understanding of scattering amplitudes. Previously, locality and unitarity were considered guiding principles, but understanding the Grassmannian structure moved these to emergent properties of the overarching principle of positivity. These considerations led to the discovery of the "Amplituhedron" [47, 48], a geometric object whose boundaries were determined by the requirement of positivity. Scattering amplitudes are related to the Amplituhedron by calculating differential forms on the boundary of the object. This geometric picture has been used to obtain a large amount of all-loop data at the level of the integrand [49, 50]. Whilst we too will be focussing on the integrand in this thesis, it is worth noting that recently connections to the symbol alphabets, which are properties of the final (integrated) amplitudes, have been made [51–54]. Furthermore, whilst we will be focussing on (planar) $\mathcal{N} = 4$, positivity has allowed the discovery of hidden structures in several other contexts, including the associahedron in bi-adjoint scalar field theory,

conformal field theory, effective field theory and ϕ^4 theory.

In this thesis we will not only be concerned with amplitudes, but other objects of $\mathcal{N} = 4$ SYM known as operators and correlators. In general, the matching between the two sides of the AdS/CFT duality is dependent on two things [2, 3]:

1. The energy of an AdS state must match the scaling dimension of a CFT local operator (we can use CFT local operators rather than states due to the operator-state correspondence).

2. The correlators of the AdS states and CFT local operators must agree.

In general, the correlators are very hard to calculate explicitly, however in the planar limit things once again become more straightforward. Here, only the leading term in the 't Hooft expansion survives, meaning only planar Feynman diagrams contribute. In fact, concrete results to all orders in λ can be calculated using powerful mathematical techniques due to the integrable nature of SYM in this limit [55]. A review of integrability as it relates to the AdS/CFT correspondence can be found in [56].

It is much more difficult to study the correspondence when allowing for sub-leading terms in the $1/N$ expansion or at finite N. However, restricting to a special class of operators known as the $\frac{1}{2}$-BPS operators, that are annihilated by half of the sixteen Poincaré supercharges in the theory, allows for more concrete results to be found even at finite N. It is of utmost importance to be careful when considering which operator in the CFT is dual to which state on the string side. Chapter 4 of this thesis shall investigate this issue for the particular example of the single particle.

Having outlined some of the extensive structure that planar $N = 4$ SYM exhibits, the context has been set for the work about to be presented here. We will now outline the main themes that will be covered in the rest of this thesis.

1.1.1 Outline of the Thesis

The thesis shall be structured as follows:

- In Chapter 2, we shall present a very brief introduction to some of the technical machinery that may be useful for the remainder of the thesis. This will include a very brief venture into $N = 4$ super Yang-Mills and various ways of representing the external momenta involved in scattering processes, as well as an introduction to various properties of the symmetric group S_n which will come in to play in Chapter 4.

- In Chapter 3, we look to determine if twistor Wilson loop diagrams provide an explicit triangulation of the amplituhedron, or any geometric region for that matter. Via the Wilson loop - amplitude duality, twistor Wilson loop diagrams (WLDs) split the amplitude into well defined pieces. The expression associated to each diagram is given by Feynman rules which we shall state, then we will show that each expression has a natural interpretation on the same space in which the amplituhedron lives. Each term has spurious poles which cancel algebraically in the sum over all diagrams to give the amplitude integrand. Therefore, one would expect that the geometric interpretations of these terms would leave no spurious boundaries when glued together. If this were true, the WLDs would give a very explicit tesselation of the amplituhedron. We will show that the diagrams do in fact give a tesselation at NMHV, but for higher helicity values there is no way to glue together the regions to end up with no spurious boundaries left over.

The work in this chapter is based off of published work given here: [57].

- In Chapter 4, we look to investigate a set of half-BPS operators which are appropriate for describing single-particle states of superstring theory on $AdS_5 \times S^5$. We refer to these as single particle operators, and they are defined to be the operators that have vanishing two-point functions with all multi-trace operators. We find explicit formulae for these operators and their two point normalisation, then look to give a number of explicit results for their free theory correlators; this will include all maximally and next-to-maximally extremal free correlators. We shall also show that at large N the single-particle operator naturally interpolates between the single-trace operator and the sphere giant graviton.

The work in this chapter is based off of published work given here: [58].

- In Chapter 5, we give a short description of N^2MHV Yangian invariants for $\mathcal{N} = 4$ SYM. Tree-level amplitudes can be written as a linear combination of Yangian invariants, which is one of many uses of them. The invariants are very important objects, and a complete understanding of their properties would be useful. As a small first step, we present all N^2MHV Yangian invaraints mapped to amplituhedron coordinates, where it is hoped it will be easier to examine their structure more carefully.

- Finally, in Chapter 6 we summarise the main results of the thesis and describe future work that would be interesting to explore.

We will provide a brief, though slightly more tailored, introduction at the beginning of Chapters $3, 4$ and 5 on the themes relevant specifically to that Chapter, as well as any more background knowledge that may be useful.

Chapter 2

Review of Concepts

2.1 The $\mathcal{N} = 4$ Supersymmetric Yang-Mills Lagrangian and Field Content

$\mathcal{N} = 4$ supersymmetric Yang-Mills theory in four dimensions is a very special theory; the β-function vanishes, therefore the conformal invariance is preserved in the quantum regime. The symmetry groups of the theory include the conformal group $SO(2,4)$ which is then uplifted to the super-conformal group $PSU(2,2|4)$, as well as a global R-symmetry $SU(4)_R \sim SO(6)_R$ that rotates the charges.

The field content of $\mathcal{N} = 4$ super Yang-Mills consists of six real scalars ϕ^i, four fermions λ_I and a gauge field A_μ. The scalars transform in the fundamental representation of of the $SO(6)$ R-symmetry group, while the fermions transform in the fundamental of the $SU(4)$. All of the fields are forced to transform in the adjoint representation of the gauge group by the extended supersymmetry; in Chapter 4 we shall consider both $U(N)$ and $SU(N)$ gauge groups.

Though we do not look to explore this in too much detail, we state the $\mathcal{N} = 4$ SYM

Lagrangian [59]:

$$\begin{aligned}\mathcal{L} = \mathrm{Tr}\Big(&\frac{1}{2}F_{\mu\nu}F^{\mu\nu} + \frac{\theta}{8\pi^2}F_{\mu\nu}\tilde{F}^{\mu\nu} + (D_\mu\phi_i)(D^\mu\phi^i) + \frac{g^2}{2}[\phi^i,\phi^j][\phi_i,\phi_j] \\ &+ 2i\bar{\lambda}_{\dot{\alpha}I}\sigma_\mu^{\alpha\dot{\alpha}}D^\mu\lambda_\alpha^I - g\left(\bar{\Sigma}_i\right)_{IJ}\lambda^{\alpha I}\left[\phi^i,\lambda_\alpha^J\right] + g(\Sigma_i)^{IJ}\bar{\lambda}_{\dot{\alpha}I}\left[\phi^i,\bar{\lambda}_J^{\dot{\alpha}}\right]\Big).\end{aligned} \tag{2.1.1}$$

The notation for the Lagrangian is as follows: $F_{\mu\nu} \equiv \partial_\mu A_\nu - \partial_\nu A_\mu + ig[A_\mu, A_\nu]$ is the field strength, with $\tilde{F}^{\mu\nu}$ corresponding to the Hodge dual defined as $\tilde{F}^{\mu\nu} = \frac{1}{2}\epsilon^{\mu\nu\rho\sigma}F_{\mu\nu}$. The covariant derivative is given by $D_\mu \equiv \partial_\mu - ig[A_\mu]$, g is the coupling strength and $(\Sigma_i)^{IJ}$, $\left(\bar{\Sigma}_i\right)_{IJ}$ are related to the Clifford Dirac matrices that relate scalars in the $SO(6)$ R-symmetry representation to their equivalent $SU(4)$ symmetry group counterpart. Finally, $\sigma_\mu \equiv (\mathbb{I}_2, \sigma_1, \sigma_2, \sigma_3)$ denotes the two by two identity matrix and the Pauli matrices, with $\alpha, \dot{\alpha} = 1, 2$.

One can rescale the gauge field to trivially remove the coupling dependence from the covariant derivative: $A_\mu \to g^{-1}A_\mu$. This also results in the coupling dependence of the field strength completely factoring out, giving $\frac{1}{2}F_{\mu\nu}F^{\mu\nu} \to \frac{1}{2g^2}F_{\mu\nu}F^{\mu\nu}$. Substituting this into (2.1.1) allows the Lagrangian to be rewritten as the "on shell" Lagrangian.

In supersymmetric theories, the on-shell degrees of freedom are balanced between bosons and fermions. In $\mathcal{N} = 4$ SYM we have eight bosons and eight fermions, which can be assembled into one on-shell superfield $\Phi(p, \eta)$ by introducing the Grassman odd parameter η^I with R-symmetry index $I = 1, 2, 3, 4$:

$$\Phi(p,\eta) = G_+ + \eta^I\Psi_I + \frac{1}{2!}\eta^I\eta^J\phi_{IJ} + \frac{1}{3!}\epsilon_{IJKL}\eta^I\eta^J\eta^K\bar{\Psi}^L + \frac{1}{4!}\epsilon_{IJKL}\eta^I\eta^J\eta^K\eta^L G^-. \tag{2.1.2}$$

The dependence on the external momenta p is contained within $G^+, \Psi_I, \phi_{IJ}, \bar{\Psi}^L$ and G^- which represent the positive-helicity gluon, positive-helicity fermions, scalars, negative-helicity anti-fermions and negative-helicity gluon respectively for a total of 1+4+6+4+1 = 16 particles in this multiplet.

2.2 Scattering Amplitudes in Planar $\mathcal{N} = 4$ SYM

Scattering amplitudes in planar SYM exhibit many beautiful mathematical properties, some of which were named briefly in the introduction. Generally an amplitude will involve some integration, which is often very non-trivial. For the considerations of this thesis, however, we shall restrict ourselves to the integrand only, i.e. before the integration is performed. The triality mentioned in the introduction holds at the level of the integrand, which will be particularly important for Chapter 3 of this thesis. The part of the integrand of the amplitude that is not dependent on the helicity of the particles involved are functions dependent on the momenta, p_a.

An n-point (planar) super-amplitude can be expanded over the Grassmann variables η_a^I with particle number $a = 1, \ldots, n$, giving

$$\mathcal{A} = \mathcal{A}_{n;2} + \mathcal{A}_{n;3} + \ldots + \mathcal{A}_{n;n-2}, \tag{2.2.1}$$

where each term $\mathcal{A}_{n;k}$ is a homogeneous polynomial in η^I of degree $4k$, with $(\eta_a)^4 \equiv \eta_a^I$. Before going any further, it is useful to introduce the spinor-helicity formalism, where we write the external kinematic data as

$$p_a^\mu (\sigma_\mu)^{\alpha\dot{\alpha}} = \begin{pmatrix} p_a^0 - p_a^3 & -p_a^1 + ip_a^2 \\ -p_a^1 - ip_a^2 & p_a^0 + p_a^3 \end{pmatrix} \equiv p_a^{\alpha\dot{\alpha}} \equiv \lambda_a^\alpha \tilde{\lambda}_a^{\dot{\alpha}} \tag{2.2.2}$$

where $\epsilon^{\alpha\beta} = -\epsilon_{\dot{\alpha}\dot{\beta}}$ are the anti-symmetric epsilon tensors with $\alpha \in \{1, 2\}, \dot{\alpha} \in \{\dot{1}, \dot{2}\}$.

Let $\mathcal{A}_{n;k}^{(l)}$ represent the l-loop n-particle N^kMHV super-amplitude. The supersymmetric generalisation of the Parke-Taylor formula is given by [60]:

$$\mathcal{A}_{n;2}^{(0)} = \frac{\delta^4 \left(\sum_{a=1}^n \lambda_a^\alpha \tilde{\lambda}_a^{\dot{\alpha}} \right) \delta^8 \left(\sum_{i=1}^n \lambda_a^\alpha \eta_a^I \right)}{\langle 12 \rangle \ldots \langle n1 \rangle}, \tag{2.2.3}$$

where $\langle ab \rangle \equiv \epsilon_{\alpha\beta} \lambda_a^\alpha \lambda_b^\beta$ and the second delta function is a Grassmann delta function that ensures conservation of supermomentum.

It is often convention that the super-amplitude is divided through by the MHV tree-level super-amplitude $\mathcal{A}_{n;2}^{(0)}$ given by (2.2.3), which roughly speaking subtracts eight powers of

η off of each partial amplitude leading to

$$\hat{\mathcal{A}} = \hat{\mathcal{A}}_{n;0} + \hat{\mathcal{A}}_{n;1} + \ldots + \hat{\mathcal{A}}_{n;n-4}, \tag{2.2.4}$$

with the standard normalisation $\hat{\mathcal{A}}_{n;0} = 1$. Once again, the $\hat{\mathcal{A}}$ are all homogeneous polynomials in η^I of degree $4k$. Each term in this sum is then further expanded over loop variables

$$\mathcal{A}_{n;k} = \sum_{l=0}^{\infty} a^l \mathcal{A}^{(l)}_{n;k}, \tag{2.2.5}$$

where we have now dropped the 'hat' notation for $\mathcal{A}$ with the understanding that when amplitudes are referred to in this thesis they will be divided by the tree level MHV super-amplitude. We refer to the expression $\mathcal{A}^{(l)}_{n;k}$ as the l-loop integrand of the amplitude. It can written as some combination of rational functions dependent on the momenta multiplied by Yangian invaraints:

$$\mathcal{A}^{(l)}_{n;k} = \sum_{ij} c_{ij} \mathcal{R}_{k;i}(\eta_a, p_1, \ldots p_n) \times \mathcal{I}^{(l)}_j(p_1, \ldots, p_{n+l}). \tag{2.2.6}$$

Notice that the rational functions $\mathcal{I}$ are dependent on the external momenta and all loop momenta for a fixed l. Furthermore, the η dependence lies within the k degree Yangian invaraints $\mathcal{R}$, meaning they act as generating functions for different helicity configurations of the superparticle given by (2.1.2).

When studying amplitudes in $\mathcal{N} = 4$ SYM, one often focusses on the gluon amplitude. The n-particle N^kMHV gluon amplitude refers to the interaction between $(k+2)$ negative helicity gluons and $(n-k-2)$ positive helicity gluons. The simplest case corresponds to the $k = 0$ case, known as the MHV gluon amplitude (see (2.2.3)). The highest value of k that results in a non-trivial gluon amplitude is known as the anti-MHV amplitude, or the $N^{n-4}\text{MHV} = \overline{\text{MHV}}$ amplitude. The amplitudes involving all positive helicity gluons, or all bar one positive with one being negative, vanish by the supersymmetric ward identities; as do their parity conjugates [61, 62]. Whilst it may seem odd at first glance that only gluon amplitudes have been considered, they can in fact be used to get the full super-amplitude using the superparticle expansion given by (2.1.2). The supersymmetric Ward

identities relate all particle amplitudes that have the same order of η dependence [62]. For example, at η^8 (before dividing by the tree-level MHV amplitude), the n-particle MHV gluon amplitude involving two negative gluons ($\sim \eta^4\eta^4$) with the rest positive gluons ($\sim \eta^0$) is related to an MHV amplitude with four scalars ($\sim \eta^2\eta^2\eta^2\eta^2$) and $(n-4)$ positive gluons.

Finally, since most of this thesis will be concerned with $\mathcal{N}=4$ SYM in the planar limit, it is worth noting one final simplification. In the planar limit, one can fix an ordering of the external momenta and calculate the "colour-ordered amplitude" corresponding to this ordering, then find the full tree level super-amplitude by summing over all non-cyclic permutations of the external momenta:

$$\mathcal{A}_n^{\text{tree}} = g^{n-2} \sum_{\sigma \in S_n/\mathbb{Z}_n} \text{Tr}\left(T^{\tilde{a}_{\sigma(1)}} \dots T^{\tilde{a}_{\sigma(n)}}\right) A_n^{\text{tree}}\left(p_{\sigma(1)}^{\Lambda\sigma(1)} \dots p_{\sigma(n)}^{\Lambda\sigma(n)}\right). \tag{2.2.7}$$

Here, $\Lambda_a = \pm 1$ gives the helicity of particle a, g is the coupling. Therefore, it makes sense to choose the canonical ordering $1, \dots, n$. For more information on this, or any topic introduced in this section, the interested reader should refer to for example [61, 62] and the references therein.

2.3 Super Momentum Twistors and Bosonisation to Amplituhedron Coordinates

In this section we introduce the so-called "momentum twistors" [63, 64], provide conventions and review some of their basic properties. We then uplift to include supersymmetry, and show how to bosonise these super-momentum twistors to write them in "amplituhedron coordinates" [47, 63].

2.3.1 Momentum Twistors and Supermomentum Twistors

Momentum twistors are defined in terms of dual coordinates x_i, defined by

$$\lambda_i^\alpha \tilde{\lambda}_i^{\dot{\alpha}} \equiv p_i^{\alpha\dot{\alpha}} \equiv x_{i+1}^{\alpha\dot{\alpha}} - x_i^{\alpha\dot{\alpha}}, \tag{2.3.1}$$

where λ_i and $\tilde{\lambda}_i$ are the usual spinor-helicity variables and $p_i^{\alpha\dot{\alpha}}$ are four dimensional null momenta. Multiplying (2.3.1) by $\lambda_{i\alpha}$ gives zero on the left hand side, leading to the following (bosonic) incidence relations:

$$x_i^{\alpha\dot{\alpha}}\lambda_{i\alpha} = x_{i+1}^{\alpha\dot{\alpha}}\lambda_{i\alpha} \equiv \mu_i^{\dot{\alpha}}, \tag{2.3.2}$$

where $i = 1, ..., n$ labels the particle number and $\alpha \in \{1, 2\}, \dot{\alpha} \in \{\dot{1}, \dot{2}\}$. Momentum conservation in dual momentum coordinates is manifest. This can be visualised as a null polygon with the x_i as the vertices, constructed by arranging the external (null) momenta head-to-tail (see Figure 2.1). There is a conformal symmetry that acts on the dual momenta known as the dual conformal group, which was shown to be a symmetry of planar $N = 4$ SYM [15–17] and ABJM theory [65–67].

Bosonic momentum twistors are then defined by taking each pair λ_i^α and $\mu_i^{\dot{\alpha}}$ and organising them as four-component projective vectors, z_i^A:

$$z_i^A \equiv \left(\lambda_i^\alpha, \mu_i^{\dot{\alpha}}\right) \in \mathbb{C}^4, \tag{2.3.3}$$

where $A \in \{1, ..., 4\}$ are indices in the fundamental representation of the dual conformal group, $SU(4)$. Using the incidence relation and (2.3.1) one finds that the x coordinates satisfy the incidence relations

$$x_a^{\alpha\dot{\alpha}} = \frac{\lambda_i^\alpha \mu_{i-1}^{\dot{\alpha}} - \lambda_{i-1}^\alpha \mu_i^{\dot{\alpha}}}{\langle i-1 i\rangle}, \tag{2.3.4}$$

where $\langle i-1 i\rangle \equiv \epsilon_{\alpha\beta}\lambda_{i-1}^\alpha \lambda_i^\beta$. These incidence relations can be derived by identifying two adjacent momentum-twistor points with a single space-time coordinate,

$$x_i^{\alpha\dot{\alpha}}\lambda_{i\alpha} = \mu_i^{\dot{\alpha}}, \qquad x_i^{\alpha\dot{\alpha}}\lambda_{i-1\alpha} = \mu_{i-1}^{\dot{\alpha}}, \tag{2.3.5}$$

and combining them in the following way:

$$\lambda_i^\alpha \mu_{i-1}^{\dot\alpha} - \lambda_{i-1}^\alpha \mu_i^{\dot\alpha} = \left(\lambda_i^\alpha \lambda_{i-1\beta} - \lambda_{i-1}^\alpha \lambda_{i\beta}\right) x_i^{\beta\dot\alpha} = \langle i-1 i\rangle \, x_i^{\alpha\dot\alpha}, \tag{2.3.6}$$

giving (2.3.4).

Under the little group scaling of $\lambda_i \to t_i \lambda_i$, the relations in (2.3.5) imply that $\mu_i \to t_i \mu_i$, meaning that the momentum twistors undergo a uniform rescaling $z_i^I \to t_i z_i^I$. Therefore, the momentum twistors are defined projectively. Momentum twistors have some very nice properties; not only do they solve the momentum conservation constraint, but they also solve the on-shell constraint.

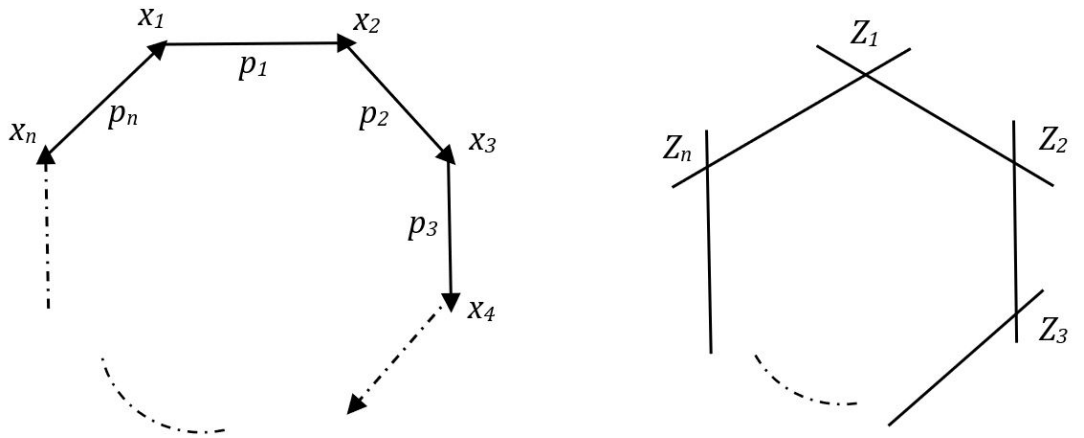

Figure 2.1: The relation between momenta p_i and the dual momenta x_i, and an indication of the transformation to momentum twistors z_i.

The incidence relations (2.3.4) imply that a point in dual momentum space, x_i, corresponds to a line in momentum twistor space, $[z_{i-1} z_i]$. Therefore, a null polygon in momentum space can be mapped to a polygon in momentum twistor space as illustrated in Figure 2.1.[1]

The momentum twistors can be used to define the natural dual-conformal invariant as the determinant of the square matrix whose columns are any four unique momentum

[1]It is worth noting that loop variables in x space also correspond to lines which do not intersect with any other lines in momentum twistor space.

twistors:

$$\langle ijkl\rangle \equiv \det\left[z_i z_j z_k z_l\right] = \epsilon_{ABCD} z_i^A z_j^B z_k^C z_l^D. \tag{2.3.7}$$

The expression generalises to higher point brackets upon adding supersymmetry then bosonising; this will be discussed below. These invariants are related to the dual space via $x_{i,j}^2 = (x_i - x_j)^2 \to \langle i-1ij-1j\rangle$. Furthermore, this four bracket can be used to express the linear dependence of any five momentum twistors as a generalised Schouten identity

$$z_i \langle jklm\rangle + (\text{cyclic in } i,j,k,l,m) = 0. \tag{2.3.8}$$

In order to extend these momentum twistors to supersymmetric theories, in analogy to (2.3.1), we define dual super momenta as

$$q_i^{\alpha I} \equiv \lambda_i^\alpha \eta_i^I \equiv \theta_{i+1}^{\alpha I} - \theta_i^{\alpha I}, \tag{2.3.9}$$

with $\theta_{n+1} = \theta_1$. The momentum twistors can now be uplifted to super-momentum twistors,

$$\mathcal{Z}_i^{\mathcal{A}} \equiv \left(\lambda_i^\alpha, \mu_i^{\dot\alpha}; \theta_i^I \cdot \lambda_i\right) \equiv \left(z_i^A; \chi_i^I\right) \in \mathbb{C}^{4|4}, \tag{2.3.10}$$

where $A = 1,...,4$ and $I = 1,...,4$ are four component bosonic and fermionic indices respectively, which we combine to form the eight component index denoted by $\mathcal{A} = 1,...,8$. The coordinates χ_i^I are Grassman-odd, and hold the necessary properties for defining the superconformal invariant that will be discussed below. Now we have incidence relations for the bosonic coordinates given in (2.3.2) and an additional set of relations for the fermionic components of the super-momentum twistors:

$$\theta_i^{\alpha I}\lambda_{i\alpha} = \theta_{i+1}^{\alpha I}\lambda_{i\alpha} \equiv \chi_i^I. \tag{2.3.11}$$

Furthermore, by equating the same superspace point to two super-momentum twistors $\chi_i^I = \theta_i^{\alpha I}\lambda_{i\alpha}$ and $\chi_{i-1}^I = \theta_i^{\alpha I}\lambda_{i-1\alpha}$, in a similar way to (2.3.6), we end up with a fermionic equivalent of (2.3.4):

$$\theta_{i\alpha}^I = \frac{\lambda_{i\alpha}\chi_{i-1}^I - \lambda_{i-1\alpha}\chi_i^I}{\langle i-1i\rangle}. \tag{2.3.12}$$

Beyond the MHV sector, superamplitudes can be written in terms of dual superconformal invariants [16]. At NMHV, the dual superconformal invariants are known as R invariants [64], and are defined as follows

$$[ijklm] \equiv \frac{\delta^{0|4}\left(\chi_i^I \langle jklm\rangle + \cdots + \chi_m^I \langle ijkl\rangle\right)}{\langle jklm\rangle \langle klmi\rangle \langle lmij\rangle \langle mijk\rangle \langle ijkl\rangle}, \tag{2.3.13}$$

where the delta function in the numerator is a fermionic delta function. The BCFW representation of the tree level n-point NMHV amplitude can be written in momentum twistor space as

$$M_n^{N\text{MHV}} = \frac{1}{2}\sum_{i,j}[1ii+1jj+1]\,. \tag{2.3.14}$$

The CSW representation of the same amplitude [43, 68] is obtained by replacing the seemingly special point "1" in this formula with a general momentum twistor, $\mathcal{Z}_1 \to \mathcal{Z}_*$. A toy example of these two representations is illustrated in Figure 3.2 and is discussed in the surrounding text. Furthermore, the general supermomentum twistor $\mathcal{Z}_*$ will be discussed more in Chapter 3 when Wilson loops are introduced.

2.3.2 Bosonisation of Supermomentum Twistors

It will be useful to switch to "bosonised superspace", where we will refer to the bosonised supermomentum twistors as being written in "amplituhedron coordinates". We provide a brief description of this process here following [47, 63].

To begin, we introduce a particle-independent fermionic variable ϕ_I^p, where $p = 1, ..., k$ and $I = 1, ..., 4$ is an R-symmetry index. The ϕ variables are then contracted with the Grassmann odd χ variables of the supermomentum twistors to give Grassmann even variables $\xi_i^p = \chi_i^I \phi_I^p$. The range of the p index is dependent on the helicity structure of the superamplitude. For N^kMHV amplitudes, $p = 1, ..., k$, therefore bosonising this superspace maps from the dimension (4|4) momentum supertwistors to purely bosonic

vectors in $4+k$ dimensions:

$$\begin{aligned} \mathbb{C}^{4|4} &\to \mathbb{C}^{4+k} \\ \mathcal{Z}(z,\chi) &\to Z(z,\xi=\chi\cdot\phi)\,. \end{aligned} \tag{2.3.15}$$

It is worth noting that the amplituhedron space itself is a subset of $\mathrm{Gr}(k,4+k)$, hence why we often refer to these bosonised supermomentum twistors as being in "amplituhedron coordinates". Using this map allows for non-trivial superconformal identities to become manifest in generalised Schouten identities (see (2.3.8)). Bosonising the momentum twistors is an essential step before being able to associate a geometry to the Wilson loop diagrams that we will introduce in Chapter 3.

We look to see how bosonising the NMHV amplitude (2.3.14) allows us to write it in a very simple way, which can be related to the volume of a polytope. Rewriting the R-invariant $[ijklm]$ by introducing a fermionic four indexed variable ϕ_I,

$$\int \mathrm{d}^4\phi\phi^4 \frac{\delta^{0|4}\left(\chi_i^I\langle jklm\rangle+\cdots+\chi_m^I\langle ijkl\rangle\right)}{\langle jklm\rangle\langle klmi\rangle\langle lmij\rangle\langle mijk\rangle\langle ijkl\rangle} \tag{2.3.16}$$

where $\phi^4=\prod_I\phi_I$. A fermionic delta function satisfies the identity $\delta^{0|4}(\theta)=\theta^4$, therefore the numerator of (2.3.16) becomes

$$\begin{aligned} &\phi^4\delta^{0|4}\left(\chi_i^I\langle jklm\rangle+\cdots+\chi_m^I\langle ijkl\rangle\right) \\ &=\phi^4\left(\chi_i^{I4}\langle jklm\rangle^4+\cdots+\chi_m^{I4}\langle ijkl\rangle^4\right) \\ &=\phi_1\phi_2\phi_3\phi_4\chi_i^1\chi_i^2\chi_i^3\chi_i^4\langle jklm\rangle^4+\cdots+\phi_1\phi_2\phi_3\phi_4\chi_m^1\chi_m^2\chi_m^3\chi_m^4\langle ijkl\rangle^4 \\ &=(\phi\cdot\chi_i\langle jklm\rangle-\phi\cdot\chi_j\langle iklm\rangle+...)^4\,. \end{aligned} \tag{2.3.17}$$

For NMHV amplitudes $k=1$, so bosonising the supermomentum twistors gives

$$Z_i^{\mathcal{A}}\equiv\left(z_i^A;\chi_i^I\phi_I\right)\in\mathbb{C}^5, \tag{2.3.18}$$

where $A=1,...,5$ labels the bosonic singlet that the supermomentum twistor has now been mapped to. With this we define the five bracket

$$\langle ijklm\rangle\equiv\det\left[Z_iZ_jZ_kZ_lZ_m\right]. \tag{2.3.19}$$

Expanding this determinant along the bottom row gives precisely (2.3.17), therefore the R-invariant can be written as the dual conformal ratio

$$[ijklm] = \frac{\langle ijklm\rangle^4}{\langle ijkl\rangle \langle jklm\rangle \langle klmi\rangle \langle lmij\rangle \langle mijk\rangle}. \tag{2.3.20}$$

The bosonised coordinates can be generalised to arbitrary helicity by the map (2.3.15), and the following $(4+k)$-bracket can be defined:

$$\langle i_1 i_2 ... i_{k+4}\rangle \equiv \det\left[Z_{i_1} Z_{i_2} ... Z_{i_{k+4}}\right]. \tag{2.3.21}$$

As a further example of how these coordinates can be useful, the $\overline{\text{MHV}}$ n-point tree level superamplitude has the following very simple form in amplituhedron coordinates:

$$\mathcal{A}^{(}0)_{n;n-4} = \frac{\langle 12...n\rangle^4}{\langle 1234\rangle \langle 2345\rangle ... \langle n123\rangle}. \tag{2.3.22}$$

2.4 Mathematical Preliminaries: Permutations and Partitions

In this section, we look to introduce some mathematical tools that will be very useful in particular for Chapter 4. The use of permutations has been a significant technical step in allowing the explicit construction of operator bases and the calculation of correlators. Here we look to give a brief overview of some of the tools that we will make use of in Chapter 4 when constructing our own bases of 1/2-BPS operators.

2.4.1 The Symmetric Group

The symmetric group, S_n, is the group of permutations of n objects. The elements of this group are often written in cycle notation, for example (123) is the reshuffling of the labels $1 \to 2, 2 \to 3, 3 \to 1$. The Young diagrams with n boxes provide a nice way of labelling the representations of the symmetric group S_n. If λ_i denotes the length of row i, the set

of possible Young diagrams consists of all diagrams which satisfy $\lambda_1 \geq \lambda_2 \geq \cdots \lambda_m \geq 0$, with $\sum_{i=1}^{m} \lambda_i = n$. Therefore, there is a one-to-one correspondence between the possible partitions of n and the set of row lengths of Young diagrams $\{\lambda_i\}$. The Young diagrams associated to the representations of S_1, S_2, S_3 and S_4 are shown in (2.4.1).

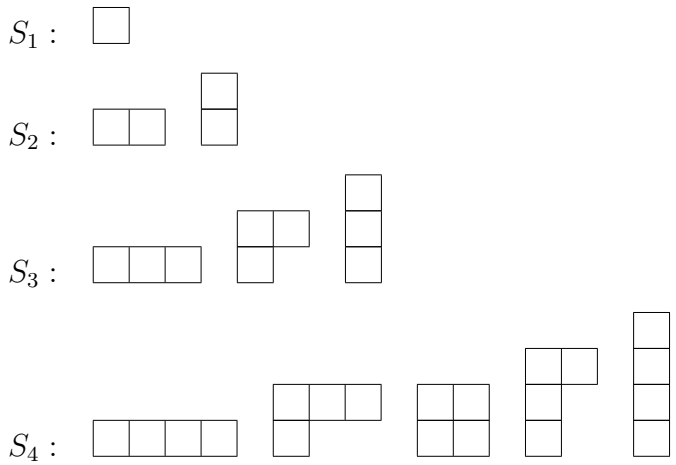

(2.4.1)

2.4.2 Conjugacy Classes of S_n

Letting $\sigma \in S_n$, the conjugacy class, $[\sigma]$, is the set of elements in S_n related to σ by conjugation:

$$[\sigma] = \Big\{\rho \in S_n : \tau\rho\tau^{-1} = \sigma \text{ for some } \tau \in S_n\Big\}. \tag{2.4.2}$$

Conjugation does not change cycle structure of the permutation, therefore the conjugacy class of σ is just the set of all permutations with the same set of row lengths. For example, the conjugacy class of $(12)(34) \in S_4$ is

$$[(12)(34)] = \Big\{(12)(34), (13)(24), (14)(23)\Big\}. \tag{2.4.3}$$

Note that the inverse of an element of S_n has the same cycle structure as the element, therefore $\sigma^{-1} \in [\sigma]$. The conjugacy classes of S_n are in one-to-one correspondence with the partitions of n, and further we will see shortly they are also in one-to-one correspondence with the $\frac{1}{2}$-BPS operators of $N = 4$ SYM.

It is straight forward to work out the size of the conjugacy class that an element $\sigma \in S_n$ belongs to, which we shall label $|[\sigma_{q_1 \ldots q_m}]|$. If all cycle lengths are distinct, i.e. $n =$

$q_1 + \ldots + q_m$ with $q_i \neq q_j$, the size of the conjugacy classes are simply $\frac{n!}{\prod_{i=1}^{m} q_i}$. If there are multiple cycles of the same length, i.e. some $q_i = q_j$ in the partition of n, then these cycles are interchangeable and we have to divide by this symmetry. To deal with this case, let $\lambda_1, \lambda_2, \ldots, \lambda_r$ be the distinct cycle lengths of the permutation σ and $k_1, k_2, \ldots, k_r$ by the number of cycles of each of those lengths respectively, such that $\prod_{j=1}^{r} \lambda_j^{k_j} = \prod_{i=1}^{m}$ and $\sum_{j=1}^{r} k_j \lambda_j = p$. Therefore, the number of elements in a conjugacy class labelled by $\{q_1 \ldots q_m\}$ is given by

$$|[\sigma_{q_1 \ldots q_m}]| = \frac{p!}{\prod_{i=1}^{r} k_i! \lambda_i^{k_i}}. \tag{2.4.4}$$

Note that the denominator is in fact the size of the symmetry group, $\mathrm{Sym}(\sigma)$, the subgroup of S_n that preserves σ under conjugation.

2.4.3 Dimension of S_n

As noted above, the Young diagrams constructed using p boxes label the representations of S_p. For example, the diagram with p boxes in the first row labels the one-dimensional trivial representation, and the diagram with p boxes in the first column labels the other one-dimensional irreducible representation, the sign representation.

Labelling a Young diagram by (r, c) where r is the row coordinate and c is the column coordinate, the hook length of a box $h(r, c)$ is obtained by summing the number of boxes to the right and the number of boxes below, plus 1 for box (r, c) itself. The Young diagram with row lengths $(4, 3, 2, 2)$ is shown in (2.4.5), labelled with the hook lengths of each box.

7	6	3	1
5	4	1	
3	2		
2	1		

(2.4.5)

The dimension of the representation R of the symmetric group is dependent on the hook lengths of the associated Young diagram. Let $d_R[S_p]$ be the dimension of representation

R of S_p. The dimension is given by

$$d_R[S_p] = \frac{n!}{\prod_{(r,c)\in R} h(r,c)}, \tag{2.4.6}$$

where the product in the denominator is over all hook lengths of the Young diagram. For example, the dimension of the representation associated to the example in (2.4.5) is given by

$$d_{\{4,3,2,2\}}(S_{11}) = \frac{11!}{7 \cdot 6 \cdot 3 \cdot 5 \cdot 4 \cdot 3 \cdot 2 \cdot 2} = 1,320. \tag{2.4.7}$$

2.4.4 Characters

Representations can be associated to matrices known as representing matrices. There are many different ways of constructing these matrices, e.g. for the symmetric group there are the natural and semi-normal representations constructed in [69] to name only a few. The character of a representation is the trace of its representation matrix. It is a constant on conjugacy classes of the group, and as such is known as a class function.

When finding an explicit formula for the single particle operators discussed in the next section, the characters of interest will be those of the symmetric group. The characters of S_2, S_3 and S_4 are shown in their character tables in Table 2.1.

S_2	()	(12)
	1	1
	1	-1

S_3	()	(12)	(123)
	1	1	1
	2	0	-1
	1	-1	1

S_4	()	(12)	(12)(34)	(123)	(1234)
	1	1	1	1	1
	3	1	-1	0	-1
	2	0	2	-1	0
	3	-1	-1	0	1
	1	-1	1	1	-1

Table 2.1: The character tables of S_2, S_3 and S_4. The labels along the top indicate the conjugacy classes, $\sigma_{q_1 \ldots q_m}$, of the symmetry groups, and the left column gives the Young diagram associated to the representation, R, in question. The main body of the tables give the characters $\chi_R(\sigma_{q_1 \ldots q_m})$.

Of particular importance will be the characters of all conjugacy classes in any 'hook representation', which are the representations that can be associated to hook-shaped Young diagrams: all non-zero rows but the first have length one and all non-zero columns but the first have height one. For example, the only non-hook representation in Table 2.1 is the S_4 representation associated to the Young diagram  . Although an explicit formula for this set of characters is unknown, they are neatly packaged in character polynomials which have a generating function defined in [70] and discussed further in [71]. See Appendix B for a short description of the generating function.

For completeness, we give two orthogonality relations for the characters of the symmetric group. Firstly, for $\sigma_1, \sigma_2 \in S_n$, summing the product of characters of these elements over the representations S_p gives

$$\sum_{R(p)} \chi_R(\sigma_1)\chi_R(\sigma_2) = \frac{p!}{|[\sigma_2]|}\delta\left([\sigma_1] = [\sigma_2]\right). \tag{2.4.8}$$

Secondly, for representations R, S of S_p, summing over the elements of S_p gives

$$\sum_{\sigma \in S_p} \chi_R(\sigma)\chi_S(\sigma) = n!\delta_{RS}. \tag{2.4.9}$$

2.4.5 Weights of $U(N)$ Representations

Young diagrams can be associated to $U(N)$ representations as well as S_n representations. Irreducible representations of $GL(N)$ are labelled by Young diagrams with at most N rows, but arbitrary number of columns. Representations of the subgroup $U(N) \subset GL(N)$ are the same and are also irreducible. For example, some representations of $U(2$ are given by

$U(2):$ **1**  $\cdots$, (2.4.10)

where the first representation is the trivial representation that maps every element of $U(2)$ to the same complex number. For more details on $U(N)$ representation theory and its relation to the symmetric group, the interested reader is encouraged to see for example [72, 73].

Once again, let each Young diagram be labelled by (r, c) where r is the row coordinate and c is the column coordinate. The weight of each box is given by $N - i + j$, e.g. for the example diagram we considered in (2.4.5), the weight of each box is given as follows:

N	$N{+}1$	$N{+}2$	$N{+}3$
$N{-}1$	N	$N{+}1$	
$N{-}2$	$N{-}1$		
$N{-}3$	$N{-}2$		

. (2.4.11)

The dimension of the $U(N)$ representation R is given by the product of the weights divided by the product of the hook lengths,

$$d_R[U(N)] = \prod_{(i,j)\in R} \frac{N - i + j}{h_{i,j}}. \tag{2.4.12}$$

For the example in (2.4.11), the dimension would be given by

$$d_{\{4,3,2,2\}}(U(N)) = \frac{N^2(N-1)^2(N+1)^2(N-2)^2(N+2)(N-3)(N+3)}{7\cdot 6\cdot 3\cdot 5\cdot 4\cdot 3\cdot 2\cdot 2}. \tag{2.4.13}$$

Another quantity that will come in useful for later considerations is the product of the weights by itself. Denoting this quantity f_R,

$$f_R \equiv \prod_{(i,j)\in R}(N-i+j) = \frac{p! d_R\left(U(N)\right)}{d_R\left(S_p\right)}. \tag{2.4.14}$$

2.4.6 Power Set

The final object that will prove useful when writing an explicit formula for the single particle operators is the power set. The power set is the set of all subsets of a set S, denoted by $\mathcal{P}(S)$, which includes the empty set and the full set S itself. For example, let $S = (\{3,2,1\})$; the power set is given by

$$\mathcal{P}(\{3,2,1\}) = \Big\{\{\},\{1\},\{2\},\{3\},\{2,1\},\{3,1\},\{3,2\},\{3,2,1\}\Big\}. \tag{2.4.15}$$

Furthermore, let $s \in \mathcal{P}(S)$. Then $|s|$ denotes the number of elements of the subset s and $\Sigma(s)$ denotes the total of all the elements in s, $\Sigma_{s_i\in s} s_i$. For example, for $s = \{3,2,1\}$ (a member of $\mathcal{P}$ in (2.4.14)) we have $|s| = 3$ and $\Sigma(s) = 6$.

Chapter 3

The Twistor Wilson Loop and the Amplituhedron

3.1 Introduction

The amplituhedron provides a beautiful description of perturbative superamplitude intergrands in $N = 4$ SYM. Inspired by the polytope structure of the six point NMHV scattering amplitude, first described by Hodges [63] then developed by Arkani-Hamed *et al* [74], Arkani-Hamed and Trnka interpreted the integrands of amplitudes in the planar theory as generalised polyhedra in positive Grassmannians called amplituhedra [47, 48][1]. The tree amplituhedron $\mathcal{A}^{(m)}_{n,k}$, with $k + m \leq n$, is defined as the image of the positive Grassmannian $\mathrm{Gr}^+(k, n)$ of k-planes in n dimensions into $\mathrm{Gr}(k, m + k)$. The positivity here dictates that all maximal $(k \times k)$ minors are non-negative. The map is induced by the $n \times (k + m)$ matrix of bosonised external kinematic data, $Z_i^{\mathcal{A}}$ with $i = 1, ..., n$ (see section 2.3), where all of the ordered maximal minors must also be positive. The amplituhedron is given by the set

$$\mathcal{A}^{(m)}_{n,k}(Z) = \{Y \subset \mathrm{Gr}(k, k + m) \ : \ Y^{\mathcal{A}}_{\alpha} = C_{\alpha i} Z^{\mathcal{A}}_i \text{ for } C \in \mathrm{Gr}^+(k, n)\} \tag{3.1.1}$$

[1] A second definition of the amplituhedron was elucidated in [75]; a topological definition directly in momentum-twistor space defined using sign-flip conditions on sequences of twistor invariants.

with $\mathcal{A} = 1, ..., k + m$ and $\alpha = 1, ..., k$. The case of $m = 4$ is of most interest to physics, as it provides a geometric basis for the computation of scattering amplitudes in $\mathcal{N} = 4$ supersymmetric Yang-Mills (SYM). The spaces involving the $m = 4$ amplituhedron are mostly what will be considered in the rest of this chapter (aside from the toy model discussed in the next section which corresponds to $m = 2$).

Before moving on, it is worth noting that the amplituhedron is a well-defined and interesting mathematical object for any m. The $m = 1$ amplituhedron can be identified with the complex of bounded faces of a cyclic hyperplane arrangement [76]. The $m = 2$ amplituhedron has a very beautiful combinatorial structure and has been well studied over the last few years [75, 77–81]. In fact, despite mostly being thought of as the toy-model for the $m = 4$ case, the $m = 2$ amplithedron has its own applications in physics. The $m = 2$, $k = 2$ amplituhedron governs the geometry of scattering amplitudes in the 'MHV' sector of $\mathcal{N} = 4$ SYM, and the $m = 2$ amplituhedron for general k has connections with the NMHV sector (and geometries of loop amplitudes) [82].

The scattering amplitude can be related to the canonical form of the $m = 4$ amplituhedron; a differential form with logarithmic singularities on the boundary and no singularities in the interior. [2] Therefore, one must consider how to calculate this canonical form. One way to construct it, which in principal is completely general and straightforward, is by finding a triangulation of the amplituhedron and summing the canonical forms of all of the pieces. Triangulating the subspace amounts to finding a non-overlapping set of $(4k)$-dimensional cells in $Gr^+(k, n)$; there have been a number of recent studies relating to this, for example [81, 83–86].

Although early polytope interpretations involved considering amplitudes via twistor Wilson loop diagrams (WLDs), the amplituhedron itself instead arose from considering the BCFW method of obtaining amplitudes. However, the WLDs seem to lend themselves very naturally and directly to a geometrical interpretation; in this chapter we wish to look again at the relationship between WLDs and the amplituhedron. Previous

[2] To see how the definition can be extended to include loops, see [47].

work examining the connection between them includes [87–89], where in particular the latter illustrated that the WLDs give a natural description of the physical boundary of the amplituhedron. Here, we examine whether it is possible to use the WLDs to define a tessellation of the amplituhedron, or further a tessellation of any "good" geometrical region. We define a *good geometrical region* as a region that contains no spurious boundaries, only physical boundaries that correspond to poles of the amplitude.

It should be highlighted here that we make no assumptions about positivity, convexity, or any particular specific form for the geometrical shape that could correspond to the WLDs. Our assumptions are only that each WLD can be assocated with a region of amplituhedron space in such a way that the canonical form of that region gives back the WLD. As we will see, each WLD contains spurious poles which geometrically correspond to spurious boundaries. We wish to give an answer to the following question: is it possible to associate a geometrical region to each WLD such that all spurious boundaries glue together correctly (locally) pairwise with those of other diagrams so that the union of all regions leaves no unmatched spurious boundaries.

The chapter will be organised as follows: in section 3.2 we will give a brief description of Wilson loop diagrams and show how to naturally associate a volume form in $\mathrm{Gr}(k, k+4)$ (the space in which the amplituhedron lives) to a WLD, in section 3.3 we show that each WLD can be associated with a tile in the tessellation of the amplituhedron, but in section 3.4 prove that for higher MHV degree this is not possible. More concretely, we prove that there does not exist a set of tiles whose canonical forms correspond to WLDs that glue together to form a geometry with no spurious boundaries. Firstly, however, we shall introduce the toy model which will prove a useful starting point for the considerations of the rest of this chapter.

This chapter is based off of work completed in [57]. Work completed at the same time dealing with the same problem using a different approach was discussed by Agarwala and Marcott in [90].

3.1.1 Toy Model: polygons in P^2

Many of the most important points in this chapter can be illustrated using the n-point, $k = 1, m = 2$ amplituhedron introduced in [47], corresponding to the space of convex polygons in P^2, complex projective space, with n vertices labelled by $Z_i^I \in P^2$, $I = 1, 2, 3$. We drop the label I for ease of notation where it is clear that it is implicitly still present. To map from the polygon X to an algebraic expression for its 'amplitude' integrand $\Omega(X)$, we associate a canonical form to the geometry. The canonical form is defined as the differential volume form with logarithmic divergences on the boundary, and no divergences inside it. In general, the canonical form for a given geometry is not easy to obtain directly [84], however they have the helpful property that the volume form of the union of (non-overlapping) geometries gives the sum of the volume forms for each. For example, the volume form of the quadrilateral constructed by taking the union of the two non-overlapping triangles X_1 and X_2 is given by by the sum of the canonical form of the two triangles i.e. $\Omega(X_1 \cup X_2) = \Omega(X_1) + \Omega(X_2)$. This property gives a simple means of obtaining the canonical form for a polygon; triangulate it and sum the canonical form for each triangle.

Consider a triangle in P^2 with vertices Z_1, Z_2 and Z_3. The interior of the triangle (region I in Figure 3.1) is the collection of points of the form

$$\begin{aligned} Y &= c_1 Z_1 + c_2 Z_2 + c_3 Z_3 \\ &= a Z_1 + b Z_2 + Z_3 \quad a, b > 0 \end{aligned} \tag{3.1.2}$$

where in the second line we use the $GL(1)$ invariance of the triplet $(c_1\ c_2\ c_3)$ to write $a = \frac{c_1}{c_3}$, $b = \frac{c_2}{c_3}$. The canonical form in these coordinates is simply given by

$$\Omega(\Delta_{\mathrm{I}}) = \frac{\mathrm{d}a\,\mathrm{d}b}{ab}, \tag{3.1.3}$$

which can be written in a co-ordinate independent way as

$$\Omega(\Delta_{\mathrm{I}}) = \frac{\langle Y\,\mathrm{d}^2 Y\rangle\,\langle 123\rangle^2}{\langle Y12\rangle\,\langle Y23\rangle\,\langle Y31\rangle}. \tag{3.1.4}$$

Here $\langle 123\rangle$ is the determinant of the matrix made by having Z_1, Z_2 and Z_3 as its columns, and one can easily get from (3.1.4) to (3.1.3) by plugging in the definition of Y above.

Moving on to the next simplest polygon, the quadrilateral with vertices Z_1, Z_2, Z_3 and Z_4 (see the right hand side of Figure 3.1) can be triangulated into two adjacent triangles with vertices Z_1, Z_2, Z_3 and Z_1, Z_3, Z_4. The triangles have two co-dimension one boundaries each that are proper boundaries of the quadrilateral, and share a co-dimension one boundary that is not a boundary of the quadrilateral; the line $[Z_1 Z_3]$. This is referred to as "spurious"; the canonical form of each triangle has a log divergence on this boundary, $Y \to \alpha Z_1 + \beta Z_3$. To calculate the canonical form of the quadrilateral we sum the forms of the two triangles:

$$\begin{aligned}\Omega\left(\Delta^4\right) &= \frac{\langle 123\rangle^2 \langle Y\, \mathrm{d}^2 Y\rangle}{\langle Y12\rangle \langle Y23\rangle \langle Y31\rangle} + \frac{\langle 134\rangle^2 \langle Y\, \mathrm{d}^2 Y\rangle}{\langle Y13\rangle \langle Y34\rangle \langle Y41\rangle} \\ &= \frac{\left(\langle 123\rangle^2 \langle Y34\rangle \langle Y41\rangle - \langle 134\rangle^2 \langle Y12\rangle \langle Y23\rangle\right)}{\langle Y12\rangle \langle Y23\rangle \langle Y34\rangle \langle Y41\rangle \langle Y31\rangle} \left\langle Y\, \mathrm{d}^2 Y\right\rangle . \end{aligned} \tag{3.1.5}$$

Adding and subtracting $\langle 123\rangle \langle 143\rangle \langle Y34\rangle \langle Y12\rangle$ from the numerator and using the following relations

$$\begin{aligned}\langle 124\rangle \langle 1Y3\rangle &= \langle 12Y\rangle \langle 143\rangle + \langle 1Y4\rangle \langle 123\rangle , \\ \langle 342\rangle \langle 31Y\rangle &= \langle 341\rangle \langle 32Y\rangle + \langle 312\rangle \langle 34Y\rangle , \end{aligned} \tag{3.1.6}$$

we can re-write (3.1.5) as

$$\Omega\left(\Delta^4\right) = \frac{\left(\langle Y12\rangle \langle 234\rangle \langle 341\rangle + \langle Y34\rangle \langle 123\rangle \langle 412\rangle\right)}{\langle Y12\rangle \langle Y23\rangle \langle Y34\rangle \langle Y41\rangle} \left\langle Y\, \mathrm{d}^2 Y\right\rangle , \tag{3.1.7}$$

which is in agreement with the canonical form for the quadrilateral calculated in [84]. We see in summing the canonical forms of the two triangles that the spurious pole cancels out and the resulting form indeed only has log divergences on the boundary of the quadrilateral itself.

A unique canonical form is associated to each polygon, however the reverse is not true; multiple geometries can have the same canonical form. For example, there are four inequivalent geometries in P^2 that are associated with the canonical form (3.1.4), given

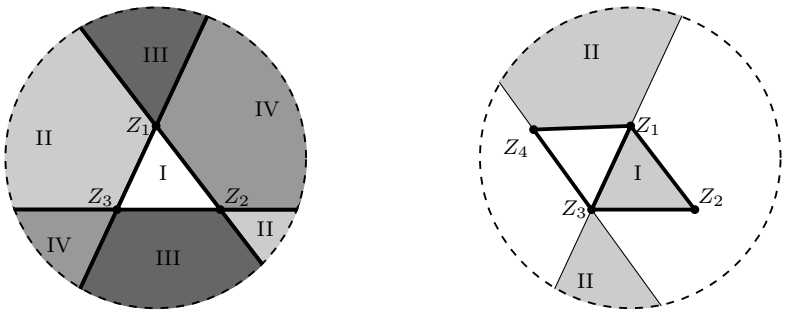

Figure 3.1: Figures illustrating polygons in P^2 represented as a disc where opposite points of the disc are identified. In Figure a) we illustrate the fact that there are four triangles $\mathrm{I}, \mathrm{II}, \mathrm{III}, \mathrm{IV}$ all of which have the same three vertices Z_1, Z_2, Z_3 and all having the same canonical form $\langle 123\rangle^2/(\langle Y12\rangle\langle Y23\rangle\langle Y31\rangle)$. In Figure b) we see a region (shaded area) which has the same canonical form as the quadrilateral $[Z_1Z_2Z_3Z_4]$, $\langle 123\rangle^2/(\langle Y12\rangle\langle Y23\rangle\langle Y31\rangle)+\langle 134\rangle^2/(\langle Y13\rangle\langle Y34\rangle\langle Y41\rangle)$ but which does not represent a good geometrical region as it has spurious boundaries.

by the sets $\{Y : Y = aZ_1 + bZ_2 + Z_3\}$ for the four possible pairs of signs of a and b i.e. $(a, b > 0)$, $(a > 0, b < 0)$, $(a < 0, b > 0)$ and $(a, b < 0)$. These sets of points simply correspond to the four inequivalent triangles in P^2 with vertices Z_1, Z_2, Z_3, as illustrated in Figure 3.1.

A necessary condition to ensure a good geometrical region given by a union of tiles is the spurious boundaries of each tile match pairwise with those of other tiles. As we saw above for the simple example of the triangle, given a canonical form the geometry associated to it can only be defined up to sign choices; it is not unique. However, if we are given a canonical form as a sum of terms containing spurious poles that cancel in the sum and look to assign a geometrical region to each term, this can not be done independently per term. The algebraic cancellation of spurious poles should correspond geometrically to a matching of the corresponding spurious boundaries.

We look again to the quadrilateral to illustrate these points. In (3.1.5) - (3.1.7) we showed that the canonical form can be written as a sum of the forms of two triangles, each with a spurious pole which cancels when summed. Geometrically this corresponds to a union

of two triangular tiles $Y_1 = aZ_1 + bZ_2 + cZ_3$ and $Y_2 = dZ_1 + eZ_3 + fZ_4$ for some choice of signs for $a, b, c, d, e, f \in \mathbb{R}$. To isolate region I on the right hand side of Figure 3.1 we take $a, b, c > 0$ and we look to see what implications that has on the sign choices for d, e and f. Taking both Y_1 and Y_2 to the co-dimension one boundary $[Z_1 Z_3]$,

$$\begin{aligned} Y_1|_{b\to 0} &= aZ_1 + cZ_3, \\ Y_2|_{f\to 0} &= dZ_1 + eZ_3. \end{aligned} \tag{3.1.8}$$

In order to obtain a good geometrical region, the two triangles must match pairwise on this boundary. For this to happen we see from (3.1.8) that the pairs a, d and c, e must have the same sign. Therefore, $d, e > 0$, and we have illustrated that signs for the geometrical region associated to each term in the canonical form of the quadrilateral cannot be decided independently if we want to match spurious boundaries. This does still leave two possible geometries corresponding to $f > 0$ and $f < 0$. For completeness, if we wish to get the inside of the quadrilateral depicted in Figure 3.1, one can use the fact that Y_2 lies to the right of the line $[Z_1 Z_3]$ to get:

$$\langle Y_2 Z_1 Z_3 \rangle = f \langle Z_1 Z_3 Z_4 \rangle > 0. \tag{3.1.9}$$

The Z_i are convex, so $\langle Z_i Z_j Z_k \rangle > 0$ for all cyclically ordered Z_i, Z_j, Z_k, therefore $f > 0$. The right hand side of Figure 3.1 shows the quadrilateral: the good region discussed above is the interior of $Z_1 ... Z_4$. The shaded region (I $\cup$ II) has the same canonical form but is not considered a good geometrical region as it has spurious boundaries. Region II would correspond to $e < 0$ (and $d, f > 0$), which was not allowed from the matching of spurious boundaries in (3.1.8).

There are two natural ways to triangulate a polygon, both of which are illustrated in Figure 3.2. The first, triangulating from one vertex of the polygon, has a natural higher dimensional analogue that is given by BCFW recursion for tree-level NMHV diagrams.

Remarkably, for the planar N^kMHV amplitude/Wilson loop, the WLDs split the amplitude into well-defined pieces. Each term can be naturally associated with a volume form

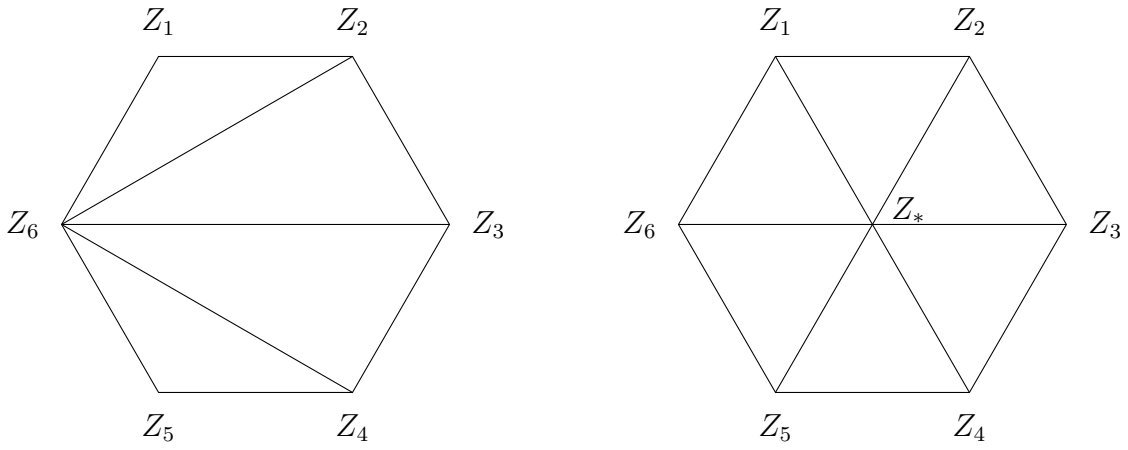

Figure 3.2: Two possibilities for triangulating a polygon. BCFW gives a generalisation of the left hand side, whereas WLDs give a generalisation of the right hand side. (for NMHV).

on the Grassmannian $\mathrm{Gr}(k, 4+k)$; the space in which the tree level $m = 4$ amplituhedron lies. The volume forms each have physical poles corresponding to the physical boundary of the amplituhedron [89], and spurious poles which cancel in the sum. This strongly suggests that the WLDs could correspond to a tessellation of the amplituhedron, with the canonical form of each tile corresponding to a WLD. Importantly, if this is true, the WLDs would give a very explicit tessellation of the amplituhedron. This idea will be explored in the rest of the chapter. In fact, the intuition described above seems to be correct for the tree-level NMHV case. NMHV twistor WIlson loop Feynman diagrams naturally give a higher dimensional analogue of the second way of triangulating a polygon by introducing an additional vertex Z_* and triangulating to that (see the right hand side of Figure 3.2). However, we find that beyond NMHV this does not seem to be the case.

3.2 WLDs and Volume Forms

There have been numerous studies looking into very interesting duality relations between three naturally gauge invariant objects in planar $N = 4$ SYM; scattering amplitudes, correlation functions and Wilson loops. The MHV gluon scattering amplitude $A_n(p_1, ..., p_n)$ was shown to be dual to a Wilson loop $W_n(x_1, ..., x_n)$ defined on a lightlike contour [19–21],

by identifying the cusp points x_i of the Wilson loop as the dual momenta of the particle p_i (see section 2.3). The correlation functions $G_n = \langle \mathcal{O}(x_1)...\mathcal{O}(x_n) \rangle$ of local gauge invariant operators $\mathcal{O}(x)$ were shown to be dual to Wilson loops, and therefore to amplitudes, in the light like limit $\lim_{x^2|_{i,i+1\to 0}} x_{12}^2...x_{n1}^2 G_n = \mathcal{W}_n$ [25,91]. The former, [22–24], and the latter, [26–28], both have supersymmetric generalisations. We utilise the amplitude/Wilson loop duality here in order to write the amplitude as a sum over twistor Wilson loop diagrams, each of which have an associated integral expression with spurious poles that cancel when summed. These expressions will then be mapped to volume forms in amplituhedron coordinates which we will attempt to give geometrical meaning to.

In this section, we provide a brief description of Wilson loops in $N = 4$ Super Yang Mills in super-twistor space and define the related Wilson loop diagrams. We will then show how to map the expression that arises from a WLD to a volume form in $\mathrm{Gr}(k, 4+k)$, the same space in which the amplituhedron lives.

3.2.1 Planar Wilson Loop Diagrams in $\mathcal{N} = 4$ SYM

The fields of $N = 4$ SYM can be described by a superfield $\mathcal{A}$, a $(0,1)$-form on supertwistor space (see for example [92,93]). It has an expansion in the fermionic twistor variables χ^A,

$$\mathcal{A} = g^+ + \chi^A \tilde{\psi}_A + \frac{1}{2}\chi^A\chi^B\phi_{AB} + \frac{1}{3!}\epsilon_{ABCD}\chi^A\chi^B\chi^C\psi^D + \frac{1}{4!}\epsilon_{ABCD}\chi^A\chi^B\chi^C\chi^D g^-, \quad (3.2.1)$$

where ψ and $\tilde{\psi}$ are the eight fermions, the antisymmetric ϕ are the six scalars and $g^\pm$ are the positive and negative helicity gluons. These are precisely the on-shell degrees of freedom for $\mathcal{N} = 4$ SYM. The twistor action of $\mathcal{N} = 4$ SYM is given by

$$S[\mathcal{A}] = \frac{i}{2\pi}\int D^{3|4}\mathcal{Z}\,\mathrm{Tr}\left(\mathcal{A}\wedge\bar{\partial}\mathcal{A} + \frac{2}{3}\mathcal{A}\wedge\mathcal{A}\wedge\mathcal{A}\right) + g^2\int \mathrm{d}^{4|8}x \log\det\left(\left(\bar{\partial}+\mathcal{A}\right)|_X\right) \quad (3.2.2)$$

where g^2 is the Yang-Mills coupling, $\left(\bar{\partial}+\mathcal{A}\right)|_X$ restricts $\bar{\partial}+\mathcal{A}$ to the projective line X in twistor space,which corresponds to the point (x,θ) in spacetime, and the integration measure is over complex projective space $D^{3|4}\mathcal{Z} = \frac{1}{4!}\epsilon_{IJKL}\,\mathrm{d}Z^I\,\mathrm{d}Z^J\,\mathrm{d}Z^K\,\mathrm{d}^4\chi$. The first

term in the action is equivalent to holomorphic Chern-Simons theory [93, 94], and the second term describes the interacting non self-dual part.[3]

To obtain the Feynman rules in twistor space, one can impose an axial gauge by choosing a reference twistor Z_* and insisting that the component of $\mathcal{A}$ in the direction of Z_* is zero, i.e. $\bar{\mathcal{Z}}_* \cdot \mathcal{A} = 0$. The cubic term in (3.2.2) is zero since imposing this gauge reduces the number of components of $\mathcal{A}$ from three down to two, and the first term, the kinetic term, defines a propagator. This is known as the CSW gauge and was first introduced in [14]. The log det term can be Taylor expanded, where in this gauge each term corresponds to an MHV amplitude. This can be expressed in twistor space and gives a Feynman diagram formalism for amplitudes known as the "MHV diagram formalism". For a more detailed description of the twistor action (3.2.2) and the expansion hinted at here, see [96] and the references therein.

The Feynman diagrams can also be used to calculate the expectation value of the polygonal holomorphic Wilson-loop in supertwistor space, with vertices being the supertwistors $\mathcal{Z}_1 ... \mathcal{Z}_n \in \mathbb{C}^{4|4}$. In the planar theory, this is equivalent via the Wilson loop/amplitude duality to n-point superamplitudes. We refer to these diagrams as Wilson loop diagrams (WLDs), and are what we are interested in going forward. Below we will discuss the Feynman rules for these diagrams. We do not look to derive these here; for their derivation see [23, 97, 98].

At tree level, the Feynman diagrams consist simply of propagators whose two ends lie on the Wilson loop contour. In the planar theory, diagrams are only valid if we can draw all the propagators inside the Wilson loop without crossing. The N^kMHV Wilson loop is the sum over all such diagrams involving k propagators; see Figure 3.3 for an example of a diagram contributing to the 8-point N^4MHV amplitude.

[3] To see motivation for the form of the log det interaction term from twistor-string theory we refer the interested reader to [92, 95]

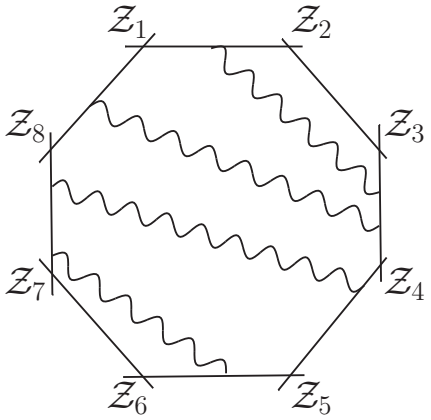

Figure 3.3: Example of a Wilson loop diagram which contributes to the 8-point N^{4}MHV amplitude.

To each propagator from edge $[\mathcal{Z}_i\mathcal{Z}_{i+1}]$ to $[\mathcal{Z}_j\mathcal{Z}_{j+1}]$ we assign the (4|4) delta function:

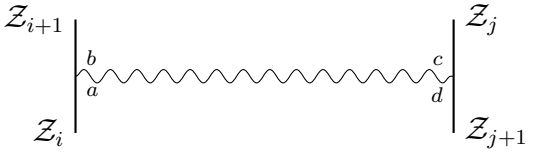

$$= \delta^{4|4}(a\mathcal{Z}_i+b\mathcal{Z}_{i+1}+c\mathcal{Z}_j+d\mathcal{Z}_{j+1}+\mathcal{Z}_*) \tag{3.2.3}$$

We then integrate over the complex integration variables associated with each end of the propagator, with a measure determined by all the propagators ending on the same edge

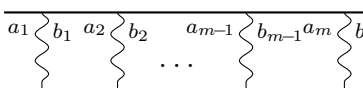

$$= \int \frac{\mathrm{d}a_1\,\mathrm{d}b_1\ldots\mathrm{d}a_m\,\mathrm{d}b_m}{b_1(a_1b_2-b_1a_2)\ldots(a_{m-1}b_m-b_{m-1}a_m)a_m} \tag{3.2.4}$$

In Figure 3.4 we illustrate these rules with two examples; firstly an example of a diagram contributing to the NMHV six-point amplitude and secondly one contributing to the N^{2}MHV six-point amplitude.

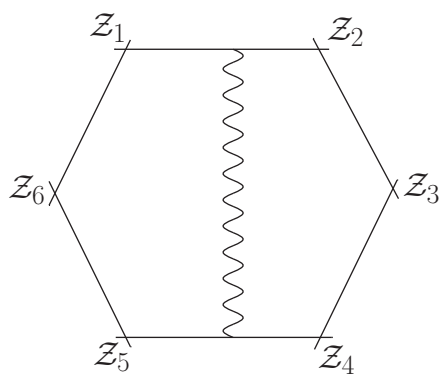

$$\int \frac{\mathrm{d}a\,\mathrm{d}b\,\mathrm{d}c\,\mathrm{d}d}{abcd}\delta^{4|4}\left(a\mathcal{Z}_1+b\mathcal{Z}_2+c\mathcal{Z}_4+d\mathcal{Z}_5+\mathcal{Z}_*\right)$$

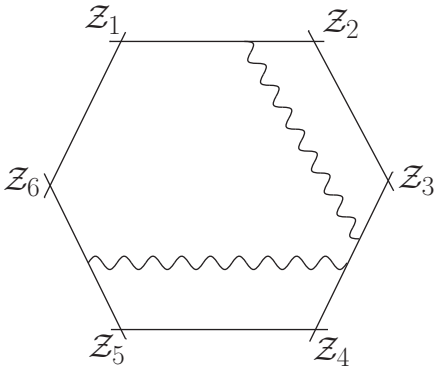

$$\int \frac{\mathrm{d}a_1\,\mathrm{d}b_1\,\mathrm{d}c_1\,\mathrm{d}d_1\,\mathrm{d}f_1\,\mathrm{d}g_1\,\mathrm{d}h_1}{a_1b_1g_1h_1e_1(c_1f_1-d_1e_1)d_1}\times$$
$$\times\delta^{(4|4)}\left(a_1\mathcal{Z}_1+b_1\mathcal{Z}_2+c_1\mathcal{Z}_3+d_1\mathcal{Z}_4+\mathcal{Z}_*\right)$$
$$\times\delta^{(4|4)}\left(e_1\mathcal{Z}_3+f_1\mathcal{Z}_4+g_1\mathcal{Z}_5+h_1\mathcal{Z}_6+\mathcal{Z}_*\right)$$

Figure 3.4: Examples of Feynman diagrams in twistor space that contribute to the 6-point NMHV / N^{2}MHV amplitude with their corresponding expressions following the rules given.

At tree level, when both propagator ends lie on the same edge or adjacent edges, the expression reduces to zero. Using this construction (with further rules for loop diagrams), it was shown the all-loop integrand at MHV can be written in dlog form, meaning the integrand is just a product of exterior derivatives of logarithms of rational functions. Beyond the MHV sector, it was shown that the integrand is in dlog form multiplied by delta functions [99, 100]. Writing the integration measure in dlog form makes associating a geometrical region to it particularly natural, as we will see below. For the remainder of this chapter, we shall focus only on the tree level integrand.

3.2.2 Volume Forms in Amplituhedron Space from WLDs

The Wilson loop diagrams are originally defined in supertwistor space, $\mathbb{C}^{4|4}$. In order to see whether the WLDs provide a tessellation of the amplituhedron, we need to somehow interpret them in the space in which the amplituhedron exists, $\mathrm{Gr}(k, 4+k)$. We show below that they have a very direct interpretation as volume forms in this "amplituhedron space".

Following their description in the previous section, we saw that all N^kMHV WLDs have the general form

$$\int \Omega_{4k}\left(a_i\right) \delta^{k\times(4|4)}\left(C\left(a_i\right).\mathcal{Z}\right) \qquad \text{[WLD]}. \tag{3.2.5}$$

The variables in (3.2.5) are defined as follows,

- a_i: the $4k$ coordinates, four for each of the k propagators of the WLD.
- $\mathcal{Z}$: the external particles in supertwistor space, organised as the rows of an $(n+1)\times(4|4)$ matrix.
- $\Omega_{4k}\left(a_i\right)$: the integration measure. A $4k$-form consisting of a product of terms of the form (3.2.4).
- $\delta^{k\times(4|4)}\left(C\left(a_i\right).\mathcal{Z}\right)$: the k delta functions, one for each propagator, written as a $k\times(n+1)$ matrix of the coordinates, $C(a_i)$, acting on the external supertwistors $\mathcal{Z}$.

We now look to interpret (3.2.5) as a canonical form in the amplituhedron space. This can be done straightforwardly via the map

$$\Omega(Y) = \Omega_{4k}(a_i) \qquad Y = C(a_i).\mathcal{Z} \in \mathrm{Gr}(k, k+4). \tag{3.2.6}$$

The coordinates are now reinterpreted as coordinates in $\mathrm{Gr}(k,k+4)$, and the $\mathcal{Z}$ here is the $(n+1)\times(4+k)$ matrix with each row corresponding to an external momentum supertwistor now bosonised in the way described in section 2.3.

We once again turn to the two examples in Figure 3.4 to illustrate this point. For the NMHV diagram, the volume form in amplituhedron space can be read off:

$$\begin{array}{ll} \int \frac{\mathrm{d}a\,\mathrm{d}b\,\mathrm{d}c\,\mathrm{d}d}{abcd}\,\delta^{4|4}\left(a\mathcal{Z}_1{+}b\mathcal{Z}_2{+}c\mathcal{Z}_4{+}d\mathcal{Z}_5{+}\mathcal{Z}_*\right) & \text{[WLD]} \\ \qquad\qquad\qquad\qquad \downarrow & \\ \Omega = \frac{\mathrm{d}a\,\mathrm{d}b\,\mathrm{d}c\,\mathrm{d}d}{abcd} \qquad Y = aZ_1{+}bZ_2{+}cZ_4{+}dZ_5{+}Z_* \in \mathbb{C}^5 & \text{[Amplituhedron Volume form]} \end{array} \tag{3.2.7}$$

This volume form can be covariantised to be written in a coordinate independent way as

$$\frac{\langle Y\,\mathrm{d}^4Y\rangle\langle Z_1Z_2Z_4Z_5Z_*\rangle^4}{\langle YZ_1Z_2Z_4Z_5\rangle\langle YZ_2Z_4Z_5Z_*\rangle\langle YZ_4Z_5Z_*Z_1\rangle\langle YZ_5Z_*Z_1Z_2\rangle\langle YZ_*Z_1Z_2Z_4\rangle}\ , \tag{3.2.8}$$

where the angle brackets denote 5×5 determinants.

For the N^2MHV example on the right hand side of Figure 3.4, the WLD can be mapped to a volume form in the amplituhedron space by

$$\begin{array}{ll} \int \frac{\mathrm{d}a_1\,\mathrm{d}b_1\,\mathrm{d}c_1\,\mathrm{d}d_1\,\mathrm{d}f_1\,\mathrm{d}g_1\,\mathrm{d}h_1}{a_1b_1g_1h_1e_1(c_1f_1-d_1e_1)d_1}\delta^{(8|8)}\left(C_1\cdot\mathcal{Z}\right) & \text{[WLD]} \\ \qquad\qquad\downarrow & \\ \Omega=\frac{\mathrm{d}a_1\,\mathrm{d}b_1\,\mathrm{d}c_1\,\mathrm{d}d_1\,\mathrm{d}f_1\,\mathrm{d}g_1\,\mathrm{d}h_1}{a_1b_1g_1h_1e_1(c_1f_1-d_1e_1)d_1} \qquad Y=C_1.Z\in \mathrm{Gr}(2,6) & \text{[Amplituhedron Volume form]} \end{array} \tag{3.2.9}$$

where $\mathcal{Z}=(\mathcal{Z}_1,\mathcal{Z}_2,\dots\mathcal{Z}_6,\mathcal{Z}_*)^T$ are the external supertwistors (together with $\mathcal{Z}_*$) viewed as a $7\times(4|4)$ matrix,

$$C_1=\begin{pmatrix} a_1 & b_1 & c_1 & d_1 & 0 & 0 & 1 \\ 0 & 0 & e_1 & f_1 & g_1 & h_1 & 1 \end{pmatrix}\in \mathrm{Gr}(2,7) \tag{3.2.10}$$

and similarly $Z=(Z_1,\dots Z_6,Z_*)^T$ are the external bosonised supertwistors (with Z_*) viewed as a 7×6 matrix.

3.3 NMHV amplituhedron from WLDs

Now that we can map the Wilson loop diagrams to a volume form in the amplituhedron space, we can take a look to the NMHV case. We show that the volume forms associated to each term in the expansion of the amplitude in terms of WLDs do indeed give a good tessellation of the amplituhedron. The spurious boundaries from each diagram all match (locally) pairwise with spurious boundaries from other diagrams, thus they can be glued together to give a good geometrical region. This is perhaps not surprising since NMHV WLDs were involved in the original polytope interpretation of amplitudes [63, 74].

3.3.1 Cancellation of spurious poles in NMHV WLDs

The n-point NMHV amplitude in the twistor Wilson loop description is given by a sum over all diagrams with a single propagator attached to any two edges of the polygon. The diagram with a propagator which has ends attached to the edges $[Z_iZ_{i+1}]$ and $[Z_jZ_{j+1}]$ can be associated to the volume form in $\mathrm{Gr}(1,5)$

$$\Omega = \frac{\mathrm{d}a\,\mathrm{d}b\,\mathrm{d}c\,\mathrm{d}d}{abcd} \qquad Y = aZ_i + bZ_{i+1} + cZ_j + dZ_{j+1} + Z_* \in \mathbb{C}^5. \tag{3.3.1}$$

Writing this in a coordinate independent form as in (3.2.8) gives

$$\frac{\langle Y\,\mathrm{d}^4Y\rangle\langle Z_iZ_{i+1}Z_jZ_{j+1}Z_*\rangle^4}{\langle YZ_iZ_{i+1}Z_jZ_{j+1}\rangle\langle YZ_{i+1}Z_jZ_{j+1}Z_*\rangle\langle YZ_jZ_{j+1}Z_*Z_i\rangle\langle YZ_{j+1}Z_*Z_iZ_{i+1}\rangle\langle YZ_*Z_iZ_{i+1}Z_j\rangle}\,. \tag{3.3.2}$$

The full NMHV amplitude is given by summing over all positions of the ends of the propagator,

$$\Omega = \langle Y\,\mathrm{d}^4Y\rangle \times \sum_{i<j} \frac{\langle Z_iZ_{i+1}Z_jZ_{j+1}Z_*\rangle^4}{\langle YZ_iZ_{i+1}Z_jZ_{j+1}\rangle\langle YZ_{i+1}Z_jZ_{j+1}Z_*\rangle\langle YZ_jZ_{j+1}Z_*Z_i\rangle\langle YZ_{j+1}Z_*Z_iZ_{i+1}\rangle\langle YZ_*Z_iZ_{i+1}Z_j\rangle}\,, \tag{3.3.3}$$

where requiring $i < j$ comes from the fact that the diagrams are invariant under the swapping of the two propagator ends.

Looking at (3.3.1), it is clear that the spurious poles for each WLD arise when any one of $a, b, c, d \to 0$. There is another pole present when $a, b, c, d \to \infty$ simultaneously, however this is a physical pole of the amplitude and does not cancel in the sum over the diagrams. From the point of view of the WLDs, the spurious poles occur when one end of the propagator approaches a vertex. However, this spurious pole is cancelled when the WLD is added together with a neighbouring diagram, where the propagator approaches the same vertex but from the adjacent edge. This is illustrated in Figure 3.5.

Algebraically this cancellation is straightforward, but for completeness we shall show it

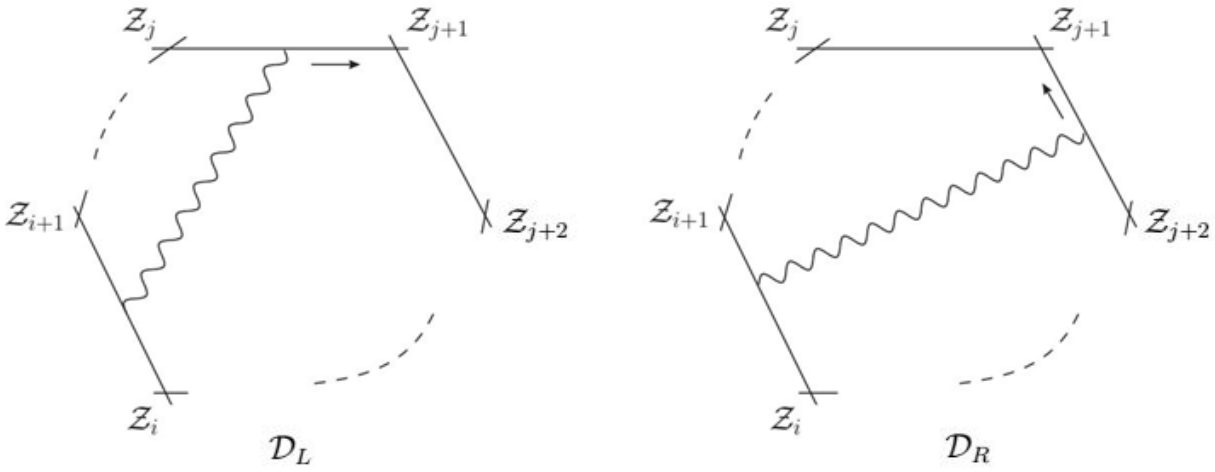

Figure 3.5: Spurious poles occur when the propagator end reaches the vertex. It is cancelled by the adjacent diagram.

explicitly for the diagrams in Figure 3.5. Using the rules from section 3.2.1, the integrals associated to the two diagrams are

$$\mathcal{I}\left(\mathcal{D}_L\right) = \int \frac{\mathrm{d}a_1\,\mathrm{d}b_1\,\mathrm{d}c_1\,\mathrm{d}d_1}{a_1 b_1 c_1 d_1} \delta^{4|4}\left(C_L \cdot \mathcal{Z}\right) \tag{3.3.4}$$

and

$$\mathcal{I}\left(\mathcal{D}_R\right) = \int \frac{\mathrm{d}a_2\,\mathrm{d}b_2\,\mathrm{d}c_2\,\mathrm{d}d_2}{a_2 b_2 c_2 d_2} \delta^{4|4}\left(C_R \cdot \mathcal{Z}\right). \tag{3.3.5}$$

The corresponding $1 \times (n+1)$ C matrices are given by

$$C_L = \begin{pmatrix} \cdots & a_1 & b_1 & \cdots & c_1 & d_1 & 0 & \cdots & 1 \end{pmatrix}, \tag{3.3.6}$$

$$C_R = \begin{pmatrix} \cdots & a_2 & b_2 & \cdots & 0 & c_2 & d_2 & \cdots & 1 \end{pmatrix}, \tag{3.3.7}$$

where the entries explicitly written out in both matrices are the $i, i+1, j, j+1, j+2$ and $n+1$ entries, with all other entries being 0.

The spurious poles being discussed here occur when $c_1 \to 0$ and $d_2 \to 0$, and the claim more precisely is that in summing the two diagrams the residues at these poles precisely cancel

$$\operatorname*{Res}_{c_1=0} \mathcal{I}(D_L) + \operatorname*{Res}_{d_2=0} \mathcal{I}(D_R) = 0. \tag{3.3.8}$$

Evaluating the two residues gives

$$\operatorname*{Res}_{c_1=0}\mathcal{I}(D_L)=\int\frac{\mathrm{d}a_1\,\mathrm{d}b_1\,\mathrm{d}d_1}{a_1b_1d_1}\delta^{4|4}\left(a_1\mathcal{Z}_i+b_1\mathcal{Z}_{i+1}+d_1\mathcal{Z}_{j+1}+\mathcal{Z}_*\right), \tag{3.3.9}$$

$$\operatorname*{Res}_{d_2=0}\mathcal{I}(D_R)=-\int\frac{\mathrm{d}a_2\,\mathrm{d}b_2\,\mathrm{d}c_2}{a_2b_2c_2}\delta^{4|4}\left(a_2\mathcal{Z}_i+b_2\mathcal{Z}_{i+1}+c_2\mathcal{Z}_{j+1}+\mathcal{Z}_*\right), \tag{3.3.10}$$

where we have expanded the product of C_L and C_R with $\mathcal{Z}$ respectively. Each entry of the two matrices can now be compared directly, and an appropriate change of variables can be done from a_2, b_2, c_2 to a_1, b_1, d_1 as dictated by matching entries of C_R to those of C_L. Therefore, we end up with

$$\int\left(\frac{\mathrm{d}a_1\,\mathrm{d}b_1\,\mathrm{d}d_1}{a_1b_1d_1}-\frac{\mathrm{d}a_1\,\mathrm{d}b_1\,\mathrm{d}d_1}{a_1b_1d_1}\right)\delta^{4|4}\left(a_1\mathcal{Z}_i+b_1\mathcal{Z}_{i+1}+d_1\mathcal{Z}_{j+1}+\mathcal{Z}_*\right)=0 \tag{3.3.11}$$

and (3.3.8) is satisfied.

It is worth mentioning a special case of this type of spurious pole which occurs when the propagator lies between next-to-adjacent edges, see Figure 3.6. Naively, it looks

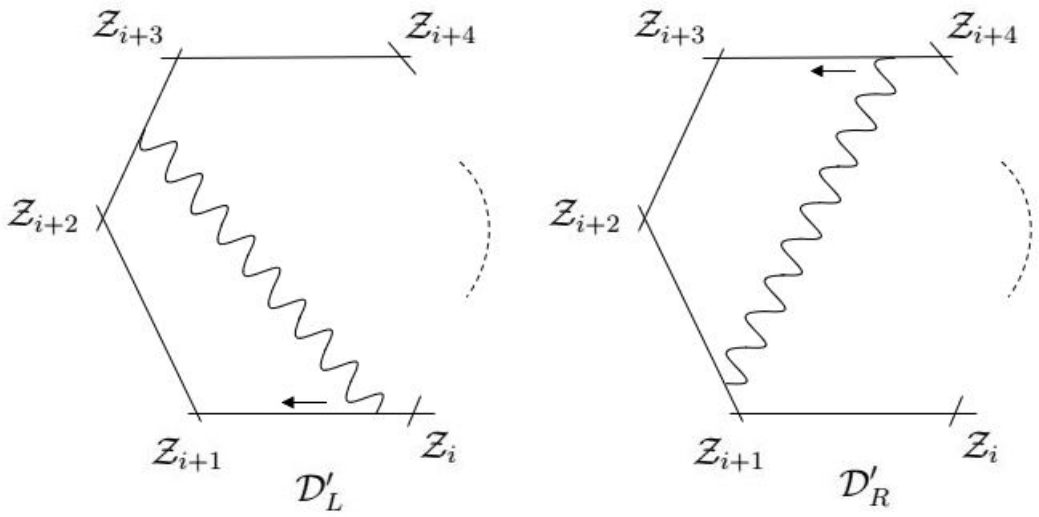

Figure 3.6: A special case of the spurious pole cancellation that occurs when the propagator ends are on next-to-adjacent edges, and one propagator end moves to the vertex closest to the other end.

like $\mathcal{D}'_L$ does not have a partner diagram that when summed with would cancel the spurious pole that occurs in the limit where the propagator end reaches the vertex $\mathcal{Z}_{i+1}$.

Following previous considerations, the partner diagram would have propagator ends lying on adjacent edges, but this diagram vanishes. Instead, it pairs with the diagram with propagator ends on edge $[\mathcal{Z}_{i+1}\mathcal{Z}_{i+2}]$ and $[\mathcal{Z}_{i+3}\mathcal{Z}_{i+4}]$, illustrated by $\mathcal{D}'_R$ in Figure 3.6. The expressions for this pair of WLDs are given by

$$\mathcal{I}(D'_L) = \int \frac{\mathrm{d}a_1\,\mathrm{d}b_1\,\mathrm{d}c_1\,\mathrm{d}d_1}{a_1b_1c_1d_1}\delta^{4|4}\left(a_1\mathcal{Z}_i + b_1\mathcal{Z}_{i+1} + c_1\mathcal{Z}_{i+2} + d_1\mathcal{Z}_{i+3} + \mathcal{Z}_*\right), \tag{3.3.12}$$

$$\mathcal{I}(D'_R) = \int \frac{\mathrm{d}a_2\,\mathrm{d}b_2\,\mathrm{d}c_2\,\mathrm{d}d_2}{a_2b_2c_2d_2}\delta^{4|4}\left(a_2\mathcal{Z}_{i+1} + b_2\mathcal{Z}_{i+2} + c_2\mathcal{Z}_{i+3} + d_2\mathcal{Z}_{i+4} + \mathcal{Z}_*\right), \tag{3.3.13}$$

and the relation for this special case is given by

$$\operatorname*{Res}_{a_1=0}\mathcal{I}(D'_L) + \operatorname*{Res}_{d_2=0}\mathcal{I}(D'_R) = 0. \tag{3.3.14}$$

3.3.2 Spurious boundary matching

There is a natural geometrical interpretation of the NMHV amplitude as a union of tiles, each giving one of the terms in (3.3.3) as its canonical form. This corresponds to

$$\bigcup_{i,j}\{Y = aZ_i + bZ_{i+1} + cZ_j + dZ_{j+1} + Z_*\,;\, a,b,c,d \geq 0\} \subset \mathrm{Gr}(1,5)\ . \tag{3.3.15}$$

It should be noted that the variables (a,b,c,d) used to describe the geometrical region in (3.3.15) are the same variables given by the WLDs, (3.3.1). The WLD integration is over complex space, however here the variables are restricted to a subspace of the real line.

If $\langle Z_iZ_jZ_kZ_lZ_m\rangle > 0$ for all cyclically ordered Z_i, Z_j, Z_k, Z_l, Z_m, corresponding to the Z's being convex, then (3.3.15) provides a tessellation of the amplituhedron as defined in [47]. This is the higher dimensional generalisation of the triangulation of the polygon in the toy model illustrated on the right hand side of Figure 3.2. In fact, this defines a good geometrical region, meaning one without spurious boundaries, even for non-convex choices of external kinematic data Z_i.

Motivated by the toy example discussed around Figure 3.1, it is interesting to determine how unique this region is. Any choice of signs for the variables a,b,c,d in each tile will associate the same canonical form to each WLD. However, as we saw for the quadrilateral,

choosing arbitrary signs for each tile independently could lead to a geometrical region which still has spurious boundaries left over even though the spurious poles in the sum of the corresponding canonical forms do cancel. Imposing that this cancellation of poles has a corresponding geometric meaning as a matching of spurious boundaries gives a correlation between the sign choices for the geometric image of the tiles.

To begin exploring whether other good geometrical regions can be determined from the canonical forms of the WLDs, let us consider a particular tile corresponding to the WLD with a propagator from edge $[Z_iZ_{i+1}]$ to edge $[Z_jZ_{j+1}]$. The most general geometry giving (3.3.1,3.3.2) as its canonical form is

$$\{Y = as_iZ_i+bs_{i+1}Z_{i+1}+cs_jZ_j+ds_{j+1}Z_{j+1}+Z_* \,:\, a,b,c,d \geq 0\}, \tag{3.3.16}$$

where $s_i, s_{i+1}, s_j, s_{j+1} = \pm 1$ are four arbitrary sign choices. Recalling the location of the spurious poles discussed in the previous section, the associated spurious boundaries arise when any one of the four coordinates $a, b, c, d \to 0$ (while a physical boundary occurring when simultaneously $a, b, c, d \to \infty$). Focussing on the spurious boundary $a \to 0$, and motivated by the fact the related spurious pole cancels by summing with a neighbouring diagram, this boundary must match the boundary when $b \to 0$ of the adjacent diagram with a propagator from edge $[Z_{i+1}Z_{i+2}]$ to edge $[Z_jZ_{j+1}]$. Defining arbitrary signs for the neighbouring diagram, $s'_{i+1}, s'_{i+2}, s'_j, s'_{j+1} = \pm 1$, we have

$$\begin{gathered}\{Y = as_iZ_i+bs_{i+1}Z_{i+1}+cs_jZ_j+ds_{j+1}Z_{j+1}+Z_* \,:\, a=0,b,c,d \geq 0\} \\ = \\ \{Y = as'_{i+1}Z_{i+1}+bs'_{i+2}Z_{i+2}+cs'_jZ_j+ds'_{j+1}Z_{j+1}+Z_* \,:\, b=0,\ a,c,d \geq 0\}.\end{gathered} \tag{3.3.17}$$

This boundary matching mimics the spurious pole cancellation in Figure 3.5 and surrounding discussion. Comparing the two regions and imposing that these two spurious boundaries match, we find a set of consistency conditions on the sign choices of the two tiles:

$$s_{i+1} = s'_{i+1}, \quad s_j = s'_j, \quad s_{j+1} = s'_{j+1}. \tag{3.3.18}$$

So, the signs associated with each vertex for different diagrams must be the same. Of course, very similar considerations can be applied for the other spurious boundaries that occur when b, c or $d \to 0$

One can continue this discussion for the spurious poles of all NMHV diagrams, moving the propagator around the edges of the polygon and fixing signs by comparing expressions similar to (3.3.17) at each step. In doing so, we see that the region

$$\bigcup_{i,j}\{Y = as_iZ_i+bs_{i+1}Z_{i+1}+cs_jZ_j+ds_{j+1}Z_{j+1}+Z_*\,;\, a,b,c,d \geq 0\} \subset \mathrm{Gr}(1,5) \qquad (3.3.19)$$

is the most general geometry matching the WLDs that has no spurious boundaries, which can be obtained by assigning a fixed sign $s_i = \pm 1$ to each vertex Z_i. This is equivalent to considering the original amplituhedron with all positive signs but flipping the sign of the external Z's. Note that at most one choice of signs for the Zs can correspond to a convex shape).

Naively, one may think that a more general possibility could have existed, consisting of assigning two sets of fixed signs per vertex rather than one, corresponding to one set per propagator end. However, in starting from one diagram and moving the propagator round the polygon, matching spurious boundaries as you go, eventually the same diagram is reached that you started on with the propagator ends switched. This reversed propagator has to correspond to the same geometrical region as the original, therefore the two sets of signs must in fact be equal to each other.

To complete the discussion of spurious boundaries for the NMHV case, it is worth double checking that this general geometrical region (3.3.19) is consistent with the special case of spurious pole cancellation illustrated in Figure 3.6 and the discussion around it. For this particular example, the geometry associated to the diagram with a propagator between edge $[Z_iZ_{i+1}]$ and edge $[Z_{i+2}Z_{i+3}]$ should match along the spurious boundary that occurs when $a = 0$ with the diagram with a propagator between edge $[Z_{i+1}Z_{i+2}]$ and edge

$[Z_{i+3}Z_{i+4}]$ along the boundary that occurs when $d = 0$. We get

$$\begin{aligned}\{Y = as_iZ_i+bs_{i+1}Z_{i+1}+cs_{i+2}Z_{i+2}+ds_{i+3}Z_{i+3}+Z_*\,;\, a=0,b,c,d\geq 0\}\\ =\\ \{Y = as_{i+1}Z_{i+1}+bs_{i+2}Z_{i+2}+cs_{i+3}Z_{i+3}+ds_{i+4}Z_{i+4}+Z_*\,;\, d=0,\ a,b,c\geq 0\}\ ,\end{aligned} \tag{3.3.20}$$

and see that indeed the spurious boundaries do match for this special case too, even for the general choice of signs.

3.4 N^2MHV

Having discussed how to obtain a "good" geometry from the WLDs for NMHV, we now look to the next highest helicity degree. We will begin by discussing new spurious poles that occur at N^2MHV, and show how they cancel algebraically. We will then prove that beyond NMHV the WLDs cannot be glued together to form a geometry without spurious boundaries. To do this, we show that this is no set of sign choices for the coordinates of each tile that is consistent with the pairwise matching of spurious boundaries. Note, by pairwise matching we mean locally; there could by more than two diagrams involved in the matching of a spurious boundary. In fact, we will see this during the discussions that follow. In order to illustrate the argument we will focus on the case of $n = 6$ in the coming sections, however we emphasise that the argument is easily generalised to all n.

3.4.1 Cancellation of spurious poles in N^2MHV WLDs

To begin, we consider the algebraic cancellation of spurious poles for N^2MHV diagrams. The discussion from Section 3.3.1 involving the spurious pole that occurs when a propagator end approaches a vertex still holds for any MHV degree. However, from N^2MHV a new spurious pole occurs; now that we have more than one propagator, there is the possibility that two propagator ends come together, which produces a pole in the integral of the WLD. Unlike the previous type of pole, there is an interesting three-way

cancellation that occurs when the three related diagrams are summed. We show how this cancellation works algebraically, and use this as motivation later when attempting to associate geometries to the WLDs (see [98, 101] for previous work also describing this mechanism).

To illustrate how the three-way cancellation works, we look to the specific set of example diagrams in Figure 3.7. Using the rules from section 3.2.1, the integrals associated to the

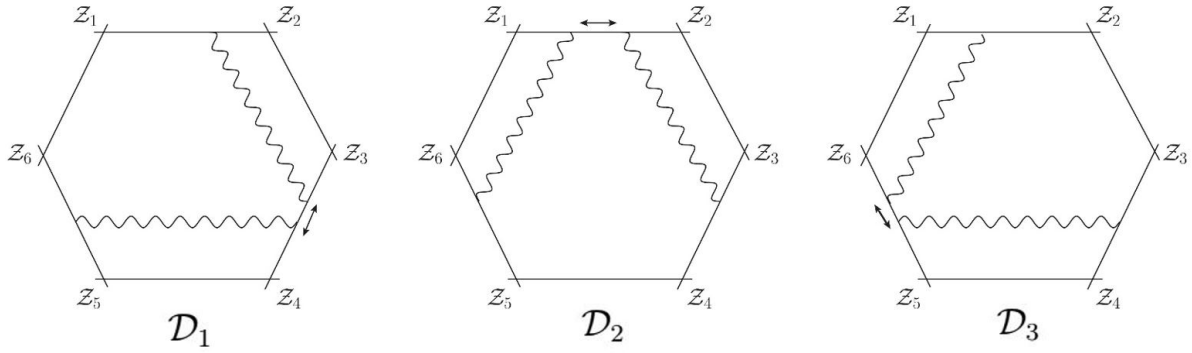

Figure 3.7: Three diagrams each having a new type of spurious pole occurring when the propagator ends touch. In the sum of the three diagrams, however, this pole cancels. Note that although this is drawn at six points for illustrative purposes, the cancellation only depends on the three sides taking part and can be directly repeated at n points.

diagrams under consideration are

$$\mathcal{I}(\mathcal{D}_1) = \int \frac{\mathrm{d}a_1\,\mathrm{d}b_1\,\mathrm{d}c_1\,\mathrm{d}d_1\,\mathrm{d}e_1\,\mathrm{d}f_1\,\mathrm{d}g_1\,\mathrm{d}h_1}{a_1 b_1 g_1 h_1 e_1 (c_1 f_1 - d_1 e_1) d_1} \delta^{(8|8)}\left(C_1 \cdot \mathcal{Z}\right) \tag{3.4.1}$$

$$\mathcal{I}(\mathcal{D}_2) = \int \frac{\mathrm{d}a_2\,\mathrm{d}b_2\,\mathrm{d}c_2\,\mathrm{d}d_2\,\mathrm{d}e_2\,\mathrm{d}f_2\,\mathrm{d}g_2\,\mathrm{d}h_2}{c_2 d_2 g_2 h_2 b_2 (a_2 f_2 - b_2 e_2) e_2} \delta^{(8|8)}\left(C_2 \cdot \mathcal{Z}\right) \tag{3.4.2}$$

and

$$\mathcal{I}(\mathcal{D}_3) = \int \frac{\mathrm{d}a_3\,\mathrm{d}b_3\,\mathrm{d}c_3\,\mathrm{d}d_3\,\mathrm{d}e_3\,\mathrm{d}f_3\,\mathrm{d}g_3\,\mathrm{d}h_3}{a_3 b_3 e_3 f_3 c_3 (d_3 g_3 - h_3 c_3) h_3} \delta^{(8|8)}\left(C_3 \cdot \mathcal{Z}\right), \tag{3.4.3}$$

with the C matrices in the above delta functions given by

$$C_1 = \begin{pmatrix} a_1 & b_1 & c_1 & d_1 & 0 & 0 & 1 \\ 0 & 0 & e_1 & f_1 & g_1 & h_1 & 1 \end{pmatrix}, \tag{3.4.4}$$

$$C_2 = \begin{pmatrix} a_2 & b_2 & 0 & 0 & c_2 & d_2 & 1 \\ e_2 & f_2 & g_2 & h_2 & 0 & 0 & 1 \end{pmatrix}, \tag{3.4.5}$$

$$C_3 = \begin{pmatrix} a_3 & b_3 & 0 & 0 & c_3 & d_3 & 1 \\ 0 & 0 & e_3 & f_3 & g_3 & h_3 & 1 \end{pmatrix}. \tag{3.4.6}$$

Each expression clearly has a pole at the point corresponding to the propagator ends coinciding (i.e. $c_1 f_1 = d_1 e_1$ for the first case, $a_2 f_2 = b_2 e_2$ for the second and $d_3 g_3 = h_3 c_3$ for the third).

The claim is that in summing the diagrams, the residues at these poles precisely cancel:

$$\operatorname*{Res}_{c_1 f_1 = d_1 e_1} \mathcal{I}(D_1) + \operatorname*{Res}_{a_2 f_2 = b_2 e_2} \mathcal{I}(D_2) + \operatorname*{Res}_{d_3 g_3 = h_3 c_3} \mathcal{I}(D_3) = 0. \tag{3.4.7}$$

In order to show this, it is useful to change variables in the following way:

$$(e_1, f_1) \to (\alpha, \epsilon_1) \qquad (e_2, f_2) \to (\beta, \epsilon_2) \qquad (g_3, h_3) \to (\gamma, \epsilon_3)$$
$$e_1 = \alpha c_1, \quad f_1 = \alpha d_1 + \epsilon_1 \quad e_2 = \beta a_2, \quad f_2 = \beta b_2 + \epsilon_2 \quad g_3 = \gamma c_3 + \epsilon_3, \quad h_3 = \gamma d_3$$

The spurious poles in question now occur when $\epsilon_1, \epsilon_2, \epsilon_3 \to 0$. Substituting these new variables into the integrals corresponding to the WLDs currently being examined gives

$$\begin{aligned} \operatorname*{Res}_{\epsilon_1=0} \mathcal{I}(D_2) &= \operatorname*{Res}_{\epsilon_1=0} \int \frac{\mathrm{d}a_1\, \mathrm{d}b_1\, \mathrm{d}c_1\, \mathrm{d}d_1\, \mathrm{d}g_1\, \mathrm{d}h_1\, \mathrm{d}\alpha\, \mathrm{d}\epsilon_1}{a_1 b_1 c_1 d_1 g_1 h_1 \alpha \epsilon_1} \delta^{(8|8)}\left(C_1 \cdot \mathcal{Z}\right) \\ &= \int \frac{\mathrm{d}a_1\, \mathrm{d}b_1\, \mathrm{d}c_1\, \mathrm{d}d_1\, \mathrm{d}g_1\, \mathrm{d}h_1\, \mathrm{d}\alpha}{a_1 b_1 c_1 d_1 g_1 h_1 \alpha} \delta^{(8|8)}\left(C_1|_{\epsilon_1=0} \cdot \mathcal{Z}\right), \end{aligned} \tag{3.4.8}$$

$$\begin{aligned} \operatorname*{Res}_{\epsilon_2=0} \mathcal{I}(D_1) &= \operatorname*{Res}_{\epsilon_2=0} \int \frac{\mathrm{d}a_2\, \mathrm{d}b_2\, \mathrm{d}c_2\, \mathrm{d}d_2\, \mathrm{d}g_2\, \mathrm{d}h_2\, \mathrm{d}\beta\, \mathrm{d}\epsilon_2}{a_2 b_2 c_2 d_2 g_2 h_2 \beta \epsilon_2} \delta^{(8|8)}\left(C_2 \cdot \mathcal{Z}\right) \\ &= \int \frac{\mathrm{d}a_2\, \mathrm{d}b_2\, \mathrm{d}c_2\, \mathrm{d}d_2\, \mathrm{d}g_2\, \mathrm{d}h_2\, \mathrm{d}\beta}{a_2 b_2 c_2 d_2 g_2 h_2 \beta} \delta^{(8|8)}\left(C_2|_{\epsilon_2=0} \cdot \mathcal{Z}\right) \end{aligned} \tag{3.4.9}$$

and

$$\begin{aligned} \operatorname*{Res}_{\epsilon_3=0} \mathcal{I}(D_3) &= \operatorname*{Res}_{\epsilon_3=0} - \int \frac{\mathrm{d}a_3\, \mathrm{d}b_3\, \mathrm{d}c_3\, \mathrm{d}d_3\, \mathrm{d}e_3\, \mathrm{d}f_3\, \mathrm{d}\gamma\, \mathrm{d}\epsilon_3}{a_3 b_3 c_3 d_3 e_3 f_3 \gamma \epsilon_3} \delta^{(8|8)}\left(C_3 \cdot \mathcal{Z}\right) \\ &= - \int \frac{\mathrm{d}a_3\, \mathrm{d}b_3\, \mathrm{d}c_3\, \mathrm{d}d_3\, \mathrm{d}e_3\, \mathrm{d}f_3\, \mathrm{d}\gamma}{a_3 b_3 c_3 d_3 e_3 f_3 \gamma} \delta^{(8|8)}\left(C_3|_{\epsilon_3=0} \cdot \mathcal{Z}\right). \end{aligned} \tag{3.4.10}$$

The measure in each expression is now simply the dlog of all the variables. The associated

C matrices in the delta functions become

$$C_1|_{\epsilon_1=0} = \begin{pmatrix} a_1 & b_1 & c_1 & d_1 & 0 & 0 & 1 \\ 0 & 0 & \alpha c_1 & \alpha d_1 & g_1 & h_1 & 1 \end{pmatrix}, \tag{3.4.11}$$

$$C_2|_{\epsilon_2=0} = \begin{pmatrix} a_2 & b_2 & 0 & 0 & c_2 & d_2 & 1 \\ \beta a_2 & \beta b_2 & g_2 & h_2 & 0 & 0 & 1 \end{pmatrix} \tag{3.4.12}$$

and

$$C_3|_{\epsilon_3=0} = \begin{pmatrix} a_3 & b_3 & 0 & 0 & c_3 & d_3 & 1 \\ 0 & 0 & e_3 & f_3 & \gamma c_3 & \gamma d_3 & 1 \end{pmatrix}. \tag{3.4.13}$$

In order to compare the three $C_i \in \mathrm{GR}(2,7)$, we must introduce a change of parameterization. Utilising the $GL(2)$ invariance, we make the following change of basis for C_2 and C_3,

$$C_2' = \begin{pmatrix} 0 & 1 \\ \frac{-\beta}{1-\beta} & \frac{1}{1-\beta} \end{pmatrix} C_2 \tag{3.4.14}$$

and

$$C_3' = \begin{pmatrix} \frac{-\gamma}{1-\gamma} & \frac{1}{1-\gamma} \\ 0 & 1 \end{pmatrix} C_3. \tag{3.4.15}$$

The three matrices C_1, C_2' and C_3' are now of the same form, meaning they have zeros and ones in the same entries and variables in the others:

$$C_2' = \begin{pmatrix} \beta a_2 & \beta b_2 & g_2 & h_2 & 0 & 0 & 1 \\ 0 & 0 & \frac{g_2}{1-\beta} & \frac{h_2}{1-\beta} & \frac{-\beta c_2}{1-\beta} & \frac{-\beta d_2}{1-\beta} & 1 \end{pmatrix}, \tag{3.4.16}$$

$$C_3' = \begin{pmatrix} \frac{-\gamma a_3}{1-\gamma} & \frac{-\gamma b_3}{1-\gamma} & \frac{e_3}{1-\gamma} & \frac{f_3}{1-\gamma} & 0 & 0 & 1 \\ 0 & 0 & e_3 & f_3 & \gamma c_3 & \gamma d_3 & 1 \end{pmatrix}. \tag{3.4.17}$$

We continue in a similar way to the simpler spurious pole discussed in Section 3.3.1 by comparing each entry in C_2' and C_3' directly to the equivalent entry in C_1. We make a change of variables for C_2' and C_3' to the variables of C_1 as dictated by matching entries:

$$C_2' : \quad \begin{matrix} a_2 \to \frac{\alpha}{\alpha-1} a_1 & b_2 \to \frac{\alpha}{\alpha-1} b_1 & g_2 \to c_1 \\ h_2 \to d_1 & c_2 \to \frac{1}{1-\alpha} g_1 & d_2 \to \frac{1}{1-\alpha} h_1 \end{matrix} \quad \beta \to \frac{-(1-\alpha)}{\alpha}, \tag{3.4.18}$$

$$C_3': \quad \begin{array}{lll} a_3 \to \frac{\alpha}{\alpha-1}a_1 & b_3 \to \frac{\alpha}{\alpha-1}b_1 & e_3 \to \alpha c_1 \\ f_3 \to \alpha d_1 & c_3 \to \frac{1}{1-\alpha}g_1 & d_3 \to \frac{1}{1-\alpha}h_1 \end{array} \quad \gamma \to 1-\alpha. \tag{3.4.19}$$

Substituting these new variables into the residues of $\mathcal{I}(\mathcal{D}_2)$ and $\mathcal{I}(\mathcal{D}_3)$ and taking the sum of all three integrals gives

$$\int \frac{\mathrm{d}a_1\,\mathrm{d}b_1\,\mathrm{d}c_1\,\mathrm{d}d_1 dg_1\,\mathrm{d}h_1\,\mathrm{d}\alpha}{a_1b_1c_1d_1g_1h_1}\left(\frac{1}{\alpha}+\frac{1}{1-\alpha}-\frac{1}{\alpha(1-\alpha)}\right)\delta^{(8|8)}\left(C_1\cdot\mathcal{Z}\right)=0. \tag{3.4.20}$$

Therefore, we have shown that (3.4.7) is satisfied.

It is worth emphasising here again that this calculation generalises to similar residues for all n. Furthermore, the propagator ends do not have to be spaced as symmetrically around the polygon as in Figure 3.7; the three way cancellation works in the same way for almost all sets of three edges that one could choose to have the propagators of the triplet of diagrams end on. There is, however, a special case when the propagator ends opposite to those coming together on the same edge sit on adjacent edges. For an example of such a diagram, see $\mathcal{D}_2'$ in Figure 3.8. The diagrams that one would naively expect to cancel

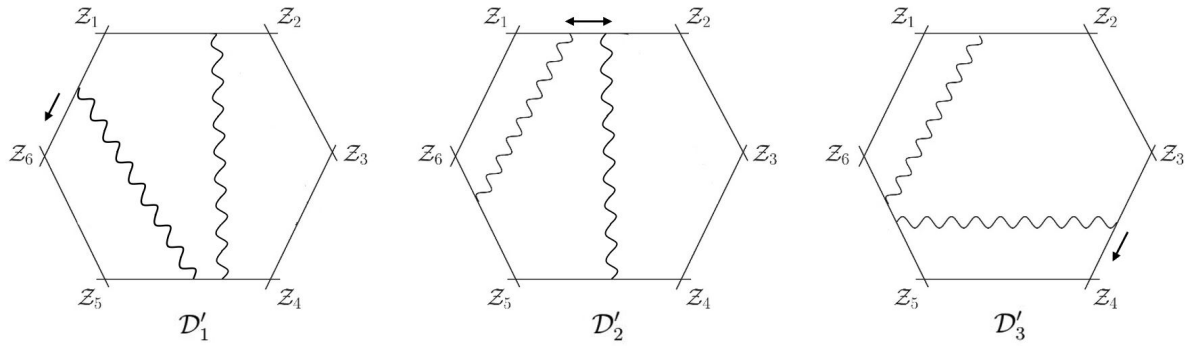

Figure 3.8: Three diagrams which when summed cancel the spurious poles illustrated by the arrows on each diagram. This is a special case of the three way cancellation.

with $\mathcal{D}_2'$ in a three-way cancellation would have a propagator between adjacent edges, which is zero. However, there does exist a different three-way cancellation involving $\mathcal{D}_1'$ and $\mathcal{D}_3'$ depicted in Figure 3.8 in the limits given by the arrows. We do not need to consider this special case to prove the mismatching of geometries of the N^2MHV WLDs

discussed in the next section, therefore we leave the proof of the spurious pole cancellation to Appendix A.

We now look to interpret the general three-way cancellation, (3.4.7), geometrically. Mapping the integrals to canonical forms via the rules discussed in section 3.2.2, we will see that there is a three-way pairwise matching of the corresponding spurious boundaries. However, we will show that there is no way to assign geometries to the canonical forms such that when glued together they are consistent with both the three-way cancellation and the simpler spurious pole cancellation discussed in section 3.3.1.

3.4.2 Spurious Boundary Matching for N^2MHV

To each N^2MHV WLD, we wish to associate a geometrical subspace of $\mathrm{Gr}(2,6)$ such then when glued together all spurious boundaries match pairwise (locally) with those of other diagrams. This may not be a sufficient condition to ensure a geometry with no spurious boundaries remaining, however it is necessary. The coordinates chosen in the previous section, for example (3.4.8), give a dlog form for the measure. Therefore, generalising from the NMHV case discussed in section 3.3.2, we expect assigning a geometry to a given WLD corresponds to making those coordinates real and assigning signs to them. Taking $\mathcal{D}_1$ in Figure 3.7 as an example and using the coordinates chosen in (3.4.8), one geometrical region (corresponding to one choice of signs) that can be associated to this canonical form is

$$\begin{gathered}\{Y = C_1.Z : a_1{>}0,\, b_1{>}0,\, d_1{>}0,\, e_1{>}0,\, g_1{>}0,\, h_1{>}0,\, \alpha > 0,\, \epsilon_1 > 0\} \\ = \\ \{Y = C_1.Z : a_1{>}0,\, b_1{>}0,\, c_1 > 0,\, d_1{>}0,\, e_1{>}0,\, g_1{>}0,\, h_1{>}0,\, f_1 c_1 > e_1 d_1\}\end{gathered} \tag{3.4.21}$$

with C_1 given in (3.4.4).

Perhaps unsurprisingly given previous discussion on the toy example and NMHV case, this region is not unique; other sign choices for the variables can be chosen to give another region with the same canonical form. There are sixteen allowed sets of sign choices

altogether. One must be careful here as the propagator ends that are on the same edge cannot cross; the geometrical region must respect this. The eight allowed possibilities for the parameters of these ends, c_1, d_1, e_1, f_1, can be seen in the following way. Choosing signs s_1, s_2 for d_1 and e_1 gives four of the possibilities immediately. However, we also require $(c_1 f_1 - e_1 d_1) > 0$: this splits each of the four cases into two disconnected regions given by $c_1, f_1 > 0$ and $c_1, f_1 < 0$, giving the expected total of eight cases. These cases can also be read off directly from the parametrisation of the WLD if one considers the parameters being real instead of complex. For the ends not to cross we need either $0 < \frac{d_1}{c_1} < \frac{f_1}{e_1}$ or $0 < \frac{e_1}{f_1} < \frac{c_1}{d_1}$. Choosing signs for d_1, e_1 gives the same eight cases as above.

In order to start our investigation of a possible geometrical region of N^2MHV WLDs, we look to the geometric interpretation of the three way cancellation described in the previous section to give some insight. To do this, we compare the C matrices in the appropriate limit after they have been rotated to match entries with each other, i.e. C_1, C_2', C_3', given by

$$C_1|_{\epsilon_1=0} = \begin{pmatrix} a_1 & b_1 & c_1 & d_1 & 0 & 0 & 1 \\ 0 & 0 & \alpha c_1 & \alpha d_1 & g_1 & h_1 & 1 \end{pmatrix} \tag{3.4.22}$$

$$C_2'|_{\epsilon_2=0} = \begin{pmatrix} \beta a_2 & \beta b_2 & g_2 & h_2 & 0 & 0 & 1 \\ 0 & 0 & \frac{g_2}{1-\beta} & \frac{h_2}{1-\beta} & \frac{-\beta c_2}{1-\beta} & \frac{-\beta d_2}{1-\beta} & 1 \end{pmatrix} \tag{3.4.23}$$

$$C_3'|_{\epsilon_3=0} = \begin{pmatrix} \frac{-\gamma a_3}{1-\gamma} & \frac{-\gamma b_3}{1-\gamma} & \frac{e_3}{1-\gamma} & \frac{f_3}{1-\gamma} & 0 & 0 & 1 \\ 0 & 0 & e_3 & f_3 & \gamma c_3 & \gamma d_3 & 1 \end{pmatrix} . \tag{3.4.24}$$

We have $\alpha = \frac{1}{1-\beta}$ and $\alpha = 1 - \gamma$ at points where the regions touch. Using this as motivation, we choose signs (positive or negative) for α, β and γ such that locally α, $\beta(\alpha)$ and $\gamma(\alpha)$ share boundaries pairwise. There are two different cases that arise from this consideration:

1. One of the variables is positive and the other two negative. Without loss of generality we consider $\alpha > 0$, $\beta, \gamma < 0$.

2. α, β and γ are all positive.

The two cases are illustrated in Figure 3.9.

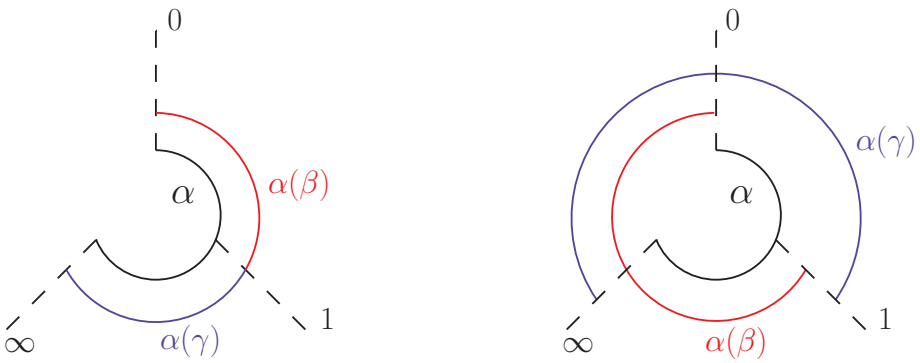

Figure 3.9: The two possibilities for three way boundary matching. We plot the range of α on a circle from $[-\infty, \infty]$ passing through 0 and 1. Black is the range of α in diagram D1, in red that of $\alpha(\beta)$ in D_2 and in blue the range of $\alpha(\gamma)$ in D_3. We see there is always a local pairwise matching of the three diagrams in both cases. In Case 1 D2 and D3 each only overlap with D1 and not with each other. For Case 2 all diagrams overlap the other two.

We look to examine both of these cases separately. Though the considerations will continue in slightly different ways, we will see the end result is the same for both; there is no way to match spurious boundaries for the three-way cancellation that is consistent with other spurious boundary matching (similar to those dealt with in Section 3.3.1) and gives a geometrical region with no spurious boundaries left unmatched when all tiles given by the WLDs are glued together.

Case 1: $\alpha > 0$**,** $\beta < 0$ **and** $\gamma < 0$

Looking at Figure 3.9a, C_1 and C_2' should overlap when $0 < \alpha < 1$ whereas C_1 and C_3' should overlap when $1 < \alpha < \infty$. At the points where the regions overlap we also need all other variables to match; in particular, this fixes the signs of the variables for the second two diagrams in terms of the first. Defining

$$\mathrm{sgn}(a_1) = s_1, \quad \mathrm{sgn}(b_1) = s_2, \quad \mathrm{sgn}(c_1) = s_3,$$

$$\text{sgn}(d_1) = s_4, \quad \text{sgn}(g_1) = s_5, \quad \text{sgn}(h_1) = s_6, \tag{3.4.25}$$

and comparing (3.4.23) and (3.4.24) to (3.4.22), we end up with a matrix of signs for C_2' and C_3':

$$\text{sgn}(C_2')|_{\epsilon_2=0} = \begin{pmatrix} -s_1 & -s_2 & s_3 & s_4 & 0 & 0 & 1 \\ 0 & 0 & s_3 & s_4 & s_5 & s_6 & 1 \end{pmatrix}, \tag{3.4.26}$$

$$\text{sgn}(C_3')|_{\epsilon_3=0} = \begin{pmatrix} s_1 & s_2 & s_3 & s_4 & 0 & 0 & 1 \\ 0 & 0 & s_3 & s_4 & -s_5 & -s_6 & 1 \end{pmatrix}. \tag{3.4.27}$$

Undoing the $GL(2)$ transformations, we end up with matrices giving signs for each entry of the original C matrices:

$$\text{sgn}(C_1)|_{\epsilon_1=0} = \begin{pmatrix} s_1 & s_2 & s_3 & s_4 & 0 & 0 & 1 \\ 0 & 0 & s_3 & s_4 & s_5 & s_6 & 1 \end{pmatrix}, \tag{3.4.28}$$

$$\text{sgn}(C_2)|_{\epsilon_2=0} = \begin{pmatrix} -s_1 & -s_2 & 0 & 0 & s_5 & s_6 & 1 \\ s_1 & s_2 & s_3 & s_4 & 0 & 0 & 1 \end{pmatrix}, \tag{3.4.29}$$

$$\text{sgn}(C_3)|_{\epsilon_3=0} = \begin{pmatrix} s_1 & s_2 & 0 & 0 & -s_5 & -s_6 & 1 \\ 0 & 0 & s_3 & s_4 & s_5 & s_6 & 1 \end{pmatrix}. \tag{3.4.30}$$

Given a set of signs for C_1, the three way cancellation fixes the signs of all entries of C_2 and C_3 for this choice of signs for α, β and γ. Crucially, despite the signs being derived by looking at their values at the spurious boundary, the signs remain unchanged inside the region away from the boundary. The only subtlety occurs with those entries depending on ϵ_i. We look to $\mathcal{D}_1$ in Figure 3.7 to illustrate this subtlety, with corresponding matrix (3.4.22).

In dealing with the three way cancellation above, we fixed signs for all variables of C_1 except for ϵ_1, as it was set to zero in the limit of the propagator ends coming together. However, away from this boundary its sign must be taken into account. In order to assign a geometrical region to this WLD, that has a canonical form given by the dlog form in the first line of (3.4.8), we must have a definite sign for ϵ_1. Letting $s_{\epsilon_1} = \pm 1$ be the sign

of ϵ_1, we focus on the entries of C_1 corresponding to the side with two propagator ends on it, away from the boundary but still using the information from the three way boundary matching considered above:

$$\left(\boldsymbol{c_1^3, c_1^4}\right) = \begin{pmatrix} c_1 & d_1 \\ e_1 & f_1 \end{pmatrix} = \begin{pmatrix} s_3 c_1' & s_4 d_1' \\ s_3 \alpha c_1' & s_4 \alpha d_1' + s_{\epsilon_1} \epsilon_1' \end{pmatrix}. \tag{3.4.31}$$

Note that here $c_1', d_1', \epsilon_1' > 0$, $s_3 c_1' = c_1$, $s_4 d_1' = d_1$, $\epsilon_1 = s_{\epsilon_1}\epsilon_1'$ and we still have $\alpha > 0$ as dictated by the three way spurious boundary matching. There are two possibilities to consider,

$$s_{\epsilon_1} = s_4 : \quad \operatorname{sgn}\left(\left(\boldsymbol{c_1^3, c_1^4}\right)\right) = \begin{pmatrix} s_3 & s_4 \\ s_3 & s_4 \end{pmatrix}, \tag{3.4.32}$$

$$s_{\epsilon_1} = -s_4 : \quad \operatorname{sgn}\left(\left(\boldsymbol{c_1^3, c_1^4}\right)\right) = \begin{cases} \begin{pmatrix} s_3 & s_4 \\ s_3 & s_4 \end{pmatrix} & \epsilon_1' < \alpha' d_1' \\ \begin{pmatrix} s_3 & s_4 \\ s_3 & -s_4 \end{pmatrix} & \epsilon_1' > \alpha' d_1'. \end{cases} \tag{3.4.33}$$

From the discussion under (3.4.21), we saw that the condition $(c_1 f_1 - e_1 d_1) > 0$ put certain constraints on what the signs of c_1, d_1, e_1 and f_1 could be. In particular, there were eight cases that satisfied this condition. Additionally, this case of the three way cancellation, with $\alpha > 0$, determined that c_1 and e_1 had to be the same sign. The matrices of signs which satisfy both conditions are

$$\begin{pmatrix} s & s \\ s & s \end{pmatrix}, \quad \begin{pmatrix} s & -s \\ s & s \end{pmatrix} \tag{3.4.34}$$

with $s = \pm 1$.[4] Relating s_3 and s_4 in (3.4.32) and (3.4.33) splits the two possibilities for

[4] These matrices give four out of eight of the cases which satisfy $(c_1 f_1 - e_1 d_1) > 0$. The other four are $\begin{pmatrix} s & s \\ -s & s \end{pmatrix}$ and $\begin{pmatrix} s & -s \\ -s & s \end{pmatrix}$ for $s = \pm 1$.

sgn $\left(\left(\boldsymbol{c_1^3}, \boldsymbol{c_1^4}\right)\right)$ into another two, for four in total:

$$s_{\epsilon_1} = s_4 = s_3 : \begin{pmatrix} s_3 & s_3 \\ s_3 & s_3 \end{pmatrix}, \quad s_{\epsilon_1} = -s_4 = -s_3 : \begin{cases} \begin{pmatrix} s_3 & s_3 \\ s_3 & s_3 \end{pmatrix} & \epsilon_1 < \alpha d_1 \\ \begin{pmatrix} s_3 & s_3 \\ s_3 & -s_3 \end{pmatrix} & \epsilon_1 > \alpha d_1, \end{cases} \tag{3.4.35}$$

$$s_{\epsilon_1} = s_4 = -s_3 : \begin{pmatrix} s_3 & -s_3 \\ s_3 & -s_3 \end{pmatrix}, \quad s_{\epsilon_1} = -s_4 = s_3 : \begin{cases} \begin{pmatrix} s_3 & -s_3 \\ s_3 & -s_3 \end{pmatrix} & \epsilon_1 < \alpha d_1 \\ \begin{pmatrix} s_3 & -s_3 \\ s_3 & s_3 \end{pmatrix} & \epsilon_1 > \alpha d_1. \end{cases}$$

The matrices coloured red do not match either of the cases in (3.4.34), therefore are not consistent with $(c_1 f_1 - e_1 d_1) > 0$. Each variable associated to the diagram $\mathcal{D}_1$ must have a definite sign to give a geometry that has the dlog form (3.4.8) as its canonical form, therefore $s_{\epsilon_1} = -s_4 = s_3$ and $s_{\epsilon_1} = -s_4 = -s_3$ are not viable as they do not satisfy the necessary conditions for the whole region of the chosen sign for ϵ_1. We also do not obtain a valid set of signs for $s_{\epsilon_1} = s_4 = -s_3$, therefore not only do we find that $s_{\epsilon_1} = s_4$, but also $s_4 = s_3$.

Similar considerations can be applied to C_2 and C_3 to find out valid sign choices away from the spurious boundary associated to the three way cancellation. For C_2, we look in particular to columns one and two:

$$\left(\boldsymbol{c_2^1}, \boldsymbol{c_2^2}\right) = \begin{pmatrix} a_2 & b_2 \\ e_2 & f_2 \end{pmatrix} = \begin{pmatrix} -s_1 a_2' & -s_2 b_1' \\ s_1 \beta' a_1' & s_2 \beta' b_1' + s_{\epsilon_2} \epsilon_2' \end{pmatrix}. \tag{3.4.36}$$

Similarly to (3.4.35), the four cases relating s_{ϵ_2}, s_1 and s_2 for C_2 are given by

$$s_{\epsilon_2}=s_2=s_1:\ \begin{pmatrix}-s_1 & -s_1\\ s_1 & s_1\end{pmatrix},\qquad s_{\epsilon_2}=-s_2=-s_1:\ \begin{cases}\begin{pmatrix}-s_1 & -s_1\\ s_1 & s_1\end{pmatrix} & \epsilon_2'<\beta' b_2'\\ \begin{pmatrix}-s_1 & -s_1\\ s_1 & -s_1\end{pmatrix} & \epsilon_2'>\beta' b_2',\end{cases}$$

$$s_{\epsilon_2}=s_2=-s_1:\ \begin{pmatrix}-s_1 & s_1\\ s_1 & -s_1\end{pmatrix},\qquad s_{\epsilon_2}=-s_2=s_1:\ \begin{cases}\begin{pmatrix}-s_1 & s_1\\ s_1 & -s_1\end{pmatrix} & \epsilon_2'<\beta' b_2'\\ \begin{pmatrix}-s_1 & s_1\\ s_1 & s_1\end{pmatrix} & \epsilon_2'>\beta' b_2'.\end{cases} \tag{3.4.37}$$

Comparing to the valid sign choices given in (3.4.34) and footnote 4, the red matrices in (3.4.37) do not satisfy $a_2f_2-b_2e_2>0$. Therefore, for ϵ_2 to be valid in the whole region of its chosen sign we must have $s_{\epsilon_2}=s_2=-s_1$.

Finally, for C_3 we concentrate on columns five and six:

$$\left(\boldsymbol{c_3^5},\boldsymbol{c_3^6}\right)=\begin{pmatrix}c_3 & d_3\\ g_3 & h_3\end{pmatrix}=\begin{pmatrix}-s_5c_3' & -s_6d_3'\\ s_5\gamma' g_3'+s_{\epsilon_3}\epsilon_3' & s_6\gamma' h_3'\end{pmatrix}. \tag{3.4.38}$$

The four cases relating s_{ϵ_3}, s_5 and s_6 for C_3 are given by

$$s_{\epsilon_3} = s_5 = s_6 : \begin{pmatrix} -s_5 & -s_5 \\ s_5 & s_5 \end{pmatrix}, \quad s_{\epsilon_3} = -s_5 = -s_6 : \begin{cases} \begin{pmatrix} -s_5 & -s_5 \\ s_5 & s_5 \end{pmatrix} & \epsilon_3' < \gamma' g_3' \\ \begin{pmatrix} -s_5 & -s_5 \\ -s_5 & s_5 \end{pmatrix} & \epsilon_3' > \gamma' g_3', \end{cases}$$

$$s_{\epsilon_3} = s_5 = -s_6 : \begin{pmatrix} -s_5 & s_5 \\ s_5 & -s_5 \end{pmatrix}, \quad s_{\epsilon_3} = -s_5 = s_6 : \begin{cases} \begin{pmatrix} -s_5 & s_5 \\ s_5 & -s_5 \end{pmatrix} & \epsilon_3' < \gamma' g_3' \\ \begin{pmatrix} -s_5 & s_5 \\ -s_5 & -s_5 \end{pmatrix} & \epsilon_3' > \gamma' g_3'. \end{cases} \tag{3.4.39}$$

For this case, we must have $d_3 g_3 > c_3 h_3$ for the propagator ends not to cross in $\mathcal{D}_3$, so the valid sets of signs are given by (3.4.34) and footnote 4 with the two columns swapped. Therefore, for ϵ_3 to be valid in the whole region of its chosen sign we must have $s_{\epsilon_3} = s_5 = -s_6$.

Substituting the three conditions found above,

$$s_{\epsilon_1} = s_4 = s_3, \quad s_{\epsilon_2} = s_2 = -s_1, \quad s_{\epsilon_3} = s_5 = -s_6, \tag{3.4.40}$$

into $\mathrm{sgn}(C_i)$, (3.4.28) - (3.4.30), leaves

$$\mathrm{sgn}(C_1) = \begin{pmatrix} s_1 & -s_1 & s_3 & s_3 & 0 & 0 & 1 \\ 0 & 0 & s_3 & s_3 & s_5 & -s_5 & 1 \end{pmatrix} \tag{3.4.41}$$

$$\mathrm{sgn}(C_2) = \begin{pmatrix} -s_1 & s_1 & 0 & 0 & s_5 & -s_5 & 1 \\ s_1 & -s_1 & s_3 & s_3 & 0 & 0 & 1 \end{pmatrix} \tag{3.4.42}$$

$$\mathrm{sgn}(C_3) = \begin{pmatrix} s_1 & -s_1 & 0 & 0 & -s_5 & s_5 & 1 \\ 0 & 0 & s_3 & s_3 & s_5 & -s_5 & 1 \end{pmatrix}. \tag{3.4.43}$$

These matrices give sets of signs for C_i relating to the WLDs in Figure 3.7 that are consistent with the matching of the spurious boundary associated to case 1 of the three-way cancellation, while ensuring that the propagators do not cross each other. These signs are valid not only on the boundary, but also away from it.

Now, we look to see if the sign choices for $\mathcal{D}_1, \mathcal{D}_2, \mathcal{D}_3$ are consistent with the consecutive matching of the other type of spurious boundary occurring when propagator ends approach vertices. We will see that the set of signs is in fact not consistent; the problem comes down to the difference in signs in the top row of (3.4.42) to those in the top row of (3.4.43).

Consider starting with diagram $\mathcal{D}_2$ in Figure 3.8 and moving the propagator defined by the second line in C_2 around the Wilson loop clockwise until it reaches a diagram equivalent to $\mathcal{D}_3$. We match spurious boundaries in a similar way to section 3.3.2; at each vertex, the whole matrix of signs in the relevant limit must match. The signs of the top row, corresponding to the propagator left fixed, must remain the same. Under this sequence of moves we get

$$\mathrm{sgn}(C_2) \to \begin{pmatrix} -s_1 & s_1 & 0 & 0 & s_5 & -s_5 & 1 \\ 0 & 0 & s_3' & s_4' & s_5' & s_6' & 1 \end{pmatrix}, \tag{3.4.44}$$

where the primed variables here represent new signs not yet fixed in the process. [5]

Comparing this new matrix to $\mathrm{sgn}(C_3)$, (3.4.43), one can see immediately that the signs on the top row are different regardless of what the primed signs in the bottom row become. Therefore, the signs found from the matching of the three-way spurious boundary are not consistent with the mathcing of the boundaries obtained by following the propagators round the Wilson loop polygon. The WLDs cannot be glued together to form a geometry without spurious boundaries with this choice of α, β and γ.

[5] In fact, we do also require $s_3' = s_3$ and $s_4' = s_3$ by the pairwise matching of consecutive spurious boundaries. However, this is not necessary for the continuation of the argument.

Case 2: $\alpha, \beta, \gamma > 0$

We now consider the second possibility for having pairwise matching boundaries, illustrated on the right hand side of Figure 3.9, with $\alpha, \beta, \gamma > 0$. Looking at the Figure, C_1 and C_2' should overlap when $1 < \alpha < \infty$ and $0 < \beta < 1$ and C_1 and C_3' should overlap when $0 < \alpha < 1$ and $0 < \gamma < 1$. Now there is an additional overlap between C_2' and C_3' when $1 < \beta < \infty$ and $1 < \gamma < \infty$.

At these overlaps, the entries of the rotated matrices (3.4.22-3.4.24) must be equal. Defining the signs of the C_1 variables as previously, (3.4.25), this means the signs of the entries of C_2' and C_3', must be the same as those of C_1 in the region where they overlap with C_1 (i.e. $0 < \beta < 1$, $0 < \gamma < 1$). However when $\beta, \gamma > 1$ some of the entries changes sign due their dependence on β or γ. Thus the signs of the entries of the rotated C matrices are as follows:

$$\mathrm{sgn}(C_1) : \begin{pmatrix} s_1 & s_2 & s_3 & s_4 & 0 & 0 & 1 \\ 0 & 0 & s_3 & s_4 & s_5 & s_6 & 1 \end{pmatrix}_{0<\alpha<\infty} \tag{3.4.45}$$

$$\mathrm{sgn}(C_2') : \begin{pmatrix} s_1 & s_2 & s_3 & s_4 & 0 & 0 & 1 \\ 0 & 0 & s_3 & s_4 & s_5 & s_6 & 1 \end{pmatrix}_{0<\beta<1}, \begin{pmatrix} s_1 & s_2 & s_3 & s_4 & 0 & 0 & 1 \\ 0 & 0 & -s_3 & -s_4 & -s_5 & -s_6 & 1 \end{pmatrix}_{1<\beta<\infty} \tag{3.4.46}$$

$$\mathrm{sgn}(C_3') : \begin{pmatrix} s_1 & s_2 & s_3 & s_4 & 0 & 0 & 1 \\ 0 & 0 & s_3 & s_4 & s_5 & s_6 & 1 \end{pmatrix}_{0<\gamma<1}, \begin{pmatrix} -s_1 & -s_2 & -s_3 & -s_4 & 0 & 0 & 1 \\ 0 & 0 & s_3 & s_4 & s_5 & s_6 & 1 \end{pmatrix}_{1<\gamma<\infty}. \tag{3.4.47}$$

Now, even before rotating C_2' and C_3' back, there is a clear problem. Looking at the matrices in 3.4.46 and 3.4.47 for $1 < \beta < \infty$ and $1 < \gamma < \infty$, the matrices do not overlap as they should. Matching diagram $\mathcal{D}_2$ with $\mathcal{D}_1$ correctly and $\mathcal{D}_3$ with $\mathcal{D}_1$ correctly fixes the signs of the respective C matrices in a way that is incompatible with $\mathcal{D}_2$ and $\mathcal{D}_3$ matching.

Therefore, there is no valid three way boundary matching for this case.

3.5 Concluding Remarks

We have shown that it is not possible to consistently assign a subspace of $\mathrm{Gr}(k, k+4)$, amplituhedron space, to each WLD consistent with its canonical form and pairwise matching of all spurious boundaries. Therefore, WLDs cannot be used to tessellate the amplituhedron, or in fact any other subspace, without spurious boundaries. This is somewhat surprising since they do have certain properties which seem promising: WLDs do have a natural, though non-unique, interpretation as subspaces in $\mathrm{Gr}(k, k+4)$ and they do sum to give the amplitude. The situation is similar to the toy example shown in Figure 3.1 where region I and II clearly have canonical forms which sum to give the quadrilateral with no spurious poles, but there are spurious boundaries left unmatched in the corresponding geometrical interpretation. For the simple example of the quadrilateral we could of course choose a more sensible set of signs to give a tessellation of the quadrilateral with no spurious boundaries left, but we have shown that for the N^2MHV WLDs and beyond this is not possible.

Despite only showing this for the N^2 MHV case, it is quite clear that the proof holds for higher helicity. One simply needs to add the extra propagators away from the three way cancellation and recycle the same argument as given here. As stated before, showing this for six points was only to easily illustrate some examples - the argument clearly holds for any number of particles. Furthermore, although we have focussed only on tree level here, it would be very surprising if the situation improved when moving to loop level.

One might hope that although the WLDs do not tessellate the amplituhedron that they may instead give a nice tessellation of the squared amplituhedron [75, 88] which has a more direct definition and for which there are 2^k copies of most diagrams. However, having attempted to make this consistent it does not seem to be the case.

Although the WLDs cannot provide a tessellation of the amplituhedron, they do still give a very concrete and suggestive "tessellation" at the level of the canonical form. It seems likely that this property generalises for more positive Grassmannians, and may prove

useful in their further mathematical study. Despite not giving a "good geometrical region" it may still be interesting to further understand the WLDs geometrically; studies in this direction have begun, see for example [102, 103].

Chapter 4

Single Particle Operators in $N = 4$ Super Yang-Mills

4.1 Introduction

The AdS/CFT correspondence, originally conjectured by Maldacena, describes a remarkable relationship between two sets of theories; on one side are the theories of quantum gravity formulated in terms of string theory, and on the other side are a type of quantum theory known as conformal field theories [1–3]. Perhaps the most noted successful confirmation of the correspondence is the relationship between the half-BPS sector of $N = 4$ SYM in four dimensions and IIB string theory on $AdS_5 \times S^5$. String states in the latter theory are related to gauge invariant operators in the former and AdS amplitudes are related to correlators of gauge invariant operators. Half-BPS operators are particularly interesting as their quantum numbers are not renormalised, and certain (extremal) correlators are protected from renormalisation. Therefore, they can be computed in the free theory then taken trivially to strong coupling. These correlation functions at large N can then be compared to a gravitational equivalent via the AdS/CFT correspondence (see for example [104–107]).

The correspondence has been used to reconstruct information on strong 't Hooft coupling

phenomena in gauge theory from semiclassical physics in AdS. For example, the operators dual to single particle operators, which will be the main focus of this chapter, are expected to vanish as the charge of the operator exceeds the number of colours N. From the gravity side, as the angular momentum of a particle moving on the S^5 increases, the point-like graviton expands into a D3-brane wrapping an $S^3 \subset S^5$, [108] which cannot grow bigger than the size of the S^5. This is the basis of the stringy exclusion principle (originally proposed in [109], see for example [110, 111] for further discussion). More recently, the correspondence has been used successfully in the other direction; analytic bootstrap techniques on the CFT side at strong coupling have allowed for more concrete investigations of perturbative quantum gravity. For example, one-loop quantum gravity amplitudes in AdS have been obtained by computing $O\left(\frac{1}{N^4}\right)$ corrections to strong coupling correlators in SYM [112–116].

In order for these investigations to be precise, and to properly account for the operator product expansion (OPE) at tree level and one loop, it was necessary for the gauge theory operators dual to single-particle supergravity states to be defined carefully. These operators are half-BPS operators, therefore are protected. However, due to the degenerate nature of the space of half-BPS operators, only in the planar limit can single particle operators be identified as the well known single-trace operators $\mathrm{Tr}\,(\phi^p)$, where p is the charge (these will be introduced in more detail below). The single trace operators were already known to receive $O\left(\frac{1}{N}\right)$ corrections from multi-trace operators [117–119]; in fact, the first order double trace corrections have recently been worked out directly from supergravity [120, 121]. However, the non-perturbative natrue of the AdS/CFT correspondence heavily indicates that a non-perturbative definition should exist for the states dual to single particles, i.e. one which remains valid for all N. Such a definition was formulated in [122]:

> *Single-particle operators are half-BPS operators which have vanishing two-point functions with all multi-trace operators.*

(4.1.1)

Up to normalisation, the above definition fixes the single particle operators uniquely as a sum of the single trace operator and multi-trace operators with pre-factors dependent on N. This definition of the operator has already been necessary for correctly determining the one-loop $O\left(\frac{1}{N^4}\right)$ supergravity correlators of operators with charges higher than four. For example, arbitrary charge correlators in position space were studied in [115] and $\langle 22pp\rangle$ correlators were calculated in Mellin space in [116].

The purpose of this chapter is to explore the properties of the single particle operators defined above, find explicit formulae for them and calculate various correlation functions involving them. We will begin by introducing the trace basis, as well as some properties of half-BPS operators in $N = 4$ SYM. We will then proceed to introduce two more bases of half-BPS operators, the dual basis and the schur polynomial basis, both of which we will refer to when writing an explicit formula for our single-particle operators. This will act as a brief review of concepts required to understand the rest of the chapter, and allow us to set up notation.

4.1.1 Half-BPS Operators in $N = 4$ SYM and the Trace Basis

Here, we will very briefly review some properties of half-BPS operators in $N = 4$ SYM. For a more thorough description see [4] and the references therein.

The half-BPS operators are built from the 6 real scalars, X_i, in the Yang-Mills theory which lie in the $(0, l, 0)$ representations of the $SU(4) \sim SO(6)$ $\mathcal{R}$-symmetry group. These are the symmetric traceless representations of $SO(6)$ that correspond to Young diagrams with one row of length l. They include single trace operators, where the trace is taken over the gauge indices of a tensor product of the real scalars, and products of these forming multi-trace operators. The $\frac{1}{2}$-BPS stress-tensor supermultiplet contains the protected half-BPS operators $\mathrm{Tr}(\phi^2)$, the stress tensor and the (on-shell) chiral Lagrangian of the theory.

In order to make sense of these operators, it is useful to introduce the $SO(6) \sim SU(4)$

null auxiliary variables Y_R, where null enforces $Y \cdot Y = 0$ and $R = 1, \ldots, 6$. The R-index coincides with the $SO(6)$ R-symmetry index. The single trace operators are then defined as follows;

$$T_p(x) = \mathrm{Tr}\, \phi(x)^p \qquad ; \qquad \phi(X, Y) = Y^R \phi_R(X), \tag{4.1.2}$$

where the variables Y^R have been used to project the elementary field ϕ_R onto the symmetric traceless representation. Therefore, a single insertion point x_i corresponds not only to a space-time coordinate X_i, but also an $SO(6)$ vector Y^R.

In this chapter, the $U(N)$ theory will be particularly useful due to its simplicity, however the bulk AdS theory is describing the $SU(N)$ part of the theory.[1] When working with the $SU(N)$ gauge group, we will denote the scalar field as $\psi(x) \equiv \psi(X, Y) = Y^R \psi_R(X)$, where now the Y^R are traceless.

To compute correlation functions in free field theory we use elementary propagators. The conformal structure of the theory dictates that the two point function of two scalar fields is given by

$$\langle \phi_a(x) \phi_b(y) \rangle = \frac{g_{ab}}{(x-y)^2}, \tag{4.1.3}$$

where the indices a, b run over the adjoint representation of the gauge group and g_{ab} is the inverse of $g^{ab} = \mathrm{Tr}\left(Y^a Y^b\right)$, the bilinear invariant. For the rest of the chapter we will only be interested in the group structure of the correlator, therefore we will drop the spacetime dependence. Taking the gauge group to be $U(N)$ or $SU(N)$, the propagator takes the form

$$\langle \phi_r^s(X_1, Y_1) \phi_t^u(X_2, Y_2) \rangle = \delta_r^u \delta_t^s g_{12} \qquad U(N) \tag{4.1.4}$$

$$\langle \psi_r^s(X_1, Y_1) \psi_t^u(X_2, Y_2) \rangle = \left(\delta_r^u \delta_t^s - \frac{1}{N} \delta_r^s \delta_t^u\right) g_{12} \qquad SU(N), \tag{4.1.5}$$

[1] A $U(N)$ gauge theory is equivalent to a free $U(1)$ vector multiplet times an $SU(N)$ gauge theory up to Z_N identifications. It was shown in [123] that the $U(1)$ part of the gauge group is a singleton field related to the centre of mass motion of the branes (the interested reader is encouraged to see [124] and the references therein.

where

$$g_{12} = \frac{Y_1 \cdot Y_2}{(X_1 - X_2)^2} \tag{4.1.6}$$

The correlators above can be related by substituting $\psi_r^s = \phi_r^s - \delta_r^s \phi_t^t / N$, into (4.1.5), giving

$$\langle \psi_r^s \psi_u^v \rangle = \left\langle \left(\phi_r^s - \delta_r^s \phi_t^t / N\right) \left(\phi_u^v - \delta_u^v \phi_w^w / N\right) \right\rangle = \delta_u^s \delta_r^v - \frac{1}{N} \delta_r^s \delta_u^v. \tag{4.1.7}$$

We will use the following notation to denote the single trace operator of charge p:

$$U(N): \quad T_p(x) \equiv \mathrm{Tr}\left(\phi(x)^p\right) \qquad SU(N): \quad T_p(x) \equiv \mathrm{Tr}\left(\psi(x)^p\right), \tag{4.1.8}$$

where the gauge group will be specified if it is not obvious from the context. It is worth highlighting that for the $SU(N)$ gauge group the field is traceless therefore there does not exist a single trace operator for $p = 1$. In addition to the single-trace operators T_p we obtain half-BPS operators from products of the form

$$T_{p_1 \ldots p_m}(x) \equiv T_{p_1}(x) \ldots T_{p_m}(x), \qquad p_1 \geq \ldots \geq p_m \geq 1. \tag{4.1.9}$$

The scaling dimension of the multi-trace operator $T_{p_1 \ldots p_m}$ is given by $(p_1 + \ldots + p_m)$. Of course, for the case of $m = 1$ reduces to the single trace operator.

We can write these operators using permutations of the symmetric group S_n.

T_1^5	(e)
$T_2 T_1^3$	(12)
$T_2^2 T_1$	$(12)(34)$
$T_3 T_1^2$	(123)
$T_3 T_2$	$(123)(45)$
$T_4 T_1$	(1234)
T_5	(12345)

Table 4.1: Table showing the 1/2-BPS operators of weight 5 in the trace basis for a $U(N)$ gauge group on the left, with a representative of the conjugacy class each corresponds to on the right. For $SU(N)$ the field is traceless, therefore only $T_3 T_2$ and T_5 survive.

Taking the set of weight five operators as an example and letting $\sigma \in S_5$, with $p_1, \ldots, p_m$ denoting the lengths of the cycles of σ ($\sum_{i=1}^{m} p_i = 5$),we write

$$\mathrm{Tr}\,(\sigma\phi(x)) \equiv T_{p_1,\ldots,p_m}(x) \equiv \phi^{i_1}_{i_{\sigma(1)}}\phi^{i_2}_{i_{\sigma(2)}}\phi^{i_3}_{i_{\sigma(3)}}\phi^{i_4}_{i_{\sigma(4)}}\phi^{i_5}_{i_{\sigma(5)}}. \tag{4.1.10}$$

For example, if $\sigma = (12)(345)$ we get the operator

$$\phi^{i_1}_{i_2}\phi^{i_2}_{i_1}\phi^{i_3}_{i_4}\phi^{i_4}_{i_5}\phi^{i_5}_{i_3} = T_3T_2 \tag{4.1.11}$$

One can see that the trace structure is only dependent on the cycle structure of the permutations; for example, the permutation (12)(345) gives the same trace structure as (14)(235). Therefore, the multi-trace operators in the $U(N)$ gauge theory are in one-to-one correspondence with the conjugacy classes of the permutation group S_n. Table 4.1 shows the correspondence between multi-trace operators of weight 5 and the conjugacy classes of S_5.

Since the fields ψ are traceless, the correspondence for the $SU(N)$ gauge theory is between multi-trace operators and conjugacy classes of S_n with no cycles of length 1, e.g. for the weight 5 example above there is an operator corresponding to the conjugacy class with elements (12)(345) and (12345) (see Table 4.1). Letting $p(n)$ denote the number of conjugacy classes of S_n, the number of conjugacy classes that do not contain a 1-cycle is $p(n) - p(n-1)$, since each element with a 1-cycle can be decomposed into a 1-cycle and an element of S_{n-1}.

We refer to the basis of half-BPS operators made of all possible $T_{p_1\ldots p_m}(x)$ as the *trace basis*, and for the remainder of the chapter will denote the basis elements with the symbol $T_{\underline{p}}$, where $\underline{p}$ stands for a partition of p. A correlation function of operators in the trace basis will have the schematic form

$$\langle T_{\underline{p_1}}(x_1)\ldots T_{\underline{p_n}}(x_n)\rangle = \sum_{\{b_{ij}\}}\prod_{i,j} g_{ij}^{b_{ij}}\ \mathcal{C}_{\{b_{ij}\},\underline{p_1}\ldots\underline{p_n}}(N), \tag{4.1.12}$$

where b_{ij} counts the number of propagators from insertion point i to j, and $\{b_{ij}\}_{i<j}$ is the collection of these bridges labelling the propagator structure. The corresponding colour

factor is given by $\mathcal{C}_{\{b_{ij}\},\underline{p_1}\ldots\underline{p_n}}(N)$.

4.1.2 Other Bases of Half-BPS Operators

Other than the trace basis, there are two other bases of the half-BPS operators that will be useful to be familiar with; the schur basis and the dual basis. Here we give the definition of these two bases, we state group theoretic formulae for them and illustrate some of their basic properties.

Schur Basis

A beautiful orthogonal basis for all half-BPS operators in the $U(N)$ theory was given in [125] in terms of Schur polynomials, where by orthogonal we mean the operators diagonalise the two point function.

The Schur polynomial basis is defined as a sum of the trace basis operators discussed in section 4.1.1 over the elements $\sigma_{p_1\ldots p_m} \in S_p$, weighted by the characters of $\sigma_{p_1\ldots p_m}$ in the representation R of S_p

$$\chi_R(\phi) = \frac{1}{n!}\sum_{\sigma\in S_p}\chi_R(\sigma)\,\mathrm{Tr}\,(\sigma\phi)\,. \tag{4.1.13}$$

As mentioned in section 2.4.3, the representations R of S_p can be labelled by Young diagrams with p boxes. Therefore, the operators in the Schur polynomial basis can also be represented by these Young diagrams. Therefore, the number of Schur polynomials of weight p is equal to the number of partitions of p. The representation R also corresponds to a representation of $U(N)$.[2] For a unitary matrix U, the character of U in representation R is given by $\chi_R(U)$ defined by (4.1.13).

The correlation function of two Schur polynomials calculated in [125] is given by

$$\left\langle \chi_R(\phi^\dagger)\chi_S(\phi)\right\rangle = \delta_{RS}f_R, \tag{4.1.14}$$

[2]This is a consequence of the fact that if V is the fundamental representation of $U(N)$, $U(N)$ and S_n have a commuting action on $V^{\bigotimes n}$. For more details see for example [72].

where f_R is defined in (2.4.14). Finally, we can invert the relation between the Schur polynomials and trace basis operators. Multiplying (4.1.13) by $\chi_R(\tau)$ and summing over the representations R we have

$$\begin{aligned}\sum_R \chi_R(\tau)\chi_R(\phi) &= \frac{1}{p!}\sum_{\sigma\in S_p}\sum_R \chi_R(\sigma)\chi_R(\tau)\,\mathrm{Tr}(\sigma\phi)\\ &= \sum_{\sigma\in S_p}\frac{1}{p!}\frac{p!}{|[\sigma]|}\delta\left([\tau]=[\sigma]\right)\mathrm{Tr}(\sigma\phi)\\ &= \mathrm{Tr}(\tau\phi),\end{aligned} \tag{4.1.15}$$

where to get to the second line we have used the orthogonality relation (2.4.9). The third line follows from the observation that the only terms in the sum over elements that survive from line two are those that have σ in the same conjugacy class as τ, of which there are $|[\tau]|$ terms.

The Schur polynomials have some very nice properties, including that they automatically truncate with N, since a $U(N)$ Young diagram with height larger than N vanishes. One can see this very easily by noticing the dimension of the representation R of $U(N)$, (2.4.12), will be zero if the number of boxes in the first column surpasses N. Therefore, this set of operators automatically satisfies one of the properties expected as a result of the AdS/CFT correspondence. However, the basis does not project onto an orthogonal basis for $SU(N)$; indeed, the operators are not even linearly independent in the $SU(N)$ theory.

Dual Basis

In [126] a non-orthogonal but linearly independent basis of all $SU(N)$ half-BPS operators was defined. This basis was later identified as the dual to the trace basis in [127] via the metric defined by the two point function, and a group theoretic expression for this basis was given:

$$\xi_{p_1\ldots p_n}(x) = \frac{|[\sigma_{p_1\ldots p_n}]|}{p!}\sum_{R\vdash p}\frac{1}{f_R}\chi_R(\sigma_{p_1\ldots p_n})\chi_R(\phi) \qquad p_1\geq\ldots\geq p_n, \tag{4.1.16}$$

where $|[\sigma_{p_1\dots p_n}]|$ is the size of the conjugacy class given labelled by the cycle lengths $p_1 \dots p_n$ (see (2.4.4)), the sum is over the representations of S_p labelled by Young diagrams with p boxes and weighted by f_R defined in (2.4.14). Here, $\chi_R(\sigma_{p_1\dots p_n})$ is the character of $\sigma_{p_1\dots p_n}$in R and $\chi_R(\phi)$ is the Schur polynomial discussed in the previous section. These are operators $\xi_{p_1\dots p_n}$ (with $p_1 \geq \dots \geq p_n$) which obey

$$\langle \xi_{p_1\dots p_m}(x_1) T_{q_1\dots q_n}(x_2)\rangle = \begin{cases} 1 & \text{if } (p_1,\dots,p_m) = (q_1,\dots,q_n)\,, \\ 0 & \text{otherwise.} \end{cases} \tag{4.1.17}$$

In other words each element of the dual to the trace basis is orthogonal to (i.e. it has vanishing two-point function with) all elements of the trace basis but one, and we then normalise it to have unit two-point coefficient with this element. This can be seen straightforwardly by substituting (4.1.15) and (4.1.16) into the two-point function:

$$\begin{aligned} \langle \xi_{p_1\dots p_m}(x_1) T_{q_1\dots q_n}(x_2)\rangle &= \frac{|[\sigma_{p_1\dots p_n}]|}{p!} \sum_{R\vdash p} \frac{1}{f_R} \chi_R(\sigma_{p_1\dots p_n}) \sum_{S\vdash p} \chi_S(\sigma_{q_1\dots q_n}) \langle \chi_R(\phi^\dagger)\chi_S(\phi)\rangle \\ &= \frac{|[\sigma_{p_1\dots p_n}]|}{p!} \sum_{R\vdash p} \chi_R(\sigma_{p_1\dots p_n})\chi_R(\sigma_{q_1\dots q_n}) \\ &= \delta_{p_1 q_1}\dots\delta_{p_m q_n}, \end{aligned} \tag{4.1.18}$$

where the second line uses the diagonal nature of the Schur basis (4.1.14) and the third line uses the orthogonality relation (2.4.8). The delta functions in the final line simply impose that the elements of S_n being considered must be in the same conjugacy class. We will refer to the basis given by the $\xi_{p_1,\dots,p_n}$ as the *dual basis*.

By definition, the change of basis matrix from the dual to the trace basis is simply the two point function:

$$\xi_{p_1\dots p_n}(x) = \sum_{\{q_1\dots q_m\}\vdash p} \langle \xi_{p_1\dots p_n} \xi_{q_1\dots q_m}\rangle T_{q_1\dots q_m}(x) \tag{4.1.19}$$

where the sum is over all partitions of p, that is all sets of integers $q_1 \geq \dots \geq q_m$ such that $q_1 + \dots + q_m = p$. Using (4.1.16) with (4.1.14), one finds the two-point function of

operators in the dual basis to be

$$\begin{aligned}\langle \xi_{p_1\dots p_n}\xi_{q_1\dots q_m}\rangle &= \frac{|[\sigma_{p_1\dots p_n}]|}{p!}\frac{|[\sigma_{q_1\dots q_m}]|}{p!}\sum_{R\vdash p}\frac{1}{f_R}\chi_R(\sigma_{p_1\dots p_n})\chi_R(\sigma_{q_1\dots q_m}) \\ p &= p_1+\ldots+p_n = q_1+\ldots+q_m\ .\end{aligned} \tag{4.1.20}$$

The considerations above have mostly been for a $U(N)$ gauge theory. However, in [127] it was shown that for SU(N) fundamental field ψ and U(N) fundamental field ϕ,

$$\xi_{p_1\dots p_n}(\psi) = \xi_{p_1\dots p_n}(\phi), \tag{4.1.21}$$

with $\psi = \phi - \frac{\mathrm{Tr}(\phi)}{N}$ and $p_i > 1$ for all $i = 1,\dots,n$, $n \geq 2$. As a consequence of this, the correlator of two members of the SU(N) dual basis must be the same as the U(N) correlator,

$$\langle \xi_{p_1\dots p_n}(\psi)\xi_{q_1\dots q_n}(\psi)\rangle = \langle \xi_{p_1\dots p_n}(\phi)\xi_{q_1\dots q_n}(\phi)\rangle, \tag{4.1.22}$$

which is given by (4.1.20).

We will see soon that the single particle operators are in fact a subset of the dual basis operators with a different normalisation (though they were not interpreted as single particle operators when defined), specifically the operators $\xi_{p_1\dots p_n}$ where $n = 1$ correspond to the SPOs. The dual basis as a whole is a more general basis of operators.

4.1.3 Summary of Chapter

The focus of the chapter will be to unpack the basic definition of the single particle operator given in (4.1.1) and explore the properties of this basis. The first result explored here is obtaining explicit formulae for the multi-trace components of the single-particle operators and examining some of their nice properties. Then, we will study some of their correlators and show that compared to the single-trace basis, the single-particle operators have a number of very surprising and nice properties. This is slightly counter-intuitive at first, because now we have to deal with an admixture of single and multi-trace operators, but nevertheless it is true in many ways, as we will demonstrate.

One of the nice properties of SPOs is the operators in the $U(N)$ theory and the $SU(N)$ theory are very closely related. In fact, writing the SPOs in terms of the trace basis, the operators in the $SU(N)$ theory are found simply by setting all T_1 to zero. Since the elementary field, ψ, in $SU(N)$ is the traceless part of the elementary field, ϕ, in $U(N)$, Indeed, in the $U(N)$ theory the single-particle operators of charge greater than or equal to two must be orthogonal to all multi-trace operators involving any $\mathrm{Tr}(\phi)$, and this automatically makes them the $SU(N)$ operators. To formalise this statement we introduce the $SU(N)$ projection on the space of the $U(N)$ operators, and show that the $U(N)$ single-particle operators belong to the $SU(N)$ subspace, which is orthogonal to the span of multi-trace operators in which at least one trace is $\mathrm{Tr}(\phi)$. It follows that correlators of $U(N)$ single-particle operators are equal to correlators of $SU(N)$ single-particle operators.

Another nice property of the single-particle operators is that they automatically vanish if the charge of the operators exceeds the number of colours N. This should be contrasted for example with the single trace basis which does not vanish, but rather decomposes into complicated linear combinations of products of lower trace operators. In [128], (sub)-determinant half-BPS operators were defined as duals to these sphere giants (discussed briefly in the introduction) and later these particles were associated with the completely antisymmetric (single column Young diagram) Schur polynomials [125]. At large N we find that the single-particle operators with charge close to N do indeed approach these (sub)-determinant operators.

The rest of the chapter will be organised as follows:

- In section 4.2 we discuss the details of the multi-trace admixture which defines the single-particle operators. We first give explicit examples at low charge, and then we use group theory techniques to obtain a general formula, *valid for any single-particle operator of any charge p.* Our formulae allow us to study the 'shape' of the operator in the large N limit, and in particular to see explicitly the interpolation between

the single-trace and the sphere giant as a function of p (see section 4.2.3). Moreover, we will be able to compute the two-point function normalisation exactly.

- In section 4.3 we uplift the defining two-point function orthogonality to a multi-point orthogonality theorem, which in turn implies vanishing of a large class of diagrams in correlators. We call these near-extremal n-point functions, where extremality will be defined as a measure of how much the diagram is connected w.r.t. the heaviest operator (see (4.3.11)). This is the first instance of hidden simplicity of multi-point single-particle correlators versus the single-trace correlators, and very interestingly, a similar feature was noticed on the (super-)gravity side in [129].

- In section 4.4, we consider the first non vanishing correlators, and we study maximally-extremal (ME) and next-to-maximally extremal (NME) n-point functions. Both are simple. The ME correlators are computed by trees and two point functions. The NME are mostly computed by weighted sums of ME correlators, which we know in general. When we compute these correlators by using Wick contractions techniques on the trace basis, the combinatorics is hard in the intermediate steps. Instead, the final result is way much simpler. We provide more evidence about this mechanism mentioning also the case of NNME three-point functions.

Most of the work here is based off of published work in [58]. I contributed at least in part to all sections being presented in this thesis. Section 5 as well as most of Appendix B and all of C from the paper are not present in this thesis as that was the work of my collaborators; I had no part in it.

4.2 Single-Particle Half-BPS Operators (SPOs)

The simple definition of the SPOs given in [122] was the following:

Single-particle operators are half-BPS operators which have vanishing two-point

functions with all multi-trace operators.

In this section we will make this definition more precise, find explicit formulae for the operators in terms of the trace basis, the eigenvalues of the operators and the Schur polynomials, and provide some examples in each of the three bases. We then show two important properties of the SPOs; one, SPOs interpolate between single-trace and giant gravitons, and two, that the operators are the same in $U(N)$ as $SU(N)$. Finally, we show the explicit formula for their two-point functions, and make some comments on the possibility of extending from single-particle operators to an orthogonal basis of multi-particle operators. For the most part we shall ignore the space-time dependence, since it is the colour factor we are most interested in; the space-time dependence can usually be reconstructed straightforwardly after the fact.

4.2.1 Definition of SPOs and Low Charge Examples

The AdS/CFT correspondence maps the spectrum of operators in $N = 4$ super Yang-Mills theory to the spectrum of IIB superstring theory on the $\mathrm{AdS}_5 \times S_5$ background. The superstring can be found in unexcited states (giving the IIB supergravity multiplet) or excited states. The half-BPS operators correspond to the supergravity states and their multi-particle products.

In the natural basis of scattering states, the multi-particle states should be orthogonal to single-particle ones. A key observation, though, for the purposes of the discussion here is that the trace basis of half-BPS operators is not an orthogonal basis with repect to the inner product given by the two-point functions. In general,

$$\langle T_p(x_1)\, T_{q_1 \ldots q_n}(x_2)\rangle \neq 0 \qquad n \geq 2\ . \tag{4.2.1}$$

In order to align with the AdS/CFT intuition, a prescription was given in [115, 122] for identifying the relevant half-BPS operators $\mathcal{O}_p$ that correspond to single particle states. The definition simply states that the operators are those which are orthogonal to all

multi-trace operators,

$$\text{Single particle operators } \equiv \{\mathcal{O} : \ \langle \mathcal{O}_p(x_1)\, T_{q_1\ldots q_n}(x_2)\rangle = 0\,, \quad (n \geq 2)\}\ . \tag{4.2.2}$$

It is worth noting that this in turn implies that if we associate multi-particle states with multi-particle operators given as a product of single particle operators, then the single particle operators are orthogonal to the multi-particle states, i.e. $\langle \mathcal{O}_p(x_1)[\mathcal{O}_{q_1}\ldots\mathcal{O}_{q_n}](x_2)\rangle = 0$.

In our normalisation, $\mathcal{O}_p$ coincides with the single-trace operators T_p up to multi-trace admixtures, i.e. the operators take the form

$$\mathcal{O}_p = T_p + \sum_{\{p_1\ldots p_n\}\vdash p} c_{p_1\ldots p_n} T_{p_1\ldots p_n} \qquad n > 2, \tag{4.2.3}$$

where $\sum_{i=1}^n p_i = p$. The coefficients can be calculated using (4.2.2) for the two-point function of (4.2.3) with each $T_{p_1\ldots p_n}$ to get a linear system of equations that can then be solved for the c's. Each multi-trace contribution is suppressed at large N, and the single-particle operators reduce to the single-trace operators in the strict large N limit. However, the novelty of the SPOs described above is precisely the fact they determine the appropriate multi-trace admixtures.

For gauge group $SU(N)$, the single trace operator and the single particle operator coincide for $p = 2, 3$ since there are no multi-trace operators for these charges,

$$\mathcal{O}_p = T_p \qquad \text{for } p = 2, 3 \qquad\qquad SU(N)\,. \tag{4.2.4}$$

In terms of supergravity states the $p = 2$ case corresponds to the superconformal primary for the energy-momentum multiplet which is dual to the graviton multiplet in AdS_5. The $p = 3$ case is the first Kaluza-Klein mode arising from reduction of the IIB graviton supermultiplet on S^5.

On the other hand, for gauge group $U(N)$ the single trace operator T_1 is not zero; the trace of the fundamental scalar does not vanish. Therefore, unlike for $SU(N)$ there is one operator of weight one; $\mathcal{O}_1 = T_1$. Furthermore, at weights two and three there are

multi-trace operators that involve T_1, specifically T_{11} for weight two and T_{21}, T_{111} for weight three, for which our single particle particle operator is defined to be orthogonal to. Therefore, they have multi-trace contributions:

$$\begin{aligned} \mathcal{O}_2 &= T_2 - \tfrac{1}{N} T_{11} \\ \mathcal{O}_3 &= T_3 - \tfrac{3}{N} T_{21} + \tfrac{2}{N^2} T_{111} \end{aligned} \qquad U(N)\,. \tag{4.2.5}$$

The additional terms compared to the $SU(N)$ operators (4.2.4) simply project out the trace part of the fundamental scalar ϕ and so the $SU(N)$ and $U(N)$ operators in fact coincide.

For $p > 3$, we have the first non-trivial admixtures in $SU(N)$ as well as $U(N)$, which can be verified using the propagator (4.1.5). This was discussed in [122], with some previous discussion in [117, 119, 130]. For example, the single particle operator for $p = 4$ is given by

$$\mathcal{O}_4 = T_4 - \frac{2N^2 - 3}{N(N^2+1)} T_{22} \qquad SU(N)\,, \tag{4.2.6}$$

where the coefficient of the double-trace contribution determined from the orthogonality condition $\langle \mathcal{O}_4 T_{22} \rangle = 0$.[3] In the $U(N)$ theory, the SPO with $p = 4$ has further contributions involving T_1. It is given by

$$\mathcal{O}_4 = T_4 - \frac{(2N^2-3)}{N\,(N^2+1)} T_{22} + \frac{10}{N^2+1} T_{211} - \frac{4}{N} T_{13} - \frac{5}{N\,(N^2+1)} T_{1111} \qquad U(N)\,, \tag{4.2.7}$$

where the coeffcients are determined by demanding orthogonality with all higher trace operators T_{22}, T_{211}, T_{13} and T_{1111}.

We see that the $SU(N)$ operators can be found from the $U(N)$ operators by imposing $T_1 = 0$. This pattern continues for $p > 4$; we give the next couple of cases to illustrate this,

$$\mathcal{O}_5 = T_5 - \frac{5\,(N^2-2)\,T_{32}}{N\,(N^2+5)} + \mathcal{U}_5, \tag{4.2.8}$$

[3] Other attempts at finding this combination can be found in [131].

$$\mathcal{O}_6 = T_6 - \frac{(3N^4 - 11N^2 + 80)\, T_{33}}{N\,(N^4 + 15N^2 + 8)} - \frac{6(N-2)(N+2)\,(N^2+5)\, T_{42}}{N\,(N^4 + 15N^2 + 8)} + \frac{7\,(N^2-7)\, T_{222}}{N^4 + 15N^2 + 8} + \mathcal{U}_6,$$

where

$$\mathcal{U}_5 = \frac{15\,(N^2-2)\, T_{221}}{N^2\,(N^2+5)} + \frac{5\,(3N^2+8)\, T_{311}}{N^2\,(N^2+5)} - \frac{35 T_{2111}}{N\,(N^2+5)} + \frac{14 T_{11111}}{N^2\,(N^2+5)} - \frac{5T_{41}}{N}, \quad (4.2.9)$$

$$\mathcal{U}_6 = \frac{42(N-1)(N+1) T_{321}}{N^4 + 15N^2 + 8} + \frac{21\,(N^2+11)\, T_{411}}{N^4 + 15N^2 + 8} - \frac{42\,(2N^2-5)\, T_{2211}}{N\,(N^4 + 15N^2 + 8)} + \\ - \frac{56\,(N^2+5)\, T_{3111}}{N\,(N^4 + 15N^2 + 8)} + \frac{126 T_{21111}}{N^4 + 15N^2 + 8} - \frac{42 T_{111111}}{N\,(N^4 + 15N^2 + 8)} - \frac{6T_{51}}{N}. \quad (4.2.10)$$

The full expressions for $\mathcal{O}_5$ and $\mathcal{O}_6$ above give the $U(N)$ operators. To reduce to the $SU(N)$ operators, the contributions denoted by $\mathcal{U}_5$ and $\mathcal{U}_6$ are imposed to vanish. The reduction from $U(N)$ single particle operators to $SU(N)$ operators by setting $T_1 = 0$ is true in general; we shall show this in 4.2.4.

4.2.2 General Formulae for SPOs

So far we have uniquely defined SPOs, up to normalisation, as operators orthogonal to all multi-trace operators and showed some examples for the $U(N)$ and $SU(N)$ gauge groups. We now look to give explicit formulae for these single particle operators. In fact, we will give three different explicit formulae; one in terms of products of traces, one in terms of eigenvalues of the elementary fields ϕ, and a third in terms of the Schur polynomials discussed in section 4.1.2. The plan will be the following:

- In section 4.2.2 we will give a formula in the trace basis, which is perhaps the most familiar basis. This formula is very non-trivial, and uses powerful group theory techniques to resolve for the expansion of the SPO in terms of multi-traces. We quote it here :

$$\mathcal{O}_p(x) = \sum_{\{q_1,\ldots,q_m\}\vdash p} C_{q_1,\ldots,q_m} T_{q_1,\ldots,q_m}(x) \quad (4.2.11)$$

$$C_{q_1,\ldots,q_m} = \frac{|[\sigma_{q_1\ldots q_m}]|}{(p-1)!} \sum_{s\in\mathcal{P}(\{q_1,..,q_m\})} \frac{(-1)^{|s|+1}(N+1-p)_{p-\Sigma(s)}(N+p-\Sigma(s))_{\Sigma(s)}}{(N)_p - (N+1-p)_p}$$

The group theory data consists of $\mathcal{P}(\{q_1, \ldots, q_m\})$, the powerset of the traces $T_{q_1,\ldots,q_m}$, then $|s|$ is the cardinality of s and $\Sigma(s) = \sum_{s_i \in s} s_i$ (see section 2.4.6). Finally, $|[\sigma_{q_1 \ldots q_m}]|$ is the size of the conjugacy classes of σ with length cycles $q_1 \ldots q_m$, given by (2.4.4).

- In section 4.2.2 we give a much simpler formula, directly in terms of the eigenvalues $E_k(z_i)$ of the elementary fields ϕ,

$$\mathcal{O}_p(x) = \sum_{k=1}^{p} d_k(p,N) E_k(z_i)(x) \tag{4.2.12}$$
$$d_k(p,N) = \frac{(-1)^{k+1} p\,(N-p+1)_{p-k}(p-1)_k}{(N)_p - (N-p+1)_p}$$

- Finally, in section 4.2.2 we give another simple formula in terms of the Schur polynomials introduced in section 4.1.2:

$$\mathcal{O}_p = \sum_{k=1}^{p} \tilde{d}_k(p,N) \chi_{R_k^p}[\phi], \tag{4.2.13}$$
$$\tilde{d}_k(p,N) = p(p-1)(-1)^{k-1} \frac{(N-k+p+1)_{k-1}(N-p+1)_{p-k}}{(N)_p - (N-p+1)_p,}$$

  where we note that only Schur polynomials of hook representations appear.

If we consider half-BPS operators to be symmetric functions of the eigenvalues of the scalar matrix ϕ_r^s, we see the three bases introduced above all correspond to well known bases for symmetric polynomials:

$$\text{Trace basis} \longleftrightarrow \text{Power sum symmetric polynomials}$$
$$\text{Eigenvalue monomials} \longleftrightarrow \text{Monomial symmetric polynomials}$$
$$\text{Schur polynomial operators} \longleftrightarrow \text{Schur polynomials},$$

where the second correspondence is true after eigenvalue monomials are summed over permutations. There are a number of well known formulae relating three bases of symmetric polynomials on the right hand side known as Newton identities. It would be interesting

to explore these relations in the context of the bases of single particle operators on the left hand side.

Formula in terms of a product of traces

In section 4.1.2 we described a linearly independent basis of half-BPS operators known as the dual basis, and gave group theoretic formulae for them and their two point functions introduced by Brown in [127]. They were operators defined to be orthogonal to all elements of the trace basis bar one; see (4.1.17). The dual field ξ_p of the single trace operator T_p satisfies

$$\langle \xi_p(x_1)\, T_{q_1\dots q_n}(x_2)\rangle = 0\,, \qquad n \geq 2. \tag{4.2.14}$$

In fact, this corresponds precisely to our single particle operators, $\mathcal{O}_p$ (see (4.2.2)), therefore the single particle operators must be equal to the dual field ξ_p up to normalisation. Since $\mathcal{O}_p = T_p +$ multi-traces, (4.2.14) and $\langle \xi_p T_p\rangle = 1$ we find

$$\langle \xi_p \mathcal{O}_p\rangle = 1, \tag{4.2.15}$$

hence

$$\xi_p(x) = \frac{\mathcal{O}_p(x)}{\langle \mathcal{O}_p \mathcal{O}_p\rangle} \qquad \text{and} \qquad \mathcal{O}_p(x) = \frac{\xi_p(x)}{\langle \xi_p \xi_p\rangle}\,. \tag{4.2.16}$$

We look to use the change of basis matrix from the dual to the trace basis given in (4.1.19) for ξ_p to find an explicit formula for the multi-trace admixtures for the single particle operator. We need the two-point function of two dual basis elements given in (4.1.20) for $\xi_{p_1\dots p_n} = \xi_p$. The conjugacy class corresponding to the single index dual basis operator consists of a cycle of length p, of which there are $(p-1)!$ possibilities meaning $|[\sigma_p]| = (p-1)!$. Furthermore, for this conjugacy class we observe that only hook representations have a non-vanishing character. More specifically,

$$\chi_R(\sigma_p) = \begin{cases} (-1)^{h_R-1} & R = \text{ hook YT of height } h_R \\ 0 & \text{otherwise,} \end{cases} \tag{4.2.17}$$

where by "hook YT" we mean that the representations R that are associated to hook-shaped diagrams: Young diagrams that only have boxes in the first row and first column. Substituting this information into (4.1.20) gives

$$\langle \xi_p \, \xi_{q_1..q_m} \rangle = \frac{1}{p} \frac{|[\sigma_{q_1..q_m}]|}{p!} \sum_{R \in \text{ hooks}} \frac{1}{f_R} (-1)^{1+h_R} \chi_R(\sigma_{q_1..q_m}) \ , \tag{4.2.18}$$

which are the coefficients of the multi-trace operators in ξ_p. In all of the many cases we have explored, we have observed that this sum over hook representations is given by the following explicit formula:

$$\langle \xi_p \, \xi_{q_1..q_m} \rangle = \frac{1}{p} \frac{|[\sigma_{q_1..q_m}]|}{p!} \frac{1}{p-1} \sum_{s \in \mathcal{P}(\{q_1,..,q_m\})} \frac{(-1)^{|s|+1}}{(N+1-\Sigma(s))_{p-1}} \, , \tag{4.2.19}$$

where the notation corresponds to the group theoretic tools introduced in section 2.4.6.

An important special case of (4.2.19) is the case $m = 1$ giving the two-point function of the dual of the single trace operator. In this case the sum is over just two elements since $\mathcal{P}(\{p\}) = \{\{\}, \{p\}\}$. The expression (4.2.19) thus simplifies to

$$\langle \xi_p \, \xi_p \rangle = \frac{1}{p^2} \frac{1}{p-1} \left(\frac{1}{(N+1-p)_{p-1}} - \frac{1}{(N+1)_{p-1}} \right) . \tag{4.2.20}$$

Finally, inserting (4.1.19), (4.2.19) and (4.2.20) into $\mathcal{O}_p(x) = \frac{\xi_p(x)}{\langle \xi_p \xi_p \rangle}$ gives an explicit expression for the single particle operator as a sum of multi-trace operators

$$\mathcal{O}_p(x) = \sum_{\{q_1..q_m\} \vdash p} C_{q_1,..,q_m} T_{q_1,..q_m}(x) \tag{4.2.21}$$

with coefficients

$$\begin{aligned} C_{q_1,..q_m} &= \frac{\langle \xi_p \, \xi_{q_1..q_m} \rangle}{\langle \xi_p \, \xi_p \rangle} \\ &= \frac{|[\sigma_{q_1..q_m}]|}{(p-1)!} \sum_{s \in \mathcal{P}(\{q_1,..,q_m\})} \frac{(-1)^{|s|+1}}{(N+1-\Sigma(s))_{p-1}} \left(\frac{1}{(N+1-p)_{p-1}} - \frac{1}{(N+1)_{p-1}} \right)^{-1} \\ &= \frac{|[\sigma_{q_1..q_m}]|}{(p-1)!} \sum_{s \in \mathcal{P}(\{q_1,..,q_m\})} \frac{(-1)^{|s|+1} (N+1-p)_{p-\Sigma(s)} (N+p-\Sigma(s))_{\Sigma(s)}}{(N)_p - (N+1-p)_p} \ , \end{aligned} \tag{4.2.22}$$

where the size of the conjugacy class is given by (2.4.4). The second equality is more useful computationally and is obtained by multiplying and dividing by $(N+1-p)_{2p-1}$

and using the identity

$$\frac{(N+1-p)_{2p-1}}{(N+1-\Sigma(s))_{p-1}} = (N+1-p)_{p-\Sigma(s)}(N+p-\Sigma(s))_{\Sigma(s)} \ . \tag{4.2.23}$$

Therefore, we have arrived at an explicit formula for computing the coefficients $C_{q_1\dots q_m}$, allowing us to write the single particle operator of any p in the trace basis. Very nicely, this formula is explicit in p and $\{q_1,\dots,q_m\}$ and depends only on the group theory data associated to such a partition.[4]

The value of m splits the single particle operator into different trace sectors. In Appendix B we provide some examples for generic $\{q_1\dots q_m\}$ when $m=2$ and $m=3$, i.e. the double trace and triple trace sectors respectively.

Formula in terms of eigenvalues

The single single particle operator can in fact be written in a much simpler way when expressed directly in terms of the eigenvalues of the adjoint scalar ϕ^s_r, which we will label $z_1, z_2, \dots, z_N$. Before we write down the explicit formula we introduce the monomial symmetric polynomials, $m_{\underline{\lambda}}(z_1\dots z_N)$:

$$m_{\underline{\lambda}}(z_1,\dots,z_N) = \sum_{\sigma'\in S_N} z_1^{\lambda_{\sigma'(1)}} z_2^{\lambda_{\sigma'(2)}} \dots z_N^{\lambda_{\sigma'(N)}}, \tag{4.2.24}$$

[4]This is unlike the formula given by Brown for the dual basis, (4.1.16), which requires the input of additional information, namely the value of the character $\chi_R(\sigma_{q_1\dots q_m})$. A coefficient in (4.2.21) can be calculated by only knowing the partition of p corresponding to the trace structure of the multi-trace operator the coefficient in question multiplies.

where the $\underline{\lambda}$ is short hand for $(\lambda_1, \ldots, \lambda_N)$ with $\lambda_1 \geq \lambda_2 \geq \ldots \geq \lambda_N$, and the sum is over all *distinct* permutations of $(\lambda_1, \lambda_2, \ldots, \lambda_N)$. Some examples of these polynomials include:

$$\begin{aligned} m_{(1,1,1)}(z_1, z_2, z_3) &= z_1 z_2 z_3, \\ m_{(3,2,0)}(z_1, z_2, z_3) &= z_1^3 z_2^2 + z_1^3 z_3^2 + z_2^3 z_1^2 + z_2^3 z_3^2 + z_3^3 z_1^2 + z_3^3 z_2^2, \\ m_{(3,1,0,0)}(z_1, z_2, z_3, z_4) &= z_1^3 z_2 + z_1^3 z_3 + z_1^3 z_4 + z_2^3 z_1 + z_2^3 z_3 + z_2^3 z_4 + z_3^3 z_1 + z_3^3 z_2 + z_3^3 z_4 \\ &\quad + z_4^3 z_1 + z_4^3 z_2 + z_4^3 z_3. \end{aligned} \tag{4.2.25}$$

It will be useful to introduce the sum over all monomials indexed by a partition of p in k parts, which we label $E_{p,k}$:

$$E_{p,k}(z_1, \ldots z_N) = \sum_{\substack{q_1 + \ldots + q_k = p \\ q_1 \geq q_2 \geq \ldots q_k > 0}} m_{[q_1, \ldots, q_k, 0^{N-k}]}(z_1, \ldots z_N). \tag{4.2.26}$$

The most obvious example of (4.2.26) is $E_{p,1}(z_1, \ldots, z_N) = z_1^p + \ldots + z_N^p = T_p$. Some other examples include

$$\begin{aligned} E_{p,p}(z_1 \ldots z_N) &= z_1 \ldots z_p + \ldots \\ E_{4,2}(z_1 \ldots z_N) &= (z_1^3 z_2 + \ldots) + (z_1^2 z_2^2 + \ldots) \end{aligned} \tag{4.2.27}$$

We find that the single-particle operators can be written as [5]

$$\mathcal{O}_p = \sum_{k=1}^{p} d_k(p, N) E_{p,k}(z_i)\,, \tag{4.2.28}$$

where the coefficient $d_k(p, N)$ is

$$d_k(p, N) = \frac{(-1)^{k+1} p\,(N - p + 1)_{p-k} (p-1)_k}{(N)_p - (N - p + 1)_p} = (-1)^k \frac{(p-1)_k}{(N - k + 1)_k} \frac{p}{1 - \frac{(N)_p}{(N-p+1)_p}} \tag{4.2.29}$$

Note that interestingly the coefficient of a monomial in this formula only depends on the number of different eigenvalues appearing in the monomial and not on any other details

[5] More precisely, in all of the many cases we explored, we always find that this formula is valid.

of the monomial.

Formula in terms of Schur polynomials

Finally we consider the SPOs written in terms of the Schur polynomial formula. In section 4.1.2 we saw a group theoretic formula (first introduced in [127]) for the dual of the trace basis in terms of the Schur polynomial basis, $\chi_R(\phi)$. The formula, (4.1.16), is:

$$\xi_{p_1\dots p_n} = \frac{|[\sigma_{p_1\dots p_n}]|}{p!}\sum_{R\vdash p}\frac{1}{f_R}\chi_R(\sigma_{p_1\dots p_n})\chi_R[\phi]\ . \tag{4.2.30}$$

The relation between the dual basis operators and single particle operators, (4.2.16), together with the observation about characters of cycle permutations, (4.2.17), therefore gives an explicit formula for SPOs directly in terms of the Schur polynomials of Hook Young diagram of height k with p boxes in total.

The Young diagrams are R^p_k:

$$R^p_k = [p-k+1, 1^{k-1}] = \begin{array}{|c|l|}\hline \uparrow & \multicolumn{1}{c|}{\leftarrow p-k \rightarrow} \\ k & \\ \downarrow & \\ \cline{1-1}\end{array}$$

and the operator is

$$\mathcal{O}_p = \sum_{k=1}^{p}\tilde{d}_k(p,N)\chi_{R^p_k}[\phi] \tag{4.2.31}$$

where

$$\begin{aligned}\tilde{d}_k(p,N) &= p(p{-}1)(-1)^{k-1}\frac{(N{-}k{+}p{+}1)_{k-1}(N{-}p{+}1)_{p-k}}{(N)_p-(N{-}p{+}1)_p} \\ &= (-)^k\frac{(p{-}1)}{p+N}\frac{(N{-}k{+}p{+}1)_k}{(N-k+1)_k}\frac{p}{1-\frac{(N)_p}{(N-p+1)_p}}\end{aligned} \tag{4.2.32}$$

The last expression is a simple rewriting, to be compared with the one in (4.2.29).

Examples of SPOs in all three bases

It is useful at this point to consider the single particle operators for some low charges, and show their representation in the three bases we just constructed.

For $\mathcal{O}_2$,

$$\begin{aligned}\mathcal{O}_2 &= T_2 - \tfrac{1}{N}T_{11} \\ \mathcal{O}_2 &= \tfrac{(N-1)}{N}E_{2,1} - \tfrac{2}{N}E_{2,2} \\ \mathcal{O}_2 &= \tfrac{(N-1)}{N}\chi_{R_1^2} - \tfrac{(N+1)}{N}\chi_{R_2^2}\end{aligned} \tag{4.2.33}$$

For $\mathcal{O}_3$,

$$\begin{aligned}\mathcal{O}_3 &= \tfrac{2}{N^2}T_{111} - \tfrac{3}{N}T_{21} + T_3 \\ \mathcal{O}_3 &= \tfrac{(N-2)(N-1)}{N^2}E_{3,1} - \tfrac{3(N-2)}{N^2}E_{3,2} + \tfrac{12}{N^2}E_{3,3} \\ \mathcal{O}_3 &= \tfrac{(N-2)(N-1)}{N^2}\chi_{R_1^3} - \tfrac{(N-2)(N+2)}{N^2}\chi_{R_2^3} + \tfrac{(N+1)(N+2)}{N^2}\chi_{R_3^3}\end{aligned} \tag{4.2.34}$$

For $\mathcal{O}_4$

$$\begin{aligned}\mathcal{O}_4 &= -\tfrac{\left(2N^2-3\right)}{N(N^2+1)}T_{22} + \tfrac{10}{N^2+1}T_{211} - \tfrac{5}{N(N^2+1)}T_{1111} - \tfrac{4}{N}T_{31} + T_4 \\ \mathcal{O}_4 &= \tfrac{(N-3)(N-2)(N-1)}{N(N^2+1)}E_{4,1} - \tfrac{4(N-3)(N-2)}{N(N^2+1)}E_{4,2} + \tfrac{20(N-3)}{N(N^2+1)}E_{4,3} - \tfrac{120}{N(N^2+1)}E_{4,4} \\ \mathcal{O}_4 &= \tfrac{(N-3)(N-2)(N-1)}{N(N^2+1)}\chi_{R_1^4} - \tfrac{(N-3)(N-2)(N+3)}{N(N^2+1)}\chi_{R_2^4} + \tfrac{(N-3)(N+2)(N+3)}{N(N^2+1)}\chi_{R_3^4} - \tfrac{(N+1)(N+2)(N+3)}{N(N^2+1)}\chi_{R_4^4}\end{aligned} \tag{4.2.35}$$

A feature of the expansion of the single-particle operator $\mathcal{O}_p$ in the Schur basis is the homogeneous degree in N of its coefficients w.r.t. the partitions of p, i.e. the different basis elements.

4.2.3 SPOs interpolate between single-trace operators and giant gravitons

The single particle operators, which have a definition directly in $\mathcal{N} = 4$ SYM, involve protected operators and are thus non-perturbative. As was anticipated in the introduction, the definition was strongly motivated via the AdS/CFT correspondence on the supergravity side by certain properties of KK modes on $AdS_5 \times S^5$ [117–119]. In this section, we shall investigate how the single particle operator behaves at large N as we vary p. This has been well understood in the gravity dual [108, 128], therefore we use this analysis to provide some further evidence that our SPOs should be identified with the single-particle half-BPS excitations of $AdS_5 \times S^5$.

Recall that the regime of validity of the gravitational description of $\mathcal{N} = 4$ SYM is the regime in which N is the largest parameter. The correspondence of the single-trace operators with the KK spectrum in the *strict* large N limit is a very well known fact. We will now show that the single particle operators do in fact become the single-trace operator in this limit.

The most direct way to see this is using the formula in terms of eigenvalues given by (4.2.28) and (4.2.29). In this formula p is explicit and held fixed in the limit. Using the Stirling approximation, namely $n! \sim \sqrt{2\pi n}\left(\frac{n}{e}\right)^n$ for $n \to \infty$, we find

$$\frac{d_k(p,N)}{d_1(p,N)} \to \frac{(-)^{k-1}}{N^{k-1}} \frac{\Gamma[p+k-1]}{\Gamma[p]} \qquad \text{as} \qquad N \to \infty. \tag{4.2.36}$$

For $k > 1$ the contribution is suppressed. As described below (4.2.26), the terms with $k = 1$ are precisely $z_1^p + \ldots + z_N^p$, i.e. the single trace term. Therefore, in the large N limit we have

$$\mathcal{O}_p \to T_p + O(1/N) \tag{4.2.37}$$

as expected.[6] The agreement of the multi-trace admixture in the $1/N$ expansion can be

[6] Though not as direct, one can see this from the formula for SPOs in the trace basis, (4.2.21)

tested from supergravity computations in [117–119], and more generally is consistent with the OPE (discussed in [115]).

In a slightly different line of consideration, drawing inspiration from the work of Myers [132], giant gravitons were predicted on the gravity side when increasing charge p, [108]. The observation was that for increasing angular momentum, equal to the charge p, the type-IIB graviton becomes less pointline on the sphere, and grows into a D3 brane wrapping an S^3 embedded in S^5. However, the radius cannot grow to be greater than the S^5, which provided the constraint $p/N \leq 1$. We will show now that the single particle operator matches with the picture described above; it cuts off if $p > N$ with both p, N finite, and becomes a giant sphere graviton in the large N limit with $p \sim N$. In particular, we will see it matches with the operator proposed to be the dual of the spherical D3 brane in [128].

Firstly, consider the charge p of the single-particle operator increasing such that eventually it exceeds the number of colours N. As $p > N$, the single trace operators become linear combinations of multi-trace operators. However, the single particle operators vanish:

$$\mathcal{O}_p = 0 \qquad ; \qquad p > N. \tag{4.2.38}$$

This is very easy to see in the explicit examples given in (4.2.33), (4.2.34) and (4.2.35). This can be explained from the original definition of SPOs; single particle operators are by definition orthogonal to all multi-trace operators. For $p > N$ there are *only* multi-trace operators, therefore the single particle operators must be orthogonal to all operators and so must vanish. This is one very evident way in which the behaviour of our single particle operators is very different from the single trace operators.

Finally, we consider the behaviour of the single particle operators in the regime in which

$$p = N - p' \qquad \text{with } p, N \gg 1 \text{ and } p' \geq 0 \text{ fixed.} \tag{4.2.39}$$

and (4.2.22), too. Each term in the sum of $C_{q_1 \ldots q_m}$ is $O(N)$, however the alternating sum provides a cancellation at each order in N for a total of m cancellations. Therefore, we end up with $O\left(1/N^{m-1}\right)$, in agreement with the considerations of the large N limit in the eigenvalue basis.

To do this, we shall consider the behaviour of coefficient $d_k(p,N)$ from the eigenvalue basis in (4.2.29) normalised with respect to $d_p(p,N)$:

$$\mathcal{D} \equiv \frac{d_k(p,N)}{d_p(p,N)} = (-1)^{k-p}\frac{\Gamma(-k+n+1)\Gamma(k+p-1)}{\Gamma(2p-1)\Gamma(n-p+1)}. \tag{4.2.40}$$

Introducing the variable $k' \equiv p-k \geq 0$, the giant graviton regime is found when k' is small. Substituting this into (4.2.40) gives

$$\mathcal{D}(k') = (-1)^{-k'}\frac{\Gamma[2p-1-k']\Gamma[1+p'+k']}{\Gamma[2p-1]\Gamma[1+p']} \qquad ; \qquad k' \equiv p-k \geq 0. \tag{4.2.41}$$

For small k', $\mathcal{D}(k') \sim O\left(1/(2p)^{k'}\right)$, and since $p \sim N$ at leading order, the $E_{p,k}$ coefficients are power-law suppressed in the large N limit, apart from the coefficient of $E_{p,p}$ which becomes the dominant term. Therefore, we obtain [7]

$$\mathcal{O}_p \;\rightarrow\; (-)^{p+1}p\left(\frac{1}{1+\frac{p}{N}}\right)^{N-p+1} E_{p,p} + O(1/N) \quad ; \quad p, N \gg 1 \text{ and } p-N \text{ fixed}, \tag{4.2.42}$$

where the pre-factor comes from the limit of $d_p(p,N)$. Therefore, the single particle operator becomes proportional to the sub-determinant operator $E_{p,p}$.

The sub-determinant operators were originally proposed in [128] to be duals to the D3 branes studied in [108]. We have seen above that the single particle operator becomes precisely the sub-determinant operator in the limit (4.2.39). Furthermore, since the sub-determinant operator corresponds to the totally antisymmetric Schur polynomial, the giant graviton limit localises the single particle operator onto the single column Schur polynomial, as is expected from [125].

4.2.4 SPOs in $U(N)$ are SPOs in $SU(N)$

As we saw for the low charge examples in (4.2.5), (4.2.7) and (4.2.8), the single particle operators in the $U(N)$ and $SU(N)$ gauge groups are very closely related. In particular,

[7] For values of $k' \to N$ we probe the contribution of other $E_{p,k}$ in the sum (4.2.28), since $k \to 1$. In this limit $\mathcal{D}(k') \sim \sqrt{\pi}N^{1/2+p'}e^{-2N\log 2}$, therefore their contribution is exponentially suppressed, and we can localise the sum on $E_{p,p}$.

despite the elementary fields of the two theories, being different in general, the $U(N)$ SPOs represented in the trace basis give the SPOs in the $SU(N)$ theory simply be setting T_1 to zero. This suggests that SPOs in $U(N)$ are SPOs in $SU(N)$; here we look to make this statement more rigorous.

Let ϕ_r^s and ψ_r^s label the fields of the $U(N)$ and $SU(N)$ theories respectively. The field ψ_r^s is the traceless part of the field ϕ_r^s,

$$\psi_r{}^s = \phi_r{}^s - \tfrac{1}{N}\delta_r^s \phi_t{}^t \ . \tag{4.2.43}$$

For any operator $O[\phi]$ in $U(N)$ we define the $SU(N)$ projection as the map,

$$\Pi : \ O[\phi] \ \rightarrow \ \hat{O}[\phi] \equiv O[\psi(\phi)] \tag{4.2.44}$$

The operator $\hat{O}[\phi]$ is then a new operator in $U(N)$. As an example, we show how the $SU(N)$ projection map works for the operator $O[\phi] = \mathrm{Tr}(\phi^2)$:

$$\begin{aligned}
\hat{O}[\phi] &= \psi_r^s(\phi)\psi_s^r(\phi) \\
&= \left(\phi_r^s - \frac{1}{N}\delta_r^s\phi_u^u\right)\left(\phi_s^r - \frac{1}{N}\delta_s^r\phi_v^v\right) \\
&= \phi_r^s\phi_s^r - \frac{1}{N}\phi_r^s\delta_s^r\phi_v^v - \frac{1}{N}\phi_s^r\delta_r^s\phi_u^u + \frac{1}{N^2}\delta_r^s\phi_u^u\delta_s^r\phi_v^v \\
&= \underbrace{\mathrm{Tr}(\phi^2)}_{O[\phi]} - \frac{1}{N}\,\mathrm{Tr}(\phi)\,\mathrm{Tr}(\phi).
\end{aligned} \tag{4.2.45}$$

More generally we find that an operator projected using the map (4.2.44) takes the form

$$\hat{O}[\phi] = O[\phi] - [T_1\tilde{O}[\phi]] \qquad ; \qquad T_1 = \mathrm{Tr}[\phi] \tag{4.2.46}$$

for some operator $\tilde{O}[\phi]$. Notice that in treating ϕ and ψ as formal variables, $O[\phi]$ is the leading term in the $\frac{1}{N}$ expansion of $\hat{O}[\phi]$.

Since the field ψ is traceless, the projection of any $U(N)$ operator made of products of traces that has T_1 in the product will be 0, with all other projections giving something non-zero of the form (4.2.46). Therefore, the map $\Pi : O \rightarrow \hat{O}$ decomposes the space of $U(N)$ operators into $Im(\Pi) \oplus Ker(\Pi)$, where all operators in the kernel are of the form

$[T_1\tilde{O}[\phi]]$.

We now look to calculate the two-point function of an operator $\hat{O}[\phi]$ with an operator in the kernel of the projection, specifically

$$\langle \hat{O}(x_1)\,[T_1\tilde{O}](x_2)\rangle_{U(N)}\ . \tag{4.2.47}$$

The operator $\hat{O}[\phi]$ is constructed from only the traceless part of ϕ^s_r. By applying Wick's theorem to compute (4.2.47), there will always be a contraction between one of the fields in $\hat{O}(x_1)$ and $T_1(x_2)$. Using the $U(N)$ theory propagator given by (4.1.4) on this particular contraction we get

$$\begin{aligned}\langle \psi^s_r(x_1)T_1(x_2)\rangle &= \langle \phi^s_r(x_1)\phi^t_t(x_2)\rangle - \tfrac{1}{N}\delta^s_r\langle \phi^u_u(x_1)\phi^t_t(x_2)\rangle \\ &= \delta^s_r - \frac{1}{N}\delta^s_r N \\ &= 0.\end{aligned} \tag{4.2.48}$$

Therefore, any operator $\hat{O}[\phi]$ constructed from only the traceless part of the field ϕ is orthogonal to any operator involving the trace as a factor, $[T_1\tilde{O}]$.

Single particle operators in $U(N)$ were defined to be orthogonal to all multi-trace operators, meaning they must be orthogonal to operators of the form $[T_1\tilde{O}]$. Therefore, single particle operators in $U(N)$ automatically live in the $SU(N)$ subspace. It is now possible that $SU(N)$ single particle operators give the $U(N)$ single particle operators. The only thing that remains to be checked is the $U(N)$ inner product restricted on the $SU(N)$ subspace is the same as the inner product of the $SU(N)$ theory. To do this we calculate the two point function of two elements of $\psi(\phi)$ using the $U(N)$ propagator

$$\langle \psi^s_r(\phi)\psi^u_t(\phi)\rangle_{U(N)} = \left\langle \left(\phi^s_r - \tfrac{1}{N}\delta^s_r\phi^v_v\right)\left(\phi^u_t - \tfrac{1}{N}\delta^u_t\phi^v_v\right)\right\rangle_{U(N)} = \delta^u_r\delta^s_t - \tfrac{1}{N}\delta^s_r\delta^u_t. \tag{4.2.49}$$

This gives precisely the $SU(N)$ propagator defined in (4.1.5).

Therefore, we conclude that $U(N)$ single-particle operators are SPOs in $SU(N)$

$$\mathcal{O}^{U(N)}_p[\phi] = \hat{\mathcal{O}}^{SU(N)}_p[\psi] \qquad p \geq 2 \tag{4.2.50}$$

and any correlators of SPOs of charge 2 or higher computed in either $U(N)$ or $SU(N)$ will be identical. This result manifests the well known feature of the free part of $\mathcal{N}=4$ SYM in the context of AdS/CFT, that the $U(1)$ part of the gauge group $U(N)$ decouples and only the $SU(N)$ remains in the interacting theory.

4.2.5 Two-point Function Properties

From the discussion of single particle operators in the trace basis (see section 4.1.1), we found that the normalisation of the two-point function of single particle operators is given by the inverse of the two-point function of dual basis elements. Letting R_p denote the N-dependent colour factor we have

$$\langle \mathcal{O}_p(x_1)\mathcal{O}_p(x_2)\rangle = R_p\, g_{12}^p \qquad ; \qquad \langle \xi_p(x_1)\xi_p(x_2)\rangle = \frac{1}{R_p} g_{12}^p \tag{4.2.51}$$

where we saw from (4.2.20) that R_p takes the form

$$R_p = p^2(p-1)\left[\frac{1}{(N-p+1)_{p-1}} - \frac{1}{(N+1)_{p-1}}\right]^{-1}. \tag{4.2.52}$$

The single particle operators vanish when $N<p$, therefore we would expect R_p to have zeros at $N=1,\ldots,p-1$. Furthermore, since it is symmetric in $N\to -N$ it would be expected that it contains explicit factors of (N^2-r^2) for $r=1,\ldots,p-1$, rather than just $(N-r)$. This property of R_p can be made manifest by writing it in the form

$$R_p = \frac{p}{Q_p(N)} \prod_{r=1}^{p-1} (N^2-r^2)\,, \tag{4.2.53}$$

where $Q_p(N)$ is a polynomial of degree $(p-2)$ in N. The first few cases of Q_p are given

below:

$$\begin{aligned} Q_2(N) &= 1 \\ Q_3(N) &= N \\ Q_4(N) &= 1+N^2 \\ Q_5(N) &= N(5+N^2) \\ Q_6(N) &= 8+15N^2+N^4 \\ Q_7(N) &= N(84+35N^2+N^4) \end{aligned} \tag{4.2.54}$$

We observe that a general formula for $Q_p(N)$ takes the form

$$Q_{p-2}(N) = \frac{(N+1)_{p-1} - (N-p+1)_{p-1}}{p(p-1)} \ . \tag{4.2.55}$$

One can make the $N \to -N$ symmetry fully manifest by using rising factorials (Pochhammers) and lowering factorials:

$$\begin{aligned} x^{\overline{p}} &= x(x+1)(x+2)\dots(x+p-1) = \prod_{k=0}^{p-1}(x+k) \\ x^{\underline{p}} &= x(x-1)(x-2)\dots(x-p+1) = \prod_{k=0}^{p-1}(x-k), \end{aligned} \tag{4.2.56}$$

where we introduced the labels $x^{\overline{p}}$ for the Pochhammer and $x^{\underline{p}}$ for the falling factorial. We find

$$R_p = p^2(p-1)\frac{(N-1)^{\underline{p-1}}(N+1)^{\overline{p-1}}}{(N+1)^{\overline{p-1}} - (N-1)^{\underline{p-1}}}. \tag{4.2.57}$$

In the form (4.2.57) it is clear that R_p is the simplest possible rational function of N^2 with the above zeros and of order $O(N^p)$ at large N.

4.2.6 On Multi-particle Operators

So far we have concerned ourselves only with the single particle operators. They alone, however, do not give a complete basis of half-BPS operators in the theory. To complete the basis, we extend to the *multi-particle basis* by taking arbitrary products of the single

particle operators:

$$\text{Multi-particle basis of weight } p: \ \Big\{\mathcal{O}_{p_1}\dots\mathcal{O}_{p_n}: \ \sum_{i=1}^{n} p_i = p, \ \ p_1 \geq p_2 \geq \dots \geq p_n > 0\Big\}, \tag{4.2.58}$$

where the second condition avoids over-counting of operators. The $U(N)$ multi-particle basis can be labelled by partitions of the integer p, while the $SU(N)$ basis can be labelled by all partitions that do not involve $p_i = 1$. The normalisation is automatically consistent with the single particle operator, in the sense that the multi-particle operator labelled by $p_1, \dots, p_n$ is of the form

$$\mathcal{O}_{p_1,\dots,p_n} \equiv \mathcal{O}_{p_1}\dots\mathcal{O}_{p_n} = T_{p_1\dots p_n} + \ \text{multi-trace admixtures.} \tag{4.2.59}$$

The multi-trace admixtures all have the same number of traces as $T_{p_1\dots p_n}$ or higher.

A similar uplift can be done going from the single trace operators to the full multi-trace basis. However, the traces over-count the operators of a given weight. In particular, any T_p with $p > N$ is not an independent operator in $U(N)$ or $SU(N)$, yet it has non-trivial two point functions with other operators. The multi-particle basis does not have this issue. For $p > N$ there are only multi-trace operators (as the single-trace operator becomes a linear combination of multi-trace operators), therefore by definition the single particle operators are orthogonal to all of these operators, hence must vanish. Remarkably, this feature is automatically implemented in the two-point function normalisation given in (4.2.57).

A very nice feature of the Schur polynomial basis of [125] is that it is both complete and orthogonal for all half-BPS operators in the $U(N)$ theory. Whilst the single particle operators are by definition orthogonal to the multi-particle operators, the multi-particle basis (4.2.58), is not orthogonal. However, unlike the Schur polynomial basis, the multi-particle basis has the advantage of being a basis for both $SU(N)$ and $U(N)$ depending simply on whether $\mathcal{O}_1$ is included or not.

To obtain an orthogonal basis of the multi-particle operators one can of course simply

implement the Gram Schmidt procedure. The idea is as follows: start with an ordered list of basis elements, leave the first element unchanged, and run over the rest in order by adding linear combinations of all previously considered elements such that the new element is orthogonal to all previous ones. As an example, for the charge six operators the trace basis operators could be ordered in the following way

$$\begin{aligned}(T_{111111}, T_{21111}, T_{2211}, T_{3111}, T_{222}, T_{321}, T_{411}, T_{33}, T_{42}, T_{51}, T_6) \qquad & U(N) \\ (T_{222}, T_{33}, T_{42}, T_6) \qquad & SU(N). \end{aligned} \tag{4.2.60}$$

Performing Gram-Schmidt orthogonalisation (with respect to either the $U(N)$ or $SU(N)$ two-point function) in the order from left to right would provide an orthogonal set of operators. Assuming the single-particle operator should be found as part of this procedure, it makes sense to have T_6 last in the ordering as this corresponds directly to the definition of the SPO. However, it is not clear if there is a canonical choice for the ordering of the other operators. Inspired by the SPO, it would be very natural to define two-particle operators as those which are orthogonal to triple traces and higher. This would give a natural ordering of trace basis elements from highest number of traces to the lowest. However, doing so still leaves ambiguity within each trace sector; even at weight six, the double trace sector has three operators T_{33}, T_{42}, T_{51} in the $U(N)$ theory and two $T_{33}, T_{4,2}$ in the $SU(N)$ theory, and it is unclear if there is a canonical choice.

Assuming the single-particles are fixed so provide a starting point for organising an ordering, a completely equivalent way of obtaining the same orthogonal basis is to start with the dual basis, list the operators in reverse order, and perform Gram-Schmidt orthogonalisation. This process yields exactly the same orthogonal basis up to normalisation. Using the weight six operators to illustrate this as above,

$$\begin{aligned}(\xi_6, \xi_{51}, \xi_{42}, \xi_{33}, \xi_{411}, \xi_{321}, \xi_{222}, \xi_{3111}, \xi_{2211}, \xi_{21111}, \xi_{111111}) \qquad & U(N) \\ (\xi_6, \xi_{42}, \xi_{33}, \xi_{222}) \qquad & SU(N) \end{aligned} \tag{4.2.61}$$

In the first approach the operator with the most traces T_{111111} (or T_{222}) remains unchanged

whereas the single-particle operator is the most complicated from the point of view of the trace-basis. In the second approach, the opposite is true; the single particle operator is ξ_p, and an operator labelled by a partition with increasing length becomes more intricate from the point of view of the ξ basis. In the end, the most intricate of such operators, a linear combination of all dual operators, must equal T_{11111} (or T_{222}).

We leave the task of extending the single-particle operators to a full orthogonal basis to a future work. Perhaps an AdS/CFT understanding of multi-particle KK modes will help us figuring out a canonical way to fix the multi-particle states in $\mathcal{N} = 4$ SYM.

4.3 Multipoint Orthogonality

In the previous section we obtained explicit expressions for the SPOs. Given that the single particle operator is constructed from all single- and multi-trace operators, one would expect such a rich structure would lead to very complicated multipoint correlation functions. In particular, one would assume that they are much more complicated than multipoint single-trace correlation functions. However, this expectation turns out to be too naive. In this section, we look to describe one unexpected simplification of multipoint correlation functions; we will prove that the defining two-point function orthogonality uplifts to a multipoint orthogonality theorem. This in turn implies that a large class of diagrams vanishes.

Multipoint Orthogonality Theorem. *Consider any diagram contributing to a half-BPS correlator that has a single particle operator $\mathcal{O}_p$ connected to two sub-diagrams, with the sub-diagrams themselves disconnected from each other. Any propagator structure consistent with this type of diagram has a vanishing colour factor. This statement holds for both $U(N)$ and $SU(N)$ free theories.*

We will consider n operators; one will be a weight p single particle operator $\mathcal{O}_p$, r operators labelled by $\underline{q_1}, \ldots, \underline{q_r}$ will form one sub-diagram and the remaining operators labelled by

$\underline{q_{r+1}}, \ldots, \underline{q_{n-1}}$ will form another sub-diagram which will be disconnected from the other (but connected to $\mathcal{O}_p$). These consist of diagrams with any propagator structure, which we will label $\mathcal{F}_{p|\underline{q_1}\ldots\underline{q_{n-1}}}$, that become disconnect upon removing $\mathcal{O}_p$; therefore, they have the shape of a dumbbell, depicted in the image below:

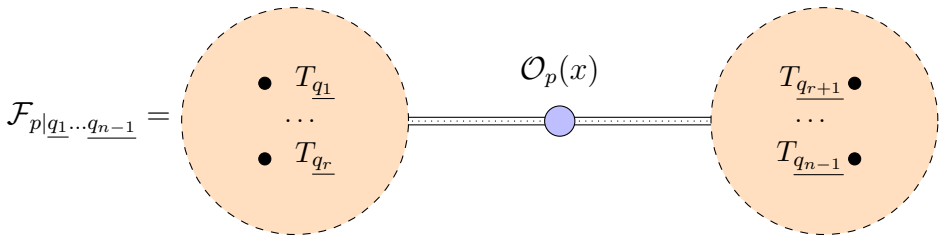

(4.3.1)

The inside of the two orange circles are two sub-diagrams, which could each have very complicated propagator structures themselves but do not connect to each other in any way. There will, though, be bridges between $\mathcal{O}_p(x)$ and points in each sub-diagram. The multipoint orthogonality theorem then states:

$$\mathcal{F}_{p|\underline{q_1}\ldots\underline{q_{n-1}}} = 0. \tag{4.3.2}$$

Note that $T_{\underline{q_i}}$ stands for *any* half-BPS operator (single trace, multi-trace, or any combination of the two) with total charge q_i.

It is worth considering how the charge of $\mathcal{O}_p$ compares to the sum of the rest of the charges. If we were considering a two-point function (or more generally, if there were no propagators between operators in the sub-diagrams) then the sum of the q charges would equal p. However, the assignment of $\underline{q_1}, \ldots, \underline{q_{n-1}}$ can be such that

$$\frac{1}{2}\left(-p + \sum_{i=1}^{n-1} q_i\right) = k \geq 0 \tag{4.3.3}$$

and still the diagram disconnects on the removal of $\mathcal{O}_p$. This becomes possible for a multipoint function because there can be $k \geq 0$ Wick contractions distributed among either $T_{\underline{q_1}}(x_1)\ldots T_{\underline{q_r}}(x_r)$ or $T_{\underline{q_{r+1}}}(x_{r+1})\ldots T_{\underline{q_{n-1}}}(x_{n-1})$ (though not between the two sets), which would not affect the diagram disconnecting upon the removal of $\mathcal{O}_p(x)$.

We will now look to prove the multi-point orthogonality theorem. Though it would be very interesting to have a combinatorial proof of the theorem, the combinatorics which lead to (4.3.2) are generally very hard. In section 4.3.1 we use an alternative route to provide a proof. Then in section 4.3.2 we give examples of how the theorem can be used to give some interesting results for multipoint correlation functions. In particular we will show that near-extremal n-point functions, defined by the constraint $k \leq n-3$, vanish. We will then present some consequences of this property through a couple of explicit examples.

4.3.1 Proof of the Theorem

The goal of this section is to show $\mathcal{F}_{p|\underline{q_1}\dots\underline{q_{n-1}}} = 0$, where $\mathcal{F}$ is a fixed propagator structure depicted schematically in (4.3.1). We will see that we can decompose F into sums over products of smaller propagator structures. We will show that each term will contain an extremal three-point function, which will be proven to be zero, therefore $\mathcal{F}$ will be zero.

To begin with, we focus only on the right hand side of the diagram. Consider Wick contractions of the fundamental fields of $\mathcal{O}_p(x)$ and $T_{\underline{q_{r+1}}}(x_{r+1})\dots T_{\underline{q_{n-1}}}(x_{n-1})$ consistent with the propagator structure $\mathcal{F}_{p|\underline{q_1}\dots\underline{q_{n-1}}}$. Since the number of bridges going between $\mathcal{O}_p$ and the sub-diagram on the right hand side is fixed and less than p, some of the fields in $\mathcal{O}_p$ will remain unlinked. This will result in a new half-BPS operator of lower charge (than p), say R, inserted at x multiplied by some propagators. This would result in:

$$\prod g_{ij}^{d_{ij}} \sum_{\underline{R}\vdash R} C_{\underline{R}}\, T_{\underline{R}}(x) \;=$$

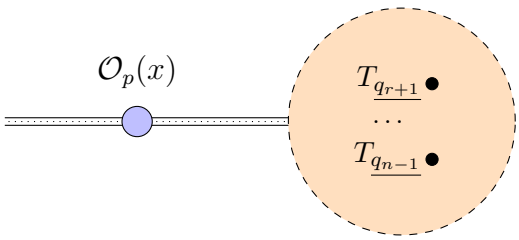

(4.3.4)

Here, the sum is over all partitions of R, the charge of the new operator that we have decomposed into a basis of half-BPS operators; the trace basis. The product $\prod g_{ij}^{d_{ij}}$ gives

the propagator structure factored out[8], and $C_{\underline{R}}$ are some coefficients which we will discuss below.

Substituting (4.3.4) into the original diagram calculation, we now have

$$\mathcal{F}_{p|\underline{q_1}\cdots\underline{q_{n-1}}} = \prod g_{ij}^{d_{ij}} \sum_{\underline{R}\vdash R} C_{\underline{R}} \times$$

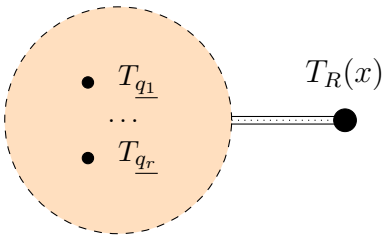

(4.3.5)

The $C_{\underline{R}}$ are still unknown; we now look to calculate them. Consider operators $T_{\underline{R}'}(x')$ at some auxiliary location x', where $\underline{R}'$ is a partition of R, that we use to bridge with the remaining fields of $\mathcal{O}_p(x)$ on the left-hand side of (4.3.4). Graphically this gives

$$\prod g_{ij}^{d_{ij}} \sum_{\underline{R}',\underline{R}\vdash R} C_{\underline{R}} \langle T_{\underline{R}'}(x')T_{\underline{R}}(x)\rangle =$$

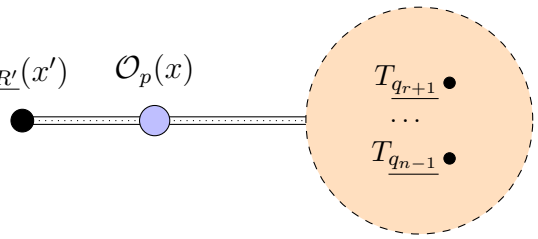

(4.3.6)

This gives a set of equations for $C_{\underline{R}}$ which can be solved by inverting the matrix of two-point functions. The coefficients $C_{\underline{R}}$ can therefore be computed using a similar dumbbell diagram to $\mathcal{F}$ but with the left hand side replaced by the operator $T_{\underline{R}'}(x')$ multiplied by the inverse of the two-point functions $\langle T_{\underline{R}'}(x')T_{\underline{R}}(x)\rangle$. These two-point functions are given by $g^R_{x'x}$ which can be factored out, multiplied by the colour factor $\mathcal{C}_{\underline{R}\underline{R}'}$. The proof does not rely on this explicit structure, therefore we will keep using the notation $\langle T_{\underline{R}'}(x')T_{\underline{R}}(x)\rangle$

[8]Here d_{ij} counts the number of propagators between insertion points x_i and x_j, and $g_{ij} = \frac{\mathrm{Tr}(T^aT^b)}{(x_i-x_j)^2}$

for clarity. Replacing the coefficients $C_{\underline{R}}$ in (4.3.5) we get

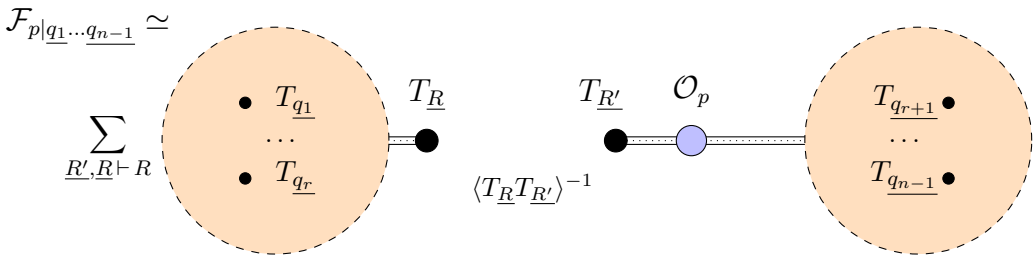

(4.3.7)

A similar discussion can be repeated to decompose the propagator structure of the right-hand side of (4.3.7) further. Introducing the operators $T_{\underline{L}}$ and $T_{\underline{L'}}$, and following similar reasoning to that given above, we conclude that the original propagator structure given by (4.3.1) can be written as

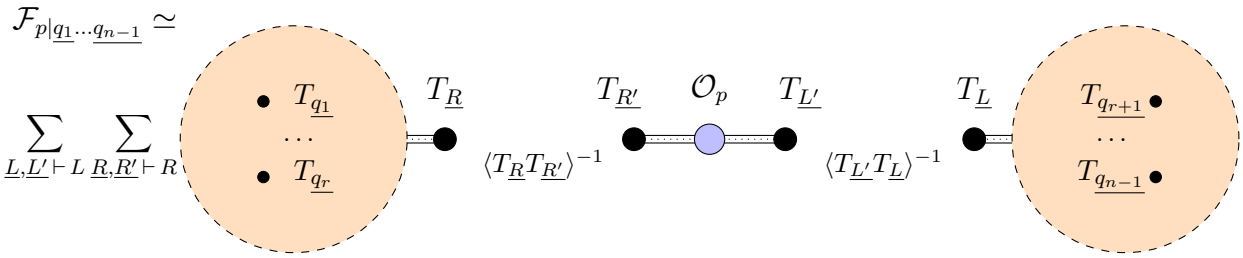

(4.3.8)

We have shown that we can decompose the full propagator structure $\mathcal{F}_{p|\underline{q_1}\cdots\underline{q_{n-1}}}$ into a sum of a product of smaller propagator structures multiplied by the inverse of two-point functions. The crucial propagator structure in each term in the sum is the middle three-point function $\langle \mathcal{O}_p T_{\underline{R'}} T_{\underline{L'}}\rangle$. There are bridges between all fundamental fields in $T_{\underline{R'}}, T_{\underline{L'}}$ and $\mathcal{O}_p$, with none going between the two T operators. Unlike the original dumbbell of (4.3.1), there can be no internal propagators within the structures connected to the single particle operator, i.e. $p = R + L$. Therefore, this three-point function is extremal. To complete the proof, we are left to show that any extremal 3-point function with an SPO at the point with largest charge vanishes

$$\langle \mathcal{O}_p(x_1) T_{\underline{Q}}(x_2) T_{\underline{R}}(x_3)\rangle = 0 \qquad ; \qquad p = Q + R\ . \tag{4.3.9}$$

This is in fact a direct consequence of the definition of the single particle operator. Since

there are no propagators running between operator $T_{\underline{Q}}$ and $T_{\underline{R}}$, the three point function can be directly related to the corresponding two-point function obtained by bringing the points 2 and 3 together. Therefore,

$$\langle \mathcal{O}_p T_{\underline{Q}} T_{\underline{R}} \rangle = \left(\frac{g_{13}}{g_{12}} \right)^R \langle \mathcal{O}_p [T_{\underline{Q}} T_{\underline{R}}] \rangle = 0 \,, \tag{4.3.10}$$

where the final equality is reached by using the fact the single particle operator is defined to be orthogonal to all multi-trace operators.

Therefore, we have shown that any propagator structure involving $\mathcal{O}_p$ which becomes disconnected on removing $\mathcal{O}_p$ vanishes, thus concluding our proof of the multipoint orthogonality theorem.

4.3.2 Vanishing Near-Extremal Correlators

The remainder of this chapter will mostly be dealing with the calculation of $n-$point functions involving the single particle operators. Before we do so, it is useful to introduce what we will refer to as the *degree of extremality*, given by k. Let p be the largest charge, and $q_1, \ldots, q_{n-1}$ be the other charges. The degree of extramilty is defined as

$$k = \tfrac{1}{2} \left(-p + \sum_{i=1}^{n-1} q_i \right) \,. \tag{4.3.11}$$

This should be familiar from (4.3.3) of the last section.

The n-point correlator $\langle \mathcal{O}_p T_{\underline{q_1}} \ldots T_{\underline{q_{n-1}}} \rangle$ is zero for $k < 0$ purely by considering the $SU(4)$ symmetry. Extremal ($k = 0$) and next-to-extremal ($k = 1$) correlators were shown to all be non-renormalised in [107, 130, 133–135], and a nice diagrammatic interpretation of the non-renormalisation for the simplest case of two-point functions was given in for example [136, 137]. Related to this quantity, the concept of "near-extremal" correlators was introduced in [129]. These are n-point correlators that satisfy the following condition

$$\text{near extremal correlator:} \qquad k \leq n - 3 \,. \tag{4.3.12}$$

For $n = 3$, only the extremal correlators ($k = 0$) are considered near-extremal by this definition. For $n = 4$ the extremal and next-to-extremal correlators are considered near-extremal, and for $n \geq 5$ the correlators that satisfy (4.3.12) go beyond even extremal and next-to-extremal functions.

We make the following claim:

Near-Extremal Correlators Vanish. *Any near-extremal $SU(N)$ correlator in free theory, where the largest charge operator is a single-particle operator, vanishes, i.e.*

$$\langle \mathcal{O}_p(x) T_{\underline{q_1}}(x_1) \dots T_{\underline{q_{n-1}}}(x_{n-1}) \rangle = 0 \qquad k \leq n-3 \ . \tag{4.3.13}$$

In the $U(N)$ theory, a similar statement can be made but with the caveat that it is true only for connected correlators.

As usual, $T_{\underline{q_i}}$ stands for any half-BPS operator with total charge q_i. We remark that *any* refers to any single- or multi-trace operator or any combination of these. A corollary of this is that any near-extremal correlator involving only SPOs vanishes.

$$\langle \mathcal{O}_p(x) \mathcal{O}_{q_1}(x_1) \dots \mathcal{O}_{q_{n-1}}(x_{n-1}) \rangle = 0 \qquad k \leq n-3 \ . \tag{4.3.14}$$

To prove (4.3.13), we will argue that every diagram contributing to the near-extremal correlator has a dumbbell shape, so the same propagator structure as in (4.3.1). This will mean every diagram gives a zero contribution, therefore the correlators are equal to zero.

Proof. Let us begin by showing that there are not enough propagators between the $T_{\underline{q_i}}$ operators to connect all of them together. The total charge of these operators is given by $\sum q_i = 2k + p$, meaning that there are $2k + p$ propagator ends connected to them. We know that p of the ends must come from propagators bridging between $\mathcal{O}_p$ and the $T_{\underline{q_i}}$, therefore there are a total of k propagators between the $T_{\underline{q_i}}$ themselves (which accounts for the $2k + p - p = 2k$ remaining ends). The minimal case that would allow all $T_{\underline{q_i}}$ to be connected to each other is if they were connected in a chain with one propagator between each; i.e. $k = n - 2$. However, from near-extremality we have $k \leq n - 3$, therefore there

are not enough bridges between these operators; we would need at least two more points. This is true for both $SU(N)$ and $U(N)$.

Since the topology of $\mathcal{O}_p(x)T_{\underline{q_1}}(x_1)\dots T_{\underline{q_{n-1}}}(x_{n-1})$ is such that it is not possible to connect all $T_{\underline{q_i}}$, a connected diagram would have to take the form of the dumbbell as in (4.3.1). Therefore, all connected diagrams for these correlators are equal to zero by the multi-point orthogonality theorem described in the previous section.

The only possible exceptional case could be when the diagram is made of two disconnected pieces i.e. one of the ends of the dumbbells is on its own completely. This would evade the vanishing property of the full dumbbell diagrams. For concreteness, let us say without loss of generality that $T_{\underline{q}_1}(x_1)\dots T_{\underline{q}_r}(x_r)$ is disconnected from $\mathcal{O}_p(x)T_{\underline{q}_{r+1}}(x_1)\dots T_{\underline{q}_n-1}(x_{n-1})$, for some value of r. We now look to investigate when the propagator structure can be disconnected in such a way. The number of propagators between the fields of the disconnected piece of the diagram, i.e. between $T_{\underline{q}_1}(x_1)\dots T_{\underline{q}_r}(x_r)$, is given by $\frac{1}{2}\left(\sum_{i=1}^{r} q_i\right)$. For the other part of the disconnected diagram, the number of bridges among the $T_{\underline{q_{r+1}}},\dots,T_{\underline{q_{n-1}}}$ which are not connecting with $\mathcal{O}_p$ is

$$k_R = \frac{1}{2}\left(-p + \sum_{i=r+1}^{n-1} q_i\right). \tag{4.3.15}$$

We assume that this part of the diagram remains connected upon the removal of $\mathcal{O}_p$, otherwise it would have a propagator structure like in (4.3.1) which would automatically give zero. For this to happen, the operators $T_{\underline{q_i}}$ with $i = r+1,\dots,n-1$ would have to all be connected to each other. The minimal way this could happen is they form a tree, which would require $k_R \geq n-r-2$ propagators.

From the near-extremality condition we have

$$k = \frac{1}{2}\left(-p + \sum_{i=1}^{n-1} q_i\right) \leq n-3. \tag{4.3.16}$$

Substituting (4.3.15) into (4.3.16) we find

$$\frac{1}{2}\sum_{i=1}^{r} q_i \leq n-3-k_R \leq r-1, \tag{4.3.17}$$

where the last inequality comes from using $k_R \geq n - r - 2$. Focussing on the first part of the inequality and the last, for this to be satisfied then at least two of the q_i must equal one. For $SU(N)$ this is not possible since there are no charge one operators, therefore there are no disconnected diagrams of the form being considered here. For the $U(N)$ theory, however, this is a possibility.

We conclude that all $SU(N)$ diagrams (and connected $U(N)$ diagrams) contributing to near extremal correlators have a dumbbell shape as in (4.3.1) and therefore equal zero. Thus, we have proven the statement made above regarding vanishing near-extremal correlators.

Further Corollaries

A useful corollary of the vanishing of near-extremal correlators occurs for lower point correlators, say m-points, which are not near extremal but have a number of multi-trace operators.,

$$\langle \mathcal{O}_p(x) T_{\underline{q_1}}(x_1) \dots T_{\underline{q_{m-1}}}(x_{m-1}) \rangle \qquad ; \qquad k = \tfrac{1}{2}(-p + \textstyle\sum q_i) \geq m - 3 \ . \tag{4.3.18}$$

Say r of the operators are multi-trace operators. We can think of (4.3.18) as the limit of an $n \geq m$ point correlator, with specific propagator structure such that there are no propagators inside any of the multi-traces. The maximum value for n is achieved by putting all parts of the multi-traces on fictitious points. If we let $l(\underline{q_i})$ measure the number of parts of $\underline{q_i}$, then

$$m \leq n = (m - r) + \sum_{i=1}^{r} l(\underline{q_i}) \tag{4.3.19}$$

If $k \leq n - 3$ then the original correlator, (4.3.18), vanishes as it can be thought of an n-point near-extremal correlator.

As a simple example of the above corollary, consider the three-point function between $\mathcal{O}_p$,

$T_{\underline{q_1}}$ and $T_{\underline{q_2}}$;

$$\text{if } \exists\ i \text{ such that } l(\underline{q_i}) \geq 2 \text{ and } k \leq 1 \quad \Rightarrow \quad \langle \mathcal{O}_p(x) T_{\underline{q_1}}(x_1) T_{\underline{q_2}}(x_2) \rangle = 0. \tag{4.3.20}$$

The correlation function is zero because one can always think of the three-point function as the limit of a near-extremal higher point function, which we have shown vanishes.

A further example is the following:

$$\text{if } \exists\ i \text{ such that } l(\underline{q_i}) \geq 2 \text{ and } k \leq m-2 \quad \Rightarrow \quad \langle \mathcal{O}_p(x) T_{\underline{q_1}}(x_1) \dots T_{\underline{q_{m-1}}}(x_{m-1}) \rangle = 0 \tag{4.3.21}$$

There are many more possibilities that arise from this corollary. In particular, in the above examples we have only considered one of the multi-trace operators being split, however multiple of the operators could be split if they have a multi-trace structure. We do not make an exhaustive list here, but point out that a consistent way of determining if a correlator falls into one of the vanishing near-extremal cases is to fully split the multi-trace operators up to consider the full n-point function, calculate the extremality k using (4.3.11), then see if it satisfies $k \leq n-3$. If this inequality is satisfied, then the n-point correlation function is zero, which in turn implies the original correlation function with multi-trace operators is zero.

4.4 Exact Results for Correlators of SPOs

In the last section we proved that all near-extremal correlators of SPOs, defined by (4.3.12), vanish. In this section, we explore correlation functions beyond the near-extremal sector, and look to give exact results for some of these correlators of single particle operators. Furthermore, we shall see some interesting results for correlators for the multi-particle basis.

4.4.1 Maximally-Extremal (ME) Correlators

The next set of correlators beyond the near-extremal sector are those of the following form:

$$\langle \mathcal{O}_p(x)\mathcal{O}_{q_1}(x_1)\dots\mathcal{O}_{q_{n-1}}(x_{n-1})\rangle \quad ; \quad k = n-2 \quad ; \quad k = \tfrac{1}{2}(-p+\sum q_i) \tag{4.4.1}$$

We will refer to these correlators as Maximally-Extremal (ME). For now we shall focus on the $SU(N)$ theory, though it is worth keeping in mind that correlators of SPOs of charge two or higher are equal in the $SU(N)$ theory and the $U(N)$ theory, as we saw in section 4.2.4.

There will be two notions of extremality referred to in this section; though they will often refer to the same correlators, we would like to make it clear to the reader what each refers to. It is worth emphasising here that the term 'Maximally-Extremal' does not refer to a specific value of k for all n; it is the name given to the set of n-point correlators which have the lowest possible value of k such that they do not give a vanishing result (which is given by $k = n-2$). For example, the ME three-point functions have extremality $k = 1$, therefore are often referred to as next-to-extremal three point functions. The ME four-point functions have extremality $k = 2$, therefore are often referred to as next-to-next-to-extremal four point functions. Within this section, we will use the term 'Maximally-Extremal' when discussing the general set of correlators satisfying $k = n-2$, but upon fixing an n we will refer to the correlators as 'next-to'^{k} extremal, or N^k extremal.

To begin we will look at the three-point ME functions, which will provide a useful simple example before giving a formula for the n-point ME functions.

3-point Functions

As mentioned in the previous section, 3-point ME functions have $k = 1$, therefore we also refer to them as next-to-extremal (NE) three-point functions. In order to compute them,

notice first that

$$\langle \mathcal{O}_p(x)\mathcal{O}_{q_1}(x_1)\mathcal{O}_{q_2}(x_2)\rangle = \langle \mathcal{O}_p(x)T_{q_1}(x_1)T_{q_2}(x_2)\rangle\,, \qquad p = q_1+q_2-2\,, \tag{4.4.2}$$

In order to get to the right hand side we have simply expanded $\mathcal{O}_{q_1}$ and $\mathcal{O}_{q_2}$ in terms of the trace basis. One would expect three-point functions involving multi-traces to also be present, however if $k = 1$ then by the results of section 4.3.2 n-point functions with $n \geq 4$ will be zero. Therefore, we are left only with the leading term in the expansion of the single particle operators.

Since we are dealing with NE three-point functions, the propagator structure will take the form:

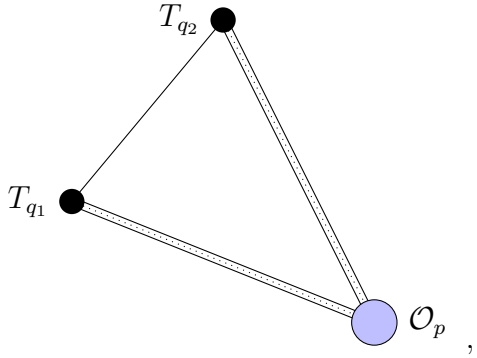

, (4.4.3)

where the thicker lines indicate the potential of having multiple propagators, and the thinner black line indicates a single propagator between T_{q_1} and T_{q_2}. The single propagator indicates there is a single Wick contraction to do between x_1 and x_2. If at the same time the two insertion points are brought together, we obtain the result,

$$\lim_{x_1\to x_2} \mathrm{Tr}(\underbrace{\phi(x_1).....\phi(x_1)}_{q_1})\,\mathrm{Tr}(\underbrace{\phi(x_2).....\phi(x_2)}_{q_2}) \simeq \mathrm{Tr}(\underbrace{\phi(x_2).....\phi(x_2)}_{p}) + \ldots \quad . \tag{4.4.4}$$

In general, the right hand side of (4.4.4) would contain all the contributions of an OPE of scalars. However, keeping in mind the three-point function we are calculating, we will contract all of these terms with the half-BPS operator $\mathcal{O}_p$. Therefore, by the two-point orthogonality with multi-traces that defines the single particle operator, any term other than the single trace does not survive. There are q_1q_2 ways to perform this Wick

contraction, so from (4.4.2) we arrive at

$$\langle \mathcal{O}_p T_{q_1} T_{q_2} \rangle = q_1 q_2 \langle \mathcal{O}_p T_p \rangle \,. \tag{4.4.5}$$

Finally, once again from the definition of the single-particle operator, we have that $\langle \mathcal{O}_p T_p \rangle = \langle \mathcal{O}_p \mathcal{O}_p \rangle$.

Putting all of this together we find a very simple explicit formula for next-to-extremal three-point functions:

$$\langle \mathcal{O}_p \mathcal{O}_{q_1} \mathcal{O}_{q_2} \rangle = q_1 q_2 \langle \mathcal{O}_p \mathcal{O}_p \rangle \qquad ; \qquad p = q_1 + q_2 - 2 \,, \tag{4.4.6}$$

with the colour factor of the two point function given by (4.2.52).

n-point Functions

We now look to go beyond 3 points, and consider the ME n-point functions of single particle operators.

Similar to the three-point case in (4.4.2), we can replace all of the operators apart from the one with the largest charge with the leading term of its expansion in the trace basis i.e. with single trace operators,

$$\langle \mathcal{O}_p(x) \mathcal{O}_{q_1}(x_1) \cdots \mathcal{O}_{q_{n-1}}(x_{n-1}) \rangle = \langle \mathcal{O}_p(x) T_{q_1}(x_1) \cdots T_{q_{n-1}}(x_{n-1}) \rangle \quad ; \quad .k = n - 2 \tag{4.4.7}$$

Again, the contributions that would occur from the multi-trace admixtures of the single-particle operators that have been expanded out are zero by the results of 4.3.2.

The connected diagrams that give non-vanishing contributions must remain connected upon removal of the charge $\mathcal{O}_p$, otherwise we would end up with a zero case described in 4.3.2. To be Maximally-Extremal, there must be $n-2$ propagators between the $n-1$ T_{q_i} operators, meaning for example there cannot be more than one propagator between any pair T_{q_i}, T_{q_j}. The number of propagators, in fact, is just enough to connect the T_{q_i}s together as a tree graph. We show two five point examples below to clarify this idea,

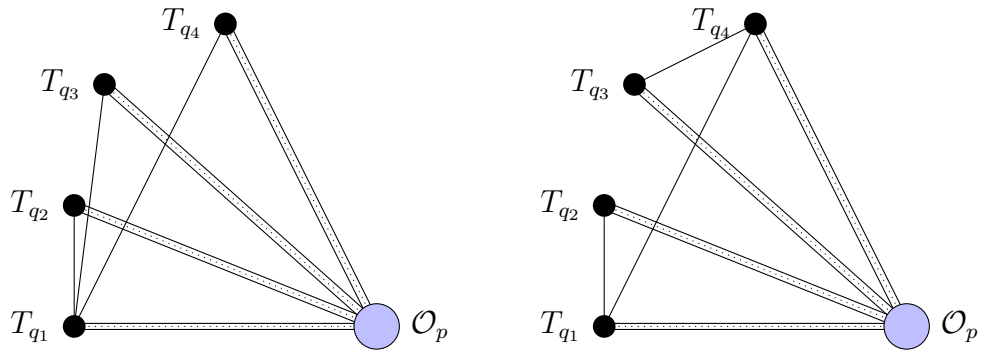

(4.4.8)

In the first case, the tree we refer to above consists of T_{q_1} connected to T_{q_2}, T_{q_3} and T_{q_4}. This is the maximum number of propagators that could have come off of T_{q_1}. In the second diagram the tree consists of T_{q_1} connected to T_{q_2} and T_{q_4}, and T_{q_3} connected to T_{q_4}.

So, the propagator structures contributing to an ME n-point correlator (4.4.7) contains a sub-propagator structure which is a tree, $\mathcal{T}$. To each tree one can associate a sequence of length $(n-3)$ called the Prüfer sequence, which uniquely labels the propagator structure of the tree linking the $(n-1)$ T_q operators. Using the structure of the trees associated with Prüfer sequences, one can show that the pairwise computation of Wick contractions represented by the trees can be given by

$$|\mathcal{W}[\mathcal{T}]| = \prod_{i=1}^{n-1} q_i(q_i-1)\dots(q_i-d_i+1). \tag{4.4.9}$$

Here d_i corresponds to the number of propagator ends within the tree structure that connects to operator T_{q_i}. We shall provide more details about this point of view in appendix D.

By performing the Wick contractions leaf by leaf on the tree as dictated by the Prüfer algorithm, and by bringing the insertion points together at each stage, we can use the same argument given in section 4.4.1 to argue that in the end gluing together the T_{q_i}s will result in a single trace operator T_p together with higher trace terms. However, the higher trace terms will not contribute in the full ME correlator as they will be limits of near-extremal functions. Therefore, the entire connected part of the ME correlator can

be written as a sum over trees, with the full sum multiplied by the two-point function $\langle \mathcal{O}_p \mathcal{O}_p \rangle$ to give:

$$\langle \mathcal{O}_p(x) \mathcal{O}_{q_1}(x_1) \cdots \mathcal{O}_{q_{n-1}}(x_{n-1}) \rangle_{\text{connected}} = \langle \mathcal{O}_p \mathcal{O}_p \rangle \left(\sum_{trees\, \mathcal{T}} |\mathcal{W}[\mathcal{T}]| \;\; \mathcal{T}(g) \right), \qquad (4.4.10)$$

where the sum is restricted to $d_i \geq 1$ and $\sum_{i=1}^{n-1} d_i = 2(n-2)$. Here $|\mathcal{W}[\mathcal{T}]|$ is given by (4.4.9) and $\mathcal{T}(g)$ gives the corresponding spacetime structure. $\mathcal{T}(g)$ is constructed by multiplying $\prod_{i=1}^{n-1} g_{n\,i}^{q_i - d_i}$ by $\prod_{\{i,j\}} g_{ij}$ where the second product is over pairs of insertion points connected by propagators dictated by the propagator structure of $\mathcal{T}$.

Note that the counting of trees of $n-1$ points is well studied, and given by Cayley's formula:

$$(n-1)^{n-3} \; . \qquad (4.4.11)$$

Finally, many trees correspond to the same arrangement of degrees d_i where $i = 1, \ldots, n-1$. Therefore, many of the trees will have the same value of $|\mathcal{W}[\mathcal{T}]|$.[9] This degeneracy is counted by the multinomial coefficient given by

$$\frac{(n-3)!}{\prod_{i=1}^{n-1}(d_i - 1)!} \; . \qquad (4.4.12)$$

Disconnected Contributions

The maximally extremal (ME) correlators can have disconnected contributions even in the $SU(N)$ theory. To see what the disconnected pieces look like, we can use similar reasoning to that given in (4.3.17) and the discussion around it. We give the argument here for completeness.

Without loss of generality, we shall say that r of the $(n-1)$ T_q operators form one of the disconnected pieces, and the other piece contains $\mathcal{O}_p, T_{r+1}, \ldots, T_{n-1}$. Upon the removal of $\mathcal{O}_p$, the rest of $T_{r+1}, \ldots, T_{n-1}$ must remain connected, otherwise we would get a near extremal diagram which we showed in 4.3.2 is equal to zero. The minimal way for this

[9] It is interesting to note, therefore, that a tree is not specified uniquely by giving the number of propagator ends that reach each point. It is only unique when the configuration of bridges is also specified.

to occur is for the other operators to be connected like a tree diagram themselves. This would lead the number of bridges between these operators, and not $\mathcal{O}_p$, to be

$$k_R = \frac{1}{2}\left(-p + \sum_{i=r+1}^{n-1} q_i\right) \geq n - r - 2. \tag{4.4.13}$$

The condition imposed by looking at Maximally-Extremal correlators is

$$k = \frac{1}{2}\left(-p + \sum_{i=1}^{n-1} q_i\right) = n - 2\ . \tag{4.4.14}$$

Therefore, using (4.4.13) with (4.4.14) we get

$$\frac{1}{2}\sum_{i=1}^{r} q_i = n - 2 - k_R \leq r\ . \tag{4.4.15}$$

The final inequality, specifically looking at $\frac{1}{2}\sum_{i=1}^{r} q_i \leq r$, indicates that the only way for disconnected propagator structures to give non-zero contributions to (4.4.7) is if the operators not connected to $\mathcal{O}_p$ are all single particle operators of charge two. Let K be the number of operators that are disconnected from $\mathcal{O}_p$, all of which are $\mathcal{O}_2$ operators, and $K \geq 2$. Let $\{k_1, \ldots, k_r\}$ label the partitions of K such that there are no 1's, meaning $k_i \geq 2$ for all i and $\sum_{i=1}^{r} k_i = K$. The disconnected part of the correlation function is given by

$$\langle\left(\prod_{i=1}^{K}\mathcal{O}_2\right)\mathcal{O}_{q_{K+1}}\ldots\mathcal{O}_{q_{n-1}}\mathcal{O}_p\rangle_{\text{discon.}} = \sum_{\{k_1,\ldots,k_r\}\vdash K}\langle\prod_{i=1}^{k_1}\mathcal{O}_2\rangle\ldots\langle\prod_{i=1}^{k_r}\mathcal{O}_2\rangle\langle\mathcal{O}_{q_{K+1}}\ldots\mathcal{O}_{q_{n-1}}\mathcal{O}_p\rangle_{\text{conn.}} \tag{4.4.16}$$

We will conclude this section with some simple examples described below.

4-point Functions

Using (4.4.11), we see there are three possible trees for the operators. Referring to the number of legs at positions $i = 1, 2, 3$ given by d_i, the three trees correspond to $d_1 = 2, d_{2,3} = 1$ and the two other unique permutations of this. There is no degeneracy,

as can be seen by (4.4.12), therefore using (4.4.10) the full result is given by

$$\langle \mathcal{O}_p \mathcal{O}_{q_1} \mathcal{O}_{q_2} \mathcal{O}_{q_3} \rangle_{\text{connected}} = q_1 q_2 q_3 \langle \mathcal{O}_p \mathcal{O}_p \rangle \Big[(q_1 - 1) g_{41}^{q_1 - 2} g_{42}^{q_2 - 1} g_{43}^{q_3 - 1} g_{12} g_{13} + \\ (q_2 - 1) g_{41}^{q_1 - 1} g_{42}^{q_2 - 2} g_{43}^{q_3 - 1} g_{12} g_{23} \ + \ (q_3 - 1) g_{41}^{q_1 - 1} g_{42}^{q_2 - 1} g_{43}^{q_3 - 2} g_{13} g_{23} \Big] . \tag{4.4.17}$$

5-point Functions

Again using (4.4.11), the number of trees is given by $4^2 = 16$, and this is the first number of points with degeneracy. There are four non-degenerate trees given by

$$d_1 = 3\,,\, d_{j=2,3,4} = 1 \quad ; \quad d_2 = 3\,,\, d_{j=1,3,4} = 1 \quad ; \quad d_3 = 3\,,\, d_{j=1,2,4} = 1 \quad ; \quad d_4 = 3\,,\, d_{j=1,2,3} = 1. \tag{4.4.18}$$

On top of that, there are the following six configurations that have degeneracy two

$$\begin{aligned} d_{i=1,2} = 2\,,\, d_{i=3,4} = 1 \quad ; \quad d_{i=1,3} = 2\,,\, d_{i=2,4} = 1 \\ d_{i=1,4} = 2\,,\, d_{i=2,3} = 1 \quad ; \quad d_{i=2,3} = 2\,,\, d_{i=1,4} = 1 \\ d_{i=2,4} = 2\,,\, d_{i=1,3} = 1 \quad ; \quad d_{i=3,4} = 2\,,\, d_{i=1,2} = 1. \end{aligned} \tag{4.4.19}$$

It is worth noting that the contribution of some of the trees might vanish for low charges. For example, consider the case $q_1 = 2$; the diagram associated to $d_1 = 3, d_{j=2,3,4} = 1$ contributes $q_1 q_2 q_3 q_4 (q_1 - 1)(q_1 - 2)$. This vanishes the case of $q_1 = 2$. In fact, if we consider the correlator $\langle \mathcal{O}_2 \mathcal{O}_2 \mathcal{O}_2 \mathcal{O}_2 \mathcal{O}_2 \rangle$ all of the non-degenerate diagrams vanish and we are left with the degenerate trees given above, all contributing with coefficient $q_1 q_2 q_3 q_4 = 16$.

4.4.2 Next-to-Maximally-Extremal Correlators

The next correlation functions to consider are the next-to-maximally-extremal functions (NME). These are the n-point correlators given by

$$\langle \mathcal{O}_p(x) \mathcal{O}_{q_1}(x_1) \dots \mathcal{O}_{q_{n-1}}(x_{n-1}) \rangle \quad ; \quad k = n - 1 \quad ; \quad k = \tfrac{1}{2}(-p + \textstyle\sum q_i) \,. \tag{4.4.20}$$

Once again, it is worth noting the difference between the two different associations with the term "extremality". The NME functions refer to the set of n-point correlators that have the second lowest value of k for which they do not vanish. However, this is not a fixed value of k for all n. At three points, the N^2E three point functions are the next-to-maximally-extremal three point functions. At four points the N^3E functions are the next-to-maximally-extremal four-point functions.

To begin we will discuss three-point next-to-maximally-extremal functions, and provide an explicit, closed formula for these functions. We will then move on to comment on n-point NME correlators.

3-Point Functions

Starting with $n = 3$ we are studying next-next-to-extremal three-point functions

$$\langle \mathcal{O}_p(x)\mathcal{O}_{q_1}(x_1)\mathcal{O}_{q_2}(x_2)\rangle \qquad ; \qquad p = q_1 + q_2 - 4. \tag{4.4.21}$$

We will see below that these correlation functions can also be related to the two-point function $\langle \mathcal{O}_p\mathcal{O}_p\rangle$, but with a more complicated pre-factor than in (4.4.6) consisting of non-factorisable polynomials.

Once again, to continue we replace $\mathcal{O}_{q_1}$ and $\mathcal{O}_{q_2}$ by their respective expansions in the trace basis. For this case, the expansion will truncate for any term involving higher than double-trace operators at a single point with all other terms vanishing due to the now familiar near-extremal argument. Furthermore, double trace operators can be replaced directly with double particle operators (meaning the product of two single particle operators) since any other terms would vanish. Therefore, we end up with the following expansion

for N^2 three-point functions:

$$\begin{aligned}\langle \mathcal{O}_p(x)\mathcal{O}_{q_1}(x_1)\mathcal{O}_{q_2}(x_2)\rangle = \; & \langle \mathcal{O}_p(x)T_{q_1}(x_1)T_{q_2}(x_2)\rangle \\ & + \sum_{p_1=2}^{\frac{q_1}{2}} C_{p_1(q_1-p_1)}\, \langle \mathcal{O}_p(x)\left[\mathcal{O}_{p_1}\mathcal{O}_{q_1-p_1}\right](x_1)\mathcal{O}_{q_2}(x_2)\rangle \\ & + \sum_{p_2=2}^{\frac{q_2}{2}} C_{p_2(q_2-p_2)}\, \langle \mathcal{O}_p(x)\mathcal{O}_{q_1}(x_1)\left[\mathcal{O}_{p_2}\mathcal{O}_{q_2-p_2}\right](x_2)\rangle \;,\end{aligned} \tag{4.4.22}$$

where $C_{(p_1p_2)}$ is the coefficient of the double trace operators $T_{p_1}T_{p_2}$ in the expansion of the single particle states. The explicit form for this mixing coefficient can be found in appendix C.

The terms involving double-traces are equivalent to the four-point ME diagrams given in the previous section. Precisely in (4.4.17). We find,

$$\langle \mathcal{O}_p(x)\left[\mathcal{O}_{p_1}\mathcal{O}_{q_1-p_1}\right](x_1)\mathcal{O}_{q_2}(x_2)\rangle = q_2(q_2-1)p_1(q_1-p_1)\, g_{xx_1}^{q_1-2}g_{xx_2}^{q_2-2}g_{x_1x_2}^2\langle \mathcal{O}_p\mathcal{O}_p\rangle \tag{4.4.23}$$

$$\langle \mathcal{O}_p(x)\mathcal{O}_{q_1}(x_1)\left[\mathcal{O}_{p_2}\mathcal{O}_{q_2-p_2}\right](x_2)\rangle = q_1(q_1-1)p_2(q_2-p_2)\, g_{xx_1}^{q_1-2}g_{xx_2}^{q_2-2}g_{x_1x_2}^2\langle \mathcal{O}_p\mathcal{O}_p\rangle \tag{4.4.24}$$

In each case there is only one term compared to (4.4.17) because there cannot be a bridge within $\left[\mathcal{O}_{p_1}\mathcal{O}_{q_1-p_1}\right](x_1)$ or $\left[\mathcal{O}_{p_2}\mathcal{O}_{q_2-p_2}\right](x_2)$.

The only unknown is therefore $\langle \mathcal{O}_p(x)T_{q_1}(x_1)T_{q_2}(x_2)\rangle$. This consists of Feynman diagrams with two propagators between T_{q_1} and T_{q_2}, of which there are $q_1(q_1-1)q_2(q_2-1)/2$ different ways of contracting the fundamental fields. However, the net colour factor has four contributions for each arrangement of Wick contraction. This is because we are using the $SU(N)$ propagator given in (4.1.5), so there will be different contributions depending on if we are using the $U(N)$ part of the propagator, $\delta_r^u\delta_t^s$, or the second part of the propagator, $-\frac{1}{N}\delta_r^s\delta_t^u$. Below we shall investigate the different contributions that we get for the Wick contractions between T_{q_1} and T_{q_2}:

- If we consider the two Wick contractions between $T_{q_1}(x_1)T_{q_2}(x_2)$ but use just the second

part of the propagator, the resulting leading term is a double trace operator:

$$\mathrm{Tr}(\underbrace{\ldots \overbrace{\phi^a_b \ldots \phi^c_d}^{\bullet} \ldots}_{q_1})\,\mathrm{Tr}(\underbrace{\ldots \overbrace{\phi^e_f \ldots \phi^g_h}^{\bullet} \ldots}_{q_2})\left(-\tfrac{1}{N}\right)\delta^a_b\delta^g_h\left(-\tfrac{1}{N}\right)\delta^c_d\delta^e_f \simeq \tfrac{1}{N^2}\,\mathrm{Tr}(\underbrace{\phi\ldots\phi}_{q_1-2})\,\mathrm{Tr}(\underbrace{\phi\ldots\phi}_{q_2-2}) \tag{4.4.25}$$

This will give zero when the final two-point function with $\mathcal{O}_p$ is taken, by the definition of the single particle operator.

- If we now consider the two Wick contractions but focussing on the $U(N)$ part of the $SU(N)$ propagator, with the fundamental fields being non-adjacent, we also end up with a double trace operator as the leading term. We get

$$\mathrm{Tr}(\underbrace{\ldots \overbrace{\phi^a_b \ldots \phi^c_d}^{\bullet} \ldots}_{q_1})\,\mathrm{Tr}(\underbrace{\ldots \overbrace{\phi^e_f \ldots \phi^g_h}^{\bullet} \ldots}_{q_2})\delta^a_h\delta^g_b\delta^c_f\delta^e_d \simeq \mathrm{Tr}(\underbrace{\phi\ldots\phi}_{q_1+i-j-k+l-2})\,\mathrm{Tr}(\underbrace{\phi\ldots\phi}_{q_2-i+j+k-l-2}) \tag{4.4.26}$$

where i, j, k, l label the positions of the fields ϕ that were written out explicitly on the left-hand side of (4.4.26) in that order. Notice that the total charge of the resultant double trace operator is $q_1 + q_2 - 4$ as expected. As with the previous case, it will give zero when the final two-point function with $\mathcal{O}_p$ is taken.

- The next two cases will both give non-vanishing results. The leading operator that comes from performing the Wick contractions between T_{q_1} and T_{q_2} we will see is the single-trace operator T_p. The first case is using the $U(N)$ part of the propagator with the fundamental fields in each T_{q_i} with bridge ends being adjacent to each other. We end up with

$$\mathrm{Tr}(\underbrace{\ldots \overbrace{\phi^a_b \phi^b_c}^{\bullet} \ldots}_{q_1})\,\mathrm{Tr}(\underbrace{\ldots \overbrace{\phi^d_e \phi^e_f}^{\bullet} \ldots}_{q_2})\delta^a_f\delta^e_b\delta^b_e\delta^d_c \simeq N\,\mathrm{Tr}(\underbrace{\phi\ldots\phi}_{p}) \tag{4.4.27}$$

where there are $q_1 q_2$ unique Wick contractions of this type. The second case that gives a non-zero contribution is taking one propagator to be the $U(N)$ part of the propagator,

and the other to be the second part of the $SU(N)$ propagator giving

$$\mathrm{Tr}(\underbrace{\ldots \phi_b^a \ldots \phi_d^c \ldots}_{q_1})\,\mathrm{Tr}(\underbrace{\ldots \phi_f^e \ldots \phi_h^g \ldots}_{q_2})\left(-\delta_h^a\delta_b^g\tfrac{1}{N}\delta_d^c\delta_f^e - \tfrac{1}{N}\delta_b^a\delta_h^g\delta_f^c\delta_d^e\right) \simeq -\tfrac{2}{N}\,\mathrm{Tr}(\underbrace{\phi\ldots\phi}_{p}) \tag{4.4.28}$$

The number of non-zero contractions of this type is given by $q_1(q_1-1)q_2(q_2-1)/2$. So, upon inputting (4.4.27) and (4.4.28) into a vev with $\mathcal{O}_p$ and using the fact that $\langle T_p\mathcal{O}_p\rangle = \langle \mathcal{O}_p\mathcal{O}_p\rangle$ we get the final result

$$\langle T_{q_1}T_{q_2}\mathcal{O}_p\rangle = q_1q_2\left[N - \frac{(q_1-1)(q_2-1)}{N}\right]\langle \mathcal{O}_p\mathcal{O}_p\rangle \ . \tag{4.4.29}$$

Inputting the calculations described above into (4.4.22) yields an explicit formula for the N^2 extremal three-point functions of single particle operators

$$\langle \mathcal{O}_p(x)\mathcal{O}_{q_1}(x_1)\mathcal{O}_{q_2}(x_2)\rangle = \langle \mathcal{O}_p\mathcal{O}_p\rangle\left[q_1q_2\Big[N - \frac{(q_1-1)(q_2-1)}{N}\Big] + \right.$$
$$\left.\sum_{p_1=2}^{\lfloor\frac{q_1}{2}\rfloor} C_{p_1(q_1-p_1)}q_2(q_2-1)p_1(q_1-p_1) + \sum_{p_2=2}^{\lfloor\frac{q_2}{2}\rfloor} C_{p_2(q_2-p_2)}q_1(q_1-1)p_2(q_2-p_2)\right]. \tag{4.4.30}$$

The two sums are symmetric and can be performed with the explicit knowledge of $C_{p_1(q_1-p_1)}$ given in appendix C. We find

$$\sum_{p_1=2}^{\lfloor\frac{q_1}{2}\rfloor} C_{p_1(q_1-p_1)}p_1(q_1-p_1) =$$
$$\frac{q_1}{2N(q_1-2)}\left[2N^2 + (q_1-1)_2N + 2(q_1-2)_2 + \frac{2(q_1-1)_2N(N)_{q_1}}{(N-q_1+1)_{q_1} - (N)_{q_1}}\right] \tag{4.4.31}$$

n-Point Functions

Whilst we are not necessarily able to provide a closed formula for n-point NME functions, the method described above can be generalised to any point. We provide a sketch of how the computation goes here.

The definition of $k = \frac{1}{2}(-p + \sum q_i) = n-1$ selects an operator $\mathcal{O}_p$ to be special in some way, and we call the others “light". The calculation begins by expanding all these “light"

operators in terms of the trace basis, where it should be clear that almost all terms in the expansion vanish since they produce correlators equivalent to near-extremal higher point diagrams. The result is the following generalisation of the three-point expansion in (4.4.22), namely

$$\langle \mathcal{O}_{q_1} \dots \mathcal{O}_{q_{n-1}} \mathcal{O}_p \rangle = \langle T_{q_1} \dots T_{q_{n-1}} \mathcal{O}_p(x_n) \rangle + \sum_{i=1}^{n-1} \sum_{p_i=2}^{\lfloor \frac{q_i}{2} \rfloor} C_{p_i(q_i-p_i)} \langle \mathcal{O}_{q_1} \dots \mathcal{O}_{q_{i-1}} [O_{p_i} \mathcal{O}_{q_i-p_i}] \mathcal{O}_{q_{i+1}} \dots \mathcal{O}_p(x_n) \rangle \ . \tag{4.4.32}$$

We can think of (4.4.32) as a separate equation for each contributing Feynman diagram independently. Note that the correlators in the sum are all contributions to $n+1$-point N^{n-1}-extremal correlators, which are maximally extremal, so we have formulae for them in section 4.4.1. The first term can then be computed by doing the partial Wick contractions, $n-1$ in total, on the single trace operators $T_{p_1} \dots T_{p_{n-1}}$ only keeping the relevant terms, just as was done in the three-point case in the discussion above (4.4.29).

4.4.3 On correlators with lower extremality

In section 4.4.1, we defined how to classify free theory correlators according to their degree of extremality with respect to the maximally-extremal correlator. The maximally-extremal n-point correlators were defined to be the simplest non-vanishing correlators, which are those which satisfy $k = n-2$, as for $k \leq n-3$ we showed in 4.3 they vanish. These functions can be computed in terms of tree graphs, and the charge dependence on p and the q_is fully factorises out for each tree graph, with the factor having a clean interpretation. The NME functions in section 4.4.2 showed more structure. They were not as simple to calculate directly, however a closed formula was found in the end for the three-point functions. We would expect that NNME functions will have ever more structure, and so on for higher extremality. Here we will explicitly show that the complexity of NNME is already evident in the three-point functions.

Let us consider the correlators $\langle \mathcal{O}_p \mathcal{O}_{q_1} \mathcal{O}_{q_2} \rangle$ with $r = p + q - 6$. In theory we can approach this calculation in the same way as for the next-to-maximally-extremal functions by expanding $\mathcal{O}_{q_1}$ and $\mathcal{O}_{q_2}$ in terms of the trace basis. For this case, however, more complicated multi-trace contributions will remain, and so when re-writing the traces in terms of the single particle operators again one must be careful to add in any extra coefficients necessary. In theory all of the contributions are known or can be calculated using the considerations of the previous sections, except for the leading term of the form $\langle \mathcal{O}_p T_{q_1} T_{q_2} \rangle$, with three bridges between T_{q_1} and T_{q_2}. The first few cases are shown below,

$$\langle \mathcal{O}_6 T_6 T_6 \rangle = \left(300 + \frac{7200}{N^2} + 36N^2\right) \langle \mathcal{O}_6 \mathcal{O}_6 \rangle \tag{4.4.33}$$

$$\langle \mathcal{O}_7 T_7 T_6 \rangle = \left(840 + \frac{12600}{N^2} + 42N^2\right) \langle \mathcal{O}_7 \mathcal{O}_7 \rangle \tag{4.4.34}$$

$$\langle \mathcal{O}_8 T_8 T_6 \rangle = \left(1680 + \frac{20160}{N^2} + 48N^2\right) \langle \mathcal{O}_8 \mathcal{O}_8 \rangle \tag{4.4.35}$$

$$\langle \mathcal{O}_8 T_7 T_7 \rangle = \left(1911 + \frac{22050}{N^2} + 49N^2\right) \langle \mathcal{O}_8 \mathcal{O}_8 \rangle \tag{4.4.36}$$

$$\langle \mathcal{O}_9 T_8 T_7 \rangle = \left(3528 + \frac{35280}{N^2} + 56N^2\right) \langle \mathcal{O}_9 \mathcal{O}_9 \rangle \tag{4.4.37}$$

where it should be noted the correlators $\langle T_{\underline{p}} T_{q_1} T_{q_2} \rangle$ are very complicated before converting the $T_{\underline{p}}$s to the single particle operator $\mathcal{O}_p$.

Using similar reasoning to that around (4.4.25) - (4.4.28), we can build up contributions to $\langle \mathcal{O}_p T_{q_1} T_{q_2} \rangle$ by considering different configurations for each of the three $SU(N)$ propagators:

(1) $O(1/N^2)$ contributions can only come from the configuration of propagators involving two $1/N$ parts and one $U(N)$ part. Completing the two $1/N$ Wick contractions leaves $T_{q_1-2}(x_1) T_{q_2-2}(x_2)$, then doing the one $U(N)$ contraction results in a single trace operator of weight p (as all multi trace contributions vanish when calculating the two-point function of it and $\mathcal{O}_p$. There are a total of $\frac{q_1(q_1-1)(q_1-2)q_2(q_2-1)(q_2-2)}{2N^2}$, where the half comes from the interchangeability of the two propagators that we take the $1/N$ terms from.

(2) $O(1/N)$ contributions can only occur from propagator configurations that have two $U(N)$ parts that are *not* consecutive, and one $1/N$ part. When the $1/N$ Wick contraction is completed we reduce to $T_{q_1-1}(x_1)T_{q_2-1}(x_2)$, then when we attach the two $U(N)$ propagators we are in a situation like (4.4.26) therefore the contribution vanishes.

(3) $O(N)$ contributions can only arise from picking three $U(N)$ propagators, with two being consecutive and the last specifically not being consecutive to the other two. The consecutive $U(N)$ propagators give a factor of N, reduce the number of legs to $q_1 + q_2 - 4$ and link the two operators. In fact, we saw in (4.4.27) that at this stage without a third propagator we would get at first order a single trace operator. The third propagator, however, gives us a similar situation to (4.4.26) again and the result vanishes.

(4) $O(N^2)$ contributions can only arise from picking three $U(N)$ propagator parts that are all consecutive. There are $q_1 q_2$ total ways of contributing to this propagator structure.

(5) $O(1)$ contributions can arise from two different configurations: a) one $1/N$ propagator part and two consecutive $U(N)$ parts. b) three $U(N)$ parts none of which can be consecutive to each other.

Notice that a) is necessarily negative, whereas b) is positive.

Putting all of this information together we find

$$\langle \mathcal{O}_p T_{q_1} T_{q_2} \rangle = \left[q_1 q_2 N^2 + 3 \times \frac{(q_1-2)_3 (q_2-2)_3}{3! N^2} + \left(-\frac{1}{N}(N c_a) + c_b \right) \right] \langle \mathcal{O}_p \mathcal{O}_p \rangle$$

where $c_a, c_b > 0$ and depend on the charges q_1 and q_2.[10]

It is not straightforward at this point to extract further information from the combinatorics, and in practice the dependence on the charges becomes hidden in the combinatorics.

[10] A simple guess is $c_b - c_a = (q_1-1)_2 (q_2-1)_2 (\frac{1}{3}(q_1-5)(q_2-5) - \frac{1}{4}(q_1-6)(q_2-6))$, which seems to be consistent with all of the above examples.

However, the surprisingly simple final results for the NNME three point function discussed above indicates that it may be possible to understand single-particle multipoint correlators in a way that avoids having to complete the brute force method of computation. We hope to make this observation more concrete in the future. For example, it would be interesting to see if the approach taken in [138], in which diagrammatic tensor space techniques are used to calculate extremal and near-extremal correlators, could provide any more insight into how to obtain explicit formulae for more classes of correlators involving single particle operators.

In [58], we present a nice alternative approach to obtaining multi-point correlation functions using the half-BPS operator product expansion. The basic idea is to bootstrap the free theory correlators by projecting onto the half-BPS states, which was an approach also pursued in [139] at order $\frac{1}{N^2}$. This method gives a different perspective to the colour factors obtained for the correlators described above. In [58], there are examples of NME, NNME and NNNME correlators; the interested reader is encouraged to take a look.

4.4.4 3-Point Functions as Multi-Particle 2-Point Functions

The work done in the previous sections has been to start from maximally extremal and next-to-maximally extremal three-point functions, compute them, and understand how to generalise the techniques to n-point functions of single particle operators. In order to deal with the three-point functions, we substituted two out of three SPOs with their corresponding expansion in the trace basis, and as such reduced part of the calculation to finding a three-point function of a single particle operator and two single-trace operators. In this section, we wish to present an interesting feature of three-point functions of the single particle operator which does not require passing to the trace basis, and is valid for any extremality. The relation works as follows,

$$\langle \mathcal{O}_p \mathcal{O}_q \mathcal{O}_r \rangle = \frac{1}{2^k k!} \langle [\mathcal{O}_p \mathcal{O}_q] \, [\mathcal{O}_r \overbrace{\mathcal{O}_2 \cdots \mathcal{O}_2}^{k}] \rangle_{\text{connected}}, \qquad p+q-r = 2k \ . \tag{4.4.38}$$

where the equality is for the color factor of the left hand side being the same as that of a two-point function of multi-particle operators of SPOs on the right hand side.

Let us first illustrate the case $k = 3$ with the following picture,

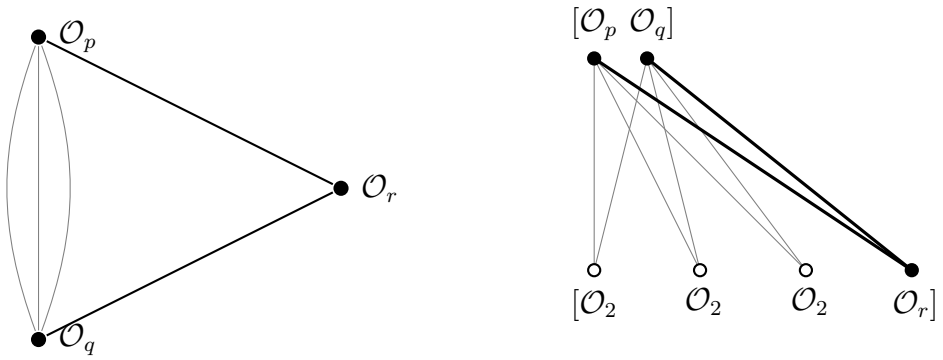

(4.4.39)

The diagram on the left is the single diagram contributing to $\langle \mathcal{O}_p \mathcal{O}_q \mathcal{O}_r \rangle$, whereas the one on the right is the only type of diagram contributing to $\langle [\mathcal{O}_p \mathcal{O}_q]\, [\mathcal{O}_r \mathcal{O}_2 \mathcal{O}_2 \mathcal{O}_2\,] \rangle$.

To show (4.4.38), consider where the two legs out of an $\mathcal{O}_2$ can end. They can not go to $\mathcal{O}_r$ as they are at the same point. If they both went to $\mathcal{O}_p$, this would result in a diagram of the form of a dumbbell in (4.3.1) (centered around $\mathcal{O}_p$) which thus vanishes. Similarly if both legs go to $\mathcal{O}_q$. The only exception to this is if p or q equals two in which case you can have a completely disconnected contribution, however the statement (4.4.38) is for the connected diagram so we do not need to consider this case. Therefore, the only remaining possibility is that one leg goes to $\mathcal{O}_p$ and one to $\mathcal{O}_q$ resulting in the diagram shown on the right. There are clearly $2^k k!$ different but equivalent diagrams of this sort, arising from the $k!$ possibilities of swapping the propagators from $\mathcal{O}_p$ to the $\mathcal{O}_2$s and from the cyclic symmetry around each $\mathcal{O}_2$.

The colour factor of $\langle \mathcal{O}_p \mathcal{O}_q \mathcal{O}_r \rangle$ is the same as one of the equivalent configuration of $\langle [\mathcal{O}_p \mathcal{O}_q]\, [\mathcal{O}_r \mathcal{O}_2 \dots \mathcal{O}_2\,] \rangle$ described above. This follows from the fact that

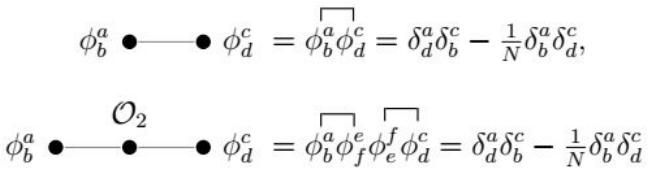

(4.4.40)

which concludes our proof of (4.4.38).[11]

While the right hand side of (4.4.38) is restricted to the connected part of the two point function (thinking of it as a limit of a higher point function) rather than the full two-point function, we need this distinction only when p or q equals 2 and $k = 1$. In this case we have

$$\langle \mathcal{O}_q \mathcal{O}_2 \mathcal{O}_q \rangle = \frac{1}{2} \left(\langle [\mathcal{O}_q \mathcal{O}_2] [\mathcal{O}_q \mathcal{O}_2] \rangle - \langle \mathcal{O}_q \mathcal{O}_q \rangle \langle \mathcal{O}_2 \mathcal{O}_2 \rangle \right). \tag{4.4.41}$$

It is worth noting that the condition giving the value of k in (4.4.38) is dependent on the order of $\mathcal{O}_p$, $\mathcal{O}_q$ and $\mathcal{O}_r$; in particular it distinguishes $\mathcal{O}_r$ from the other two operators. However the colour factor of the three-point function *does not depend on this ordering*. For example, consider the three point function of $\mathcal{O}_3$, $\mathcal{O}_4$ and $\mathcal{O}_5$, we can have three multi-particle two-point functions with $k = 1, 2, 3$ respectively,

$$\begin{array}{ccccccc} \langle \mathcal{O}_3 \mathcal{O}_4 \mathcal{O}_5 \rangle & = & \langle \mathcal{O}_3 \mathcal{O}_5 \mathcal{O}_4 \rangle & = & \langle \mathcal{O}_4 \mathcal{O}_5 \mathcal{O}_3 \rangle & = & \dfrac{60 \prod_{i=1}^{4} (N^2 - i^2)}{N(5+N^2)} \\ \| & & \| & & \| & & \\ \frac{1}{2} \langle [\mathcal{O}_3 \mathcal{O}_4] [\mathcal{O}_5 \mathcal{O}_2] \rangle & & \frac{1}{8} \langle [\mathcal{O}_3 \mathcal{O}_5] [\mathcal{O}_4 \mathcal{O}_2 \mathcal{O}_2] \rangle & & \frac{1}{48} \langle [\mathcal{O}_4 \mathcal{O}_5] [\mathcal{O}_3 \mathcal{O}_2 \mathcal{O}_2 \mathcal{O}_2] \rangle & & \end{array} \tag{4.4.42}$$

All three multi-particle two-point functions are then equal!.

We conclude that for a triplet of single-particle operators all multi-particle two-point functions which correspond to different dispositions of the three SPOs give the same color factor up to a multiplicity counted by $2^k k!$.

While the discussion above required $\mathcal{O}_p$ and $\mathcal{O}_q$ to be SPOs, it nowhere relied on $\mathcal{O}_r$ to be an SPO. Thus the following more general relation holds for any half-BPS operator $T_{r_1,\ldots,r_l}$:

$$\langle \mathcal{O}_p \mathcal{O}_q T_{r_1,\ldots,r_l} \rangle = \frac{1}{2^k k!} \langle [\mathcal{O}_p \mathcal{O}_q] [T_{r_1,\ldots,r_l} \overbrace{\mathcal{O}_2 \cdots \mathcal{O}_2}^{k}] \rangle |_{\text{connected}}, \tag{4.4.43}$$

with $r_1 + \ldots + r_l = r$ and $p + q - r = 2k$.

[11] The ideas of our proof here can be generalised to multipoint correlators as well. For example those which are equivalent to the l.h.s. of (4.4.43).

4.4.5 Some Formulae for Two-Point Functions of Multi-Particle Operators

Zeroes

Looking at the two point functions of multi-particle operators with two-particle operators of weight p, we can predict when they are zero. The statement is as follows:

$$\langle [\mathcal{O}_{p-p_1}\mathcal{O}_{p_1}][\mathcal{O}_{q_1}...\mathcal{O}_{q_j}]\rangle = 0, \quad j > p_1, \tag{4.4.44}$$

where $p-p_1$ is the largest charge. By thinking of (4.4.44) as the limit of a higher point, p_1 extremal function, this is a direct consequence of the fact that near extremal correlators vanish. All diagrams contributing to p_1 extremal functions are zero if the number of points is p_1+3 or above. $\langle [\mathcal{O}_{p-p_1}\mathcal{O}_{p_1}][\mathcal{O}_{q_1}...\mathcal{O}_{q_j}]\rangle$ is a $j+2$-point function, therefore for $j > p_1$ all diagrams are zero and we arrive at (4.4.44).

In fact, the statement can be generalised to

$$\langle [\mathcal{O}_{p_i}\mathcal{O}_{p_1}...\mathcal{O}_{p_{i-1}}][\mathcal{O}_{q_1}...\mathcal{O}_{q_j}]\rangle = 0, \quad j \geq \sum_{k=1}^{i-1} p_k - i + 3. \tag{4.4.45}$$

where $i < j$ and p_i is the largest charge. The reasoning follows in a similar way to the two-particle case above, noting that the two point function (4.4.45) is the limit of a higher point, $\sum_{k=1}^{i-1} p_k$ extremal function.

Multi-particle two point functions proportional to single particle two-point functions

Considering again two point functions of multi-particle operators with two-particle operators of weight p, we find

$$\langle [\mathcal{O}_{p-p_1}\mathcal{O}_{p_1}][\mathcal{O}_{q_1}...\mathcal{O}_{q_j}]\rangle = p_1! \left(\prod_{k=1}^{j} q_j\right) \langle \mathcal{O}_{p-p_1}\mathcal{O}_{p-p_1}\rangle, \quad j = p_1, \tag{4.4.46}$$

where $p-p_1$ is the largest charge. To show this, we first note that

$$\langle[\mathcal{O}_{p-p_1}\mathcal{O}_{p_1}][\mathcal{O}_{q_1}...\mathcal{O}_{q_j}]\rangle = \langle[\mathcal{O}_{p-p_1}T_{p_1}][T_{q_1}...T_{q_j}]\rangle \tag{4.4.47}$$

which can be seen by expanding all bar the first single particle operators in the trace basis and noting that for $j=p_1$ all other contributions are near extremal and therefore zero. The only diagrams that contribute to (4.4.47) are those with one propagator between the charge p_1 and each of the charges $q_1,...,q_j$; the others either reduce to dumbbell diagrams that are known to be zero, or factorise into two two-point functions of a single particle operator with a multi-particle operator, which are zero by definition. Doing these p_1 contractions gives

$$\lim_{x_1\to x_2}\mathrm{Tr}(\underbrace{\phi(x_1)\dots\phi(x_1)}_{p_1})\,\mathrm{Tr}(\underbrace{\phi(x_2)\dots\phi(x_2)}_{q_1})\dots\mathrm{Tr}(\underbrace{\phi(x_2)\dots\phi(x_2)}_{q_j}) \simeq \mathrm{Tr}(\underbrace{\phi(x_2)\dots\phi(x_2)}_{p-p_1}) + \dots \tag{4.4.48}$$

and since the right hand side is being contracted with the single particle operator $\mathcal{O}_{p-p_1}$, only the $p-p_1$ single trace term will be non-zero in the end.

There are $p_1!\prod_{k=1}^{j}q_k$ ways of doing the above contractions, therefore

$$\langle[\mathcal{O}_{p-p_1}\mathcal{O}_{p_1}][\mathcal{O}_{q_1}...\mathcal{O}_{q_j}]\rangle = p_1!\left(\prod_{k=1}^{j}q_j\right)\langle\mathcal{O}_{p-p_1}T_{p-p_1}\rangle. \tag{4.4.49}$$

Finally, using the fact that $\langle\mathcal{O}_pT_p\rangle = \langle\mathcal{O}_p\mathcal{O}_p\rangle$ for all p due to the orthogonality of $\mathcal{O}_p$, we arrive at (4.4.46).

4.4.6 Three-point Functions of Multi-Particles Involving $\mathcal{O}_2$s

In this section we present some formulae for two- and three-point functions of multi-particle operators constructed using single particle operators of charge 2. We then take the large N limit of the normalised correlators we have calculated. The motivation behind studying these correlation functions was to try to make contact with the AdS giant gravitons, which we expected to be related to a product of $\mathcal{O}_2$s in the multi-particle

basis. In the Schur basis the AdS giants are given by the Schur polynomial operators associated to the completely symmetric Young diagram. By comparing to results detailed in [140] we will see that these limits are in fact not in agreement with the AdS giant graviton calculation on the string theory side. However, the explicit expressions for the correlators may be useful in the future so we present them here even though they do not have the interpretation we expected in the large N limit.

We begin by calculating the three point function of the form $\langle \mathcal{O}_2[\mathcal{O}_2...\mathcal{O}_2][\mathcal{O}_2...\mathcal{O}_2]\rangle$. Firstly, from many examples we observe the two-point function of products of $\mathcal{O}_2$'s is given by

$$\langle [\overbrace{\mathcal{O}_2...\mathcal{O}_2}^{k}][\overbrace{\mathcal{O}_2...\mathcal{O}_2}^{k}]\rangle = 2^{k-1}k!\langle \mathcal{O}_2\mathcal{O}_2\rangle \prod_{i=1}^{k-1}(2i-1+N^2) \tag{4.4.50}$$

$$= 2^{2(k-1)}k!\left(\frac{1}{2}(1+N^2)\right)_{k-1}\langle \mathcal{O}_2\mathcal{O}_2\rangle. \tag{4.4.51}$$

This particular two-point function will be useful for calculating the rest of the correlators considered in this section. Note that for the rest of the section we shall use the variables k and l to represent the number of $\mathcal{O}_2$ operators in a multi-particle operator, and q and r for when we are referring to the total charge of the multi-particle operator.

The only non-zero correlators of the form $\langle \mathcal{O}_2[\overbrace{\mathcal{O}_2...\mathcal{O}_2}^{\frac{q}{2}}][\overbrace{\mathcal{O}_2...\mathcal{O}_2}^{\frac{r}{2}}]\rangle$ are those with $\frac{q}{2}=\frac{r}{2}=k$ and $\frac{q}{2}=k$, $\frac{r}{2}=k-1$. The three-point functions are given by

$$\langle \mathcal{O}_2[\overbrace{\mathcal{O}_2...\mathcal{O}_2}^{k}][\overbrace{\mathcal{O}_2...\mathcal{O}_2}^{k-1}]\rangle = \langle [\overbrace{\mathcal{O}_2...\mathcal{O}_2}^{k}][\overbrace{\mathcal{O}_2...\mathcal{O}_2}^{k}]\rangle, \tag{4.4.52}$$

$$\langle \mathcal{O}_2[\overbrace{\mathcal{O}_2...\mathcal{O}_2}^{k}][\overbrace{\mathcal{O}_2...\mathcal{O}_2}^{k}]\rangle = 2\cdot 2k\langle [\overbrace{\mathcal{O}_2...\mathcal{O}_2}^{k}][\overbrace{\mathcal{O}_2...\mathcal{O}_2}^{k}]\rangle. \tag{4.4.53}$$

Relation (4.4.52) is clear from the point of view of the correlator as a limit of the $2k$-point function of $\mathcal{O}_2$'s. There cannot be a contributing diagram with a propagator between the individual $\mathcal{O}_2$ and any of the $k-1$ group of $\mathcal{O}_2$'s, as there is no consistent propagator structure that can link the rest of the fields of the $\mathcal{O}_2$s. Therefore, the diagrams contributing to (4.4.52) are the same as the diagrams contributing to the two-

point function (4.4.50). The relation (4.4.53) comes from the same considerations as in section 4.4.1, and the observation that

$$\langle [\overbrace{\mathcal{O}_2...\mathcal{O}_2}^{k}][\overbrace{T_2...T_2}^{k}]\rangle = \langle [\overbrace{\mathcal{O}_2...\mathcal{O}_2}^{k}][\overbrace{\mathcal{O}_2...\mathcal{O}_2}^{k}]\rangle,$$

which is a result of near-extremal correlators vanishing.

We consider the limit of the normalised three-point functions (4.4.52) and (4.4.53) where $N \to \infty$, and $q, r \to \infty$ such that $q' = \frac{q}{N}, r' = \frac{r}{N}$ are fixed. We find the limit of (4.4.52) is given by

$$\frac{\langle \mathcal{O}_2[\overbrace{\mathcal{O}_2...\mathcal{O}_2}^{k}][\overbrace{\mathcal{O}_2...\mathcal{O}_2}^{k-1}]\rangle}{\sqrt{\langle \mathcal{O}_2\mathcal{O}_2\rangle\langle [\underbrace{\mathcal{O}_2...\mathcal{O}_2}_{k}][\underbrace{\mathcal{O}_2...\mathcal{O}_2}_{k}]\rangle\langle [\underbrace{\mathcal{O}_2...\mathcal{O}_2}_{k-1}][\underbrace{\mathcal{O}_2...\mathcal{O}_2}_{k-1}]\rangle}} \to \sqrt{\frac{q'N}{2}}, \tag{4.4.54}$$

and the limit of (4.4.53) is given by

$$\frac{\langle \mathcal{O}_2[\overbrace{\mathcal{O}_2...\mathcal{O}_2}^{k}][\overbrace{\mathcal{O}_2...\mathcal{O}_2}^{k}]\rangle}{\sqrt{\langle \mathcal{O}_2\mathcal{O}_2\rangle\langle [\underbrace{\mathcal{O}_2...\mathcal{O}_2}_{k}][\underbrace{\mathcal{O}_2...\mathcal{O}_2}_{k}]\rangle\langle [\underbrace{\mathcal{O}_2...\mathcal{O}_2}_{k}][\underbrace{\mathcal{O}_2...\mathcal{O}_2}_{k}]\rangle}} \to \sqrt{2}\frac{q}{N}. \tag{4.4.55}$$

In fact, equation (4.4.52) can be generalised to the following set of extremal three-point functions:

$$\langle [\overbrace{\mathcal{O}_2...\mathcal{O}_2}^{k}][\overbrace{\mathcal{O}_2...\mathcal{O}_2}^{l}][\overbrace{\mathcal{O}_2...\mathcal{O}_2}^{k+l}]\rangle = \langle [\overbrace{\mathcal{O}_2...\mathcal{O}_2}^{k+l}][\overbrace{\mathcal{O}_2...\mathcal{O}_2}^{k+l}]\rangle. \tag{4.4.56}$$

There are no diagrams with propagators between the group of k $\mathcal{O}_2$'s and the group of l $\mathcal{O}_2$'s, therefore the diagrams contributing to the three-point function on the left-hand side of (4.4.56) are the same as the diagrams contributing to the two-point function on the right-hand side of (4.4.56).

Now, taking the limit $N \to \infty$, but $q \to \infty$ such that $q' = \frac{q}{N}$ is fixed:

$$\frac{\langle [\overbrace{\mathcal{O}_2...\mathcal{O}_2}^{k}][\overbrace{\mathcal{O}_2...\mathcal{O}_2}^{l}][\overbrace{\mathcal{O}_2...\mathcal{O}_2}^{k+l}]\rangle}{\sqrt{\langle [\underbrace{\mathcal{O}_2...\mathcal{O}_2}_{k}][\underbrace{\mathcal{O}_2...\mathcal{O}_2}_{k}]\rangle\langle [\underbrace{\mathcal{O}_2...\mathcal{O}_2}_{l}][\underbrace{\mathcal{O}_2...\mathcal{O}_2}_{l}]\rangle\langle [\underbrace{\mathcal{O}_2...\mathcal{O}_2}_{k+l}][\underbrace{\mathcal{O}_2...\mathcal{O}_2}_{k+l}]\rangle}} \to \sqrt{\frac{N^k q'^k}{2^k k!}} \left(= \sqrt{\frac{l^k}{k!}}\right). \tag{4.4.57}$$

The 3-point function scales as $N^{\frac{k}{2}}$. The expression for $k = 1$ is in agreement with (4.4.54).

Finally, equation (4.4.53) can be generalised to the following set of next-to-extremal three-point functions:

$$\langle[\overbrace{\mathcal{O}_2...\mathcal{O}_2}^{k}][\overbrace{\mathcal{O}_2...\mathcal{O}_2}^{l}][\overbrace{\mathcal{O}_2...\mathcal{O}_2}^{k+l-1}]\rangle = 2k\cdot 2l\langle[\overbrace{\mathcal{O}_2...\mathcal{O}_2}^{k+l-1}][\overbrace{\mathcal{O}_2...\mathcal{O}_2}^{k+l-1}]\rangle. \tag{4.4.58}$$

This relies on the following;

$$\langle[\overbrace{\mathcal{O}_2...\mathcal{O}_2}^{k}][\overbrace{\mathcal{O}_2...\mathcal{O}_2}^{k}]\rangle = \langle[\overbrace{T_2...T_2}^{k}][\overbrace{\mathcal{O}_2...\mathcal{O}_2}^{k}]\rangle, \tag{4.4.59}$$

$$\langle[\overbrace{\mathcal{O}_2...\mathcal{O}_2}^{k}][\overbrace{\mathcal{O}_2...\mathcal{O}_2}^{l}][\overbrace{\mathcal{O}_2...\mathcal{O}_2}^{k+l-1}]\rangle = \langle[\overbrace{T_2...T_2}^{k}][\overbrace{T_2...T_2}^{l}][\overbrace{\mathcal{O}_2...\mathcal{O}_2}^{k+l-1}]\rangle, \tag{4.4.60}$$

both of which are a consequence of the vanishing of near extremal functions.

Now, taking the limit $N\to\infty$, but $q\to\infty$ such that $q'=\frac{q}{N}$ is fixed:

$$\begin{aligned}&\frac{\langle[\overbrace{\mathcal{O}_2...\mathcal{O}_2}^{k}][\overbrace{\mathcal{O}_2...\mathcal{O}_2}^{l}][\overbrace{\mathcal{O}_2...\mathcal{O}_2}^{k+l-1}]\rangle}{\sqrt{\langle[\underbrace{\mathcal{O}_2...\mathcal{O}_2}_{k}][\underbrace{\mathcal{O}_2...\mathcal{O}_2}_{k}]\rangle\langle[\underbrace{\mathcal{O}_2...\mathcal{O}_2}_{l}][\underbrace{\mathcal{O}_2...\mathcal{O}_2}_{l}]\rangle\langle[\underbrace{\mathcal{O}_2...\mathcal{O}_2}_{k+l-1}][\underbrace{\mathcal{O}_2...\mathcal{O}_2}_{k+l-1}]\rangle}}\\ &\to 2kq'N\sqrt{\frac{N^{k-3}q'^{k-1}}{2^k k!}} = 2k\sqrt{\frac{N^{k-1}q'^{k+1}}{2^k k!}},\end{aligned} \tag{4.4.61}$$

where $q=2l$. The 3-point function scales as $N^{\frac{k-1}{2}}$, so is only finite for $k=1$. As a sanity check, the expression for $k=1$ is in agreement with (4.4.55).

As mentioned at the beginning of this section, the limits can be compared to the string theory calculation of the AdS giant gravitons given in [140]. They do not appear to agree, therefore it seems that the products of $\mathcal{O}_2$ are not the right objects to compare to the AdS giant graviton. It would be interesting to work out what object in the multi-particle basis is related to the AdS giant graviton, but we shall leave this to future work.

4.5 Conclusions

In this chapter, we explored a new basis of half-BPS operators in $\mathcal{N}=4$ super Yang-Mills. The basis was developed out of a need to be very precise when discussing the definition of the operator dual to the single particle supergravity states on $AdS_5\times S^5$.

Products of these single particle operators were then used to extend the basis to a full multi-particle basis. We provide explicit formulae for these operators, and showed that they interpolate between point-like gravitons and giant (sphere) gravitons in the relevant limits, as they should. We then went on to consider free theory correlators of these operators. A particularly interesting and useful result was found that stated all near-extremal correlators of SPOs, namely n-point correlators with extremality degree strictly less than $n-2$, vanish. We would assume that this is tied to the conjecture given in [129] that the corresponding supergravity couplings vanish. We then continued to consider the maximally extremal correlators, which were nicely directly related to tree diagrams with $n-1$ vertices. The next-to-maximally extremal correlators were then studied; despite finding that the complexity increases as the extremality is lowered, we found additional simplicity compared to the single-trace correlators. Finally, we gave a few exact results of two- and three-point functions of multi-particle operators, and particularly interestingly proved a relation between the three-point functions of single particle operators and two-point functions of multi-particle operators that held for all extremality.

It is interesting to revisit past discussions involving half-BPS operators, especially concerning large N limits and the relation to string theory computations via AdS/CFT, in the light of our new basis of SPOs. As we saw in section 4.2.3, the SPOs correctly interpolate between single trace operators and the operators conjectured to be dual to S^5 giant graviton operators in the relevant limit. In [140] the half-BPS three-point functions of two giant graviton operators and one point-like graviton was performed and compared with the analogous computation in gauge theory. The gauge theory was computed using two large Schur polynomial operators and one single trace operator. The results were found to not quite agree and it was conjectured the reason was related to the inability of the Schur polynomials to correctly interpolate between giant and point-like gravitons. The SPOs on the other hand do precisely interpolate between the two as show in section 4.2.3. However, the extremal correlators of SPOs simply vanish! In [141] this issue was revisited and it was argued that indeed there were subtleties in the extremal case which are not present

in the next-to-extremal case. The NE three-point functions with two giant gravitons and one point-like graviton were computed in gauge theory (using Schur polynomials for the giant gravitons and single trace operators for the point-like operator) as well as in string theory and this time found agreement. Since we have explicit formulae for the NE 3-point functions we can check this agrees here also.

We start with the next-to-extremal three-point function of unit normalised single particle operators. From (4.4.6) we have

$$\frac{\langle \mathcal{O}_p \mathcal{O}_q \mathcal{O}_r \rangle}{\sqrt{\langle \mathcal{O}_p \mathcal{O}_p \rangle \langle \mathcal{O}_q \mathcal{O}_q \rangle \langle \mathcal{O}_r \mathcal{O}_r \rangle}} = pq \sqrt{\frac{\langle \mathcal{O}_r \mathcal{O}_r \rangle}{\langle \mathcal{O}_p \mathcal{O}_p \rangle \langle \mathcal{O}_q \mathcal{O}_q \rangle}}, \quad p+q = r+2. \tag{4.5.1}$$

Now consider the limit $N \to \infty$ with p staying finite, but $q, r \to \infty$ such that $q' = q/N, r' = r/N$ are fixed. Taking the appropriate limits of the two point functions (4.2.52) we find

$$\frac{\langle \mathcal{O}_p \mathcal{O}_q \mathcal{O}_r \rangle}{\sqrt{\langle \mathcal{O}_p \mathcal{O}_p \rangle \langle \mathcal{O}_q \mathcal{O}_q \rangle \langle \mathcal{O}_r \mathcal{O}_r \rangle}} \to \sqrt{p} \frac{r}{N} \left(1 - \frac{r}{N}\right)^{\frac{p-2}{2}}, \quad p+q = r+2 \tag{4.5.2}$$

which is in precise agreement with [141].

We can also compute the normalised next-to-next-to-extremal three-point function given by (4.4.30)-(4.4.31) in the same limit, $N \to \infty$ with $p, q' = q/N, r' = r/N$ fixed

$$\frac{\langle \mathcal{O}_p \mathcal{O}_q \mathcal{O}_r \rangle}{\sqrt{\langle \mathcal{O}_p \mathcal{O}_p \rangle \langle \mathcal{O}_q \mathcal{O}_q \rangle \langle \mathcal{O}_r \mathcal{O}_r \rangle}} \to \sqrt{p} \frac{r}{N} \left(1 - \frac{r}{N}\right)^{\frac{p-4}{2}} \left(1 - \frac{(p-1)r}{2N}\right), \quad p+q = r+4. \tag{4.5.3}$$

It would be interesting to compare with the corresponding string theory computation.

We shall provide some examples of interesting paths that could lead to the continuation of this work in Chapter 6.

Chapter 5

A Note on N^2MHV Yangian Invariants for $N = 4$ SYM

5.1 Introduction

Yangian invariants are the basic building blocks of many quantities of interest related to amplitudes in $\mathcal{N} = 4$ super Yang-Mills (see for example [43–45, 64, 142–145]). Some examples of the quantities they can be used to construct include any tree-level amplitude which can be written as a linear combination of Yangian invariants [146], and any leading singularity of a loop level integrand which are themselves Yangian invariants [147]. Therefore, a full understanding of all Yangian invariant functions and their properties would be extremely useful. There have been considerable steps made recently in understanding these functions, for example all positive n-particle N^kMHV Yangian invariants with $n = 5k$ were classified in [148]. Furthermore, all rational $m = 2$ (corresponding to the toy model of $\mathcal{N} = 4$ SYM) Yangian invariants were classified very nicely in terms of generalised triangles inside the $m = 2$ amplituhedron [80].

In Section 2.3 we introduced the five particle R invariant in the context of the n-point NMHV superamplitude integrand, and showed that it can be written in bosonised dual momentum superspace co-ordinates (or amplituhedron coordinates) as the following dual

conformal ratio:

$$[ijklm] = \frac{\langle ijklm\rangle^4}{\langle ijkl\rangle \langle jklm\rangle \langle klmi\rangle \langle lmij\rangle \langle mijk\rangle}. \tag{5.1.1}$$

For any k, these Yangian invariants can be understood as residues of a Grassmannian integral. It would be useful to understand how these residues of the Grassmannian can be taken directly in amplituhedron space, which would give covariant forms for higher-k analogues of the R invariants given by (5.1.1). A procedure for calculating expressions for the R invariants in amplituhedron coordinates was outlined in [31], which was used to calculate the 6 and 7 particle N^2MHV Yangian invariants.

In this chapter, we look to extend those considerations to all other N^2MHV Yangian invariants. We will begin by briefly introducing the Grassmannian representation for the Yangian invariants, and give an outline of the procedure used in [31] to calculate them in amplituhedron coordinates. Finally, we will use this procedure to calculate all bar one of the rest of the fourteen N^2MHV Yangian invariants.

5.1.1 Yangian Invariants from the Grassmannian

The Grassmannian representation of n-particle N^kMHV Yangian invariants is given by [45]

$$\frac{1}{\text{vol}[GL(k)]} \int_{C\subset\Gamma_\sigma} \frac{\mathrm{d}^{k\times n}C_{\alpha i}}{M_1 M_2 \cdots M_n} \prod_{\alpha=1}^{k} \delta^{4|4}\left(C_{\alpha i}\mathcal{Z}_i^{\mathcal{A}}\right), \tag{5.1.2}$$

where $C_{\alpha a}$ is the $k \times n$ matrix defining a Grassmannian of k-planes in n dimensions, $\text{Gr}(k,n)$, and $\mathcal{Z}_i^{\mathcal{A}}$ are super momentum twistor co-ordinates. The M_i variables in the denominator are the ordered, adjacent, maximal minors of C, e.g $M_1 = \det[C_1 \dots C_k]$, $M_2 = \det[C_2 \dots C_{k+1}], \dots, M_n = \det[C_n \dots C_{k-1}]$. The $\text{GL}(k)$ redundancy reflects a change of basis for the k planes coordinates of which are given by the matrix of variables C. The integral is $k \times (n-k)$ dimensional after taking into account the $\text{GL}(k)$ invariance. There are $4k$ bosonic delta functions, which would then leave a total of $k \times (n-k-4)$ non-trivial integrals. A spanning set of all possible integrals of this form is provided by the residues of these poles, which define a co-dimension $k \times (n-k-4)$ integration region.

This corresponds to a $4k$ dimension cell of $\mathrm{Gr}(k,n)$; it was shown that these cells can be classified by permutations in [45].

One can obtain positive canonical coordinates for this cell inside $\mathrm{Gr}(k,n)$ which we will label $\alpha_1,\ldots,\alpha_{4k}$. By positive we mean that the ordered minors of the Grassmannian matrix are all strictly positive if and only if $\alpha_i > 0$ for all i. In these coordinates, the measure in (5.1.2) reduces to the following simple d log form:

$$\Omega_{k(n-k)} \equiv \frac{1}{\mathrm{vol}[GL(k)]}\frac{\mathrm{d}^{k\times n}C_{\alpha i}}{M_1 M_2\cdots M_n} \quad \rightarrow \quad \Omega_{4k} = \frac{\mathrm{d}\alpha_1\ldots\mathrm{d}\alpha_{4k}}{\alpha_1\ldots\alpha_{4k}}. \tag{5.1.3}$$

We now wish to write the full Yangian invariant in amplituhedron coordinates. The Grassmannian integral in (5.1.2) becomes

$$\int \Omega_{4k}\delta^{4k}(Y;Y_0), \tag{5.1.4}$$

where we have defined $Y_\alpha^{\mathcal{A}} \equiv C_{\alpha i}Z_i^{\mathcal{A}}$, and

$$Y_{0\alpha}^{\mathcal{B}} \equiv \left(0_\alpha^b, \delta_\alpha^\beta\right) = \begin{pmatrix} 0_{4\times k} \\ 1_{k\times k}\end{pmatrix}. \tag{5.1.5}$$

Notice that when defining Y_0 we split the $4+k$ index $\mathcal{B}$ into an ordinary four dimensional twistor index B and k additional indices β. The delta function (5.1.4) is the natural Grassmannian invariant δ-function,

$$\delta^{4k}(Y;Y_0) = \int g^{k\ timesk}(\rho)_\alpha^\beta \det(\rho)^4 \delta^{k\times(k+4)}\left(Y_\alpha^I - \rho_\alpha^\beta Y_{0\beta}^I\right), \tag{5.1.6}$$

whose precise definition can be found in [47].

The natural brackets in amplituhedron space, $\mathbb{C}^{4+k}$, are $(4+k)$-brackets. One can construct $4+k$-brackets using four bosonised momentum-twistor coordinates and $Y \in \mathrm{Gr}(k,k+4)$ in the following way:

$$\langle Ypqrs\rangle \equiv \langle Y_1\ldots Y_k Z_p Z_q Z_r Z_s\rangle \equiv \det\left(Y_1,\ldots,Y_k,Z_pZ_qZ_rZ_s\right). \tag{5.1.7}$$

We can use these brackets to write the reduced measure Ω_{4k} as a differential form on

$\mathrm{Gr}(k, k+4)$, giving

$$\Omega_{4k} = \left\langle Y\,\mathrm{d}^4Y_1\right\rangle \ldots \left\langle Y\,\mathrm{d}^4Y_k\right\rangle \times \mathcal{Y}_{n;k}(Z_1, \ldots, Z_n, Y). \tag{5.1.8}$$

The full form is rendered covariant in the Y variables as the weights of the brackets with the differentials are offset by the weight $-(k+4)$ $\mathcal{Y}_{n;k}$. Here, $\langle Y\,\mathrm{d}^4Y_1\rangle \ldots \langle Y\,\mathrm{d}^4Y_k\rangle$ is the natural Grassmannian invariant measure which uses the brackets defined in (5.1.7) but with the Zs replaced by the anti-symmetric differential form d^4Y. Explicitly these brackets are given by

$$\left\langle Y\,\mathrm{d}^4Y_i\right\rangle \propto \epsilon^{\alpha_1\ldots\alpha_k}\epsilon_{\mathcal{A}_1\ldots\mathcal{A}_{k+4}}Y_{\alpha_1}^{\mathcal{A}_1}\ldots Y_{\alpha_k}^{\mathcal{A}_k}\,\mathrm{d}Y_i^{\mathcal{A}_{k+1}}\ldots\mathrm{d}Y_i^{\mathcal{A}_{k+4}}. \tag{5.1.9}$$

If Ω_{4k} can be written as (5.1.8), then the Yangian invariant (5.1.4) can be written as

$$\int \Omega_{4k}\delta^{4k}(Y; Y_0) = \mathcal{Y}_{n;k}(Z_1, \ldots, Z_n, Y_0). \tag{5.1.10}$$

Due to the form of Y_0 given in (5.1.5), the brackets involving Y reduce to the 4-brackets $\langle Y_0 ijkl\rangle = \langle ijkl\rangle$. Note that there is really no integral to perform here; the delta functions fully fix Y.

Using the above construction will allow us to jump directly from the canonical coordinates and corresponding $\mathrm{d}\log$ from (5.1.3) to the Yangian invariant $\mathcal{Y}_{n;k}(Z_1, \ldots, Z_n, Y_0)$. In this chapter, we shall be paying particular attention to the N^2MHV Yangian invariants, i.e. for $k = 2$. For this case, Ω in (5.1.4) becomes a $(4 \cdot 2) = 8$-form, which if we use the *canonical positive coordinates* on the Grassmannian defined in [45] is given by

$$\Omega = \int \frac{\mathrm{d}\alpha_1 \ldots \mathrm{d}\alpha_8}{\alpha_1 \ldots \alpha_8}. \tag{5.1.11}$$

Therefore, we can jump straight to the Yangian invariant in amplituhedron space by solving

$$\Omega = \int \frac{\mathrm{d}\alpha_1 \ldots \mathrm{d}\alpha_8}{\alpha_1 \ldots \alpha_8} = \left\langle Y\,\mathrm{d}^4Y_1\right\rangle \left\langle Y\,\mathrm{d}^4Y_2\right\rangle \times \mathcal{Y}_{n;2}(Z_1, \ldots, Z_n, Y) \tag{5.1.12}$$

In the next section, we work through an example of a covariantisation procedure in

detail for a seven-point $k = 2$ Yangian invariant, as detailed in [31]. This process gives a methodical way of finding some expression for $\mathcal{Y}$. However, we note that this process does not necessarily have to be pursued; if one were to guess a function $\mathcal{Y}$ such that (5.1.12) was satisfied, then we would have immediately found an expression for the Yangian invariant. This is mostly what was done when calculating the rest of the N^2MHV invariants; specifically when looking to write some in a simple way. We will show these results in 5.2.

5.1.2 Covariantising the Seven-Point Yangian Invariants

Here we shall show an example of a covariantisation method for calculating the Yangian invariants for $n = 7$. Though this is specified for $n = 7$, these invariants are also valid for higher n.

From (5.1.2), any 7-point N^2MHV Yangian invariant can be represented as the following Grassmannian integral:

$$\frac{1}{\text{vol}[GL(2)]}\int_{C\subset\Gamma_\sigma}\frac{\mathrm{d}^{2\times n}C_{\alpha i}}{(12)(23)(34)(45)(56)(71)}\prod_{\alpha=1}^{2}\delta^{4|4}\left(C_{\alpha i}\mathcal{Z}_i^{\mathcal{A}}\right), \tag{5.1.13}$$

where $(jj+1) = \det[C_jC_{j+1}]$ where j labels column j of the C matrix. The integration is $14-4 = 10$ dimensional after dividing by vol[GL(2)], and there are 8 bosonic delta functions, which leaves two non-trivial integrations. Therefore, we can choose to circle two of the poles (corresponding to two of the minors given in the denominator) and use the residue theorem.

There are three classes of residues given by the following pairs of vanishing minors

$$(67) = (71) = 0, \qquad (12) = (34) = 0 \qquad (12) = (45) = 0, \tag{5.1.14}$$

where all other invariants are related by cyclicity. Each of these poles is directly related to one type of Yangian invariant present at seven points. The simplest case corresponds to the residue at the first pole in the list, $(67) = (71) = 0$. As mentioned in the previous

section, we can choose to use the positive canonical coordinates given in [45] to produce

$$C_{\alpha i} = \begin{pmatrix} 1 & \alpha_2+\alpha_4+\alpha_6+\alpha_8 & (\alpha_2+\alpha_4+\alpha_6)\alpha_7 & (\alpha_2+\alpha_4)\alpha_5 & \alpha_2\alpha_3 & 0 & 0 \\ 0 & 1 & \alpha_7 & \alpha_5 & \alpha_3 & \alpha_1 & 0 \end{pmatrix}, \tag{5.1.15}$$

giving the canonical form in (5.1.11). The goal now is to solve (5.1.12) in order to jump straight to the Yangian invariant in amplituhedron space.

Using the GL(6) invariance of the external momenta, we can choose amplituhedron coordinates

$$Z_a^{\mathcal{A}} = \begin{pmatrix} 1 & 0 & 0 & 0 & 0 & 0 & a_1 \\ 0 & 1 & 0 & 0 & 0 & 0 & b_1 \\ 0 & 0 & 1 & 0 & 0 & 0 & c_1 \\ 0 & 0 & 0 & 1 & 0 & 0 & d_1 \\ 0 & 0 & 0 & 0 & 1 & 0 & e_1 \\ 0 & 0 & 0 & 0 & 0 & 1 & f_1 \end{pmatrix}, \tag{5.1.16}$$

which when projected using (5.1.15) through $Y = C_{\alpha i} Z_i^{\mathcal{A}}$ gives

$$Y_\alpha^{\mathcal{A}} = \begin{pmatrix} 1 & \alpha_2+\alpha_4+\alpha_6+\alpha_8 & (\alpha_2+\alpha_4+\alpha_6)\alpha_7 & (\alpha_2+\alpha_4)\alpha_5 & \alpha_2\alpha_3 & 0 \\ 0 & 1 & \alpha_7 & \alpha_5 & \alpha_3 & \alpha_1 \end{pmatrix}. \tag{5.1.17}$$

Using (5.1.17), the covariant differential form is given by

$$\left\langle Y\, \mathrm{d}^4 Y_1 \right\rangle \left\langle Y\, \mathrm{d}^4 Y_2 \right\rangle = \alpha_1\alpha_3\alpha_5\alpha_7\, \mathrm{d}\alpha_1 \ldots \alpha_8. \tag{5.1.18}$$

Since the differential form is of weight 6 in Y, we can divide by any six brackets defined in (5.1.7) to obtain a Y-weightless volume form. For example, we can choose the following:

$$\frac{\langle Y\, \mathrm{d}^4 Y_1\rangle \langle Y\, \mathrm{d}^4 Y_2\rangle}{\langle Y1234\rangle \langle Y1236\rangle \langle Y1456\rangle \langle Y2345\rangle \langle Y2346\rangle \langle Y3456\rangle} = \frac{\mathrm{d}\alpha_1 \ldots \mathrm{d}\alpha_8}{\alpha_1\alpha_2\alpha_3^2\alpha_4\alpha_8}, \tag{5.1.19}$$

meaning the residue (67) = (71) = 0 is given by

$$\Omega_{(67),(71)} \equiv \frac{\mathrm{d}\alpha_1 \ldots \mathrm{d}\alpha_8}{\alpha_1 \ldots \alpha_8} = \frac{\alpha_3 \langle Y\, \mathrm{d}^4 Y_1\rangle \langle Y\, \mathrm{d}^4 Y_2\rangle}{\alpha_5\alpha_6\alpha_7 \langle Y1234\rangle \langle Y1236\rangle \langle Y1456\rangle \langle Y2345\rangle \langle Y2346\rangle \langle Y3456\rangle}. \tag{5.1.20}$$

The final step is to covariantise the α variables on the right hand side of (5.1.20). The expressions must be Y-weightless in order for the expression to remain Y-weightless overall. We find the following:

$$\alpha_3 = -\frac{\langle Y2346\rangle}{\langle Y3456\rangle}, \quad \alpha_5 = \frac{\langle Y2356\rangle}{\langle Y3456\rangle}, \quad \alpha_6 = -\frac{\langle Y1256\rangle\,\langle Y3456\rangle}{\langle Y2356\rangle\,\langle Y2456\rangle}, \quad \alpha_7 = -\frac{\langle Y2456\rangle}{\langle Y3456\rangle}. \tag{5.1.21}$$

Substituting these values into (5.1.20), we arrive at

$$\Omega_{(67)(71)} \to \frac{\langle Y\,\mathrm{d}^4Y_1\rangle\,\langle Y\,\mathrm{d}^4Y_2\rangle}{\langle Y1234\rangle\,\langle Y2345\rangle\,\langle Y3456\rangle\,\langle Y4561\rangle\,\langle Y5612\rangle\,\langle Y6123\rangle}. \tag{5.1.22}$$

Whilst the above expression is weightless in Y, it is not weightless on the external particles. We can easily correct this by multiplying by $\langle 123456\rangle^4$ which is equal to one, giving us the final covariant expression[1]

$$\Omega_{(67)(71)} \to \frac{\langle Y\,\mathrm{d}^4Y_1\rangle\,\langle Y\,\mathrm{d}^4Y_2\rangle\,\langle 123456\rangle^4}{\langle Y1234\rangle\,\langle Y2345\rangle\,\langle Y3456\rangle\,\langle Y4561\rangle\,\langle Y5612\rangle\,\langle Y6123\rangle}. \tag{5.1.23}$$

So, the Yangian invariant is given by the piece of (5.1.23) not involving the differentials upon removing the Ys, which corresponds to integrating with the delta function. It should be noted that this example was particularly straight forward, because this invariant is actually the unique six-point N^2MHV Yangian invariant. Despite being slightly more complicated, the other invariants can be calculated following this procedure.

There are two Yangian invariants present at $n = 7$, which correspond to the other poles given by (5.1.14). The calculation of the remaining invariants was presented in [31]; since their derivation is very similar to the above example, we do not go through them here. Instead, we state the final results:

$$R^{(k=2)}_{(67)(71)} \equiv \frac{\langle 123456\rangle^4}{\langle 1234\rangle\,\langle 2345\rangle\,\langle 3456\rangle\,\langle 4561\rangle\,\langle 5612\rangle\,\langle 6123\rangle}, \tag{5.1.24}$$

[1] In general this result would seem to be dependent non-trivially on the unfixed coordinates $a_1, b_1, c_1, d_1, e_1, f_1$. We can write these in the following forms, which are all weightless in Y: $a_1 = -\langle 234567\rangle$, $b_1 = \langle 134567\rangle$, $c_1 = -\langle 124567\rangle$, $d_1 = \langle 123567\rangle$, $e_1 = -\langle 123467\rangle$ and $f_1 = \langle 123457\rangle$.

$$R^{(k=2)}_{(12)(34)} \equiv \frac{\left(\langle [1|567\rangle \langle |2]34567\rangle\right)^4}{\langle 1267\rangle \langle 1567\rangle \langle 2567\rangle \langle 3456\rangle \langle 3567\rangle \langle 4567\rangle \langle 125[7|\rangle \langle 345|6]\rangle \langle 12[6|7\rangle \langle 34|5]7\rangle}, \tag{5.1.25}$$

$$R^{(k=2)}_{(12)(45)} \equiv \frac{\left(\langle [2|367\rangle \langle |1]34567\rangle\right)^4}{\langle 1237\rangle \langle 1267\rangle \langle 1367\rangle \langle 2367\rangle \langle 3456\rangle \langle 3467\rangle \langle 4567\rangle \langle 123[7|\rangle \langle 345|6]\rangle}, \tag{5.1.26}$$

where $\langle [1|567\rangle \langle |2]34567\rangle \equiv \langle 1567\rangle \langle 234567\rangle - \langle 2567\rangle \langle 134567\rangle$ is an ordered antisymmetrisation of the two points enclosed in the square brackets.

5.2 Results of N^2MHV Yangian Invariants

We now present the results of the rest of the N^2MHV Yangian invariant functions, except for one which unfortunately we were not yet able to find in a nice form. Unlike in section 5.1.2, we will not be going through a complete step-by-step procedure to calculate the invariants; a number of them were calculated by going through many covariant brackets expanded in the canonical coordinates given in [45] by hand to try to match (5.1.11). To begin with, we will set up some notation.

There are fourteen cyclically distinct Yangian-invariant functions for $k = 2$; a unique six point invariant, two more at seven points, six more at eight points (one of which we have not yet calculated), four more at nine points and a final Yangian invariant at ten points. For ease of notation we shall label these invariants by $\mathcal{Y}^{(n)}_p$, where n corresponds to the particle number for which the invariant first exists, and p runs over the integers $1, \ldots, 14$ and references the pole structure. The number of non-trivial integrations, therefore the number of poles required, corresponding to particle number n is given by $n \cdot 2 - 4 - 8 = 2n - 12$. The unique six particle invariant is just labelled by $p = 1$ and there is no non-trivial integration to do in this case. The pole structures of the other

thirteen values of p are given by:

$$\begin{aligned}
p=2:\ (12)(34) \qquad & p=3:\ (12)(45)\\
p=4:\ (12)(23)(45)(56) \qquad & p=5:\ (12)(23)(56)(67)\\
p=6:\ (12)(23)(45)(67) \qquad & p=7:\ (12)(23)(45)(78)\\
p=8:\ (12)(23)(56)(78) \qquad & p=9:\ (12)(34)(56)(78)\\
p=10:\ (12)(23)(34)(56)(67)(78) \qquad & p=11:\ (12)(23)(34)(56)(67)(89)\\
p=12:\ (12)(23)(34)(56)(78)(89) \qquad & p=13:\ (12)(23)(45)(56)(78)(89)\\
p=14:\ (12)(23)(34)(45)(67)(78)(89)(9\,10) &
\end{aligned} \tag{5.2.1}$$

where the pairs of values correspond to the minors being set to zero. If the Y dependence had been kept, then equations (5.1.24), (5.1.25) and (5.1.26) would correspond to $\mathcal{Y}_1^{(6)}$, $\mathcal{Y}_2^{(7)}$ and $\mathcal{Y}_3^{(7)}$ respectively. Note, the Yangian invariant corresponding to the pole structure given by $p=9$ is the invariant we have not yet managed to write down in a nice way. The procedure described in the previous section should still follow through for this example.

The coordinates we shall use, as a natural extension to (5.1.16), will be given by

$$Z_i^{\mathcal{A}} = \begin{pmatrix}
1 & 0 & 0 & 0 & 0 & 0 & a_1 & \cdots & a_{n-6}\\
0 & 1 & 0 & 0 & 0 & 0 & b_1 & \cdots & b_{n-6}\\
0 & 0 & 1 & 0 & 0 & 0 & c_1 & \cdots & c_{n-6}\\
0 & 0 & 0 & 1 & 0 & 0 & d_1 & \cdots & d_{n-6}\\
0 & 0 & 0 & 0 & 1 & 0 & e_1 & \cdots & e_{n-6}\\
0 & 0 & 0 & 0 & 0 & 1 & f_1 & \cdots & f_{n-6}
\end{pmatrix}, \tag{5.2.2}$$

where the Y independent forms of each variable can be written in the following way:

$$\begin{gathered}
a_i = (-1)^i \langle 23456 a_{n+i}\rangle\,, \quad b_i = (-1)^{i+1}\langle 13456 b_{n+i}\rangle\,, \quad c_i = (-1)^i\langle 12456 c_{n+i}\rangle\\
d_i = (-1)^{i+1}\langle 123567 a_{n+i}\rangle\,, \quad e_i = (-1)^i\langle 123467 b_{n+i}\rangle\,, \quad f_i = (-1)^{i+1}\langle 123457 c_{n+i}\rangle\\
\langle 123456\rangle = 1.
\end{gathered} \tag{5.2.3}$$

The final piece of notation that we shall need is

$$\langle Y\,(i_1j_1k_1l_1m_1)\cap(i_2j_2k_2l_2m_2)\rangle = \langle Y_1i_1j_1k_1l_1m_1\rangle\,\langle Y_2i_2j_2k_2l_2m_2\rangle - \langle Y_2i_1j_1k_1l_1m_1\rangle\,\langle Y_1i_2j_2k_2l_2m_2\rangle\,, \tag{5.2.4}$$

which we introduce to simplify the expressions, and hint toward the notation used in [80] where it was helpful to introduce such notation to very nicely classify all $m = 2$ Yangian invariants. Using this notation, we can write the numerators of (5.1.25) and (5.1.26) as:

$$\left(\langle[1|567\rangle\,\langle|2]34567\rangle\right)^4 = \langle Y(12567)\cap(34567)\rangle^4\,, \tag{5.2.5}$$

$$\left(\langle[2|367\rangle\,\langle|1]34567\rangle\right)^4 = \langle Y(12367)\cap(34567)\rangle^4\,. \tag{5.2.6}$$

We shall now present the results of the Yangian invariants, $\mathcal{Y}_p^{(n)}$. At each new n, the canonical coordinates taken from [45] will be stated, then the Yangian invariants newly present at that value of n will be written down.

5.2.1 $n = 8$ Invariants

Here we present the Yangian invaraints corresponding to $p = 4, \ldots, 8$ in (5.2.1). Labelling the 2×8 matrices of canonical coordinates by $C^{(p)}$, [45] gives

$$C^{(4)} = \begin{pmatrix} 1 & \alpha_1 & \alpha_2 & (\alpha_3+\alpha_4) & (\alpha_3+\alpha_4)\alpha_5 & (\alpha_3+\alpha_4)\alpha_6 & \alpha_4\alpha_7 & 0 \\ 0 & 0 & 0 & 1 & \alpha_5 & \alpha_6 & \alpha_7 & \alpha_8 \end{pmatrix} \tag{5.2.7}$$

$$C^{(5)} = \begin{pmatrix} 1 & \alpha_1 & \alpha_2 & (\alpha_3+\alpha_4) & \alpha_4\alpha_5 & \alpha_4\alpha_6 & \alpha_4\alpha_7 & 0 \\ 0 & 0 & 0 & 1 & \alpha_5 & \alpha_6 & \alpha_7 & \alpha_8 \end{pmatrix} \tag{5.2.8}$$

$$C^{(6)} = \begin{pmatrix} 1 & \alpha_1 & \alpha_2 & (\alpha_3+\alpha_4) & (\alpha_3+\alpha_4)\alpha_5 & \alpha_4\alpha_6 & \alpha_4\alpha_7 & 0 \\ 0 & 0 & 0 & 1 & \alpha_5 & \alpha_6 & \alpha_7 & \alpha_8 \end{pmatrix} \tag{5.2.9}$$

$$C^{(7)} = \begin{pmatrix} 1 & \alpha_1 & \alpha_2 & (\alpha_3+\alpha_4) & (\alpha_3+\alpha_4)\alpha_5 & \alpha_4\alpha_6 & 0 & 0 \\ 0 & 0 & 0 & 1 & \alpha_5 & \alpha_6 & \alpha_7 & \alpha_8 \end{pmatrix} \tag{5.2.10}$$

$$C^{(8)} = \begin{pmatrix} 1 & \alpha_1 & \alpha_2 & (\alpha_3+\alpha_4) & \alpha_4\alpha_5 & \alpha_4\alpha_6 & 0 & 0 \\ 0 & 0 & 0 & 1 & \alpha_5 & \alpha_6 & \alpha_7 & \alpha_8 \end{pmatrix}, \tag{5.2.11}$$

where it is understood in each case that $Y = C^{(p)} \cdot Z$ with Z given in (5.2.2) for $n = 8$.

The goal is to find a rational expression which is weightless in Y and the external momenta for each case, which along with the measure reproduces (5.1.11). We find we can write the Yangian invariants as follows

$$\mathcal{Y}_4^{(8)} = \frac{\langle Y(12378) \cap (45678)\rangle^4}{\langle Y1238\rangle \langle Y1278\rangle \langle Y1378\rangle \langle Y2378\rangle \langle Y4567\rangle \langle Y4578\rangle \langle Y4678\rangle \langle Y5678\rangle \langle Y123[7|\rangle \langle Y456|8]\rangle} \tag{5.2.12}$$

$$\mathcal{Y}_5^{(8)} = \frac{\langle Y(12348) \cap (45678)\rangle^4}{\langle Y1234\rangle \langle Y2348\rangle \langle Y3481\rangle \langle Y4812\rangle \langle Y8123\rangle \langle Y4567\rangle \langle Y5678\rangle \langle Y6784\rangle \langle Y7845\rangle \langle Y8456\rangle} \tag{5.2.13}$$

$$\begin{aligned}\mathcal{Y}_6^{(8)} = &\frac{(\langle Y5678\rangle \langle Y(12348) \cap (45678)\rangle + \langle Y6784\rangle \langle Y(12358) \cap (45678)\rangle)^4}{\langle Y5678\rangle \langle Y4678\rangle \langle Y4578\rangle \langle Y4568\rangle \langle Y4567\rangle \langle Y1238\rangle} \\ &* \langle Y13[6|8\rangle \langle Y45|7]8\rangle \langle Y12[6|8\rangle \langle Y45|7]8\rangle \langle Y23[6|8\rangle \langle Y45|7]8\rangle (\langle Y123[6|\rangle \langle Y45|7]8\rangle + \langle Y1238\rangle \langle Y4567\rangle)\end{aligned} \tag{5.2.14}$$

$$\begin{aligned}\mathcal{Y}_7^{(8)} = &\frac{\left(\begin{array}{c}\langle Y4567\rangle \langle Y4678\rangle \langle Y(12358) \cap (45678)\rangle + \langle Y8456\rangle \langle Y6784\rangle \langle Y(12357) \cap (45678)\rangle + \\ \langle Y4567\rangle \langle Y5678\rangle \langle Y(12348) \cap (45678)\rangle + \langle Y8456\rangle \langle Y5678\rangle \langle Y(12347) \cap (45678)\rangle\end{array}\right)^4}{\langle Y4578\rangle^4 \langle Y4567\rangle \langle Y4568\rangle \langle Y4678\rangle \langle Y5678\rangle \langle Y123[7|\rangle \langle Y456|8]\rangle} \\ &\langle Y126[7|\rangle \langle Y456|8]\rangle \langle Y136[7|\rangle \langle Y456|8]\rangle \langle Y236[7|\rangle \langle Y456|8]\rangle (\langle Y123[7|\rangle \langle Y456|8]\rangle - \langle Y1236\rangle \langle Y4578\rangle)\end{aligned} \tag{5.2.15}$$

$$\begin{aligned}\mathcal{Y}_8^{(8)} = &\frac{(\langle Y4567\rangle \langle Y(12348) \cap (45678)\rangle + \langle Y4568\rangle \langle Y(12347) \cap (45678)\rangle)^4}{\langle Y4567\rangle \langle Y4568\rangle \langle Y4578\rangle \langle Y4678\rangle \langle Y5678\rangle \langle Y1234\rangle} \\ &* \langle Y123[7|\rangle \langle Y456|8]\rangle \langle Y124[7|\rangle \langle Y456|8]\rangle \langle Y134[7|\rangle \langle Y456|8]\rangle \langle Y234[7|\rangle \langle Y456|8]\rangle\end{aligned}. \tag{5.2.16}$$

When the relevant canonical coordinates are substituted in to each expression, we find that

$$\left\langle Y\, \mathrm{d}^4 Y_1 \right\rangle \left\langle Y\, \mathrm{d}^4 Y_2 \right\rangle \mathcal{Y}_8^{(p)} = \frac{\mathrm{d}\alpha_1 \ldots \mathrm{d}\alpha_8}{\alpha_1 \ldots \alpha_8}, \tag{5.2.17}$$

therefore from (5.1.12) we can conclude the expressions above are indeed representations of the Yangian invariants in amplituhedron coordinates.

5.2.2 $n = 9$ Invariants

At $n = 9$, there are four more cyclically distinct R-invariants. The canonical coordinates are given by the following

$$C^{(10)} = \begin{pmatrix} 1 & \alpha_1 & \alpha_2 & \alpha_3 & \alpha_4 & \alpha_4\alpha_5 & \alpha_4\alpha_6 & \alpha_4\alpha_7 & 0 \\ 0 & 0 & 0 & 0 & 1 & \alpha_5 & \alpha_6 & \alpha_7 & \alpha_8 \end{pmatrix} \tag{5.2.18}$$

$$C^{(11)} = \begin{pmatrix} 1 & \alpha_1 & \alpha_2 & \alpha_3 & \alpha_4 & \alpha_4\alpha_5 & \alpha_4\alpha_6 & 0 & 0 \\ 0 & 0 & 0 & 0 & 1 & \alpha_5 & \alpha_6 & \alpha_7 & \alpha_8 \end{pmatrix} \tag{5.2.19}$$

$$C^{(12)} = \begin{pmatrix} 1 & \alpha_1 & \alpha_2 & \alpha_3 & \alpha_4 & \alpha_4\alpha_5 & 0 & 0 & 0 \\ 0 & 0 & 0 & 0 & 1 & \alpha_5 & \alpha_6 & \alpha_7 & \alpha_8 \end{pmatrix} \tag{5.2.20}$$

$$C^{(13)} = \begin{pmatrix} 1 & \alpha_1 & \alpha_2 & \alpha_3 & \alpha_3\alpha_4 & \alpha_3\alpha_5 & 0 & 0 & 0 \\ 0 & 0 & 0 & 0 & 1 & \alpha_5 & \alpha_6 & \alpha_7 & \alpha_8 \end{pmatrix} \tag{5.2.21}$$

We find the Yangian invariants for these cases can be written as

$$\mathcal{Y}_{10}^{(9)} = \frac{\langle Y(12349) \cap (56789)\rangle^4}{\langle Y1234\rangle \langle Y1239\rangle \langle Y1249\rangle \langle Y1349\rangle \langle Y2349\rangle \langle Y5678\rangle \langle Y5679\rangle \langle Y5689\rangle \langle Y5789\rangle \langle Y6789\rangle} \tag{5.2.22}$$

$$\mathcal{Y}_{11}^{(9)} = \frac{(\langle Y5678\rangle \langle Y(12349) \cap (56789)\rangle + \langle Y9567\rangle \langle Y(12348) \cap (56789)\rangle)^4}{\langle Y1234\rangle \langle Y5678\rangle \langle Y5679\rangle \langle Y5689\rangle \langle Y5789\rangle \langle Y6789\rangle \langle Y123[8|\rangle \langle Y567|9]\rangle \langle Y124[8|\rangle \langle Y567|9]\rangle \langle Y134[8|\rangle \langle Y567|9]\rangle \langle Y234[8|\rangle \langle Y567|9]\rangle} \tag{5.2.23}$$

$$\mathcal{Y}_{12}^{(9)} = \frac{(\langle Y6789\rangle \langle Y(12345) \cap (56789)\rangle + \langle Y7895\rangle \langle Y(12346) \cap (56789)\rangle)^4}{\langle Y1234\rangle \langle Y5678\rangle \langle Y5679\rangle \langle Y5689\rangle \langle Y5789\rangle \langle Y6789\rangle \langle Y123[5|\rangle \langle Y|6]789\rangle \langle Y124[5|\rangle \langle Y|6]789\rangle \langle Y134[5|\rangle \langle Y|6]789\rangle \langle Y234[5|\rangle \langle Y|6]789\rangle} \tag{5.2.24}$$

$$\mathcal{Y}_{13}^{(9)} = -\phi \frac{\left(\begin{array}{c} \langle Y6123\rangle \langle Y7894\rangle \langle Y(12356) \cap (45789)\rangle + \langle Y1235\rangle \langle Y7894\rangle \langle Y(12356) \cap (46789)\rangle + \langle Y1234\rangle \langle Y7894\rangle \langle Y(12356) \cap (56789)\rangle + \\ \langle Y6123\rangle \langle Y5789\rangle \langle Y(12346) \cap (45789)\rangle + \langle Y1235\rangle \langle Y5789\rangle \langle Y(12346) \cap (46789)\rangle + \langle Y1234\rangle \langle Y7895\rangle \langle Y(12346) \cap (56789)\rangle + \\ \langle Y1236\rangle \langle Y6789\rangle \langle Y(12345) \cap (45789)\rangle + \langle Y5123\rangle \langle Y6789\rangle \langle Y(12345) \cap (46789)\rangle + \langle Y1234\rangle \langle Y6789\rangle \langle Y(12345) \cap (56789)\rangle \end{array}\right)^4}{\begin{array}{c} (\langle Y1236\rangle \langle Y4578\rangle - \langle Y1235\rangle \langle Y4678\rangle + \langle Y1234\rangle \langle Y5678\rangle)(\langle Y1236\rangle \langle Y4579\rangle - \langle Y1235\rangle \langle Y4679\rangle + \langle Y1234\rangle \langle Y5679\rangle) \\ (\langle Y1236\rangle \langle Y4589\rangle - \langle Y1235\rangle \langle Y4689\rangle + \langle Y1234\rangle \langle Y5689\rangle)(\langle Y123[4|\rangle \langle Y|5]789\rangle)^2(\langle Y123[4|\rangle \langle Y|6]789\rangle)^2 \\ (\langle Y1256\rangle \langle Y4789\rangle - \langle Y1246\rangle \langle Y5789\rangle + \langle Y1245\rangle \langle Y6789\rangle)(\langle Y1356\rangle \langle Y4789\rangle - \langle Y1346\rangle \langle Y5789\rangle + \langle Y1345\rangle \langle Y6789\rangle) \\ (\langle Y2356\rangle \langle Y4789\rangle - \langle Y2346\rangle \langle Y5789\rangle + \langle Y2345\rangle \langle Y6789\rangle) \end{array} \tag{5.2.25}$$

where

$$\phi = \frac{\langle Y45(123) \cap (789)\rangle \langle Y46(123) \cap (789)\rangle}{\langle Y56(123) \cap (789)\rangle}.$$

Once again, when the relevant canonical coordinates are substituted in to each expression, we find that it satisfies (5.2.17). Therefore, from (5.1.12) we can conclude the expressions above are representations of the Yangian invariants in amplituhedron coordinates.

5.2.3 $n = 10$ Invariants

There is one final Yangian invariant present at ten points and beyond. The canonical coordinates for this term are given by

$$C^{(14)} = \begin{pmatrix} 1 & \alpha_1 & \alpha_2 & \alpha_3 & \alpha_4 & 0 & 0 & 0 & 0 & 0 \\ 0 & 0 & 0 & 0 & 0 & 1 & \alpha_5 & \alpha_6 & \alpha_7 & \alpha_8 \end{pmatrix}, \tag{5.2.26}$$

with $Y = C^{(14)} \cdot Z$. The corresponding Yangian invariant is given by

$$\frac{\langle Y(12345) \cap (6789(10)) \rangle^4}{\langle Y1234 \rangle \langle Y1235 \rangle \langle Y1245 \rangle \langle Y1345 \rangle \langle Y2345 \rangle \langle Y6789 \rangle \langle Y679(10) \rangle \langle Y689(10) \rangle \langle Y789(10) \rangle \langle Y678(10) \rangle} \tag{5.2.27}$$

5.3 Concluding Remarks

In this chapter, we have presented expressions for most of the N^2MHV Yangian invariants for $\mathcal{N} = 4$ SYM in amplituhedron coordinates. There are a number of advantages in writing the invariants in amplituhedron coordinates over the original coordinates. For example, non-trivial identities which are very hard to see in the superspace formalism arise naturally as Schouten-like identities in the bosonised quantities.

By writing the $m = 2$ Yangian invariants in $(m = 2)$ amplituhedron coordinates, it was shown that the n-point N^kMHV Yangian invariants can be classified by labelling them as a general configuration of k non-intersecting triangles in an n sided polygon. One would hope that there may be a way to generalise this classification to $m = 4$ Yangian invariants, or at least use an uplifted version of this construction to describe some subset of the invariants. We already see that some of the N^2MHV invariants have very simple forms; see for example (5.1.25), (5.1.26) with numerators written in the form given in (5.2.5), as well as (5.2.12), (5.2.22) and (5.2.27). It would be interesting to investigate why these forms are particularly simple, and see if they can be generalised to a subset of invariants with $k > 2$. It would also be interesting to see if the invariants with more complicated expressions can be written in a simpler way, and further, see if all $k = 2$ invariants can be classified in a simple geometric way that can be extended to $k > 2$.

Moreover, these Yangian invariants can be used to continue the work of [31]. There, the authors managed to extract individual amplitudes from the four-point correlator by assuming Yangian symmetry and an appropriate basis of planar dual conformal integrands. Writing the R invariants in amplituhedron coordinates was a necessary ingredient of the method which they tested up to seven points and two loops. In order to move to higher points, the $n = 8$ invariants are required; it would be beneficial to first find a way to write $\mathcal{Y}_9^{(8)}$ in as simple a way as possible.

Chapter 6

Conclusion

To conclude, let us briefly review the main results of each chapter, and indicate some directions in which the research could be continued.

In this thesis, we have continued the exploration of three fundamental objects in four dimensional planar supersymmetric Yang-Mills theory; amplitudes, operators and invariants.

In chapter 3, we utilised the Wilson loop / amplitude duality in the hopes of finding a very explicit tesselation of the amplituhedron using Wilson loop diagrams (WLDs). The WLDs split the amplitude into well defined pieces as a sum of planar Feynman diagrams and whilst each individual expression contains spurious poles, they all cancel when summed leaving only the physical poles of the amplitude. Motivated by this property, and the fact that each diagram could be naturally associated with a canonical form of a geometrical object in the same subspace as the amplituhedron, $\mathrm{Gr}(k, k+4)$, we set out to explore whether the geometrical regions given by each diagram could be glued together to give a final "good geometry" i.e. one with no spurious boundaries left unmatched (locally) pairwise. Whilst this was possible for the NMHV case, we proved that it is not possible for N^2MHV and beyond. The principle of the proof can be very nicely summed up by Figure 6.1.

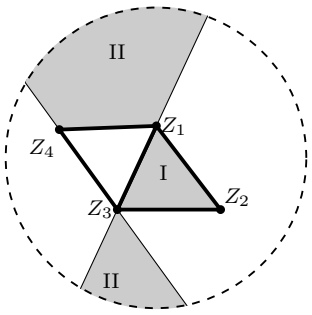

Figure 6.1: Regions I and II clearly have a spurious boundary along the edge $[Z_1 Z_3]$ despite their canonical forms summing to cancel the associated spurious pole.

The canonical forms associated to regions I and II sum and result in only poles that correspond to logarithmic singularities along the boundary of the quadrilateral labelled $Z_1 Z_2 Z_3 Z_4$. However, the geometrical region clearly still has unmatched spurious boundaries. In this simple example, region II could instead be chosen to be the interior of the triangle with vertices Z_1, Z_3 and Z_4, allowing it to maintain the same canonical form and match the spurious boundary along the edge $[Z_1 Z_3]$. Our proof shows that for N^2MHV, it is not possible to choose geometries that are consistent with the canonical form dictated by the WLDs and the pairwise matching of the boundaries. Therefore, we conclude that the WLDs do not provide a tesselation of the amplituhedron, or any geometrical region.

Whilst the WLDs do not provide a geometrical tesselation of the amplituhedron, they do still give a very concrete 'tesselation' at the level of its canonical form. It may be interesting to see if this property generalises to more general positive Grassmannians. Furthermore, it may be interesting to explore the final geometry the WLDs provide from a mathematical perspective despite them not having the physical interpretation we had hoped for. It was noted in [90] that it may be interesting to see if the WLDs correspond to some characteristic class of the manifold, for which the Amplituhedron volume forms may be seen as a special case.

In Chapter 4 we initiated an investigation into the properties of single particle operators, $\mathcal{O}_p$, and their correlation functions. The operators defined to be orthogonal to all multi-

trace operators, and are appropriate for describing single-particle states of superstring theory on $AdS_5 \times S^5$. We found explicit formulae for them in three different bases: the trace basis, the basis corresponding to the eigenvalues of the operators and in the Schur polynomial basis. Furthermore, we found an explicit expression for their two point function, and show that for weight greater than one the $U(N)$ SPOs are simply the $SU(N)$ SPOs, or more precisely in substituting $\psi = \phi - \frac{\mathrm{Tr}\,\phi}{N}$ we have

$$\mathcal{O}_p^{U(N)}[\phi] = \mathcal{O}_p^{SU(N)}[\psi] \qquad p \geq 2.$$

We made contact with the gravity side, and pointed out that in the large N limit, as the length of the operator increases the single-particle operator naturally interpolates between the single-trace and the sphere giant graviton.

The extension of single particle operators to a full basis of half-BPS operators was then discussed by simply taking products of the operators; we referred to these as multi-particle operators. This new basis has the advantage of being valid in $U(N)$ and $SU(N)$ gauge theories (by either allowing O_1 contributions in the product or not respectively), and naturally cuts off when the length of any of the single-particle operators exceeds the number of colours.

We then went on to study correlators of single particle operators, beginning with a very interesting theorem regarding multipoint orthogonality:

Multipoint Orthogonality Theorem. *Consider any diagram contributing to a half-BPS correlator that has a single particle operator $\mathcal{O}_p$ connected to two sub-diagrams, with the sub-diagrams themselves disconnected from each other. Any propagator structure consistent with this type of diagram has a vanishing colour factor. This statement holds for both $U(N)$ and $SU(N)$ free theories.*

This theorem meant that a huge number of diagrams thought to contribute to various correlators of SPOs were actually zero, simplifying a number of calculations that followed. In particular, an important corollary of this theorem was the following:

Near-Extremal Correlators Vanish. *Any near-extremal $SU(N)$ correlator in free theory, where the largest charge operator is a single-particle operator, vanishes, i.e.*

$$\langle \mathcal{O}_p(x) T_{\underline{q_1}}(x_1) \dots T_{\underline{q_{n-1}}}(x_{n-1}) \rangle = 0 \qquad k \leq n-3 \ . \tag{6.0.1}$$

In the $U(N)$ theory, a similar statement can be made but with the caveat that it is true only for connected correlators.

Using the above results, we were able to calculate expressions for all maximally and next-to-maximally extremal free correlators, and were able to calculate explicit expressions for some multi-particle two and three point functions.

There are a number of ways in which this topic can be further explored. Firstly, there are still a large number of things left to calculate even in the free theory. For example, the simple nature of the end formula for lowering extremality three-point functions hints that there may be a way to write a general formula for all N^k maximally extremal three-point functions. As mentioned previously, the multi-particle basis is not orthogonal; it would be interesting to see if a canonical way of orthogonalising the single particle operators could be discovered, perhaps by exploring the string theory point of view further.

One could try to generalise the story of single particle operators described here to beyond the half-BPS sector. Bases do exist already for more general operators beyond the half-BPS sector [149–155], but it would be interesting to revisit these from the perspective of the single-particle operators.

In a slightly different direction, one would assume that the definition of the single particle operator holds beyond the $U(N)$ and $SU(N)$ gauge theories, to the orthogonal and symplectic gauge groups in $\mathcal{N} = 4$ SYM. These can be obtained via a $\mathbb{Z}_2$ orientifold projection of the standard $\mathrm{AdS}_5 \times S^5$ set-up [156]. There have been studies on half-BPS operators in these theories [157–160], so it would be useful to consider single particle operators in these gauge theories and see how they compare to those operators already studied. It would also be interesting to study single particle states for other backgrounds,

for example AdS_3 [161], ABJM, and for the slightly mysterious six-dimensional $(2,0)$ theory on $AdS_7 \times S^4$.

Finally, it would be interesting to consider aspects of the dynamics of the single-particle operators that have not yet been explored, and go beyond the computation of the one-loop amplitudes in [115], along the lines suggested in [162]. The trace basis is widely used in the context of integrability, and in turn integrability based techniques have allowed the computation of exact correlators (see work on the octagon configuration in [163–167] and the five-point analogue called the decagon configuration in [168]). It would be very interesting to understand how the integrability based techniques [169, 170] modify or adapt when correlators of single particle operators are considered.

Finally, in Chapter 6 we looked to write all the N^2MHV Yangian invariants of $\mathcal{N} = 4$ SYM in amplituhedron coordinates. We began be describing a covariantisation algorithm detailed in [31] that made this possible. Then we presented results for all bar one of the 14 N^2MHV Yangian invaraints. It was evident that some had particular simple forms; it would be interesting to see if there exists a nice geometrical way of classifying (a subset of) Yangian invariants for all $k > 2$, in a similar way that was done for all $m = 2$ invariants in [80].

Appendix A

Spurious Pole Cancellation for Special N^2MHV Three-Way Case

Here, we show how the algebraic cancellation works for the special three-way cancellation illustrated in Figure 3.8 and the surrounding discussion:

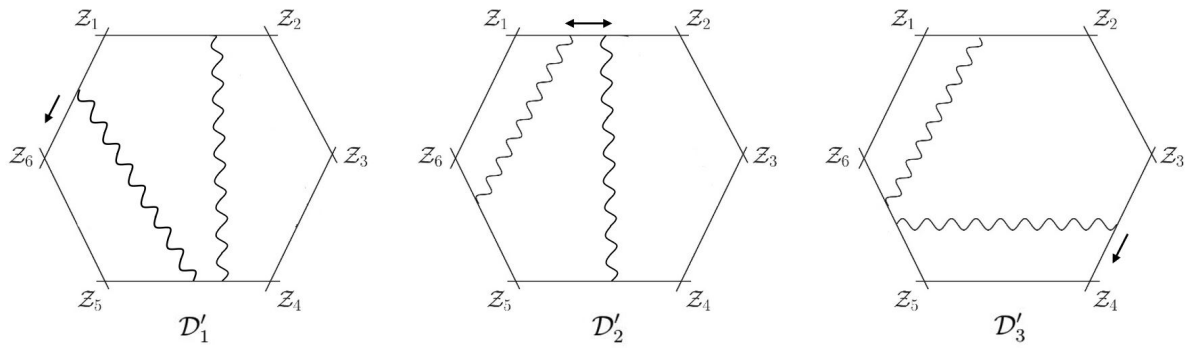

Figure A.1: The WLDs corresponding to the special three way cancellation, with the limits of the residues illustrated by the arrows on each WLD.

To begin, the three integrals given by the WLDs in Figure A.1 are

$$\mathcal{I}(\mathcal{D}_1') = \int \frac{\mathrm{d}a_1\,\mathrm{d}b_1\,\mathrm{d}c_1\,\mathrm{d}d_1\,\mathrm{d}e_1\,\mathrm{d}f_1\,\mathrm{d}g_1\,\mathrm{d}h_1}{a_1 b_1 g_1 h_1 e_1 (c_1 f_1 - d_1 e_1) d_1} \delta^{(8|8)}\left(C_1' \cdot \mathcal{Z}\right) \tag{A.0.1}$$

$$\mathcal{I}(\mathcal{D}_2') = \int \frac{\mathrm{d}a_2\,\mathrm{d}b_2\,\mathrm{d}c_2\,\mathrm{d}d_2\,\mathrm{d}e_2\,\mathrm{d}f_2\,\mathrm{d}g_2\,\mathrm{d}h_2}{c_2 d_2 g_2 h_2 a_2 (e_2 b_2 - a_2 f_2) f_2} \delta^{(8|8)}\left(C_2' \cdot \mathcal{Z}\right) \tag{A.0.2}$$

and

$$\mathcal{I}(\mathcal{D}_3') = \int \frac{\mathrm{d}a_3\,\mathrm{d}b_3\,\mathrm{d}c_3\,\mathrm{d}d_3\,\mathrm{d}e_3\,\mathrm{d}f_3\,\mathrm{d}g_3\,\mathrm{d}h_3}{a_3b_3e_3f_3c_3(d_3g_3-h_3c_3)h_3}\delta^{(8|8)}\left(C_3'\cdot\mathcal{Z}\right), \tag{A.0.3}$$

with the C matrices in the above delta functions given by

$$C_1' = \begin{pmatrix} a_1 & b_1 & 0 & c_1 & d_1 & 0 & 1 \\ h_1 & 0 & 0 & e_1 & f_1 & g_1 & 1 \end{pmatrix}, \tag{A.0.4}$$

$$C_2' = \begin{pmatrix} a_2 & b_2 & 0 & c_2 & d_2 & 0 & 1 \\ e_2 & f_2 & 0 & 0 & g_2 & h_2 & 1 \end{pmatrix}, \tag{A.0.5}$$

$$C_3' = \begin{pmatrix} a_3 & b_3 & 0 & 0 & c_3 & d_3 & 1 \\ 0 & 0 & e_3 & f_3 & g_3 & h_3 & 1 \end{pmatrix}. \tag{A.0.6}$$

The claim is that in summing the diagrams, the residues at the poles diagrammatically represented by the arrows in Figure A.1 precisely cancel:

$$\operatorname*{Res}_{h_1=0}\mathcal{I}(D_1') + \operatorname*{Res}_{a_2f_2=b_2e_2}\mathcal{I}(D_2') + \operatorname*{Res}_{e_3=0}\mathcal{I}(D_3') = 0. \tag{A.0.7}$$

To show this, we will change variables of C_2

$$(e_1,f_1)\to(\alpha,\epsilon_1) \qquad (e_2,f_2)\to(\beta,\epsilon_2) \qquad (g_3,h_3)\to(\gamma,\epsilon_3)$$
$$e_1=\alpha c_1, \quad f_1=\alpha d_1+\epsilon_1 \quad e_2=\beta a_2+\epsilon_2, \quad f_2=\beta b_2 \quad g_3=\gamma c_3+\epsilon_3, \quad h_3=\gamma d_3$$

The spurious poles in question now occur when $h_1,\epsilon,e_3\to 0$.

Substituting these new variables into the integrals corresponding to the WLDs currently being examined gives

$$\begin{aligned}\operatorname*{Res}_{h_1=0}\mathcal{I}(D_1') &= \operatorname*{Res}_{h_1=0}\int \frac{\mathrm{d}a_1\,\mathrm{d}b_1\,\mathrm{d}c_1\,\mathrm{d}d_1\,\mathrm{d}g_1\,\mathrm{d}h_1\,\mathrm{d}\alpha\,\mathrm{d}\epsilon_1}{a_1b_1c_1d_1g_1h_1\alpha\epsilon_1}\delta^{(8|8)}\left(C_1\cdot\mathcal{Z}\right)\\ &= -\int \frac{\mathrm{d}a_1\,\mathrm{d}b_1\,\mathrm{d}c_1\,\mathrm{d}d_1\,\mathrm{d}g_1\,\mathrm{d}\alpha\,\mathrm{d}\epsilon_1}{a_1b_1c_1d_1g_1\alpha\epsilon_1}\delta^{(8|8)}\left(C_1|_{h_1=0}\cdot\mathcal{Z}\right),\end{aligned} \tag{A.0.8}$$

$$\begin{aligned}\operatorname*{Res}_{\epsilon_2=0}\mathcal{I}(D_2') &= \operatorname*{Res}_{\epsilon_2=0}\int \frac{\mathrm{d}a_2\,\mathrm{d}b_2\,\mathrm{d}c_2\,\mathrm{d}d_2\,\mathrm{d}g_2\,\mathrm{d}h_2\,\mathrm{d}\beta\,\mathrm{d}\epsilon_2}{a_2b_2c_2d_2g_2h_2\beta\epsilon_2}\delta^{(8|8)}\left(C_2\cdot\mathcal{Z}\right)\\ &= \int \frac{\mathrm{d}a_2\,\mathrm{d}b_2\,\mathrm{d}c_2\,\mathrm{d}d_2\,\mathrm{d}g_2\,\mathrm{d}h_2\,\mathrm{d}\beta}{a_2b_2c_2d_2g_2h_2\beta}\delta^{(8|8)}\left(C_2|_{\epsilon_2=0}\cdot\mathcal{Z}\right)\end{aligned} \tag{A.0.9}$$

and

$$\begin{aligned}\operatorname*{Res}_{e_3=0}\mathcal{I}(D_3') &= \operatorname*{Res}_{e_3=0}\int \frac{\mathrm{d}a_3\,\mathrm{d}b_3\,\mathrm{d}c_3\,\mathrm{d}d_3\,\mathrm{d}e_3\,\mathrm{d}f_3\,\mathrm{d}\gamma\,\mathrm{d}\epsilon_3}{a_3b_3c_3d_3e_3f_3\gamma\epsilon_3}\delta^{(8|8)}\left(C_3\cdot\mathcal{Z}\right)\\ &= \int \frac{\mathrm{d}a_3\,\mathrm{d}b_3\,\mathrm{d}c_3\,\mathrm{d}d_3\,\mathrm{d}f_3\,\mathrm{d}\gamma\,\mathrm{d}\epsilon_3}{a_3b_3c_3d_3f_3\gamma\epsilon_3}\delta^{(8|8)}\left(C_3|_{e_3=0}\cdot\mathcal{Z}\right). \end{aligned} \tag{A.0.10}$$

The measure in each expression is now simply the dlog of all the variables. The associated C matrices in the delta functions become

$$C_1'|_{h_1=0} = \begin{pmatrix} a_1 & b_1 & 0 & c_1 & d_1 & 0 & 1\\ 0 & 0 & 0 & \alpha c_1 & \alpha d_1+\epsilon_1 & g_1 & 1\end{pmatrix}, \tag{A.0.11}$$

$$C_2'|_{\epsilon_2=0} = \begin{pmatrix} a_2 & b_2 & 0 & c_2 & d_2 & 0 & 1\\ \beta a_2 & \beta b_2 & 0 & 0 & g_2 & h_2 & 1\end{pmatrix}, \tag{A.0.12}$$

$$C_3'|_{e_3=0} = \begin{pmatrix} a_3 & b_3 & 0 & 0 & c_3 & d_3 & 1\\ 0 & 0 & 0 & f_3 & \gamma c_3+\epsilon_3 & \gamma d_3 & 1\end{pmatrix}. \tag{A.0.13}$$

In order to compare the three $C_i' \in \mathrm{GR}(2,7)$, we must introduce a change of parameterization. Utilising the $GL(2)$ invariance, we make the following change of basis for C_1' and C_3',

$$C_1'' = \begin{pmatrix} 1 & 0\\ \frac{-\alpha}{1-\alpha} & \frac{1}{1-\alpha}\end{pmatrix} C_1' \tag{A.0.14}$$

and

$$C_3'' = \begin{pmatrix} \frac{-\gamma}{1-\gamma} & \frac{1}{1-\gamma}\\ 1 & 0\end{pmatrix} C_3'. \tag{A.0.15}$$

The three matrices C_1'', C_2' and C_3'' are now of the same form, meaning they have zeros and ones in the same entries and variables in the others:

$$C_1'' = \begin{pmatrix} a_1 & b_1 & 0 & c_1 & d_1 & 0 & 1\\ \frac{-\alpha a_1}{1-\alpha} & \frac{-\alpha b_1}{1-\alpha} & 0 & 0 & \frac{\epsilon_1}{1-\alpha} & \frac{g_1}{1-\alpha} & 1\end{pmatrix}, \tag{A.0.16}$$

$$C_3'' = \begin{pmatrix} \frac{-\gamma a_3}{1-\gamma} & \frac{-\gamma b_3}{1-\gamma} & 0 & \frac{f_3}{1-\gamma} & \frac{\epsilon_3}{1-\gamma} & 0 & 1\\ a_3 & b_3 & 0 & 0 & c_3 & d_3 & 1\end{pmatrix}. \tag{A.0.17}$$

We make a change of variables for C_1'' and C_3'' to the variables of C_2' as dictated by matching entries:

$$C_1'': \quad \begin{array}{lll} a_1 \to a_2 & b_1 \to b_2 & c_1 \to c_2 \\ d_1 \to d_2 & \epsilon_1 \to \frac{1}{1-\beta} g_2 & g_1 \to \frac{1}{1-\beta} h_1 \end{array} \quad \alpha \to \frac{-\beta}{1-\beta}, \tag{A.0.18}$$

$$C_3'': \quad \begin{array}{lll} a_3 \to \beta a_2 & b_3 \to \beta b_2 & f_3 \to \frac{-\beta c_2}{1-\beta} \\ \epsilon_3 \to \frac{-\beta d_2}{1-\beta} & c_3 \to g_2 & d_3 \to h_2 \end{array} \quad \gamma \to \frac{1}{1-\beta}. \tag{A.0.19}$$

Substituting these new variables into the residues of $\mathcal{I}(\mathcal{D}_1')$ and $\mathcal{I}(\mathcal{D}_3')$ and taking the sum of all three integrals gives

$$\int \frac{\mathrm{d}a_2\, \mathrm{d}b_2\, \mathrm{d}c_2\, \mathrm{d}d_2\, \mathrm{d}g_2\, \mathrm{d}h_2\, \mathrm{d}\beta}{a_1 b_1 c_1 d_1 g_1 h_1} \left(-\frac{1}{\beta(1-\beta)} + \frac{1}{\beta} + \frac{1}{1-\beta} \right) \delta^{(8|8)}(C_2' \cdot \mathcal{Z}) = 0. \tag{A.0.20}$$

Therefore, we have shown that (A.0.7) is indeed satisfied.

Appendix B

Character Polynomials

As we saw in section 4.1.2, group theoretic formula for the dual operators to the trace basis was given by Brown in [127]. This formula was dependent on the character of any conjugacy class of the symmetric group in any hook representation, where the hook representations consisted of the representations associated to Young diagrams with one column and one row. An explicit formula for this set of characters is unknown, however they are neatly packaged in character polynomials. We give a brief explanation of them here and show how to calculate the characters given in the character tables in (2.1) using this technique.[1]

In [70], the following generating function was defined for the character polynomials for characters of all hook representations:

$$\sum_{k=0}^{\infty} q_{1^k} t^k = \frac{1}{1+t} \prod_{i=1}^{\infty} \left(1 - (-t)^i\right)^{c_i} . \tag{B.0.1}$$

Here, q_{1^k} is the character polynomial for the hook representation correponding to the Young diagram with $k+1$ boxes in the first column and a row of any length), and c_i denotes the number of cycles of length i the element $\sigma \in S_n$ has.

[1] We were able to re-write the sum for the single particle operators in terms of other group theoretic quantities described in section 2.4.6, which turned the coefficients of the multi-traces into formulae explicit in the weight p and the conjugacy class of the trace structure $\{q_1, \ldots, q_m\}$. So, calculating these characters explicitly did not end up being relevant when continuing to discuss SPOs.

The simplest way to understand this generating function is by illustrating its use with an example. To do this, we shall calculate the character table for S_4. There are four representations that have the required hook shape:

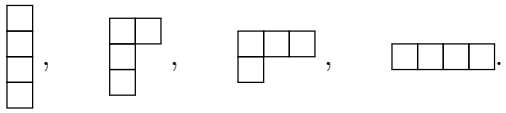

(B.0.2)

The left hand side of (B.0.1) must be expanded to $k = 3$ giving

$$q_{1^0} + q_{1^1}t + q_{1^2}t^2 + q_{1^3}t_3. \tag{B.0.3}$$

Now to expand the right hand side. Plugging in the relevant c_i gives a different expansion for each conjugacy class, which we show below:

$$() : \quad \frac{1}{1+t}(1-(-t)^1)^4 = 1 + 3t + 3t^2 + t^3, \tag{B.0.4}$$

$$(12) : \quad \frac{1}{1+t}(1-(-t)^2)(1-(-t))^2 = 1 + t - t^2 - t^3, \tag{B.0.5}$$

$$(12)(34) : \quad \frac{1}{1+t}(1-(-t)^2)^2 = 1 - t - t^2 + t^3, \tag{B.0.6}$$

$$(123) : \quad \frac{1}{1+t}(1-(-t)^3)(1-(-t)) = 1 + t^3 \tag{B.0.7}$$

$$(1234) : \quad \frac{1}{1+t}(1-(-t)^4) = 1 - t + t^2 - t^3 \tag{B.0.8}$$

By comparing (B.0.3) to each of the polynomials on the right hand side of (B.0.4), we can construct the part of the S_4 character table involving hook representations. Note that the set of coefficients of the polynomials in t each give one column of the character table. The result is below:

S_4	()	(12)	(12)(34)	(123)	(1234)
	1	1	1	1	1
	3	1	-1	0	-1
	3	-1	-1	0	1
	1	-1	1	1	-1

Table B.1: The character table involving hook representations, using characters calculated using the generating function (B.0.1)

,

We see that the results of B.1 are in full agreement with the S_4 character table we showed in (2.1).

Appendix C

Trace Sector Formulae

In section 4.2.2 we obtained the result

$$\mathcal{O}_p = \sum_{\{q_1..q_m\}\vdash p} C_{q_1,..,q_m} T_{q_1,..q_m} \tag{C.0.1}$$

$$C_{q_1,..q_m} = \frac{||[\sigma_{q_1..q_m}]||}{(p-1)!} \sum_{s\in\mathcal{P}(\{q_1,..,q_m\})} \frac{(-1)^{|s|+1}(N+1-p)_{p-\Sigma(s)}(N+p-\Sigma(s))_{\Sigma(s)}}{(N)_p - (N+1-p)_p} \tag{C.0.2}$$

which is explicit in p and $q_1 \dots q_m$, and depends on group theory data which we explained in section 2.4.6.

The value of m distinguishes the splitting of $\mathcal{O}_p$ into m traces we. We will give explicit examples for the double trace sector $m = 2$, and the triple trace sector $m = 3$.

C.1 Double Trace Sector

Consider the partition $q_1 + q_2 = p$. The powerset in the sum is

$$\mathcal{P}\left(\{q_1 q_2\}\right) = \{\{\}, \{q_1\}, \{q_2\}, \{q_1, q_2\}\} \tag{C.1.1}$$

and the corresponding values of Σ are

$$\Sigma(\{\}) = 0\ ,\ \Sigma(\{q_1\}) = q_1\ ,\ \Sigma(\{q_2\}) = q_2\ ,\ \Sigma(\{q_1, q_2\}) = q_1 + q_2 = p. \tag{C.1.2}$$

Furthermore the size of the conjugacy class is $|[q_1q_2]| = p!/(q_1q_2)$ as long as $q_1 \neq q_2$. Otherwise $q_1 = q_2 = p/2$ and $|[q_1q_2]| = p!/(2q_1q_2) = (p-1)!/(2p)$. With these informations, the coefficient of $T_{q_1}T_{q_2}$ in $\mathcal{O}_p$, from (C.0.2), is

$$C_{q_1q_2} = \begin{cases} \dfrac{p}{q_1q_2} \times \dfrac{-(N-p+1)_p - (N)_p + (N-p+1)_{q_2}(N+q_2)_{p-q_2} + (N-p+1)_{q_1}(N+q_1)_{p-q_1}}{(N)_p - (N-p+1)_p} \\ \dfrac{2}{p} \times \dfrac{-(N-p+1)_p - (N)_p + 2(N-p+1)_{p/2}(N+p/2)_{p/2}}{(N)_p - (N-p+1)_p} \end{cases} \tag{C.1.3}$$

The above formula holds for the coefficients of the double trace contributions to the single particle operator of any weight.

C.2 Triple Trace Sector

Consider the partition $q_1 + q_2 + q_3 = p$. By making explicit (C.0.2) we find,

$$\begin{aligned} C_{q_1q_2q_3} = & \frac{p}{q_1q_2q_3} \frac{-(N-p+1)_p + (N)_p}{(N)_p - (N-p+1)_p} + \\ & \frac{p}{q_1q_2q_3} \frac{-\sum_{i=1}^3 (N-p+1)_{q_i}(N+q_i)_{p-q_i} + \sum_{i=1}^3 (N-p+1)_{p-q_i}(N+p-q_i)_{q_i}}{(N)_p - (N-p+1)_p} \end{aligned} \tag{C.2.1}$$

The other two possible cases, in which $q_i = q_j$ and $q_1 = q_2 = q_3 = p/3$, only differ compared to the result above by the the size of the conjugacy class. In the first case we have to further divide by 2, and in the second case by 6. This formula thus cover all possible triple trace contributions to single particle operators of any weight.

For any value of m, i.e. for any trace sector, the function $C_{\underline{q}}$ can be made very explicit in a similar way to the examples above.

Appendix D

Prüfer Sequences and Trees

The Prüfer sequence, which we write as $s = (s_1 \ldots)$ gives a unique way of labelling a tree diagram. The construction was described in [171]; here we look to give a brief description on how this works.

Consider a tree made of points at positions $1, \ldots, n-1$, with each point i having d_i legs attached to it. For example, the trees associated with the T_{q_i} operators and the propagators between them in (4.4.8) are given in Figure D.1.

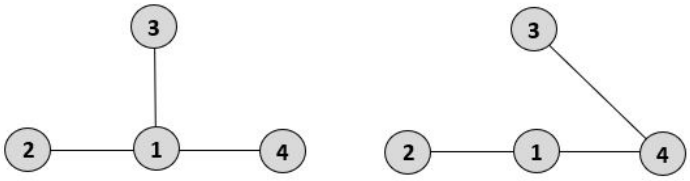

Figure D.1: Tree diagrams corresponding to the diagrams given in (4.4.8). The label i corresponds to the propagator T_{q_i} and the branches of the trees correspond to the propagators.

We define a leaf in a tree to be a pair of positions (a, b) such that a has one and only one bridge connecting to it, and b is the node at the other side of that one bridge. The Prüfer algorithm works as follows: at step k of the algorithm remove the leaf (a, b) where a has the smallest label, and assign $s_k = b$ to the sequence. To relate this to the number

of possible Wick contractions for that propagator, write down the contribution

$$|\mathcal{W}(a,b)| = (q_a - d_a + 1)(q_b - R(b)), \tag{D.0.1}$$

where q_a, q_b corresponds to the charge of the operator at position a, b respectively and $R(b)$ corresponds to the number of times b has appeared in the sequence previous (i.e. steps $< k$). The Prüfer sequence stops when there is only one leaf left, i.e. one pair of nodes left. However, we do have to write down that final contribution to the number of Wick contractions given by (D.0.1).

For example, on the left hand side of Figure D.1, the Prüfer algorithm would give the sequence $\{1, 1\}$, and the number of Wick contractions at each step would correspond to $\{|\mathcal{W}(2,1)| = q_2 q_1,\ |\mathcal{W}(3,1)| = q_3(q_1 - 1)\}$. The total number of wick contractions for the whole tree though would be the product of the right hand side of each element in that sequence, multiplied by the result of the final leaf given by $|\mathcal{W}(3,1)| = q_4(q_1 - 2)$. Therefore, for this example

$$|\mathcal{W}(\mathcal{T})| = q_1 q_2 q_3 (q_1 - 1)(q_1 - 2). \tag{D.0.2}$$

It is very straightforward to continue these considerations to as complicated a tree as you like.

It is quite evident that the Prüfer Sequence gives a very nice way of ordering Wick contractions for the purposes of counting the total number of possibilities. It is clear that the first time two operators i and j appear in the sequence, they count with $q_i q_j$, because necessarily $d_i = 1$ or $d_j = 1$. The second time one of this operators appears again, it counts with $q_i - 1$ or $q_j - 1$, and so on. The total number of Wick contractions is then,

$$|\mathcal{W}[\mathcal{T}]| = \prod_{i=1}^{n-1} q_i (q_i - 1) \dots (q_i - d_i + 1) \tag{D.0.3}$$

which is the result we quoted in (4.4.9).

Bibliography

[1] Juan Maldacena. The Large N Limit of Superconformal Field Theories and Supergravity. *International Journal of Theoretical Physics*, 38(4):1113–1133, 1999.

[2] S.S. Gubser, I.R. Klebanov, and A.M. Polyakov. Gauge Theory Correlators from Non-Critical String Theory. *Physics Letters B*, 428(1-2):105–114, May 1998.

[3] Edward Witten. Anti-de Sitter Space and Holography. *Adv. Theor. Math. Phys.*, 2:253–291, 1998.

[4] Ofer Aharony, Steven S. Gubser, Juan Maldacena, Hirosi Ooguri, and Yaron Oz. Large N Field Theories, String Theory and Gravity. *Physics Reports*, 323(3-4):183–386, Jan 2000.

[5] Gerard 't Hooft. A Planar Diagram Theory for Strong Interactions. *Nucl. Phys. B*, 72:461, 1974.

[6] Stephen J. Parke and T.R. Taylor. Gluonic Two Goes to Four. *Nucl. Phys. B*, 269:410–420, 1986.

[7] Stephen J. Parke and T.R. Taylor. An Amplitude for n Gluon Scattering. *Phys. Rev. Lett.*, 56:2459, 1986.

[8] Zvi Bern, Lance Dixon, David C. Dunbar, and David A. Kosower. One-Loop n-Point Gauge Theory Amplitudes, Unitarity and Collinear Limits. *Nuclear Physics B*, 425(1-2):217–260, Aug 1994.

[9] Ruth Britto, Freddy Cachazo, and Bo Feng. Generalized Unitarity and One-Loop Amplitudes in Super-Yang–Mills. *Nuclear Physics B*, 725(1-2):275–305, Oct 2005.

[10] J.M. Drummond, J. Henn, G.P. Korchemsky, and E. Sokatchev. Generalized Unitarity for Super-Amplitudes. *Nuclear Physics B*, 869(3):452–492, Apr 2013.

[11] Zvi Bern and Yu-tin Huang. Basics of Generalized Unitarity. *Journal of Physics A: Mathematical and Theoretical*, 44(45):454003, Oct 2011.

[12] Ruth Britto, Freddy Cachazo, and Bo Feng. New Recursion Relations for Tree Amplitudes of Gluons. *Nuclear Physics B*, 715(1-2):499–522, May 2005.

[13] Ruth Britto, Freddy Cachazo, Bo Feng, and Edward Witten. Direct Proof of the Tree-Level Scattering Amplitude Recursion Relation in Yang-Mills Theory. *Physical Review Letters*, 94(18), May 2005.

[14] Freddy Cachazo, Peter Svrcek, and Edward Witten. MHV Vertices And Tree Amplitudes in Gauge Theory. *Journal of High Energy Physics*, 2004(09):006–006, Sep 2004.

[15] James M Drummond, Johannes Henn, Vladimir A Smirnov, and Emery Sokatchev. Magic Identities for Conformal Four-Point Integrals. *Journal of High Energy Physics*, 2007(01):064–064, Jan 2007.

[16] J.M. Drummond, J. Henn, G.P. Korchemsky, and E. Sokatchev. Dual Superconformal Symmetry of Scattering Amplitudes in Super Yang–Mills Theory. *Nuclear Physics B*, 828(1-2):317–374, Mar 2010.

[17] Andreas Brandhuber, Paul Heslop, and Gabriele Travaglini. Note on Dual Superconformal Symmetry of the $\mathcal{N} = 4$ Super Yang-Mills S Matrix. *Physical Review D*, 78(12), Dec 2008.

[18] Andreas Brandhuber, Paul Heslop, and Gabriele Travaglini. Proof of the Dual Conformal Anomaly of One-Loop Amplitudes in $\mathcal{N} = 4$ SYM. *Journal of High Energy Physics*, 2009(10):063–063, Oct 2009.

[19] Luis F Alday and Juan Maldacena. Gluon Scattering Amplitudes at Strong Coupling. *Journal of High Energy Physics*, 2007(06):064–064, Jun 2007.

[20] J.M. Drummond, G.P. Korchemsky, and E. Sokatchev. Conformal Properties of Four-Gluon Planar Amplitudes and Wilson Loops. *Nuclear Physics B*, 795(1-2):385–408, May 2008.

[21] Andreas Brandhuber, Paul Heslop, and Gabriele Travaglini. MHV Amplitudes in Super Yang–Mills and Wilson Loops. *Nuclear Physics B*, 794(1-2):231–243, May 2008.

[22] S. Caron-Huot. Notes on the Scattering Amplitude — Wilson Loop Duality. *Journal of High Energy Physics*, 2011(7), Jul 2011.

[23] Lionel Mason and David Skinner. The Complete Planar S-matrix of $\mathcal{N} = 4$ SYM as a Wilson Loop in Twistor Space. *Journal of High Energy Physics*, 2010(12), Dec 2010.

[24] A.V. Belitsky, G.P. Korchemsky, and E. Sokatchev. Are Scattering Amplitudes Dual to Super Wilson Loops? *Nuclear Physics B*, 855(2):333–360, Feb 2012.

[25] Luis F. Alday, Burkhard Eden, Gregory P. Korchemsky, Juan Maldacena, and Emery Sokatchev. From Correlation Functions to Wilson Loops. *Journal of High Energy Physics*, 2011(9), Sep 2011.

[26] Burkhard Eden, Paul Heslop, Gregory P. Korchemsky, and Emery Sokatchev. The Super-Correlator/Super-Amplitude Duality: Part I. *Nuclear Physics B*, 869(3):329–377, Apr 2013.

[27] Burkhard Eden, Paul Heslop, Gregory P. Korchemsky, and Emery Sokatchev. The Super-Correlator/Super-Amplitude Duality: Part II. *Nuclear Physics B*, 869(3):378–416, Apr 2013.

[28] Tim Adamo, Mathew Bullimore, Lionel Mason, and David Skinner. A Proof of the Correlation Function/Supersymmetric Wilson Loop Correspondence. *Journal of High Energy Physics*, 2011(8), Aug 2011.

[29] James Drummond, Johannes Henn, and Jan Plefka. Yangian Symmetry of Scattering Amplitudes in $\mathcal{N} = 4$ Super Yang-Mills Theory. *Journal of High Energy Physics*, 2009(05):046–046, May 2009.

[30] Jacob L. Bourjaily, Paul Heslop, and Vuong-Viet Tran. Amplitudes and Correlators to Ten Loops Using Simple, Graphical Bootstraps. *Journal of High Energy Physics*, 2016(11), Nov 2016.

[31] Paul Heslop and Vuong-Viet Tran. Multi-Particle Amplitudes from the Four-Point Correlator in Planar $\mathcal{N} = 4$ SYM. *Journal of High Energy Physics*, 2018(7), Jul 2018.

[32] Nathan Berkovits and Juan Maldacena. Dual superconformal symmetry, and the amplitude/Wilson loop connection. *Journal of High Energy Physics*, 2008(09):062–062, Sep 2008.

[33] Niklas Beisert, Riccardo Ricci, Arkady A. Tseytlin, and Martin Wolf. Dual superconformal symmetry from $AdS_5 \times S_5$ superstring integrability. *Physical Review D*, 78(12), Dec 2008.

[34] Luis F. Alday and Radu Roiban. Scattering amplitudes, Wilson loops and the string/gauge theory correspondence. *Physics Reports*, 468(5):153–211, Nov 2008.

[35] J.M. Drummond, J. Henn, G.P. Korchemsky, and E. Sokatchev. On planar gluon amplitudes/Wilson loops duality. *Nuclear Physics B*, 795(1-2):52–68, May 2008.

[36] J.M. Drummond, J. Henn, G.P. Korchemsky, and E. Sokatchev. Conformal Ward identities for Wilson loops and a test of the duality with gluon amplitudes. *Nuclear Physics B*, 826(1-2):337–364, Feb 2010.

[37] Zvi Bern, Lance J. Dixon, and Vladimir A. Smirnov. Iteration of planar amplitudes in maximally supersymmetric Yang-Mills theory at three loops and beyond. *Physical Review D*, 72(8), Oct 2005.

[38] J.M. Drummond, J. Henn, G.P. Korchemsky, and E. Sokatchev. The hexagon Wilson loop and the BDS ansatz for the six-gluon amplitude. *Physics Letters B*, 662(5):456–460, May 2008.

[39] Z. Bern, L. J. Dixon, D. A. Kosower, R. Roiban, M. Spradlin, C. Vergu, and A. Volovich. Two-loop six-gluon maximally helicity violating amplitude in maximally supersymmetric Yang-Mills theory. *Physical Review D*, 78(4), Aug 2008.

[40] J.M. Drummond, J. Henn, G.P. Korchemsky, and E. Sokatchev. Hexagon Wilson loop = six-gluon MHV amplitude. *Nuclear Physics B*, 815(1-2):142–173, Jul 2009.

[41] Mathew Bullimore and David Skinner. Holomorphic Linking, Loop Equations and Scattering Amplitudes in Twistor Space, 2011.

[42] N. Arkani-Hamed, F. Cachazo, C. Cheung, and J. Kaplan. A Duality for the S Matrix. *Journal of High Energy Physics*, 2010(3), Mar 2010.

[43] N. Arkani-Hamed, J. Bourjaily, F. Cachazo, and J. Trnka. Local Spacetime Physics from the Grassmannian. *Journal of High Energy Physics*, 2011(1), Jan 2011.

[44] N. Arkani-Hamed, J. Bourjaily, F. Cachazo, and J. Trnka. Unification of Residues and Grassmannian Dualities. *Journal of High Energy Physics*, 2011(1), Jan 2011.

[45] Nima Arkani-Hamed, Jacob L. Bourjaily, Freddy Cachazo, Alexander B. Goncharov, Alexander Postnikov, and Jaroslav Trnka. Scattering Amplitudes and the Positive Grassmannian, 2014.

[46] Nima Arkani-Hamed, Jacob Bourjaily, Freddy Cachazo, Alexander Goncharov, Alexander Postnikov, and Jaroslav Trnka. *Grassmannian Geometry of Scattering Amplitudes*. Cambridge University Press, 2016.

[47] Nima Arkani-Hamed and Jaroslav Trnka. The Amplituhedron. *Journal of High Energy Physics*, 2014(10), Oct 2014.

[48] Nima Arkani-Hamed and Jaroslav Trnka. Into the Amplituhedron. *Journal of High Energy Physics*, 2014(12), Dec 2014.

[49] Nima Arkani-Hamed, Cameron Langer, Akshay Yelleshpur Srikant, and Jaroslav Trnka. Deep Into the Amplituhedron: Amplitude Singularities at All Loops and Legs. *Phys. Rev. Lett.*, 122:051601, Feb 2019.

[50] Cameron Langer and Akshay Yelleshpur Srikant. All-Loop Cuts from the Amplituhedron. *Journal of High Energy Physics*, 2019(4), Apr 2019.

[51] I. Prlina, M. Spradlin, J. Stankowicz, and S. Stanojevic. Boundaries of Amplituhedra and NMHV Symbol Alphabets at Two Loops. *Journal of High Energy Physics*, 2018(4), Apr 2018.

[52] I. Prlina, M. Spradlin, J. Stankowicz, S. Stanojevic, and A. Volovich. All-Helicity Symbol Alphabets from Unwound Amplituhedra. *Journal of High Energy Physics*, 2018(5), May 2018.

[53] T. Dennen, I. Prlina, M. Spradlin, S. Stanojevic, and A. Volovich. Landau Singularities from the Amplituhedron. *Journal of High Energy Physics*, 2017(6), Jun 2017.

[54] Lance J. Dixon, Matt von Hippel, Andrew J. McLeod, and Jaroslav Trnka. Multi-Loop Positivity of the Planar $\mathcal{N} = 4$ SYM Six-Point Amplitude. *Journal of High Energy Physics*, 2017(2), Feb 2017.

[55] Niklas Beisert and Matthias Staudacher. The SYM Integrable Super Spin Chain. *Nuclear Physics B*, 670(3):439–463, Oct 2003.

[56] Niklas Beisert, Changrim Ahn, Luis F. Alday, Zoltán Bajnok, James M. Drummond, Lisa Freyhult, Nikolay Gromov, Romuald A. Janik, Vladimir Kazakov, Thomas Klose, and et al. Review of AdS/CFT Integrability: An Overview. *Letters in Mathematical Physics*, 99(1-3):3–32, Oct 2011.

[57] Paul Heslop and Alastair Stewart. The Twistor Wilson Loop and the Amplituhedron. *Journal of High Energy Physics*, 2018(10), Oct 2018.

[58] Francesco Aprile, J. M. Drummond, Paul Heslop, Hyneck Paul, Francesco Sanfilippo, Michele Santagata, and Alastair Stewart. Single Particle Operators and their Correlators in Free $\mathcal{N} = 4$ SYM. *Journal of High Energy Physics*, 2020(72), Aug 2020.

[59] Eric D'Hoker and Daniel Z. Freedman. Supersymmetric gauge theories and the AdS / CFT correspondence. In *Theoretical Advanced Study Institute in Elementary Particle Physics (TASI 2001): Strings, Branes and EXTRA Dimensions*, pages 3–158, 1 2002.

[60] V.P. Nair. A Current Algebra for Some Gauge Theory Amplitudes. *Phys. Lett. B*, 214:215–218, 1988.

[61] Zvi Bern, Lance J. Dixon, David C. Dunbar, and David A. Kosower. Fusing Gauge Theory Tree Amplitudes into Loop Amplitudes. *Nucl. Phys. B*, 435:59–101, 1995.

[62] Henriette Elvang and Yu tin Huang. Scattering Amplitudes, 2014.

[63] Andrew Hodges. Eliminating Spurious Poles from Gauge-Theoretic Amplitudes, 2009.

[64] Lionel Mason and David Skinner. Dual Superconformal Invariance, Momentum Twistors and Grassmannians. *Journal of High Energy Physics*, 2009(11):045–045, Nov 2009.

[65] Dongmin Gang, Yu-tin Huang, Eunkyung Koh, Sangmin Lee, and Arthur E. Lipstein. Tree-Level Recursion Relation and Dual Superconformal Symmetry of the ABJM Theory. *Journal of High Energy Physics*, 2011(3), Mar 2011.

[66] Yu-tin Huang and Arthur E. Lipstein. Dual Superconformal Symmetry of $\mathcal{N} = 6$ Chern-Simons Theory. *Journal of High Energy Physics*, 2010(11), Nov 2010.

[67] Till Bargheer, Florian Loebbert, and Carlo Meneghelli. Symmetries of Tree-Level Scattering Amplitudes in $\mathcal{N} = 6$ Superconformal Chern-Simons Theory. *Physical Review D*, 82(4), Aug 2010.

[68] Mathew Bullimore. MHV Diagrams from an All-Loop Recursion Relation. *Journal of High Energy Physics*, 2011(8), Aug 2011.

[69] Wei Wu and Qianer Zhang. The Orthogonal and the Natural Representation for Symmetric Groups. *International Journal of Quantum Chemistry*, 50(1):55–67, 1994.

[70] Alain Goupil. Generating Functions for Irreducible Characters of S_n Indexed with Multiple Hooks. *Annales des Sciences Mathématiques du Québec*, 23, 01 1999.

[71] Ahmed Umer Ashraf. Character Polynomials for Two Rows and Hook Partitions, 2018.

[72] W. Fulton and J. Harris. *Representation Theory: A First Course*. Graduate texts in mathematics. Springer, 1991.

[73] A.O. Barut and R. Raczka. *Theory of Group Representations and Applications*. 1986.

[74] N. Arkani-Hamed, J. Bourjaily, F. Cachazo, A. Hodges, and J. Trnka. A Note on Polytopes for Scattering Amplitudes. *Journal of High Energy Physics*, 2012(4), Apr 2012.

[75] Nima Arkani-Hamed, Hugh Thomas, and Jaroslav Trnka. Unwinding the Amplituhedron in Binary. *Journal of High Energy Physics*, 2018(1), Jan 2018.

[76] Steven N Karp and Lauren K Williams. The $m = 1$ Amplituhedron and Cyclic Hyperplane Arrangements. *International Mathematics Research Notices*, 2019(5):1401–1462, Jul 2017.

[77] Tomasz Lukowski, Matteo Parisi, and Lauren K. Williams. The positive tropical Grassmannian, the hypersimplex, and the $m = 2$ amplituhedron, 2020.

[78] Tomasz Lukowski. On the Boundaries of the $m = 2$ Amplituhedron, 2019.

[79] Huanchen Bao and Xuhua He. The $m = 2$ amplituhedron, 2019.

[80] Tomasz Łukowski, Matteo Parisi, Marcus Spradlin, and Anastasia Volovich. Cluster Adjacency for $m = 2$ Yangian Invariants. *Journal of High Energy Physics*, 2019(10), Oct 2019.

[81] Steven N. Karp, Lauren K. Williams, and Yan X Zhang. Decompositions of Amplituhedra, 2017.

[82] Ryota Kojima and Cameron Langer. Sign flip triangulations of the amplituhedron. *Journal of High Energy Physics*, 2020(5), May 2020.

[83] Livia Ferro, Tomasz Łukowski, Andrea Orta, and Matteo Parisi. Towards the Amplituhedron Volume. *Journal of High Energy Physics*, 2016(3), Mar 2016.

[84] Nima Arkani-Hamed, Yuntao Bai, and Thomas Lam. Positive Geometries and Canonical Forms. *Journal of High Energy Physics*, 2017(11), Nov 2017.

[85] Pavel Galashin and Thomas Lam. Parity Duality for the Amplituhedron, 2018.

[86] Livia Ferro, Tomasz Łukowski, and Matteo Parisi. Amplituhedron Meets Jeffrey–Kirwan Residue. *Journal of Physics A: Mathematical and Theoretical*, 52(4):045201, Dec 2018.

[87] Susama Agarwala and Eloi Marin-Amat. Wilson Loop Diagrams and Positroids. *Communications in Mathematical Physics*, 350(2):569–601, Jul 2016.

[88] Burkhard Eden, Paul Heslop, and Lionel Mason. The Correlahedron. *Journal of High Energy Physics*, 2017(9), Sep 2017.

[89] Susama Agarwala and Sian Fryer. A study in $\mathbb{G}_{\mathbb{R},\geq 0}$: from the Geometric Case Book of Wilson Loop Diagrams and SYM $\mathcal{N} = 4$, 2018.

[90] Susama Agarwala and Cameron Marcott. Wilson Loops in SYM $\mathcal{N} = 4$ do not Parametrize an Orientable Space, 2018.

[91] Burkhard Eden, Gregory P. Korchemsky, and Emery Sokatchev. From Correlation Functions to Scattering Amplitudes. *Journal of High Energy Physics*, 2011(12), Dec 2011.

[92] Rutger Boels, Lionel Mason, and David Skinner. Supersymmetric Gauge Theories in Twistor Space. *Journal of High Energy Physics*, 2007(02):014–014, Feb 2007.

[93] Edward Witten. Perturbative Gauge Theory as a String Theory in Twistor Space. *Communications in Mathematical Physics*, 252(1-3):189–258, Oct 2004.

[94] E. Sokatchev. Action for $\mathcal{N} = 4$ Supersymmetric Self-Dual Yang-Mills Theory. *Physical Review D*, 53(4):2062–2070, Feb 1996.

[95] Lionel J Mason. Twistor Actions for Non-Self-Dual Fields; a New Foundation for Twistor-String Theory. *Journal of High Energy Physics*, 2005(10):009–009, Oct 2005.

[96] Tim Adamo, Mathew Bullimore, Lionel Mason, and David Skinner. Scattering Amplitudes and Wilson Loops in Twistor Space. *Journal of Physics A: Mathematical and Theoretical*, 44(45):454008, Oct 2011.

[97] Dmitry Chicherin and Emery Sokatchev. $\mathcal{N} = 4$ Super Yang-Mills in LHC Superspace Part I: Classical and Quantum Theory. *Journal of High Energy Physics*, 2017(2), Feb 2017.

[98] Dmitry Chicherin, Paul Heslop, Gregory P. Korchemsky, and Emery Sokatchev. Wilson Loop Form Factors: A New Duality, 2016.

[99] Arthur E. Lipstein and Lionel Mason. From the holomorphic Wilson loop to "d log" loop-integrands of super-Yang-Mills amplitudes. *Journal of High Energy Physics*, 2013(5), May 2013.

[100] Arthur E. Lipstein and Lionel Mason. From d logs to dilogs; the super Yang-Mills MHV amplitude revisited. *Journal of High Energy Physics*, 2014(1), Jan 2014.

[101] D. Chicherin, R. Doobary, B. Eden, P. Heslop, G. P. Korchemsky, L. Mason, and E. Sokatchev. Correlation Functions of the Chiral Stress-Tensor Multiplet in $\mathcal{N} = 4$ SYM, 2015.

[102] Susama Agarwala, Siân Fryer, and Karen Yeats. Combinatorics of the Geometry of Wilson Loop Diagrams I: Equivalence Classes via Matroids and Polytopes, 2019.

[103] Susama Agarwala, Siân Fryer, and Karen Yeats. Combinatorics of the Geometry of Wilson Loop Diagrams II: Grassmann Necklaces, Dimensions, and Denominators, 2019.

[104] Daniel Z. Freedman, Samir D. Mathur, Alec Matusis, and Leonardo Rastelli. Correlation Functions in the CFT(d)/AdS($d + 1$) Correspondence. *Nuclear Physics B*, 546(1-2):96–118, Apr 1999.

[105] Sangmin Lee, Shiraz Minwalla, Mukund Rangamani, and Nathan Seiberg. Three Point Functions of Chiral Operators in $D = 4$, $\mathcal{N} = 4$ SYM at large N. *Adv. Theor. Math. Phys.*, 2:697–718, 1998.

[106] B. Eden, P.S. Howe, A. Pickering, E. Sokatchev, and P.C. West. Four-Point Functions in $N = 2$ Superconformal Field Theories. *Nuclear Physics B*, 581(1-2):523–558, Aug 2000.

[107] B Eden, P.S Howe, E Sokatchev, and P.C West. Extremal and Next-to-Extremal n-Point Correlators in Four-Dimensional SCFT. *Physics Letters B*, 494(1-2):141–147, Nov 2000.

[108] John McGreevy, Leonard Susskind, and Nicolaos Toumbas. Invasion of the Giant Gravitons from Anti-de Sitter Space. *Journal of High Energy Physics*, 2000(06):008–008, Jun 2000.

[109] Juan Maldacena and Andrew Strominger. AdS3 Black Holes and a Stringy Exclusion Principle. *Journal of High Energy Physics*, 1998(12):005–005, Dec 1998.

[110] Pei-Ming Ho, Sanjaye Ramgoolam, and Radu Tatar. Quantum Space-Times and Finite Effects in 4D Super Yang–Mills Theories. *Nuclear Physics B*, 573(1-2):364–376, May 2000.

[111] Antal Jevicki and Sanjaye Ramgoolam. Non-Commutative Gravity from the AdS / CFT Correspondence. *JHEP*, 04:032, 1999.

[112] F. Aprile, J. M. Drummond, P. Heslop, and H. Paul. Quantum Gravity from Conformal Field Theory. *Journal of High Energy Physics*, 2018(1), Jan 2018.

[113] Luis F. Alday and Simon Caron-Huot. Gravitational S-matrix from CFT Dispersion Relations. *Journal of High Energy Physics*, 2018(12), Dec 2018.

[114] F. Aprile, J. M. Drummond, P. Heslop, and H. Paul. Loop Corrections for Kaluza-Klein AdS Amplitudes. *Journal of High Energy Physics*, 2018(5), May 2018.

[115] F. Aprile, J.M. Drummond, P. Heslop, and H. Paul. One-Loop Amplitudes in $AdS5 \times S5$ Supergravity from $\mathcal{N} = 4$ SYM at Strong Coupling. *Journal of High Energy Physics*, 2020(3), Mar 2020.

[116] Luis F. Alday and Xinan Zhou. Simplicity of AdS Supergravity at One Loop, 2020.

[117] G. Arutyunov and S. Frolov. Some Cubic Couplings in Type IIB Supergravity on $AdS5 \times S5$ and Three-Point Functions in Four-Dimensional Super Yang-Mills Theory at Large N. *Physical Review D*, 61(6), Feb 2000.

[118] Gleb Arutyunov and Sergey Frolov. On the Correspondence Between Gravity Fields and CFT Operators. *Journal of High Energy Physics*, 2000(04):017–017, Apr 2000.

[119] Leonardo Rastelli and Xinan Zhou. How to Succeed at Holographic Correlators Without Really Trying. *Journal of High Energy Physics*, 2018(4), Apr 2018.

[120] Gleb Arutyunov, Rob Klabbers, and Sergei Savin. Four-Point Functions of All-Different-Weight Chiral Primary Operators in the Supergravity Approximation. *Journal of High Energy Physics*, 2018(9), Sep 2018.

[121] Gleb Arutyunov, Rob Klabbers, and Sergei Savin. Four-Point Functions of 1/2-BPS Operators of Any Weights in the Supergravity Approximation. *Journal of High Energy Physics*, 2018(9), Sep 2018.

[122] Francesco Aprile, James Drummond, Paul Heslop, and Hynek Paul. Double-Trace Spectrum of $\mathcal{N} = 4$ Supersymmetric Yang-Mills Theory at Strong Coupling. *Physical Review D*, 98(12), Dec 2018.

[123] G. W. Gibbons and P. K. Townsend. Vacuum Interpolation in Supergravity via Super p-Branes. *Physical Review Letters*, 71(23):3754–3757, Dec 1993.

[124] Moshe Flato, Christian Fronsdal, and Daniel Sternheimer. Singleton Physics. 1 1999.

[125] Steve Corley, Antal Jevicki, and Sanjaye Ramgoolam. Exact Correlators of Giant Gravitons from Dual $\mathcal{N} = 4$ SYM Theory. *Adv. Theor. Math. Phys.*, 5:809–839, 2002.

[126] Robert de Mello Koch and Rhiannon Gwyn. Giant Graviton Correlators from Dual SU(N) super Yang–Mills Theory. *Journal of High Energy Physics*, 2004(11):081–081, Nov 2004.

[127] T.W Brown. Half-BPS SU(N) Correlators in $\mathcal{N} = 4$ SYM. *Journal of High Energy Physics*, 2008(07):044–044, Jul 2008.

[128] Vijay Balasubramanian, Micha Berkooz, Asad Naqvi, and Matthew J Strassler. Giant Gravitons in Conformal Field Theory. *Journal of High Energy Physics*, 2002(04):034–034, Apr 2002.

[129] Eric D'Hoker, Johanna Erdmenger, Daniel Z. Freedman, and Manuel Pérez-Victoria. Near-Extremal Correlators and Vanishing Supergravity Couplings in AdS/CFT. *Nuclear Physics B*, 589(1-2):3–37, Nov 2000.

[130] Eric D'Hoker, Daniel Z. Freedman, Alec Matusis, and Leonardo Rastelli. Extremal Correlators in the AdS/CFT Correspondence. *The Many Faces of the Superworld*, page 332–360, Jul 2000.

[131] G. Arutyunov, S. Penati, A. Santambrogio, and E. Sokatchev. Four-Point Correlators of BPS Operators in SYM at Order g^4. *Nuclear Physics B*, 670(1-2):103–147, Oct 2003.

[132] Robert C. Myers. Dielectric branes. *JHEP*, 12:022, 1999.

[133] Massimo Bianchi and Stefano Kovacs. Nonrenormalization of Extremal Correlators in $\mathcal{N} = 4$ SYM theory. *Phys. Lett. B*, 468:102–110, 1999.

[134] B. Eden, P.S. Howe, C. Schubert, E. Sokatchev, and P.C. West. Extremal Correlators in Four-Dimensional SCFT. *Physics Letters B*, 472(3-4):323–331, Jan 2000.

[135] J. Erdmenger and M. Pérez-Victoria. Nonrenormalization of Next-to-Extremal Correlators in $\mathcal{N} = 4$ Super Yang-Mills Theory and the AdS/CFT Correspondence. *Physical Review D*, 62(4), Jul 2000.

[136] Silvia Penati, Alberto Santambrogio, and Daniela Zanon. Two-Point Functions of Chiral Operators in $\mathcal{N} = 4$ SYM at Order g^4. *Journal of High Energy Physics*, 1999(12):006–006, Dec 1999.

[137] Silvia Penati, Alberto Santambrogio, and Daniela Zanon. More on Correlators and Contact Terms in SYM at Order g^4. *Nuclear Physics B*, 593(3):651–670, Jan 2001.

[138] Steve Corley and Sanjaye Ramgoolam. Finite factorization equations and sum rules for bps correlators in n=4 sym theory. *Nuclear Physics B*, 641(1-2):131–187, Oct 2002.

[139] Simon Caron-Huot and Anh-Khoi Trinh. All Tree-Level Correlators in $AdS5 \times S5$ Supergravity: Hidden Ten-Dimensional Conformal Symmetry. *Journal of High Energy Physics*, 2019(1), Jan 2019.

[140] A. Bissi, C. Kristjansen, D. Young, and K. Zoubos. Holographic Three-Point Functions of Giant Gravitons. *Journal of High Energy Physics*, 2011(6), Jun 2011.

[141] Pawel Caputa, Robert de Mello Koch, and Konstantinos Zoubos. Extremal vs. Non-Extremal Correlators with Giant Gravitons. *Journal of High Energy Physics*, 2012(8), Aug 2012.

[142] Nima Arkani-Hamed, Freddy Cachazo, and Clifford Cheung. The Grassmannian Origin of Dual Superconformal Invariance. *Journal of High Energy Physics*, 2010(3), Mar 2010.

[143] J. M. Drummond and L. Ferro. Yangians, Grassmannians and T-Duality. *Journal of High Energy Physics*, 2010(7), Jul 2010.

[144] J. M. Drummond and L. Ferro. The Yangian Origin of the Grassmannian Integral. *Journal of High Energy Physics*, 2010(12), Dec 2010.

[145] Sujay K. Ashok and Eleonora Dell'Aquila. On the Classification of Residues of the Grassmannian. *Journal of High Energy Physics*, 2011(10), Oct 2011.

[146] J.M Drummond and J.M Henn. All Tree-Level Amplitudes in $\mathcal{N} = 4$ SYM. *Journal of High Energy Physics*, 2009(04):018–018, Apr 2009.

[147] N. Arkani-Hamed, J. Bourjaily, F. Cachazo, S. Caron-Huot, and J. Trnka. The All-Loop Integrand for Scattering Amplitudes in Planar $\mathcal{N} = 4$ SYM. *Journal of High Energy Physics*, 2011(1), Jan 2011.

[148] Luke Lippstreu, Jorge Mago, Marcus Spradlin, and Anastasia Volovich. Weak Separation, Positivity and Extremal Yangian Invariants. *Journal of High Energy Physics*, 2019(9), Sep 2019.

[149] T.W Brown, P.J Heslop, and S Ramgoolam. Diagonal Multi-Matrix Correlators and BPS Operators in $\mathcal{N} = 4$ SYM. *Journal of High Energy Physics*, 2008(02):030–030, Feb 2008.

[150] Rajsekhar Bhattacharyya, Storm Collins, and Robert de Mello Koch. Exact Multi-Matrix Correlators. *Journal of High Energy Physics*, 2008(03):044–044, Mar 2008.

[151] T.W Brown, P.J Heslop, and S Ramgoolam. Diagonal Free Field Matrix Correlators, Global Symmetries and Giant Gravitons. *Journal of High Energy Physics*, 2009(04):089–089, Apr 2009.

[152] Robert de Mello Koch, Jelena Smolic, and Milena Smolic. Giant Gravitons — with Strings Attached (I). *Journal of High Energy Physics*, 2007(06):074–074, Jun 2007.

[153] Robert de Mello Koch, Jelena Smolic, and Milena Smolic. Giant Gravitons — with Strings Attached (II). *Journal of High Energy Physics*, 2007(09):049–049, Sep 2007.

[154] David Bekker, Robert de Mello Koch, and Michael Stephanou. Giant Gravitons - with Strings Attached (III). *Journal of High Energy Physics*, 2008(02):029–029, Feb 2008.

[155] Christopher Lewis-Brown and Sanjaye Ramgoolam. Quarter-BPS States, Multi-Symmetric Functions and Set Partitions, 2020.

[156] Edward Witten. Baryons and Branes in Anti de Sitter Space. *Journal of High Energy Physics*, 1998(07):006–006, Jul 1998.

[157] Ofer Aharony, Yaron E Antebi, Micha Berkooz, and Ram Fishman. 'Holey Sheets' - Pfaffians and Subdeterminants as D-brane Operators in Large N Gauge Theories. *Journal of High Energy Physics*, 2002(12):069–069, Dec 2002.

[158] Pawel Caputa, Robert de Mello Koch, and Pablo Diaz. A Basis for Large Operators in $\mathcal{N} = 4$ SYM with Orthogonal Gauge Group. *Journal of High Energy Physics*, 2013(3), Mar 2013.

[159] Pawel Caputa, Robert de Mello Koch, and Pablo Diaz. Operators, Correlators and Free Fermions for SO(N) and Sp(N). *Journal of High Energy Physics*, 2013(6), Jun 2013.

[160] Christopher Lewis-Brown and Sanjaye Ramgoolam. BPS Operators in $\mathcal{N} = 4$ SO(N) Super Yang-Mills Theory: Plethysms, Dominoes and Words. *Journal of High Energy Physics*, 2018(11), Nov 2018.

[161] Marika Taylor. Matching of Correlators in AdS3/CFT2. *Journal of High Energy Physics*, 2008(06):010–010, Jun 2008.

[162] Francesco Aprile and Pedro Vieira. Large p Explorations. From SUGRA to Big STRINGS in Mellin Space, 2020.

[163] Frank Coronado. Perturbative Four-Point Functions in Planar $\mathcal{N} = 4$ SYM from Hexagonalization. *Journal of High Energy Physics*, 2019(1), Jan 2019.

[164] Frank Coronado. Bootstrapping the Simplest Correlator in Planar $\mathcal{N} = 4$ Supersymmetric Yang-Mills Theory to All Loops. *Physical Review Letters*, 124(17), Apr 2020.

[165] A.V. Belitsky and G.P. Korchemsky. Exact Null Octagon. *Journal of High Energy Physics*, 2020(5), May 2020.

[166] A. V. Belitsky and G. P. Korchemsky. Octagon at Finite Coupling. *Journal of High Energy Physics*, 2020(7), Jul 2020.

[167] A. V. Belitsky and G. P. Korchemsky. Crossing Bridges with Strong Szego Limit Theorem, 2020.

[168] Thiago Fleury and Vasco Goncalves. Decagon at Two Loops. *Journal of High Energy Physics*, 2020(7), Jul 2020.

[169] Till Bargheer, Frank Coronado, and Pedro Vieira. Octagons I: Combinatorics and Non-Planar Resummations. *Journal of High Energy Physics*, 2019(8), Aug 2019.

[170] Till Bargheer, Frank Coronado, and Pedro Vieira. Octagons II: Strong Coupling, 2019.

[171] H Prufer. Neuer Bewis Eines Satzes Uber Permutationnen. *Arch. Math. Phys.*, 27:742–744, 1918.